Pathophysiological role of RhoA/Rho-kinase under oxygen-glucose deprivation/reperfusion and hyperglycaemia

Kirtiman Srivastava

Division of Stroke, School of Clinical Sciences,

Faculty of Medicine and Health Sciences,

The University of Nottingham, City Hospital,

Nottingham, NG5 1PB

Thesis submitted to the University of Nottingham for

The Degree of Philosophy

December 2013

Abstract

Introduction: Oxygen-glucose deprivation (OGD)±reperfusion and hyperglycaemia exacerbate the ischaemic cerebral injuries during or after a stroke. The key biochemical events associated with these pathologies include excessive cytoskeletal remodelling, modulation of tight junction proteins and the induction of oxidative stress. Recently, the overactivities of protein kinase C (PKC), RhoA/Rho-kinase, and pro-oxidant NADPH oxidase have been shown to account for the development of these events and the consequent disruption of human blood-brain barrier (BBB) integrity.

Objectives: This thesis focused on the putative roles of RhoA/Rho-kinase signalling in OGD and OGD+reperfusion-evoked modulation of cytoskeletal remodelling, tight junction proteins and oxidative stress in human brain microvascular endothelial cells (HBMEC). The effects of hyperglycaemia-mediated PKC overactivities in modulating the RhoA/Rho-kinase pathway with reference to the aforementioned parameters i.e. cytoskeletal remodelling and tight junction protein expression and localisation have also been the focus of this thesis.

Methods: For the OGD studies, the HBMEC were exposed to normoxia (controls), OGD (4, 20 hours) alone and followed by reperfusion (20 hours). The HBMEC-human astrocyte (HA) cocultures were established to mimic human BBB before exposing them to the experimental conditions. The integrity and function of HBMEC-HA cocultures were measured by transendothelial electrical resistance (TEER) and flux of permeability markers sodium fluorescein (NaF) and Evan's blue-labelled albumin (EBA), respectively. For the hyperglycaemia studies, the HBMEC monolayers and the cocultures were exposed to normoglycaemia (5.5 mM D-glucose), hyperglycaemia (25 mM D-glucose), and hyperglycaemia with inhibitors of Rho-kinase, PKC, PKC-α, PKC-β, PKC-β_{II}, PKC-δ; and the BBB integrity and function were measured by the TEER and flux studies, respectively.

Fold differences in the protein expression or activity of RhoA, Rho-kinase-2, mono- and di-phosphorylated myosin light chain-2 (MLC2), total MLC2, gp91-phox (a pivotal NADPH oxidase subunit), catalase, occludin, claudin-5, zonula occludens-1 (ZO-1), β-catenin, and vinculin were either measured by in-cell or ordinary Western analyses.

Results from the OGD studies: OGD compromised the barrier integrity as observed by decreases in TEER values and concomitant increases in flux of EBA and NaF across the cocultures. Transfection of HBMEC with constitutively active RhoA also decreased the TEER and increased the NaF paracellular permeability, whereas inactivation of RhoA by anti-RhoA-IgG electroporation exerted barrier protective effects. Moreover, OGD alone and after constitutively active RhoA transfection introduced stress fibres in HBMEC, which were abrogated by inactivation of RhoA and the specific inhibition of its main effector Rho-kinase by Y-27632. In addition, dramatic increases in the protein expressions of RhoA-GTP, Rho-kinase-2, gp91-phox, and antioxidant catalase were observed in HBMEC exposed to OGD+reperfusion conditions. These along with increases in the NADPH oxidase activity and total superoxide anion levels confirmed the oxidative stress in HBMEC under these experimental conditions. A marked rise in the protein expressions of claudin-5 and β-catenin observed after OGD (20 hours) alone and followed by reperfusion may represent the effects of oxidative stress on tight and adherens junction proteins stability, respectively. These results also concurred with marked decreases in TEER and concomitant increases in the flux of EBA across the *in vitro* models of human BBB exposed to OGD±reperfusion conditions when compared with the controls. Cotreatment with Y-27632 under OGD±reperfusion normalised the protein expressions of RhoA, Rho-kinase-2, gp91-phox, claudin-5, catalase; activities of RhoA and NADPH oxidase; and total superoxide anions levels, alongside improving the expression of occludin and the coculture integrity under the OGD±reperfusion conditions.

Results from the hyperglycaemia studies: Hyperglycaemia also increased RhoA-GTP, Rho-kinase-2, mono- and di-phosphorylated MLC2 protein levels and total PKC activity. These changes were consistent with the actin stress fibre formations, ZO-1 and occludin redistribution from HBMEC periphery. Hyperglycaemia-mediated endothelial-barrier dysfunction was further characterised by reduction in TEER and elevation in flux of EBA. Glucose normalisation, RhoA neutralisation by anti-RhoA-IgG electroporation and Rho-kinase-2 inhibition by Y-27632 normalised all abovementioned protein expressions, restored actin and tight junction protein localisations and barrier integrity. Cotreatment of HBMEC with hyperglycaemia and a general PKC inhibitor namely, bisindolylmaleimide-I normalised the Rho-kinase-2, mono- and di-phosphorylated MLC2 levels. Moreover, specific inhibitors of PKC-α (Ro-32-0432), PKC-β (LY333531), PKC-β_{II} (CGP53353) attenuated the PKC overactivity, normalised all protein expressions, restored actin localisation and improved barrier integrity. In addition, the PKC-α and PKC-β siRNA transfections mimicked the effects of the specific inhibitors and attenuated the hyperglycaemia-evoked RhoA-GTP, mono- and di-phosphorylated MLC2 protein levels and stress fibre formations.

Conclusions: The RhoA/Rho-kinase overactivities compromise the endothelial-barrier integrity, in part, by modulating the cytoskeletal remodelling and inducing the NADPH oxidase-evoked oxidative stress under OGD±reperfusion pathology. Moreover, hyperglycaemia-mediated increases in PKC-α and PKC-β activities exacerbate the endothelial-barrier dysfunction by modulating RhoA/Rho-kinase signalling pathway.

Summary: These findings support the hypothesis that OGD±reperfusion and hyperglycaemia perturb BBB integrity through regulation of RhoA/Rho-kinase activity and modulation of cytoskeletal reorganisation, oxidative stress and tight junction protein expressions or localisations.

Acknowledgement

I am very thankful to all those who helped, inspired and motivated me during my doctoral study. I take immense pleasure to thank my supervisor Dr. Ulvi Bayraktutan for giving me an opportunity to pursue doctoral studies in the Division of Stroke. The experiments and the thesis writing would not have been possible without the support and guidance of Dr. Bayraktutan over the last three years. I am particularly indebted to Dr. Bayraktutan as he was always available and willing to help me in designing the experiments and supervising my work in the laboratories. His enthusiasm in vascular research has motivated me and kept me going in pursuit of quality data for publications in high impact peer-review journals. I owe a big thank you to Dr. Claire Allen who was the research fellow when I joined the group and to my fellow PhD students Kamini, Beili, Zuraidah and Manik for helping me in optimising the experimental protocols, being nice, friendly and supportive to me during my doctoral studies.

I would like to thank Wim for providing technical assistance, making me smile, and for organising regular curry nights with Graham and company. I would like to thank the technical staff at Clinical Sciences Building, Nottingham City Hospital for keeping the laboratories up to date and functional. I am grateful to Dr. Sadaf Ashraf and Dr. Paul Mapp from Academic Rheumatology for teaching and allowing me to use their fluorescent microscopes. I also like to thank my fellow researchers from Divisions of Respiratory Medicine, Haematology and Oncimmune for their help and support towards my research work.

I would like to thank my family for believing in me and for all that they have done for me. It would have been difficult to study PhD without their love and support. Lastly, I am thankful to god almighty for giving me an opportunity to work and study at the prestigious University of Nottingham, UK.

List of publications

Manuscripts

1. **Srivastava K**, Shao B, Bayraktutan U. Inhibition of PKCβ reverses hyperglycaemia-induced *in vitro* brain barrier permeability via RhoA/Rho-kinase/MLC2 pathway. (***J Cereb Blood Flow Metab.*** 2013; accepted)
2. **Srivastava K**, Bath PMW, Bayraktutan U. Current Therapeutic strategies to mitigate the eNOS dysfunction in ischaemic stroke. ***Cell Mol Neurobiol.*** 2012; 32:319-336.
3. Allen CL, **Srivastava K**, Bayraktutan U. Small GTPase RhoA and its effector Rho-kinase mediate oxygen glucose deprivation-evoked *in vitro* cerebral barrier dysfunction. ***Stroke***. 2010; 41:2056-2063.
4. Vashisht K, **Srivastava K**, Bayraktutan U. Oxidative stress impairs *in vitro* brain-barrier function through regulation of matrix metalloproteinase and urokinase. (***PLOS one***; submitted)
5. **Srivastava K**, Shao B, Bayraktutan U. PKC-α overactivity potentiates brain microvascular barrier dysfunction under hyperglycaemia. (***Microvasc Res***; submitted)
6. **Srivastava K**, Bayraktutan U. The role RhoA/Rho-kinase in the endothelial-barrier dysfunction. (***Int J Stroke***; in preparation)

Abstracts and Poster presentations

1. **Srivastava K**, Shao B, Bayraktutan U. Protein kinase C overactivity augments *in vitro* cerebral-barrier dysfunction through RhoA/ROCK pathway. ***Cerebrovasc Dis.*** 2012; 33(suppl 2): 431. (European stroke conference 2012, Lisbon)
2. Vashisht K, **Srivastava K**, Bayraktutan U. Blood-brain barrier breakdown after ischaemic stroke: the role of oxidative stress, plasminogen activators and matrix metalloproteinases. ***Cerebrovasc Dis.*** 2012; 33(suppl 2): 435. (European stroke conference 2012, Lisbon)

3. **Srivastava K**, Bayraktutan U. Rho/Rho-kinase pathway exacerbates the hyperglycaemia-mediated blood-brain barrier (BBB) disruption. ***Int. J Stroke.*** 2010, 4(suppl. 2). (UK stroke conference 2010, Glasgow)
4. **Srivastava K**, Bayraktutan U. Hyperglycaemia perturbs blood-brain barrier by inducing redistribution of tight junction proteins. ***Cerebrovasc Dis***. 2010; 29(suppl 2). (European stroke conference 2010, Barcelona)
5. **Srivastava K**, Bayraktutan U. Elevated Oxidative stress status contributes to breakdown of the blood brain-barrier under ischaemic conditions. ***Cerebrovasc Dis***. 2009; 27:191. (European stroke conference 2009, Paraguay)
6. Allen CL, **Srivastava K**, Bayraktutan U. The role of RhoA and its effector protein Rho kinase in ischaemia-mediated blood-brain barrier breakdown. ***Cerebrovasc Dis***. 2009; 27:190. (European stroke conference 2009, Paraguay)
7. **Srivastava K**, Bayraktutan U. Oxidative stress compromises blood-brain barrier integrity through up-regulation of urokinase plasminogen activator and its receptor. ***Int. J Stroke***. 2009, 4(suppl 2): 14. (UK stroke conference 2009, Glasgow)
8. Allen CL, **Srivastava K**, Bayraktutan U. The role of GTP-binding protein RhoA and its effector protein Rho kinase in ischaemia-mediated blood-brain barrier breakdown. ***Int. J Stroke***. 2009, 4(suppl 2): 13. (UK stroke conference 2009, Glasgow)

Table of Contents

List of Figures

List of abbreviations

ADP	: Adenosine diphosphate
AGE	: Advanced glycation endproducts
ANOVA	: Analysis of variance
ATP	: Adenosine triphosphate
BBB	: Blood-brain barrier
Bis-I	: Bisindolylmaleimide-I
BSA	: Bovine serum albumin
CaM	: Ca^{2+}-calmodulin
CNS	: Central Nervous System
COX	: Cyclooxygenase
CPI-17	: 17 kDa PKC-potentiated protein phosphatase-1 inhibitor protein
DAPI	: 4',6-diamidino-2-phenylindole
df1	: Degree of freedom (between groups)
df2	: Degree of freedom (within groups)
DMEM	: Dulbecco's Modified Eagles Medium
DMPK	: Myotonic dystrophy kinase
EBA	: Evan's blue-labelled albumin
EDTA	: Ethylene diamine tetraacetic acid
EGTA	: Ethylene glycol tetraacetic acid
ERK	: Extracellular signal-regulated kinase
ERM	: Ezrin/radixin/moesin
F-actin	: Filamentous-actin
GAP	: GTPase-activating proteins
GDI	: Guanine dissociation inhibitors

GDP : Guanosine diphosphate

GEF : Guanine-nucleotide exchange factors

GPCR : G-protein coupled receptors

GTP : Guanosine triphosphate

HIF : Hypoxia inducible factor

HA : Human astrocytes

HBMEC : Human brain microvascular endothelial cells

HBSS : Hank's buffered salt solution

HG : Hyperglycaemia

HMG-CoA : 3-hydroxy-3-methyl-glutaryl-coenzyme A

H_2O_2 : Hydrogen peroxide

H_2O : Water molecule

IL : Interleukin

IR : Ischaemia-reperfusion

JAK : Janus Kinase

JAM : Junction adhesion molecules

LIMK : LIM kinase

MAPK : Mitogen activated protein kinase

MCAO : Middle cerebral artery occlusion

mDia : Mammalian diaphanous

MLB : Mg^{2+} lysis buffer

MLC : Myosin light chain

MLCK : Myosin light chain kinase

MLCP : Myosin light chain phosphatase

MYPT : Myosin phosphatase targeting subunit

NADPH : Nicotinamide adenine dinucleotide phosphate-reduced

NaF : Sodium fluorescein

NF-κB : Nuclear factor-kappa B

NG : Normoglycaemia

NO : Nitric oxide

NOS : Nitric oxide synthase

O_2 : Molecular oxygen

$O_2^{\bullet-}$: Superoxide anion

OGD : Oxygen-glucose deprivation

OGD±R : Oxygen-glucose deprivation with or without reperfusion

PAK : p21-activated protein kinase

PBS : Phosphate buffer saline

PH : Pleck-strain homology

PI 3-K : Phosphatidylinositol 3-kinase

PKA : Protein kinase A

PKC : Protein kinase C

PKN : Protein kinase N

PMSF : Phenylmethylsulfonyl fluoride

RB : Rho binding

RNA : Ribonucleic acid

ROS : Reactive oxygen species

SAPK : Stress-activated protein kinase

SDS : Sodium dodecyl sulphate

SEM : Standard error measurement

siRNA : Small interfering ribonucleic acid

SOD	: Superoxide dismutase
STAT	: Signal transducer and activator of transcription
TNF	: Tumour necrosis factor
TGase	: Transglutaminase
TEER	: Transendothelial electric resistance
VEGF	: Vascular endothelial growth factor
ZO	: Zonula occludens

Introduction

The blood-brain barrier (BBB) serves as a selectively permeability barrier between systemic circulation and the central nervous system (CNS) whereby it plays a crucial role in maintaining the integrity and normal function of CNS. Several conditions associated with vascular abnormalities including hypertension, hyperglycaemia, ischaemia and hypercholesterolaemia exacerbate brain endothelial-barrier dysfunction and cause paracellular flow of circulating molecules into the brain parenchyma, leading to vasogenic oedema and possibly death after a stroke (Sydow, 2003, Hayashi et al., 2004). A plethora of deleterious molecular events are responsible for the endothelial-barrier dysfunction, which prominently include enhanced oxidative stress and inflammatory mediators (Petty and Wettstein, 2001, Brouns and De Deyn, 2009). Recently, the roles of small GTP-binding protein RhoA and its effector Rho-kinase have been highlighted in several cerebrovascular pathologies associated with increased vascular tone and endothelial remodelling (Chrissobolis and Sobey, 2006). This thesis focuses on the specific roles of RhoA/Rho-kinase pathway in cellular contractility, induction of the oxidative stress, modulation of tight junction and adherens junction proteins under physiological and pathological conditions, namely oxygen-glucose deprivation alone and followed by reperfusion (OGD±R) and hyperglycaemia.

1. BBB structure and function

It is important to maintain the fragile extracellular microenvironment of the neuronal parenchyma for the normal functioning of the brain. The BBB is responsible for this protection and maintenance against noxious chemicals, variations in blood compositions and breakdown of concentration gradient and therefore regarded as the physical and the metabolic barrier between the CNS and the systemic circulation (Huber et al., 2001, Petty and Lo, 2002).

The normal BBB phenotype consists of cerebral endothelial cells and their basement membrane together with perivascular cells including pericytes embedded within the basement membrane, perivascular monocytes, astrocytes and microglia. The cerebral microvasculature is ensheathed by astrocytic endfeet, which play an essential role in maintaining the BBB phenotype. It has been shown that astrocytes confer a protective role on the BBB against the hypoxia and aglycemia (Huber et al., 2001, Ballabh et al., 2004). The BBB accounts for two main functions which are to protect the brain from the blood-borne substances that may damage its fragile extracellular environment and to ensure the supply of nutrients through specific transport systems, namely transcellular pathway (passage through the endothelial cells) and paracellular pathway (passage between the endothelial cells) (Zhang and Pardridge, 2001). The endothelial cells at the BBB are specially adapted to prevent the flow of molecules either between or across cells because these cells have a low rate of transcytosis and limited transcellular solutes trafficking (Vorbrodt and Dobrogowska, 2003). Moreover, the presence of the continuous strands of tight junction proteins completely seal the paracellular cleft between the lateral endothelial cells (Gloor et al., 2001).

The tight junction and the adherens junctions together form the junctional complex between the adjacent endothelial cells at the BBB (Petty and Lo, 2002). The number of tight junction strands and their frequency is variable. The tight junction is composed of three integral membrane proteins; claudins, occludins and the junction adhesion molecules (JAM) (Figure 1). The adherens junctions consist of a cadherin–catenin complex and its associated protein. The third set of proteins includes the cytoplasmic accessory proteins such as zonula occludens (ZO-1, ZO-2, ZO-3) and cingulin. These proteins link the membrane proteins to actin, which is the main

cytoskeleton protein maintaining the structure and functionality of endothelium (Ballabh et al., 2004).

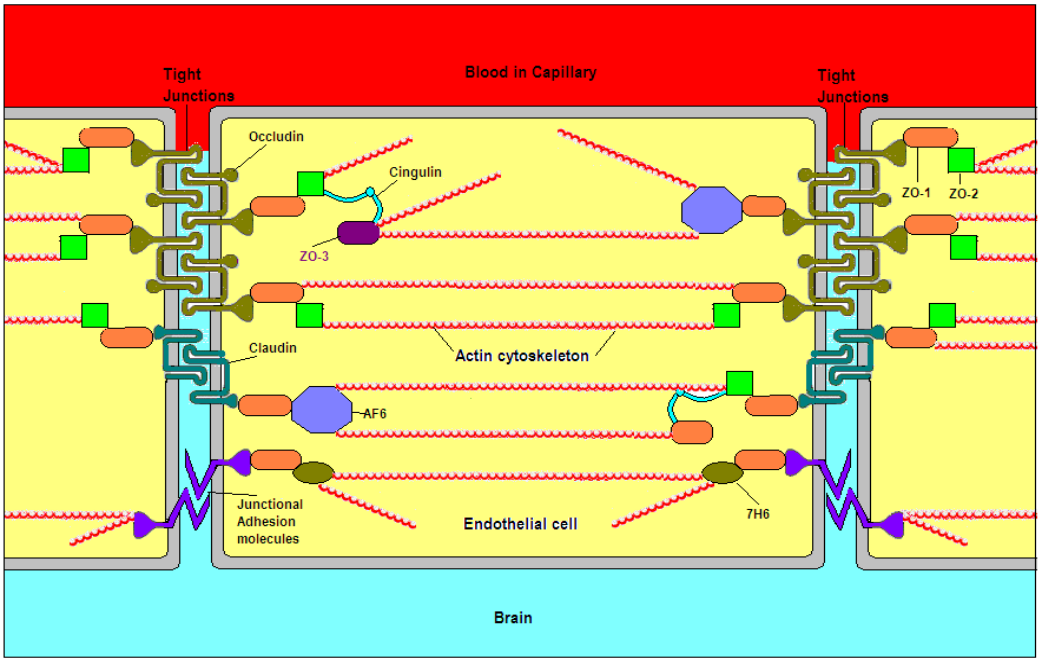

Figure 1. A schematic representation of tightly sealed human brain microvascular endothelial cells forming a typical BBB. ZO: Zonula occludens; AF6, 7H6: accessory proteins.

2. Proteins which mediate BBB integrity

2.1. Tight junction proteins

The three integral proteins of the tight junction are occludin, claudins and JAMs. The former two constitute the backbone of tight junction strands while JAMs play an important role in routine trafficking of T-lymphocytes, neutrophils and dentritic cells from lymphoid and vascular compartments of tissue (Furuse et al., 1993, González-Mariscal et al., 2003).

2.1.1. Claudins

Claudins are small phosphoproteins of about 20-22 kDa in size and have four transmembrane domains. They have two extracellular loops where the first one is significantly longer than the second one, and a short carboxy-intracellular tail. The last few amino acid of this tail are highly conserved within the family. The primary seal of tight junction is formed by the claudin dimers which bind homotypically to claudins on adjacent endothelial cells (Huber et al., 2001). Mammalian endothelial cells express solely claudin-1 and claudin-5 of which claudin-5 is expressed primarily in endothelial cells of blood vessels (Petty and Lo, 2002).

2.1.2. Occludins

Occludins are phosphoproteins of 60-65 kDa in size. They are significantly larger than claudins and show no similarities to the claudins at amino acid sequence level (Wolburg and Lippoldt, 2002). Occludins have four transmembrane domains with amino and carboxy-terminals located intracellularly. They have two similar size extracellular loops and three cytoplasmic domains. Their extracellular loops have 45 amino acids mainly tyrosine and glycine and are involved in cell-cell adhesion (Petty and Lo, 2002). Moreover, these extracellular loops of claudins and occludins originating from neighbouring endothelial cells form the paracellular barrier of tight junction at the BBB. The cytoplasmic domain of occludin is directly associated with the ZO proteins. The expression of occludin is much higher in brain endothelial cells as compared to nonneural tissues and they together with claudins contribute to the electrical resistance across the BBB (Sonoda et al., 1999, Gloor et al., 2001).

2.1.3. ,Junctional adhesion molecules

The JAM make up the third type of transmembrane tight junction proteins (Martìn-Padura et al., 1998). The JAM belong to immunoglobulin super family and are about 40 kDa in size. They have a single transmembrane domain and their extracellular portion (215 residues) contains two domains with intra-chain disulfide bonds typical of immunoglobulin like loops of the V-type (Citi and Cordenonsi, 1998). Three JAM related proteins have been identified while JAM-1 is expressed in endothelial and epithelial cells; JAM-2 and JAM-3 are expressed in most vascular endothelial cells (Ando-Akatsuka et al., 1996, Palmeri et al., 2000, Wolburg and Lippoldt, 2002). JAM are involved in cell-cell adhesion and contribute to monocyte extravasation.

2.2. Adherens junction proteins

The adherens junction proteins also play a significant role in sealing the adjacent endothelial cells and participate in preserving the endothelial-barrier integrity by stabilising the tight junction proteins. Like tight junction proteins, the adherens junction proteins also have transmembrane components like Ca^{2+}-dependent cadherins, and the cytoplasmic components which include β-catenin, γ-catenin, vinculin, α-actinin, and p120-catenin. The cytoplasmic proteins link cadherins with actin cytoskeleton via α-catenin (Ballabh et al., 2004, Dejana et al., 2008).

2.3. Cytoplasmic Accessory proteins

The cytoplasmic accessory proteins are involved in linking the membrane proteins to the cytoskeleton (Citi and Cordenonsi, 1998). They include ZO-1, ZO-2 and ZO-3, cingulin, 7H6 and several others. The ZO proteins belong to the membrane–associated guanylate kinase proteins family which is involved in the coupling of the transmembrane proteins to cytoskeleton (Gloor et al., 2001). The ZO-1 (220 kDa),

ZO-2 (160 kDa) and ZO-3 (130 kDa) contains three PDZ domains (PDZ-1, PDZ-2 and PDZ-3), one SH3 domain and one guanyl kinase like domain and bind to the actin filaments providing structural support to the endothelial cells (Gloor et al., 2001, Petty and Lo, 2002, Wolburg and Lippoldt, 2002). The other cytoplasmic accessory proteins include AF6 (180 kDa), 7H6 (155 kDa) and cingulin (140-160kDa). These are phosphoproteins which are found to localise on the cytoplasmic surface of the tight junctions and are pivotal in maintaining the tight junction complex stability and function. (Denker and Nigam, 1998).

3. Physiology of RhoA/Rho-kinase pathway

3.1. Rho GTPases

The low-molecular-weight (20-30 kDa) or small GTP-binding protein superfamily consists of more than 100 structurally similar proteins which act as molecular "on-off" switches and control multiple intracellular signalling pathways. They are broadly divided into 5 families i.e. Ras, Rho, Arf, Rab, and Ran (Heo and Meyer, 2003). Among them, the Rho GTPase family has received much of the attention in recent years mainly because of their role in actin-cytoskeleton remodelling, cell adhesion, motility, migration and contraction (Takai et al., 1995, Narumiya et al., 1997). Moreover, their activation also alters signalling pathways that regulate cell proliferation, gene expression, smooth muscle contraction, ion channel activity, endothelial permeability, reactive oxygen species (ROS) production and phospholipids metabolism (Burridge and Wennerberg, 2004, Schwartz, 2004). The Rho family members differ from other small GTPases by the presence of a Rho-specific insert domain and are approximately 25% identical to the members of Ras family (Ridley, 2001a, Boureux et al., 2007). So far, 20 members of Rho family have been identified in mammals, which are divided into 8 different subfamilies including

a Rho subfamily consisting of 3 members: RhoA, RhoB and RhoC (Miyagi et al., 2000, Miao et al., 2001, Miao et al., 2002, Chrissobolis et al., 2004). The best studied members of Rho-GTPase family are RhoA, Rac1 and Cdc42 for their contribution to cell migration, cell division and contraction. Past studies have shown that RhoA regulates the actin stress fibre assembly, whereas Rac and Cdc42 regulate actin polymerization and cellular protrusions respectively (Ridley and Hall, 1992, Ridley et al., 1992). This precise regulation is reflected in a diverse set of cellular events, such as leukocyte infiltration, smooth muscle contraction, axon growth, cytokinesis and angiogenesis (Schlessinger, 1993, Ridley, 2001b, Etienne-Manneville and Hall, 2002, De Smet et al., 2009). Moreover, recent studies have shown cumulative roles of RhoA, Rac1 and Cdc42 in regulation and maintenance of endothelial barrier integrity, during various vascular pathologies (Wojciak-Stothard and Ridley, 2002, Vandenbroucke et al., 2008). In addition, it has been shown that RhoA plays a pivotal role in Ca^{2+} sensitization in both cerebral and noncerebral vascular tissues (Akopov et al., 1998).

The effects of active Rho GTPase on the actin cytoskeleton and cell morphology are mediated via stimulation of downstream effector kinases. These include citron kinase, p140 mammalian diaphanous (mDia), protein kinase N (PKN), p21-activated protein kinase (PAK), rhophillin, and rhotekin. However, the best known downstream effectors of RhoA are Rho-kinase and mDia (Leung et al., 1995, Ishizaki et al., 1996, Matsui et al., 1996, Riento and Ridley, 2003).

3.2. Activation and regulation of RhoA

As mentioned earlier, RhoA is involved in regulation of various cellular activities like motility, proliferation, adhesion, remodelling, apoptosis, and gene expression (Burridge and Wennerberg, 2004). It regulates these activities by functioning as a

molecular "on-off" switch, cycling between an active GTP-bound state and an inactive GDP-bound state. 3 classes of enzymes regulate the cycle between active and inactive form of RhoA (Figure 2): (a) guanine-nucleotide exchange factors (GEF) that catalyses the exchange of GDP for GTP in the switch regions of RhoA and rendering RhoA activation; (b) GTPase-activating proteins (GAP) which inactivates active RhoA by accelerating intrinsic GTPase activity and dephosphorylating GTP to GDP and (c) guanine dissociation inhibitors (GDI) which keep RhoA in its inactive state by inhibiting the dissociation of bound GDP thereby preventing the membrane translocation of RhoA from the cytoplasm (Aspenström, 1999, Beckers et al., 2010).

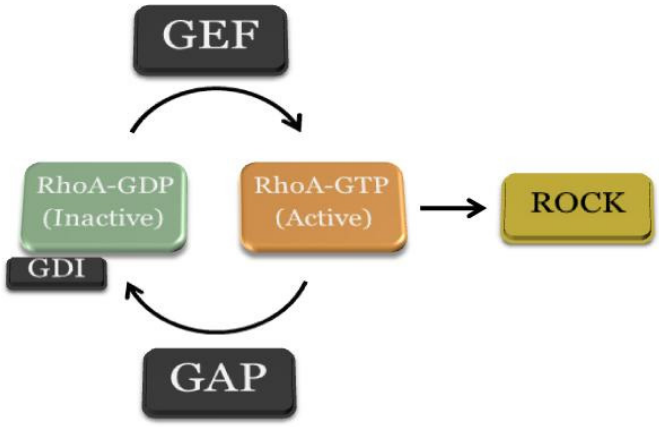

Figure 2. Activation and inactivation of RhoA regulated by small peptides

There are various agonists that regulate the activity of RhoA through heterotrimeric G protein coupled receptors (GPCR). It has been observed in non-muscle cells that following stimulation by agonists like thrombin and thromboxane A_2, the activated subunit of GPCR, $G\alpha_{13}$ binds to p115Rho GEF and stimulates its activity to catalyze the GDP exchange for GTP on RhoA (Hart et al., 1998, Seasholtz et al., 1999). However, it has been reported that protein kinase C-α (PKC-α) and focal

adhesion kinase can also phosphorylate the serine and tyrosine residues of GEFs and activate them (Siehler, 2009).

3.3. Rho-kinases

Rho-kinases are the ubiquitously expressed Ca^{2+}-sensitizing serine-threonine kinases that were found to be the first downstream effectors of RhoA (Chikumi et al., 2002). They are 40-50% homologous to other actin cytoskeleton kinases such as myotonic dystrophy kinase (DMPK), myotonic dystrophy-related Cdc42-binding kinase and citron kinase (Riento and Ridley, 2003). Rho-kinases have a 3 domain structure consisting of an amino-terminal kinase domain, followed by a mid-coiled-coil-forming lesion containing a Rho-binding (RB) domain, and a carboxy-terminal cysteine-rich domain located within the pleck-strain homology (PH) motif. Rho-kinase exists in 2 isoforms in the mammalian system; Rho-kinase-1 and Rho-kinase-2. Rho-kinase-1, also known as ROK-β and p160ROCK, is located on chromosome 18 encoding a 1354 amino acids protein. On the other hand, Rho-kinase-2 also called ROK-α, is located on chromosome 12 and contains 1388 amino acids. Rho-kinase-1 is 65% homologues to Rho-kinase-2 in amino acid sequence and 92% homologues in its kinase domain (Ishizaki et al., 1996, Matsui et al., 1996). The amino-terminal kinase domain has 72% amino acid sequence homology with the kinase domain of DMPK.

It has been observed that the binding of RB domain to GTP-RhoA enhances the Rho-kinase activity through depression of the carboxy-terminal RB-PH domain on the amino-terminal kinase domain, leading to an active “open” kinase conformation. Moreover, the lack of carboxy-terminal portion by cleavage also orientates Rho-kinase to an open kinase conformation in a constitutively active form (Feng et al., 1999b). By contrast, the kinase-activity-deficient form or the C-terminal fragments

lacking kinase domain, represent the dominant-negative form of Rho-kinase in cells (Leung et al., 1996, Amano et al., 1997, Amano et al., 1998). The dominant-negative form of Rho-kinase containing RB domain, specifically inhibits Rho-kinase activity and is used alongside several specific Rho-kinase inhibitors like Y-27632 and fasudil (HA1077) in many studies evaluating functional data in cells (Amano et al., 1999, Liao et al., 2007).

As mentioned earlier, Rho-kinases are ubiquitously expressed in mammals. In mouse tissues, Rho-kinase-1 mRNA was significantly expressed in lung, liver, spleen, kidney, and testis. In contrast, Rho-kinase-2 mRNA was highly expressed in the heart and brain (Nakagawa et al., 1996, Di Cunto et al., 2000). Moreover, the immunolocalization and cell fractionation studies have revealed that Rho-kinase-2 is distributed mainly in the cytoplasm, and is translocated to cell membrane after being activated by GTP-RhoA. In addition the subcellular localization of Rho-kinase-1 has been attributed to centrosomes (Kimura et al., 1996, Chevrier et al., 2002). Since Rho-kinases control the actin cytoskeleton assembly and cellular contractility, they regulate cellular apoptosis, growth, migration, and metabolism by phosphorylation and inhibition of myosin phosphatase, phosphorylation of myosin light chain (MLC), and facilitating the interaction of myosin with F-actin, thereby initiating the formation of stress fibres and focal adhesion complexes (Uehata et al., 1997).

3.4. Myosin kinases

The phosphorylation of regulatory light chain of myosin-II molecule induces a change in its conformation and promotes the actomyosin filament assembly (van Nieuw Amerongen and van Hinsbergh, 2001). Rho-kinase-2 and myosin light chain kinases (MLCK) are responsible for this phosphorylation at Ser^{19} and Thr^{18} of MLC,

when induced by agonists that stimulate MLC phosphorylation (Amano et al., 1996). However, Rho-kinase-2-mediated phosphorylation of MLC was found to be ~3 times lower than that of MLCK, hence MLCK are considered to be principally responsible for MLC phosphorylation (Gong et al., 1996). The MLCK are Ca^{2+}/calmodulin (CaM)-activated protein kinases which occur in several isoforms ranging from 130 to 150 kDa in size (Gallagher et al., 1997). Studies on endothelial cells have reported few MLCK which are bigger in size and immunologically distinct from their original isoforms and are also regulated by Ca^{2+}/CaM molecule (Gallagher et al., 1995, Garcia et al., 1997).

3.5. RhoA/Rho-kinase regulated actomyosin contractility

It has been well documented that activated Rho-kinases control the polymerization/assembly of actin monomers and also regulate the cellular contractility. They do so by serine-threonine phosphorylation of their effectors like ezrin/radixin/moesin (ERM) proteins, LIM kinase (LIMK), α-adducin, MLC-phosphatase (MLCP), 17 kDa PKC-potentiated protein phosphatase-1 inhibitor protein (CPI-17), MLC and calponin (Kawano et al., 1999, Koyama et al., 2000, Sumi et al., 2001). These actin cytoskeletal proteins have consensus amino acid sequences for phosphorylation as R/KXS/T or R/KXXS/T (R: arginine; K: lysine; X: any amino acid; S: serine; T: threonine), and can also be phosphorylated by other serine-threonine kinases like protein kinase A (PKA), PKC and G-kinases (Hartshorne, 1998).

3.5.1. Actin polymerization

Actin polymerization and reorganization are the pioneers in the cascade of events responsible for cellular contraction. The cellular protein cofilin binds to actin filament

and exhibits actin-depolymerizing activity (Carlier et al., 1997, Bamburg et al., 1999). This activity of cofilin is inhibited by phosphorylation at Ser^{3} by LIMK1 and LIMK2 (Arber et al., 1998, Yang et al., 1998). It has been reported that Rho-kinase activates LIMK1 by phosphorylation at Thr^{508} and LIMK2 at Thr^{505}, thereby curtailing the cofilin-mediated actin depolymerization (Ohashi et al., 2000, Sumi et al., 2001).

The ERM proteins are three closely related proteins, which function as cross-linkers between plasma membrane proteins and actin filaments (Bretscher, 1983). Studies have shown that Rho-kinase phosphorylates ERM proteins at Thr^{567} of ezrin, Thr^{564} of radixin, and Thr^{558} of moesin. This results in the disruption of intermolecular head-to-tail association of ERM proteins and initiates actin cytoskeleton reorganization (Matsui et al., 1998). Studies have also shown that Rho-kinase-2 phosphorylates and activates α-adducin, which assembles spectrin to the ends of actin filament, thereby increasing contractile response of actin cytoskeleton (Fukata et al., 1999).

3.5.2. Actomyosin contraction

The actomyosin contraction is corroborated by the formation of actomyosin bundles of anti-parallel actin filaments cross-linked by myosin-II, called as stress fibres (Narumiya et al., 2009). The formation and assembly of stress fibres is triggered by the Rho-kinase-mediated and MLCK-mediated phosphorylation of the regulatory subunit of MLC at Ser^{19}. This causes major conformational changes within myosin molecule, and facilitates the cellular contraction by increasing actin-myosin interaction and propelling myosin to slide along the actin filaments (van Nieuw Amerongen and van Hinsbergh, 2001).

Moreover, in many studies it was found that Rho-kinase further augments the MLC phosphorylation by inhibiting the MLC dephosphorylation activity of MLCP. MLCP holoenzyme is made of 3 subunits: a catalytic subunit (PP1δ), a myosin phosphatase targeting subunit-1 (MYPT1) composed of a 58 kDa head and 32 kDa tail region, and a small non-catalytic subunit, M21. Rho-kinase phosphorylates MYPT1 at Thr^{697}, Thr^{855} and attenuates MLCP activity and in some studies, causes the dissociation of MLCP from myosin (Essler et al., 1998, Feng et al., 1999a, Fukata et al., 2001).

In another study, the inactivation of MLCP has also been attributed to CPI-17. CPI-17 is a phosphorylation-dependent inhibitory protein specific for MLCP. It was found that CPI-17 is also a downstream effector of Rho-kinase, and its phosphorylation increases the inhibitory effect of CPI-17 on MLCP activity (Koyama et al., 2000). Thus, Rho-kinase manoeuvres the MLC activity and actomyosin contractility by virtue of two processes: MLC phosphorylation and MLCP inactivation. In addition, calponin has also been reported as a downstream effector of Rho-kinase and plays a pivotal role in actin cytoskeleton remodelling. Calponin is an actin filament-associated protein and its binding to actin filament cast an inhibitory effect on the actin-activated myosin ATPase activity. Upon phosphorylation by various kinases like Rho-kinase, PKC and CaM-dependent protein kinase-II, the binding activity of calponin to actin filament gets significantly reduced, thereby regulating the actomyosin contractility (Kaneko et al., 2000).

4. Ischaemic pathophysiology

Microglias are the resident immune cells in the brain that play a critical role in maintaining cerebral homeostasis and the BBB integrity (Gehrmann et al., 1995,

Hawkins and Davis, 2005). Upon activation following a cerebral injury like focal cerebral ischaemia, microglia migrate to the site of injury to exert a neuroprotective role through their ability to clear the dead tissue, inhibit excitotoxic neuronal damage and generate neuroprotective growth factors (Nakajima et al., 2001, Lu et al., 2005, Neumann et al., 2006, Turrin and Rivest, 2006, Ito et al., 2007). Contrary to this notion, previous *in vitro* studies under oxygen-glucose deprivation condition, which represents an aspect of ischaemia, have shown that the pharmacological inhibition of ischaemia-activated microglia attenuates the BBB disruption and the cerebral injury (Yenari et al., 2006). Activated microglia are implicated in the progression of cerebral neuro-inflammatory processes by increasing the production of pro-inflammatory cytokines such as interleukin-1β (IL-1β) and TNFα as well as chemokines, proteases, lipases, inducible nitric oxide synthase (iNOS), ROS and reactive nitrogen species which collectively compromise the BBB integrity and promote neuronal apoptosis (Wood, 1995, Flavin et al., 1997, del Zoppo et al., 2000, Wang et al., 2007). Indeed, a recent study focusing on an ischaemia-reperfusion (IR)-linked cerebral lesion, namely periventricular leukomalacia has shown that the activation of microglia is closely associated with increases in iNOS expression and activity (Haynes et al., 2009). Besides activated microglia, ischaemia-mediated astrocyte hyperactivity has also been linked to dramatic elevations in iNOS expression and activity and consequent cerebral damage further exacerbated by enhanced nitro-oxidative stress and increased infarct size, neuronal death and remodelling responses (Endoh et al., 1994, Yasuda et al., 2004, Askalan et al., 2006, Haynes et al., 2009). In this context, inhibitions of iNOS and cyclooxygenases-2 (COX-2) activities via suppression of phosphoinositidyl 3-kinase (PI3-K)/Akt, hypoxia inducible factor-1α (HIF-1α), nuclear factor-kappa B (NF-κB), Janus Kinase/Signal Transducer and Activator of Transcription

(JAK/STAT) and JNK/Stress-Activated Protein Kinase (SAPK) signalling pathways have been proposed as important molecular targets to mitigate the activated microglia-induced brain damage after ischaemia (Lu et al., 2006, Son et al., 2009, Oh et al., 2010, Kacimi et al., 2011).

5. Alterations to BBB structure/function under ischaemic conditions

The detrimental effects of ischaemic stroke are brought upon the BBB as a result of cerebral thrombosis or embolism which decreases the blood supply to the CNS. This phenomenon evokes a cascade of deleterious biochemical events which include a rapid depletion of ATP molecules, activation of inflammatory processes, induction of proteases and oxidative stress (Assenza et al., 2009).

These events in turn disrupt extracellular matrix and contribute to the remodelling of endothelial cells thereby causing vasogenic oedema. Restoration of blood flow to ischaemic parts of brain is associated with enhanced tissue damage mediated partly by oxidative stress which results from the imbalance between generation and metabolism of superoxide anion ($O_2^{\bullet -}$), the foundation molecule of other ROS (Raat et al., 2009).

It has been reported that in IR injury, the rapid ATP depletion impairs the Na^+/K^+ATPase in membrane and the Ca^{2+}ATPase in endoplasmic reticulum, causing an increase in the intracellular Ca^{2+}-concentration. Moreover, the influx of Ca^{2+} during reperfusion induces the activation of Ca^{2+}-dependent enzymes and subsequently the actomyosin contractility (Solaini and Harris, 2005). Since rapid ATP depletion is also attributed to the ROS production, the ROS-mediated activation of RhoA has been demonstrated in vascular smooth muscles during IR injury (Ferrari et al., 1993, Jin et al., 2004). In recent years, the role of RhoA/Rho-kinase pathway has been studied in detail in cerebral and coronary vasospasm (Sato et al., 2000,

Masumoto et al., 2002). In various rat models of stroke, the inhibitors of RhoGTPase and Rho-kinase have been shown to improve the blood flow to ischaemic brain areas, decrease infarct volume, improve neurological functions and prevent neutrophil accumulation (Ohtaki and Tranmer, 1994, Satoh et al., 1999, Satoh et al., 2001). Recent studies using human endothelial cell lines have shown that protein levels of RhoA GTPase and Rho-kinase are increased significantly after 5 hours of hypoxia (Jin et al., 2006). Keeping that in mind our recent study has shown that ischaemia increases the expression and activity of RhoA GTPase and Rho-kinase, promotes the MLC2 phosphorylation and induces the actin stress fibre formation in human brain microvascular endothelial cells (HBMEC). By treating HBMEC with Y-27632 and electroporating with anti-RhoA-IgG, the effects of ischaemia were significantly attenuated. These observations were further substantiated by improved integrity and function of *in vitro* model of human BBB exposed to RhoA/Rho-kinase pathway inhibitors in the presence of OGD (Allen et al., 2010). A recent study has reported that during IR injury, ROS can directly activate RhoA in cells by oxidative modification of the critical cysteine residues within the redox-active motif of RhoA. Moreover, this mechanism of regulating RhoA/Rho-kinase pathway is independent but parallel to classical regulation by GEF and GAP (Aghajanian et al., 2009).

6. Impact of hyperglycemia on BBB structure/function

Diabetes, a metabolic disorder associated with defects in either insulin production or utilisation, is one of the well-known risk factors for stroke. Approximately 40% of stroke patients have hyperglycaemia and nearly 50% of these patients have previously unrecognised glucose tolerance abnormalities. Hence, it is safe to state that hyperglycaemia plays an independent and possibly additive role in IR-mediated endothelial dysfunction during stroke (Goldstein et al., 2001, Allen and Bayraktutan,

2008). Hyperglycaemia-mediated endothelial dysfunction and injury has been attributed to increased oxidative stress, activation of polyol pathway, glucose auto-oxidation, upregulation of diacylglycerol, activation of PKC, and the non-enzymatic glycation of proteins and lipids with the irreversible formation/deposition of advanced glycation endproducts (AGEs) in a variety of recent studies (Brownlee, 2001, Vlassara and Palace, 2002, Allen and Bayraktutan, 2009b).

It has been reported in many studies, that AGE in high concentration ($\geq$ 0.6 μM) induce the formation and upregulation of hyperpermeability mediators like pro-inflammatory cytokines e.g. TNF-α and IL-1 (Bonnardel-Phu et al., 1999, Otero et al., 2001). Moreover, hyperglycaemia has also been reported to upregulate another hyperpermeability mediator namely vascular endothelial growth factor (VEGF) and its receptor VEGFR-2. These mediators are known to produce vasoactive and cytotoxic effects on vascular endothelium and activate a number of signalling pathways that promote endothelial remodelling and hyperpermeability (Caldwell et al., 2005, Kumar et al., 2009). In recent years, several studies have confirmed a direct relationship between diabetes and increased cerebrovascular RhoA/Rho-kinase activity. Moreover, the use of fasudil has shown to ameliorate hyperglycaemia-induced microvascular damage in retinas of diabetic rats (Miao et al., 2002, Arita et al., 2009). The increased RhoA/Rho-kinase activity has also been confirmed by looking into the functional data from cerebral arterioles of type-2 diabetic mice which showed an enhanced dilator response to Y-27632 compared to control mice (Didion et al., 2005). Hence it is possible that through the activation and upregulation of RhoA/Rho-kinase pathway, hyperglycaemia augments the endothelial barrier dysfunction and remodelling thereby perturbing the BBB integrity and further

contributing to the vascular injury during ischaemic stroke (Srivastava and Bayraktutan, 2010).

7. Drugs and inhibitors of Rho/Rho-kinase pathway

Aberrant Rho/Rho-kinase pathway activation has been reported in various cardiovascular, cerebrovascular, respiratory and dietary disorders. The Rho-kinase inhibitors have shown considerable improvement in Alzheimer's disease, bronchial asthma, cancers, glaucoma and osteoporosis (Liao et al., 2007). Y-27632 has been used in several animal models as well as in our recent cell culture studies with HBMEC mainly because it is a small cell-permeable molecule. Another cell-permeable Rho-kinase inhibitor, fasudil has been shown to prevent cerebral vasospasm after subarachnoid haemorrhage (Sato et al., 2000). Both of these inhibitors block the Rho-kinase activity by competing with ATP for binding and are therefore equipotent in inhibiting both isoforms of Rho-kinase. Moreover, higher concentrations of these inhibitors have been reported to inhibit other serine-threonine kinases, like PKA and PKC. On the contrary, the hydroxyl form of fasudil, hydroxyfasudil, is relatively more selective for Rho-kinases than fasudil and Y-27632 and has a half-life greater than 5 hours compared to the extremely short half-life of fasudil (0.5 hours) (Rikitake et al., 2005).

In recent studies, RhoA GTPase has been targeted as an alternative to Rho-kinase inhibition to attenuate the Rho/Rho-kinase pathway. Ca^{2+}-dependent enzyme, Transglutaminase2 (TGase2) catalyses the post-translational modification of RhoA by polyamination or deamidation at Gln^{63} and constitutively activates RhoA (Masuda et al., 2000, Singh et al., 2001). It has been reported that cystamine, an oxidized dimer of cysteamine and an inhibitor of TGase2 significantly prevented rat cardiomyocytes to IR-mediated injuries by inhibiting enhanced TGase-mediated RhoA/Rho-kinase

pathway during IR (Shin et al., 2008). C3-exoenzyme (transferase), another RhoA inhibitor has produced significant decreases in size of cerebral infarcts in mice models of middle cerebral artery occlusion (MCAO) (Laufs et al., 2000).

Moreover, the 3-hydroxy-3-methyl-glutarul coenzyme A (HMG-CoA) reductase inhibitors, commonly known as statins have been used to inhibit the RhoA/Rho-kinase pathway. For many years, statins have been prescribed to reduce plasma cholesterol levels (Liao and Laufs, 2005). Recently, a number of pleiotropic effects of statins have been reported that extend beyond their cholesterol lowering activity. As indicated above statins block the cholesterol biosynthesis by inhibition of HMG-CoA reductase and subsequent synthesis of isoprenoid intermediate (farnesyl pyrophosphate or geranylgeranyl pyrophosphate). Importantly, the geranylgeranylation of RhoA is a prerequisite for Rho activation by facilitating its conformational change and interaction with plasma membrane where GDP-GTP exchange occurs. Hence, by inhibiting Rho isoprenylation, statins decrease membrane targeting and subsequent activation of RhoA GTPase (Takemoto and Liao, 2001).

8. NADPH oxidase enzyme and superoxide anion metabolism

Cerebral reperfusion, achieved by the reestablishment of blood flow to ischaemic part of the brain is associated with enhanced tissue damage mediated in part by oxidative stress which emerges due to an imbalance between generation and metabolism of $O_2^{\bullet-}$, the foundation molecule of all ROS (Raat et al., 2009). Although a number of enzymatic and nonenzymatic mechanisms (Figure 3) including leakage from the mitochondrial electron transport system, xanthine oxidase, COX, lipooxygenase, and uncoupled endothelial NOS may account for exaggerated production of $O_2^{\bullet-}$ in the brain, the nicotinamide adenine dinucleotide phosphate-

oxidase (NADPH oxidase) has recently attracted much of the attention as it has been found to represent the major source of ROS in endothelial cells of different origins (Margaill et al., 2005, Selemidis et al., 2008). NADPH oxidase was first identified in phagocytic cells, and since then numerous isoforms of 'classical' NADPH oxidase have been identified in vascular cells which primarily differ in the nature of their catalytic 'Nox' subunit i.e. gp91-phox (Miller et al., 2006). To date, 7 other Nox isoforms have been discovered which are homologus to gp91-phox (Nox2), namely Nox1–Nox7. Among these Nox1, Nox2, Nox4, and Nox5 are highly expressed in vascular tissues and are the major source of ROS production in cardiovascylar system (Lassegue and Griendling, 2010). NADPH oxidase is a multi-component enzyme system comprising several cytosolic subunits such as small G protein Rac1, p47-phox, p67-phox and a membrane-bound cytochrome b_{558} domain consisting of gp91-phox and a stabiliser protein p22-phox that upon activation form functional enzyme complex. The $O_2^{\bullet-}$ produced from NADPH oxidase acts as a signalling molecule and activates a cascade of intracellular signalling mechanisms including mitogen-activated protein kinases (MAPK), PKC and PI3K. Furthermore, elevated levels of $O_2^{\bullet-}$ has also been implicated in the BBB hyperpermeability to large molecules in mice after IR injury (Stenmark et al., 2006, Chrissobolis and Faraci, 2008, Sandoval and Witt, 2008).

The $O_2^{\bullet-}$ produced from various enzyme complexes is dismutased by antioxidant enzyme superoxide dismutase (SOD) to generate hydrogen peroxide (H_2O_2), another ROS. In physiological conditions, low levels of intracellular or extracellular ROS including $O_2^{\bullet-}$ and H_2O_2 participate in many cellular functions such as intracellular signalling and defence against invading microorganisms. However, high levels of ROS are implicated in the pathogenesis of many vascular complications which

include hypercholesterolemia, atherosclerosis, diabetes, hypertension, and myocardial infaction. In mammals, three isoforms of oxidoreductase SOD have been identified which are SOD1 (CuZn-SOD), SOD2 (Mn-SOD), and SOD3 (extracellular-SOD). The dismutation reactions vary slightly with these SOD isoforms because of different redox active transition metal required for the enzyme activity (Fukai and Ushio-Fukai, 2011). The H_2O_2 generated after dismutation reaction is further metabolised to water and molecular oxygen by other antioxidant enzymes namely; catalase and glutathione peroxidase. It is of note here that recent *in vivo* studies using transgenic mice overexpressing catalase alone or with CuZn-SOD have been shown to be resistant to atherosclerosis due to their vascular protective effects (Yang et al., 2004).

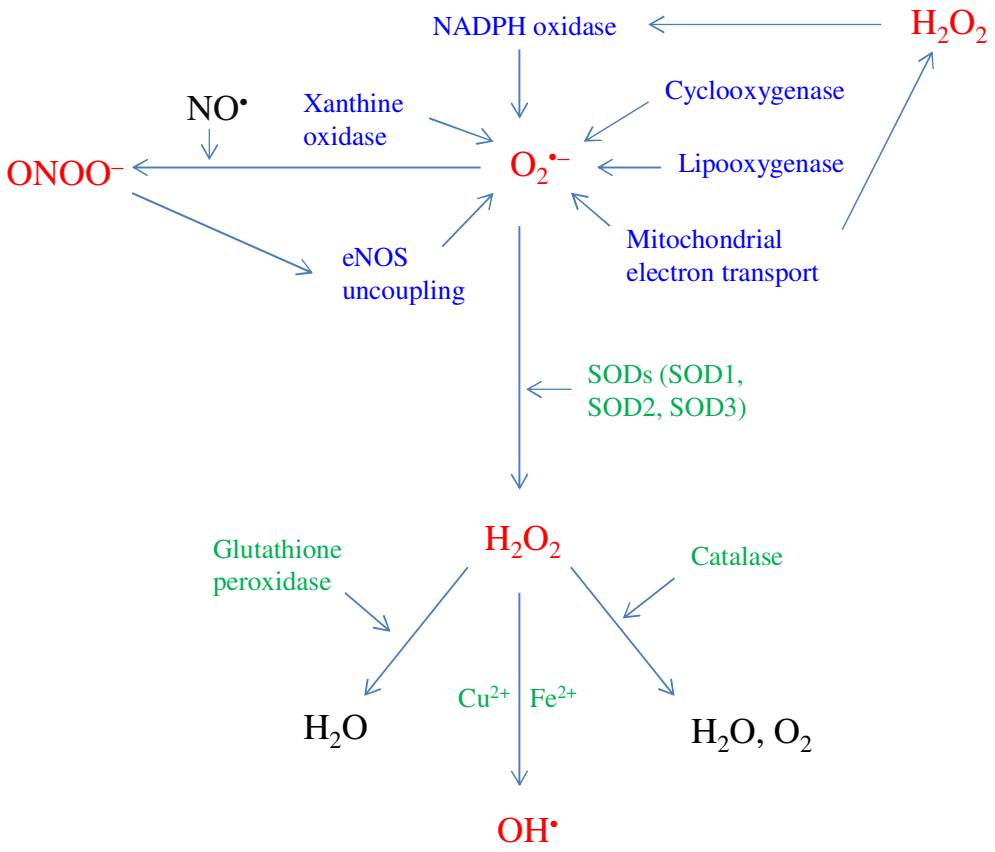

Figure 3. Metabolism of the reactive oxygen species (ROS). The prooxidant enzyme complexes (blue) generate ROS ($O_2^{\bullet-}$), which under physiological conditions are rapidly converted into less toxic/non-toxic products by enzymatic and nonenzymatic protective mechanisms (green). $ONOO^-$: peroxynitrite; $NO^{\bullet}$: Nitric oxide, $O_2^{\bullet-}$: superoxide anion; H_2O_2: hydrogen peroxide; $OH^{\bullet}$: hydroxyl radical; H_2O: water; O_2: oxygen.

9. Protein kinase C

The PKC is a family of enzymes that modulate the function of other proteins through phosphorylation of serine and threonine residues on them. The family possesses ten different isoforms that are classified into three different subfamilies, namely conventional (α, β_I, β_{II} and γ), novel (δ, ε, θ, η) and atypical (ζ and λ), on the

basis of their second messenger requirements (Geraldes and King, 2010). Due to the multiplicity of isozymes, the PKC is amenable to activation by many patho-physiological stimuli and thus involved in a wide spectrum of functions ranging from the mediation of immune responses to modulation of cell growth, contractility and permeability. Recent data have shown that activation of PKC, especially its β isoform, results in vascular hyper-permeability in organs that present ischaemic injury- or diabetes-mediated damage such as heart and retina (Hink et al., 2001, Bayraktutan, 2002, Geraldes and King, 2010). Specific increases in PKC-α and PKC-β protein expressions have also been reported in the brain infarcts of deceased ischaemic stroke patients (Xu et al., 2010). Given the profound involvements of PKC in the regulation of endothelial function and pathologies associated with barrier failure such as oxidative stress and inflammatory responses, it is safe to hypothesise that several PKC isoform(s) may be involved in the prevention or reversal of hyperglycaemia-evoked cerebrovascular damage (Stamatovic et al., 2006). In support of this notion, pharmacological inhibitions of PKC-α or PKC-β isoforms have previously been shown to exert vasculoprotection through negating the advanced glycation end products-induced inflammation and inhibitions of ZO-1 translocation, occludin phosphorylation and small GTP-binding protein RhoA glucosylation (Hink et al., 2001, Chen et al., 2002, Harhaj et al., 2006, Stamatovic et al., 2006, Xu et al., 2010).

10. Hypotheses

As mentioned earlier, occludins are implicated in increased tightness of the junctions and ZO-1 are known to anchor transmembrane proteins to endothelial cells (Furuse et al., 1998). Therefore, hyperglycaemia-induced putative changes in HBMEC phenotype and/or tight junction assembly may account for endothelial barrier hyperpermeability and endothelial-barrier dysfunction. Although several

mechanisms including the irreversible formation and accumulation of AGE, the activation of polyol pathway or stimulation of PKC have been implicated in diabetes-mediated peripheral vascular pathologies, the mechanisms involved in hyperglycaemia-mediated cerebral barrier failure remain largely unknown (Bayraktutan, 2002). Recently, the roles of small GTP-binding protein RhoA and its effector Rho-kinase have been highlighted in several cerebrovascular pathologies including diabetes that are inextricably linked with cerebral barrier hyperpermeability. Once activated RhoA activates Rho-kinase which promotes MLC2 phosphorylation, actin stress fibre formation and mitigates the nitric oxide (NO) bioavailability (Van Aelst and D'Souza-Schorey, 1997, Takemoto et al., 2002). Since increased MLC2 phosphorylation is linked to destabilization of the tight junction proteins and promote actomyosin contractility followed by hyperpermeability, it is possible that the suppression of RhoA/Rho-kinase pathway may be of clinical significance in reverting the hyperglycaemia-evoked barrier dysfunction by stabilising the endothelium effected by diabetes mellitus (Allen and Bayraktutan, 2009a). Thus, current thesis hypothesises that the activation of PKC and RhoA/Rho-kinase pathways under hyperglycaemia may perturb the physiological role of endothelial cells and compromise the BBB integrity. This may be due to enhanced cytoskeletal remodelling and modulation of junctional complexes. Studying these signaling pathways will enable us to identify new potential pharmacological targets/strategies for the stroke treatment.

Recent *in vitro* and *in vivo* studies on mice model of ischaemic stroke have shown that IR injury is associated with enhanced cytoskeletal remodelling and induction of oxidative stress which is responsible for the endothelial barrier hyperpermeability (Solaini and Harris, 2005, Raat et al., 2009). It has been shown that oxidative stress

modulates the tight junction and adherens junction proteins and disrupts the cerebral barrier integrity (Guntaka et al., 2011). However, the molecular mechanisms behind the IR-mediated cerebral barrier faliure remain largly unexplored. Hence, the current thesis also hypothesises that OGD±R may compromise the BBB integrity via enhanced cytoskeletal remodelling and induction of oxidative stress which could be associated with the RhoA/Rho-kinase pathway. This will lead to a better understanding of the signalling pathway and will help in identifing new molecular targets against oxidative stress-mediated pathologies which include ischaemic stroke and myocardial infarction.

Material

And

Methods

General methods and approach

The following list of chemicals and equipment were used in various experimental methodologies outlined in this chapter.

1. Chemicals and equipment

Materials	Company	Origin
Human brain microvascular endothelial cells	ScienCell research Labs	USA
Human astrocytes	ScienCell research Labs	USA
Dulbecco's Modified Eagle's Medium	Sigma-Aldrich	UK
Bisindolylmaleimide-I	Calbiochem (Merck)	UK
SB203580	Calbiochem (Merck)	UK
Y-27632	Calbiochem (Merck)	UK
LY333531	Calbiochem (Merck)	UK
Ro-32-0432	Calbiochem (Merck)	UK
CGP53353	Calbiochem (Merck)	UK
Rottlerin	Calbiochem (Merck)	UK
His-RhoA-L63	Cytoskeleton	USA
Odyssey blocking buffer	Li-Cor Biosciences	Germany
Rhodamine phalloidin dye	Invitrogen	UK
Bovine serum albumin	Sigma-Aldrich	UK
Foetal bovine serum (FBS)	Sigma-Aldrich	UK
Leupeptin	Sigma-Aldrich	UK
Aprotinin	Sigma-Aldrich	UK
Trypsin 10X	Sigma-Aldrich	UK
Protease cocktail inhibitor	Sigma-Aldrich	UK
Phenylmethanesulfonyl fluoride (PMSF)	Sigma-Aldrich	UK
Triton X-100	Sigma-Aldrich	UK
4',6-diamidino-2-phenylindole (DAPI)	Sigma-Aldrich	UK
Formaldehyde	Sigma-Aldrich	UK
Paraformaldehyde	Sigma-Aldrich	UK
Tween-20	Sigma-Aldrich	UK
D-mannitol	Sigma-Aldrich	UK
Evan's blue	Sigma-Aldrich	UK
40% Acrylamide	Sigma-Aldrich	UK
Sodium fluorescein	Sigma-Aldrich	UK
Cytochrome C	Sigma-Aldrich	UK
NADPH	Sigma-Aldrich	UK
Lucigenin	Sigma-Aldrich	UK
L-NAME	Sigma-Aldrich	UK
Rotenone	Sigma-Aldrich	UK

Allopurinol	Sigma-Aldrich	UK
Indomethacin	Sigma-Aldrich	UK
Rho activation assay kit	Upstate Millipore	USA
Non-radioactive Peptag total PKC activity kit	Promega	UK
siRNA oligonucleotides (PKC-α, PKC-β)	Dharmacon	USA
siRNA transfection reagents 1, 4	Dharmacon	USA
Antibodies		
Occludin	Santa Cruz biotechnology	Germany
RhoA	Santa Cruz biotechnology	Germany
Rho-kinase-2	Santa Cruz biotechnology	Germany
Myosin light chain-2 (MLC2)	Santa Cruz biotechnology	Germany
p-MLC2Ser^{19}	Santa Cruz biotechnology	Germany
p-MLC2Thr^{18}/Ser^{19}	Santa Cruz biotechnology	Germany
gp91-phox	Santa Cruz biotechnology	Germany
Vinculin	Santa Cruz biotechnology	Germany
PKC-α	Santa Cruz biotechnology	Germany
PKC-β_I	Santa Cruz biotechnology	Germany
CuZn-SOD	Sigma-Aldrich	UK
Catalase	Sigma-Aldrich	UK
β-catenin	Sigma-Aldrich	UK
β-actin	Sigma-Aldrich	UK
Claudin-5	Abcam	UK
Zonula occludens-1	Abcam, Invitrogen	UK
α-tubulin	Abcam	UK
Infrared (IR) dye 700/800 secondary antibody	Li-Cor Biosciences	Germany
FITC-conjugated secondary antibody	Axxora	USA
Equipment/apparatus		
6-well tissue culture plates	Corning Life sciences	UK
12-well tissue culture plates	Corning Life sciences	UK
96-well tissue culture plates	Corning Life sciences	UK
Tissue culture flasks (T-25, T-75, T-225)	Corning Life sciences	UK
12mm diameter, 0.4μm pore size, polyester membrane transwell inserts	Corning Life sciences	UK
Cell scrappers	TPP	Switzerland
8-chamber tissue culture slides	BD Biosciences	UK
Fluorescence plate reader	TECAN GENios	USA
Absorbance/luminescence plate reader	BMG LABTECH Omega	USA
Spectrophotometer	Berthold Technologies	USA
Zeiss fluorescence microscope	Carl Zeiss GmbH	Germany
Odyssey IR imaging system	Li-Cor Biosciences	Germany
PAGE apparatus	Bio-Rad	UK
Amersham hybond PVDF membrane	GE Healthcare	UK

O_2-controlled hypoxic tissue culture incubator	Sanyo	USA
CO_2-controlled tissue culture incubator	Sanyo	USA
N_2 cylinders	Airproducts	UK
Electroporator (1.8 kV)	Equibio Easyject Prima	USA
Electroporation cuvettes	Fisher scientific	UK

2. Human tissue culture

HBMEC and human astrocytes (HA) were cultured up to passage 7 to retain the barrier specific properties in Dulbecco's Modified Eagle's Medium (DMEM) containing 10% foetal bovine serum, penicillin (100 units/mL), and streptomycin (100 µg/mL) in a humidified atmosphere (95% relative humidity) under normal conditions (70% N_2, 25% O_2, 5% CO_2 and 5.5 mM D-glucose at 37ºC).

2.1. Experiments under hyperglycaemic conditions

To study the effects of hyperglycaemia, HBMEC were exposed to normoglycaemia (5.5 mM D-glucose), hyperglycaemia (25 mM D-glucose), D-mannitol (5.5 mM D-glucose + 19.5 mM D-mannitol) for 72 hours with media replacement every 24 hours to maintain the constant glucose levels. Experiments with D-mannitol were performed to assess how much of the putative changes that may be observed with hyperglycaemia could be attributed to an increase in osmolality. To determine the possible therapeutic effects of glucose normalisation on hyperglycaemia-mediated barrier dysfunction, in some experiments HBMEC were successively subjected to equal periods (72 hours) of hyperglycaemia followed by normoglycaemia (HG/NG). The relevance of Rho-kinase (Y-27632; 2.5 µM), p38MAPK (SB203580; 10 µM), PKC (Bis-I; 5 µM) and its specific isoforms PKC-α (Ro-32-0432; 1-5 µM), PKC-β (LY333531; 0.5-5 µM), PKC-β_{II} (CGP53353; 1 µM), PKC-δ (rottlerin; 5 µM), to hyperglycaemia-mediated barrier damage was assessed by

coexposure of HBMEC to hyperglycaemia and their specific inhibitors indicated in brackets.

2.2. Experiments under oxygen-glucose deprivation condition

To study the effects of IR injury mimicked by OGD±R, the confluent HBMEC were cultured in glucose-free RPMI-1640 media under hypoxic (94% N_2, 1% O_2 and 5% CO_2 at 37ºC) conditions. To study the reperfusion-mediated pathological alterations, some of the HBMEC flasks were reintroduced to the normal conditions for 20 hours after exposure to OGD. HBMEC cultured under normal conditions served as controls. The therapeutic effects of Rho-kinase inhibition on HBMEC were studied by cotreatments with Y-27632 (10 μM) and OGD±R. The HA were cultured in DMEM under normal conditions and were used in establishing the *in vitro* models of human BBB. The normal morphologies of HBMEC and HA cultured on coverslips in complete DMEM have been illustrated in figure 4.

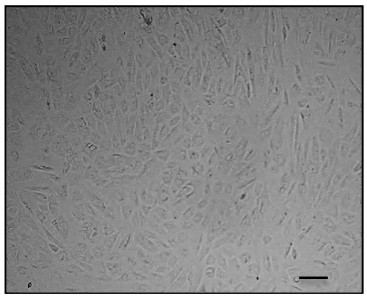

HBMEC

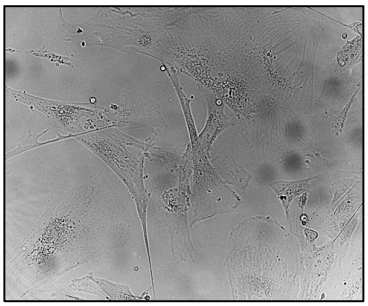

HA

Figure 4. HBMEC and HA cultured to subconfluence in complete DMEM as observed by 20X magnification on a light microscope. Bar scale: 50 μm.

3. *In vitro* model of human blood-brain barrier

To generate an *in vitro* model of human BBB, HBMEC were cocultured with HA to maximum confluence. This enabled HBMEC to maintain their barrier specific properties. HA (~75,000 cells/150 µL DMEM) were seeded on the basolateral side of polyester membrane Transwell inserts (12 mm diameter, 0.4 µm pore size) directed upside down in the 6-well tissue culture plates. Following overnight adherence of HA to the membranes, the inserts were inverted the correct way in sterile 12-well tissue culture plates containing fresh DMEM (1.5 mL) and were kept under normal tissue culture conditions until attainment of ~90% confluence. Thereafter, the HBMEC (~50,000 cells/150 µL DMEM) were seeded onto the inner part of the same inserts, and the cells were cultured to the maximum confluence under normal conditions before exposing the *in vitro* model of BBB to the experimental conditions. Equal number of HBMEC and HA used to start the preparation of the *in vitro* model of BBB were also seeded separately to form monolayers on the fresh inserts to monitor the cell proliferation rate and confluence simultaneously with the cocultures. A diagrammatic representation of the *in vitro* model of human BBB in a single well of a 12-well plate is illustrated in figure 5.

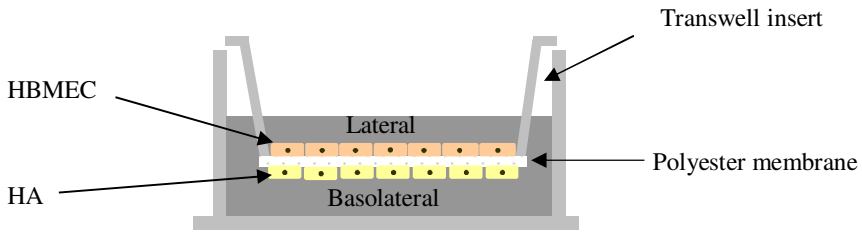

Figure 5. The *in vitro* model of human BBB consisting of HBMEC and HA

To study the effects of hyperglycaemia on the BBB, HBMEC and HA cocultures were incubated for 72 hours under abovementioned conditions in the presence and absence of specific inhibitors outlined earlier in this chapter. Similarly, the cocultures were also exposed to OGD±R.

3.1. Measurements of the *in vitro* blood brain-barrier integrity and function

The integrity and function of HBMEC and HA cocultures were assessed by measurements of transendothelial electrical resistance (TEER) and the flux of permeability markers sodium fluorescein (NaF; 376 Da), and Evan's blue-labelled with 0.1% albumin (EBA; 67 kDa) across the barrier, respectively. After exposures to experimental conditions TEER across the cocultures were measured by EVOM electrodes on an EVOM resistance meter and expressed relative to the surface area of HBMEC monolayer in "Ωcm^2". Thereafter, the inserts were transferred to the fresh wells in sterile 12-well plates containing Hank's buffered salt solution (HBSS; 2 mL) in basolateral side. To the lateral side of the inserts, either NaF (10 µg/mL) or EBA (165 µg/mL; 0.5 mL) was gently added and the permeability of markers were analysed by carefully collecting the lateral and basolateral samples (400 µL) after 1 hour of incubation. The concentration of EBA and fluorescein molecules in the samples were measured by using a BMG LABTECH Omega plate reader (absorbance: 610 nm) and fluorescent TECAN GENios plate reader (excitation: 440 nm, emission: 525 nm) and the flux of permeability markers were calculated as cleared volume (µL) by the formula: Cleared volume = $Concentration_{(basolateral\ reading)}$ x $Volume_{(basolateral)}$ x $Concentration_{(lateral\ reading)}^{-1}$. The average cleared volumes were represented as histograms to display the NaF and EBA passage across the cocultures subjected to pathological versus normal conditions. A diagrammatic representation of

the TEER measurement and NaF, EBA flux across the *in vitro* model of human BBB is illustrated in figure 6.

A

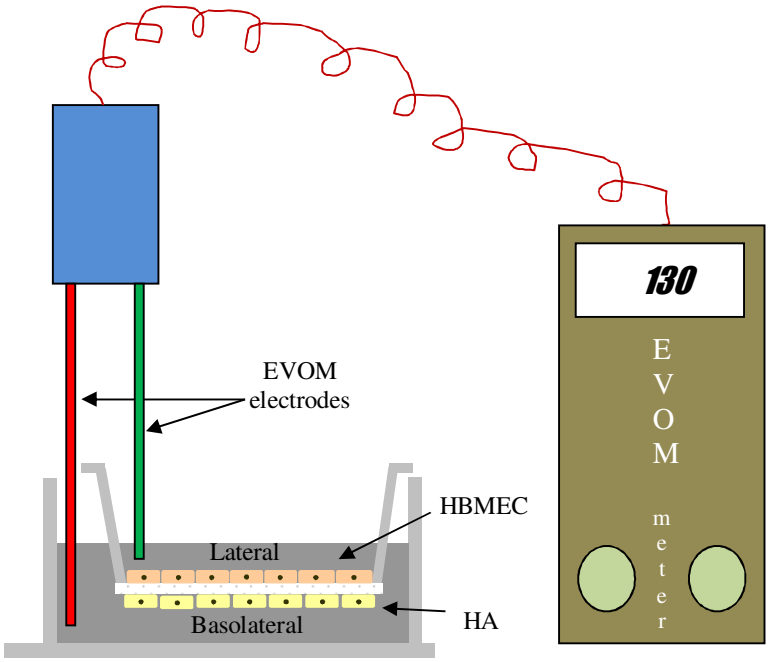

B

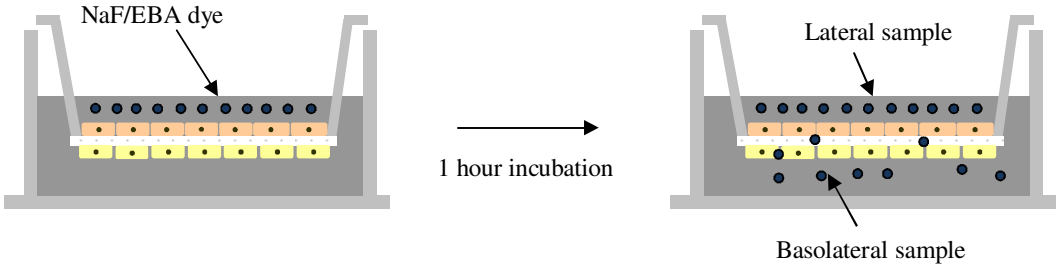

Figure 6. Measurements of the blood-brain barrier integrity and function by (A) TEER and (B) flux of NaF or EBA, respectively.

4. In-cell Western analysis

To detect the differences in the intracellular protein expressions, HBMEC (~5000 cells/well) were seeded on sterile 96-well tissue culture plates and were exposed to normal tissue culture conditions to proliferate into subconfluent monolayers before subjecting to experimental and corresponding control conditions. For example, after treatment with hyperglycaemia in the presence or absence of inhibitors, the DMEM was aspirated carefully and the HBMEC monolayers were fixed in fixing solution composed of 3.7% formaldehyde/phosphate buffer saline (PBS), (20 minutes), followed by permeabilisation by Triton washing solution (0.1% Triton X-100/PBS, 20 minutes) and blocking by either Odyssey blocking buffer or 1% BSA/PBS (1 hour) at room temperature. Following the blocking step, HBMEC were then successively incubated with primary antibodies (1-5 µg/mL, overnight at 4º C) raised against human RhoA, Rho-kinase-2, total MLC2, p-MLC2-Ser^{19}, p-MLC2-Thr^{18}/Ser^{19}, occludin, ZO-1 and α-tubulin. Thereafter, the cells were washed with Tween washing solution (0.1% Tween-20/PBS, 25 minutes at room temperature) on an orbital shaker and incubated with species-specific infrared 700/800-dye-tagged secondary antibodies (1 hour, room temperature) in dark. The cells were further washed as previously described and the plates were inverted to remove any residual washing solution. The plates were protected from light and were scanned on the Odyssey infrared imaging system to measure the infrared intensities corresponding to the intracellular protein levels in the HBMEC monolayer. Using the Li-Cor imaging software, the fold differences in the protein levels were calculated after normalisation against the infrared intensities corresponding to the internal control α-tubulin in the same well to eliminate the possibilities of unequal cell numbers.

5. Protein sample preparation and quantification

Firstly, the cells grown in cell culture flasks were washed twice with sterile PBS. The cells were dislodged from the flask by a sterile cell scrapper and were concentrated in the cell-lysis buffer (0.1% Triton X-100/PBS) containing protease cocktail inhibitor and phenylmethanesulfonyl fluoride (PMSF). The cells were lysed by sonication and cell homogenates were collected in pre-cooled eppendorf tubes on ice. Half of the cell homogenates were aliquoted and stored at -80ºC and cell debris in the remaining protein samples were removed by centrifugation (12,000 rpm/10 minutes) followed by storage at -80ºC. A small volume of protein samples and cell homogenates were used for protein quantification by Bradford assay using detergent-sensitive Coomassie plus assay kit.

The total proteins in samples were quantified by Coomassie plus assay kit to ensure that equal amount of proteins are used in Western blottings and enzyme activity assays. Briefly, in a 96-well plate the bovine serum albumin (BSA) standards (10 µL) with known protein concentrations (0, 25, 125, 250, 500, 750, 1000, 1500 and 2000 µg/mL) were mixed with Coomassie plus reagent (300 µL) in duplicates and a standard curve with its equation were derived from the absorbance values (610 nm) measured on the BMG LABTECH Omega plate reader after the colorimetric analysis. The figure 7 illustrates a representative standard curve and its equation used to quantify the protein levels in the unknown HBMEC samples.

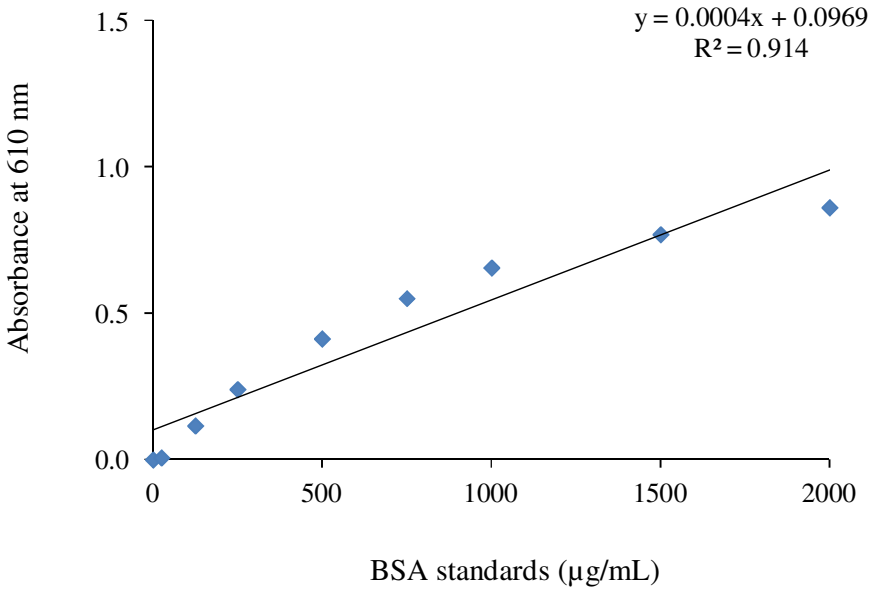

Figure 7. The BSA standard curve and corresponding equation of a straight line for the protein quantification in tissue culture samples.

6. Western blotting

Western blotting is a technique to resolve proteins depending on their molecular weight on polyacrylamide gels, and to compare the fold differences in their levels observed by immuno-specific reactions on the PVDF or nitrocellulose membranes. Various buffers including running buffer, transfer buffer, and washing buffer were used during Western blotting procedure to resolve and transfer the proteins onto the membranes followed by washing to remove excess of antibodies to minimise the background and maximise the signal intensity. A detailed recipe of these buffers and polyacrylamide gels are illustrated in appendix I.

Equal quantities of protein samples and cell homogenates were reduced (2-mercaptoethanol in 2X Laemmli dye) and denatured to open tertiary/quaternary

structures (100ºC, 5 minutes). The samples were resolved on SDS-polyacrylamide gels (7.5-15%) and proteins were transferred on the methanol-activated PVDF membranes followed by blocking (either with 5% dry milk, or with 5% BSA/PBS; 1 hour). The membranes were probed with primary antibodies against human antigens illustrated in appendix II followed by washing with the wash buffer (1X TBST). The membranes were subsequently probed with species-specific infrared 700/800-tagged secondary antibodies (1 hour) and were again washed to remove excessive antibodies to reduce the background and increase the signal intensities. The protein bands on the membrane were visualised by scanning on the Odyssey infrared imaging system and band intensities obtained by Li-Cor imaging software were used to calculate the relative band intensities between different treatment regimens after normalisation against the loading control β-actin.

7. Rho activation assay

To measure the RhoA activity in HBMEC under abovementioned treatment regimens, the "Rho pulldown assay" was used to detect active RhoA-GTP isoform.. Briefly, the HBMEC were lysed in 1X Mg^{2+} lysis buffer in the presence of protease inhibitors aprotinin (10 µg/mL), leupeptin (10 µg/mL) and protease cocktail inhibitor at 4ºC. The cell homogenates were centrifuged (14,000 g for 5 minutes at 4ºC) and cell lysates were collected for total protein quantification by Bradford assay. Equal amount of protein samples were incubated with rhotekin-RhoA binding peptide immobilised on agarose beads (10 µL) for 45 minutes at 4ºC with gentle shaking followed by centrifugation (14,000 g for 10 seconds at 4ºC). The pellets were rinsed three times with 1X Mg^{2+} lysis buffer and dislodged in 2X laemmli reducing buffer (25 µL). 20 µL of suspension samples were resolved on SDS-polyacrylamide gels (10%) followed by transfer of proteins on methanol-activated PVDF membranes. The

membranes were probed with primary antibody raised against human RhoA and subsequently with species-specific infrared 800-tagged secondary antibody. The protein bands on the membrane were visualised by scanning on the Odyssey infrared imaging system and band intensities obtained by Li-Cor imaging software were used to calculate the relative RhoA activities between different treatment regimens after normalisation against the total RhoA levels detected as described above.

8. Immunocytochemistry

To analyse the cellular localisation of proteins of interest, the HBMEC were cultured on glass coverslips to subconfluence under experimental and corresponding control conditions. Following the treatments, the DMEM was carefully aspirated and the cells were fixed (4% paraformaldehyde/PBS, 15 minutes), permeabilised (0.1% Triton X-100/PBS, 15 minutes) and blocked (10% BSA/PBS, 1 hour) at room temperature. The cells were either incubated with Rhodamine-labelled phalloidin dye for F-actin staining (200 U/mL, 20 minutes, room temperature) or with primary antibodies against human tight junction proteins i.e. occludin (20 µg/mL) and ZO-1 (4 µg/mL), human RhoA (2.5 µg/mL) and human Rho-kinase-2 (2.5 µg/mL) for overnight at 4º C in 1% BSA/PBS. The coverslips were washed by Tween washing solution (0.1% Tween-20/PBS, three times 5 minutes, room temperature) and the cells were incubated with FITC-labelled species-specific secondary antibody (1:100 in 1% BSA/PBS, 1 hour, room temperature) in dark. The coverslips were washed and incubated in 4',6-diamidino-2-phenylindole (DAPI) (5 minutes, room temperature) in dark. The excessive DAPI was removed by washing and the coverslips were mounted using glycerol/PBS (3:1), and the edges were sealed by nail polish. The cellular localisation of tight junction proteins and F-actin were observed under 40X

magnification on a Zeiss Axio Observer fluorescence microscope and pictures captured by Sony cybershot digital camera.

9. Transfection experiments

To modulate the RhoA GTPase activity, HBMEC (~$5x10^6$) were resuspended in a FBS and antibiotics-free RPMI 1640 media (100 µL) in a pre-chilled sterile electrode cuvette. 3 µg/cuvette of either His-RhoA-L63 or anti-RhoA-IgG was added to the cell suspension before electroporation at 1.8 kV. Similar procedure with equal volume of ultrapure H_2O served as electroporation controls. The viabilities of the electroporated cells were quickly analysed by trypan blue exclusion assay and the cells were quickly seeded in tissue culture flasks under normal tissue culture conditions. Once the electroporated cells were settled, they were subjected to experimental conditions followed by immunocytochemistry or the proteins harvestion to analyse the relative RhoA activities as previously described.

10. siRNA gene knockdown studies

To substantiate the pharmacological inhibition data and to confirm the specific PKC isoform-mediated effects under hyperglycaemia, semiconfluent HBMEC were washed with sterile PBS to remove traces of antibiotics. The transfection media was prepared by diluting DharmaFECT siRNA transfection reagent 4 (containing 50-100 nM of ON-TARGET plus SMART pool siRNA oligonucleotides against human PKC-α and PKC-β isoforms) in antibiotics-free complete DMEM. The cells were incubated with equal volume of transfection media (2 mL) for 24 hours followed by the hyperglycaemia treatment. Similar procedure was adopted for tranfecting HBMEC with ON-TARGET plus Non-targetting siRNA pool, which served as negative controls before exposing them to the normal and hyperglycaemic treatments. The cells

were homogenised after 72 hours of treatment, and transfection efficiency followed by protein downregulation were confirmed by detecting human PKC-α and PKC-β isoforms by Western blotting. Since the amount of DharmaFECT reagent and siRNA used in this study were proportional to the transfected cell numbers (in accordance with the manufacturer's guidelines), the cellular death rates observed appeared to be negligible. The appendix III shows the oligonucleotide sequences of the siRNA used to knockdown PKC isoforms.

11. Total PKC activity assay

To evaluate the total PKC activities under hyperglycaemia and to delineate the PKC isoforms modulating the hyperglycaemic effects, the total PKC activity was measured in HBMEC lysates using the PepTag non-radioactive PKC activity assay kit. Briefly, HBMEC pellets were resuspended and homogenised in cold PKC extraction buffer prior to elution of PKC-containing fraction through the use of pre-equilibrated Bio-spin columns with DEAE sepharose beads (1 mL). The eluted samples were mixed with PKC reaction mixture containing PepTag C1 peptide before loading onto 0.8% agarose/Tris-HCl (50 mM) gels to separate phosphorylated and nonphosphorylated PepTag peptide bands. The portion of the gel containing the phosphorylated bands was then excised and solubilised by melting (65ºC) followed by solubilisation in acetic acid. The samples (50 µL) were aliquoted in duplicates on a 96-well plate and absorbance (570 nm) was measured on a BMG LABTECH Omega plate reader. The absorbances were used to determine the relative PKC activities (units/mL) in accordance with the manufacturer's guidelines by Beer's law $A=\varepsilon BC$, where A=absorbance of the samples, ε=the molar absorptivity of the peptide, B=the width of the light cell, C=the concentration of the peptide in mol/L of the sample read.

The appendix IV shows the detailed recipe of the buffers used in the total PKC activity assay.

12. Total NADPH oxidase activity assay

The total NADPH oxidase activity was measured in HBMEC homogenates by lucigenin-enhanced chemiluminascent detection assay to address the role of NADPH oxidase enzyme complex in inducing the oxidative stress under OGD±R. The HBMEC were trypsinised and stored as pellets at -80ºC, and were homogenised only on the day of activity measurement to preserve maximum enzymatic activity. The HBMEC pellets were homogenised in phosphate lysis buffer (KH_2PO_4; 300 mM) containing ethylene glycol tetraacetic acid (EGTA; 50 mM) aprotinin, leupeptin, phenylmethylsulfonyl fluoride (PMSF) and protease cocktail inhibitors. Cell homogenates (50 µL) were aliquoted in duplicates in a white 96-well plate containing reaction mixture (100 µL) of phosphate buffer (50 mM), lucigenin (5 µM), sucrose (150 mM) and EGTA (1 mM). To ascribe all the lucigenin-enhanced chemiluminescent to NADPH oxidase activity, specific inhibitors of other ROS genetating enzyme complexes and rections namely; L-NAME (100 µM, NOS inhibitor), indomethacin (50 µM, COX inhibitor), allopurinol (100 µM, xanthine oxidase inhibitor) and rotenone (50 µM, mitochondrial complex I inhibitor) were added simultaneously to aliquots. The plates were incubated in a temperature controlled BMG LABTECH Omega plate reader (37ºC) for 15 minutes and the reaction substrate NADPH (100 µM; 100 µL) was added to each well by injectors in the plate reader to initiate the reaction. The luminescence value was recorded after every minute from each well for 3 hours and average luminescence corresponding to different samples were calculated by Mars data analysis software. The relative

NADPH oxidase activities (units/µg) were recorded by normalising the average luminescence values against the total protein levels in homogenates used.

13. Total $O_2^{\bullet-}$ detection assay

The total $O_2^{\bullet-}$ levels were measured in HBMEC homogenates by lucigenin-enhanced chemiluminescent detection assay. The HBMEC were trypsinised and stored as pellets at -80ºC, and were homogenised only on the day of activity measurement to preserve maximum enzyme activity. The HBMEC pellets were homogenised in phosphate lysis buffer (KH_2PO_4; 300mM) containing EGTA, aprotinin, leupeptin, PMSF and protease cocktail inhibitor. Cell homogenates (50 µL) were aliquoted in duplicates in a white 96-well plate containing reaction mixture (100 µL) of lucigenin (5 µM), sucrose (150 mM), EGTA (1 mM). The plates were incubated in a temperature controlled BMG LABTECH Omega plate reader (37ºC) for 15 minutes and the reaction substrate NADPH (100 µM; 100 µL) was added to each well by injectors in the plate reader to initiate the reaction. The luminescence value was recorded after every minute from each well for 3 hours and average luminescence corresponding to different samples were calculated by Mars data analysis software. The relative $O_2^{\bullet-}$ levels (units/µg) were recorded by normalising the average luminescence values against the total protein levels in homogenates used.

14. Cytochrome C reduction assay

The NADPH oxidase activity was measured in cell homogenates by colorimetric assay, which monitored the reduction of cytochrome C in the presence of electron rich NADPH substrate. HBMEC pellets comprising of 20 $x10^6$ cells were homogenised in cold HEPES buffer (20 mM, pH 7.2), containing EGTA (1 mM), mannitol (210 mM) and sucrose (70 mM). Equal volume (50 µL) of cell homogenate samples or positive

controls were added in 1 mL cuvette containing cytochrome C working solution (36 µM, 950 µL) at 25°C. To ascribe all the cytochrome C reduction to NADPH oxidase, specific inhibitors of other ROS-generating enzymes including L-NAME (100 µM), rotenone (50 µM), allopurinol (100 µM), and indomethacin (50 µM) were added to the reaction mixture. The reaction components were mixed gently and the reaction was initiated by addition of NADPH working solution (0.85 mg/mL) just before measuring the absorbance values. The absorbance values were measured on a temperature controlled (25°C) spectrophotometer at 550 nM by initial delay of 5 seconds followed by recordings of 7 readings with 10 seconds interval. The total $O_2^{\bullet-}$ anion levels were also measured by the cytochrome C reduction assay. Equal volume (50 µL) of HBMEC homogenates were added in 1 mL cuvette containing cytochrome C working solution (950 µL) at 25°C. The reaction was initiated by the addition of NADPH working solution followed by a gentle mix. The absorbance values were measured as previously described on a temperature controlled (25°C) spectrophotometer at 550 nM. The enzyme activities and total $O_2^{\bullet-}$ anion levels (units/µg) were measured following subtraction of background levels at 550 nm by following equation:

Units/µg= $\Delta A_{550/min}$/(21.1 x amount of protein used (µg)), where A=absorbance at 550nm.

15. Cell counting and cell viability detection assay

The HBMEC or HA counting was regularly carried out either to seed accurate number of cells or to monitor the cellular viability rates after transfection experiments. A small aliquot of cell suspension (10 µL) was mixed with equal volume of 0.1% trypan blue for 5 minutes and the mixture was carefully pipetted on haemacytometer for cell counting. Cells situated on the 5 big grids were counted by

the aid of a light microscope, and cells/mL was calculated by the following formula: Total cells/mL = Average cells in each grid x dilution factor x 10^4; dilution factor = Total volume of cell suspension in trypan blue/original volume of cell suspension.

The viable cells were calculated by counting the cells which were not stained by trypan blue in 5 big grids, and total viable cells/mL was calculated as follows: Total viable cells/mL = Average viable cells in each grid x dilution factor x 10^4. Hence, the cell viability was represented as percentage of viable cells by the following calculation: Cell viability = Total viable cells/mL x Total cells/mL^{-1} x 100

16. Statistical analyses

Results were presented as mean±SEM. Statistical analysis was performed by using IBM SPSS 20.0 software and comparing the mean by student's t-test and one-way analysis of variance (ANOVA) followed by Dunnet's *post hoc* analysis. The $P<0.05$ was considered to be significant in all the experiment.

Results

Chapter 1

OGD-evokes *in vitro* BBB disruption through regulation of RhoA/Rho-kinase pathway

1.1. Aims

To study,

1. whether OGD alters the *in vitro* model of human BBB integrity and function,

2. whether RhoA and Rho-kinase play a significant role in the OGD-mediated hyperpermeability,

3. the cellular localisation of RhoA and Rho-kinase during OGD,

4. whether RhoA evokes cytoskeletal remodelling under OGD,

5. whether specific inhibition of Rho-kinase exert any cerebrovascular protective effects.

1.2. Results

1.2.1. Effects of OGD on the *in vitro* cerebral-barrier integrity and function

To evaluate the effects of OGD on the integrity of an *in vitro* model of human BBB, HBMEC and HA cocultures were exposed to short and longer periods of OGD (4 and 20 hours) using a hypoxic chamber. The integrity of the cocultures were analysed by measuring TEER values which were indicative of physical disruption, and the flux of NaF which represented the functional impairment of the endothelial-barrier. Our data have shown that OGD compromised the *in vitro* cerebral-barrier integrity as evidenced by time-dependent decreases in TEER values ($P<0.05$), and concomitant increases in the flux of NaF across cocultures compared to the cocultures exposed to normoxia which served as controls ($P<0.05$). Moreover, the cocultures exposed to longer periods of OGD further compromised the BBB integrity and function thereby showing the deleterious effects of OGD ($P<0.05$) (Figure 1.1A, B).

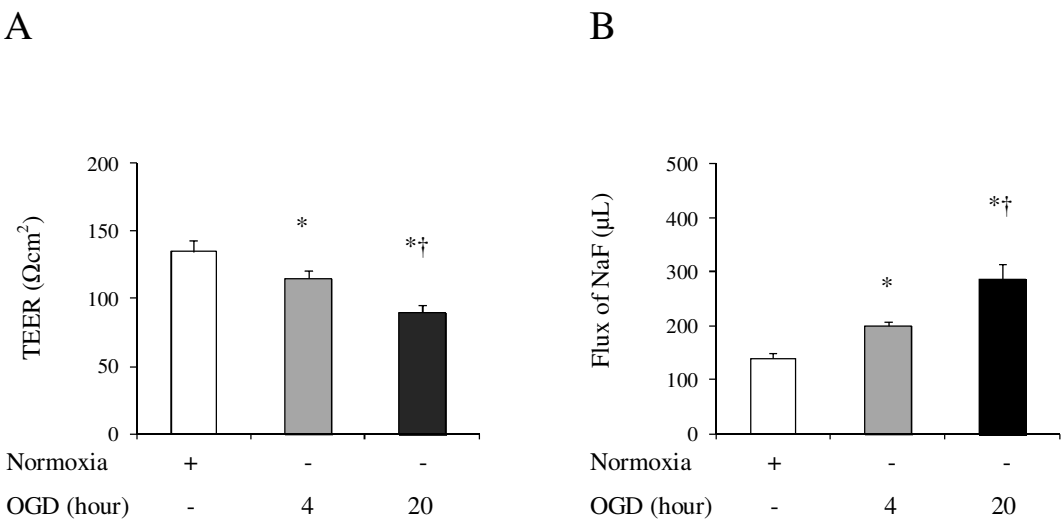

Figure 1.1. Effects of OGD on integrity and function of an *in vitro* model of human BBB. **(A)** Transendothelial electrical resistance (TEER) and **(B)** flux of sodium fluorescein (NaF) across the cocultures subjected to short and longer OGD (4 and 20 hours). Data are expressed as mean±SEM from 5 different experiments. Statistical analysis was done using ANOVA with Dunnet's *post hoc* test for multiple comparisons (A: $P<0.0001$, $F=37.212$, $df1=2$, $df2=6$), (B: $P<0.0001$, $F=174.817$, $df1=2$, $df2=6$). $^{*}P<0.05$ compared to normoxia, $^{\dagger}P<0.05$ compared to OGD (4 hours).

1.2.2. RhoA and Rho-kinase are involved in OGD-mediated hyperpermeability

To evaluate the role of RhoA under OGD-mediated barrier permeability, the cocultures were established using HBMEC electroporated with constitutively active human recombinant RhoA protein (His-RhoA-L63). Here, the cocultures developed by the HBMEC electroporated with either anti-human RhoA-IgG, or with ultrapure water served as electroporation controls to ensure that the changes observed were not dependent on electroporation-evoked cell death.

The studies investigating the effects of electroporation on the BBB function revealed no significant differences in the patterns of TEER and flux of NaF between the nonelectroporation controls and the electroporation controls as OGD disrupted the cerebral barrier measured by decreases in the TEER values and increases in the flux of NaF across the cocultures ($P<0.05$). These results indicate that the observed alterations to the coculture integrity are reflective of the treatments *per se* (Figure 1.2A). The His-RhoA-L63 electroporation in HBMEC led to a marked decrease in the TEER values under normoxia and OGD, respectively ($P<0.05$). These data indicate that RhoA overexpression in HBMEC mediate and exacerbate the cerebral-barrier disruption under normoxia and OGD, respectively. Concomitant increases observed in the flux of NaF across the respective cocultures supported these findings ($P<0.05$) (Figure 1.2B). In contrast to these, the cocultures established with anti-human RhoA-IgG electroporated HBMEC showed a significantly improved TEER and concurrent reduction in the flux of NaF after OGD compared to the respective cocultures subjected to normoxic conditions ($P<0.05$) (Figure 1.3A). These data indicate that inhibition of RhoA may be cerebral-barrier protective under OGD condition.

In addition, cotreatment with Y-27632 (2.5 μM), a specific Rho-kinase inhibitor, during normoxia and OGD exposures appeared to blocked the synergistic effects of His-RhoA-L63 electroporation and OGD as confirmed by improvement in TEER values and decrease in the flux of NaF across these cocultures, thus suggesting a cerebral barrier protective role of the Rho-kinase inhibition during pathological conditions like OGD ($P<0.05$) (Figure 1.3B).

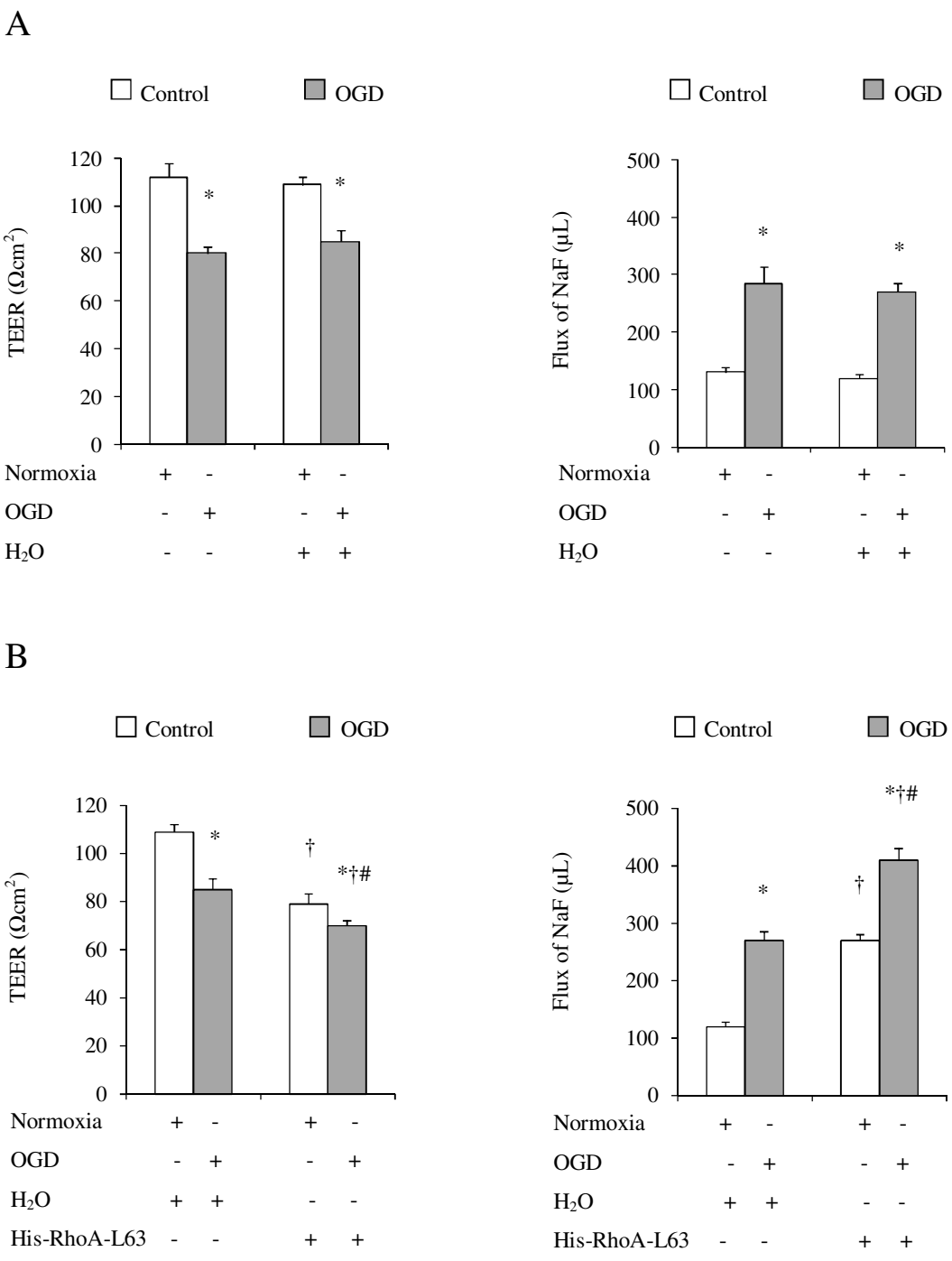

Figure 1.2. RhoA-mediated increase in the paracellular permeability under OGD. Transendothelial electrical resistance (TEER) and flux of sodium fluorescein (NaF) across cocultures established by HBMEC electroporated with **(A)** H_2O which served as electroporation controls, and with **(B)** His-RhoA-L63 or H_2O. Data are expressed

as mean±SEM from 5 different experiments. Univariate comparisons were made using Student's t-test. $^{*}P<0.05$ compared to normoxia in the same group, $^{\dagger}P<0.05$ compared to normoxia in the electroporation control group, $^{\#}P<0.05$ compared to OGD in the electroporation control group.

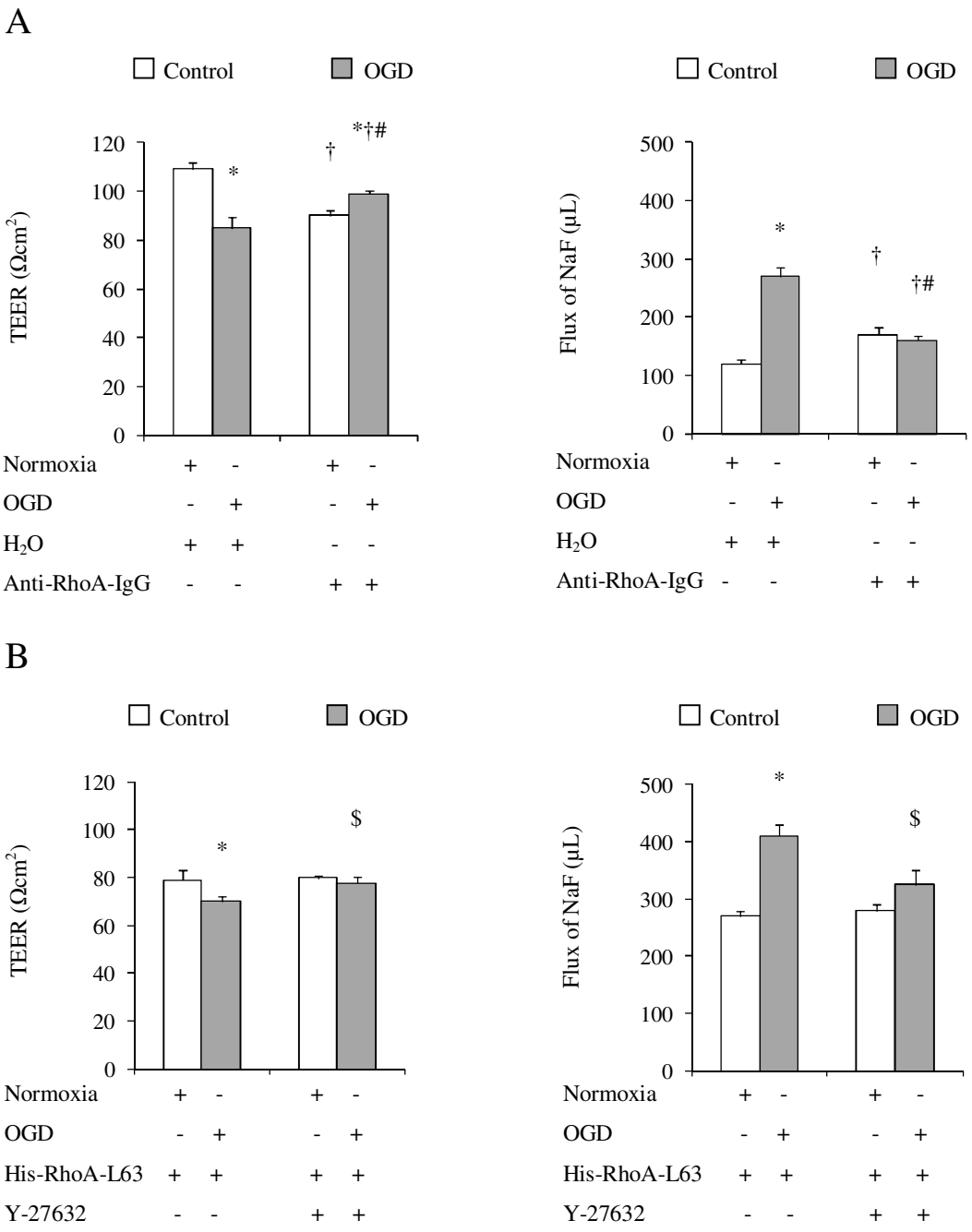

Figure 1.3. RhoA/Rho-kinase-mediated increase in the paracellular permeability after OGD. Transendothelial electrical resistance (TEER) and flux of sodium fluorescein (NaF) across cocultures established by HBMEC electroporated with **(A)** Anti-RhoA-IgG or H_2O, and with **(B)** His-RhoA-L63 or H_2O in the presence or absence of Y-

27632. Data are expressed as mean±SEM from 5 different experiments. Univariate comparisons were made using Student's t-test. $^{*}P<0.05$ compared to normoxia in the same group, $^{\dagger}P<0.05$ compared to normoxia in the electroporation control group, $^{\#}P<0.05$ compared to OGD in the electroporation control group, $^{\$}P<0.05$ compared to the OGD in the His-RhoA-L63 electroporated group.

1.2.3. Cellular localisation of RhoA and Rho-kinase

Small GTPase have been shown to localise to cytoplasm, hence the cellular localisation of RhoA and Rho-kinase proteins have been investigated in HBMEC exposed to normoxia and OGD (20 hours). Under normoxia, RhoA was uniformly distributed in the HBMEC cytoplasm as represented by faint intracellular stainings. However, after the OGD increased intracellular stainings of RhoA protein (arrows) marked by a relatively brighter stainings were recorded. In addition, the intracellular staining of Rho-kinase showed a faint uniform staining under OGD, which were similar to the Rho-kinase stainings observed under normoxic conditions (Figure 1.4).

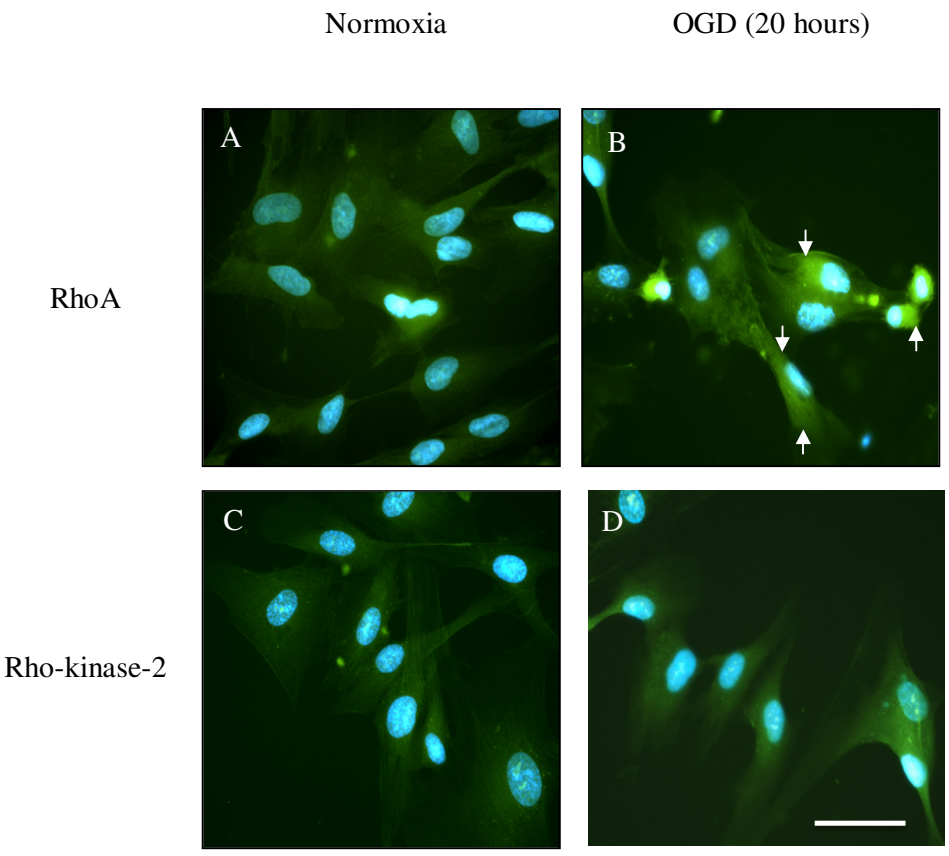

Figure 1.4. Cellular localisation of RhoA **(A, B)** and Rho-kinase-2 **(C, D)** in HBMEC exposed to normoxia and OGD (20 hours). Arrows indicate the effect of OGD on RhoA localisation. The cellular RhoA and Rho-kinase-2 levels were detected by primary antibodies against human RhoA and human Rho-kinase-2 followed by species specific secondary antibodies-tagged with FITC. The cells were incubated with DAPI and were identified by blue coloured nuclei by 40X magnification on a fluorescent microscope. Bar scale: 50 μm.

1.2.4. RhoA-induced cytoskeletal remodelling under OGD

To investigate whether the RhoA-evoked paracellular permeability may in part be due to OGD-induced cytoskeletal remodelling, the filamentous actin (F-actin) cytoskeletal detection were carried out in HBMEC electroporated with either H_2O, His-RhoA-L63 or anti-RhoA-IgG before exposure to normoxia and OGD (20 hours), respectively. The H_2O-electroporated HBMEC cultured under normoxia displayed marginal actin band distribution while OGD led to formation of stress fibres (arrows) and morphological changes characterised by cuboidal or elongated appearance. While RhoA overactivity induced by His-RhoA-L63 electroporation led to the formation of thick stress fibres similar to cells exposed to OGD, the inhibition of RhoA by anti-human RhoA-IgG electroporation eradicated all phenotypic changes and produced morphologies resembling to those seen in normal HBMEC (Figure 1.5).

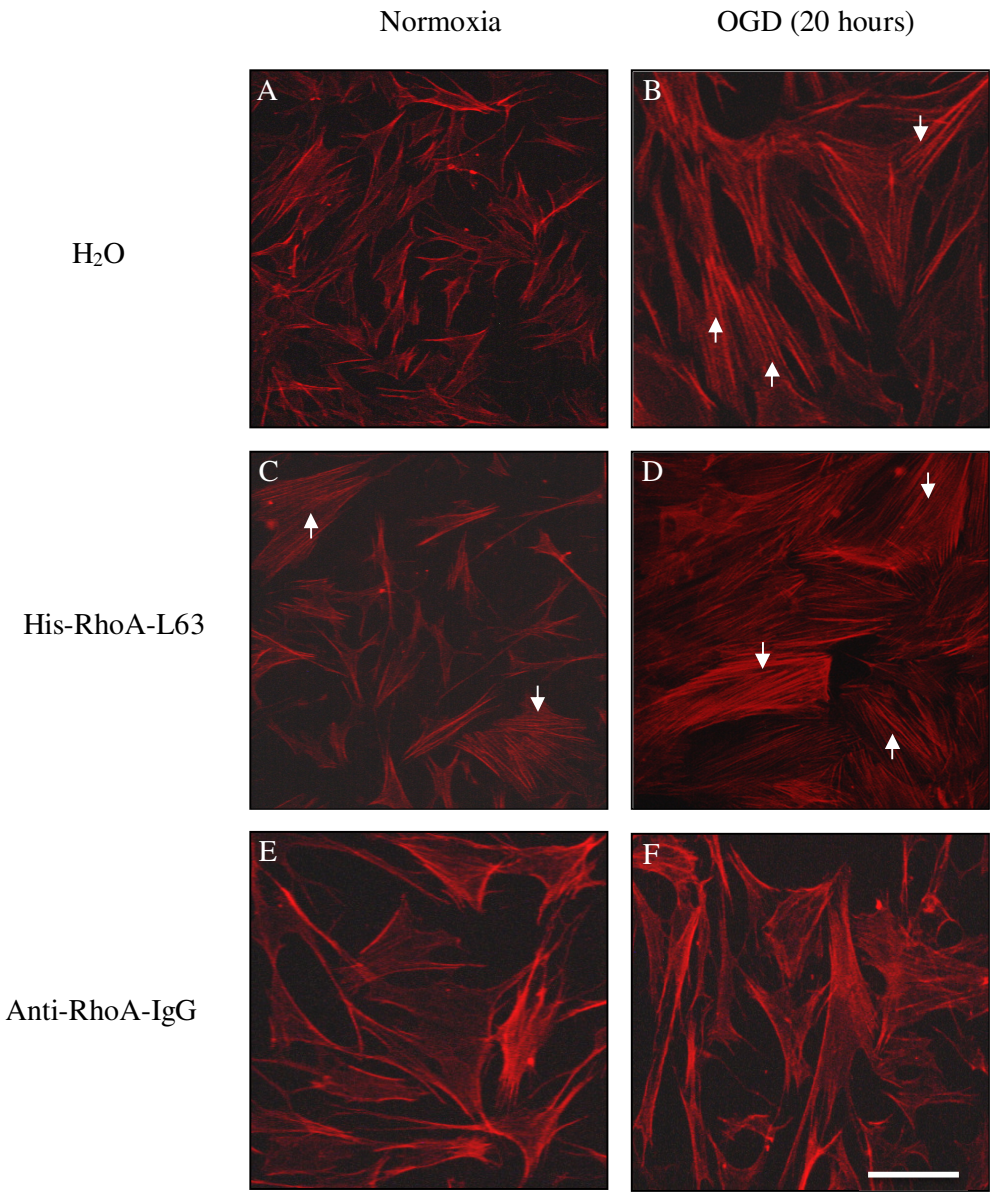

Figure 1.5. The F-actin stainings in HBMEC electroporated with H_2O **(A, B)**, His-RhoA-L63 **(C, D)**, and anti-RhoA IgG **(E, F)** before exposure to normoxia and OGD. Arrows indicate the stress fibres. The F-actin were detected by Rhodamine-labelled phalloidin dye by 40X magnification on fluorescent microscope. Bar scale: 50 µm.

1.2.5. Rho-kinase inhibition attenuate the cytoskeletal remodelling

Since the inhibition of Rho-kinase by Y-27632 abrogated RhoA-induced cerebral barrier, it was examined whether the cerebrovascular protective effects of Y-27632 may in part be attributed to the regulation of the RhoA/Rho-kinase-mediated cytoskeletal remodelling. As described earlier, the HBMEC cultured under normoxia displayed marginal actin staining, while OGD promoted the formation of thick bundles of stress fibres. Cotreatment of HBMEC during OGD with Y-27632 neutralised the effects of OGD on actin fibres and normalised the cellular morphology similar to those seen in normoxic HBMEC (Figure 1.6).

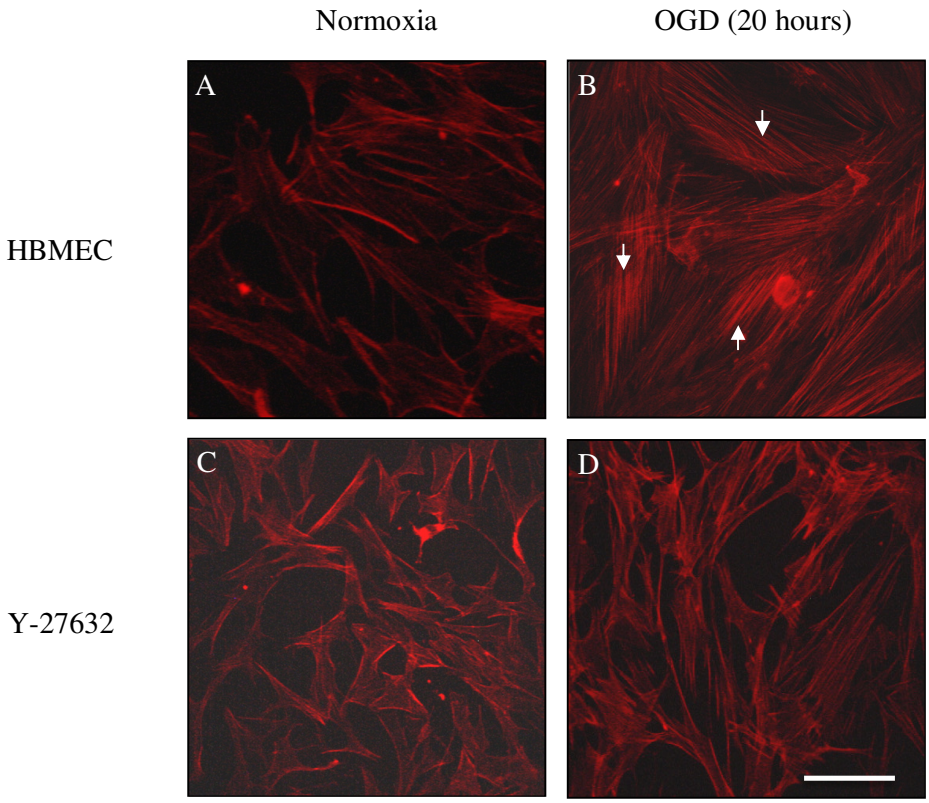

Figure 1.6. F-actin stainings with Rhodamine-labelled phalloidin dye in HBMEC exposed to normoxia **(A, C)** and OGD (20 hours) **(B, D)** in the absence and presence of Y-27632 (2.5 μM). Arrows represent the stress fibre formations. The F-actin stainings were observed by 40X magnification on a fluorescent microscope. Bar scale: 50 μm.

1.3. Discussion

Breakdown of the BBB, associated with formation of brain oedema, constitutes one of the leading causes of mortality after ischaemic strokes. Despite a consensus on endothelial cell dysfunction, the underlying mechanism(s) of this defect during ischaemic injury remains largely unknown (Hou and MacManus, 2002). Using an *in vitro* model of human cerebral barrier consisting of HBMEC and HA, the current study explored the involvement of RhoA in OGD-evoked barrier impairment and showed marked increase in intracellular levels of RhoA protein in OGD- versus normoxia-exposed HBMEC in consistence with our recent study (Allen et al., 2010). Similar increases in RhoA protein levels have previously been reported in stroke brain sections and in various cellular components of rodent cerebrovasculature after exposure to global ischaemia (Brabeck et al., 2003, Zhou et al., 2003). In the latter study, suppression of neuronal RhoA levels via hyperbaric oxygen confirms the ability of ischaemia to regulate GTPase expression (Zhou et al., 2003).

In previous *in vitro* studies, we have shown that OGD dramatically increases the activities of RhoA and Rho-kinase in HBMEC (Allen et al., 2010). Suppression of Rho-kinase activity in mice with fasudil or Y-27632, specific Rho-kinase inhibitors, before transient MCAO decreased infarct volume and kinase activity by ~50% and substantiated the relevance of Rho-kinase overactivity to ischaemic cerebral damage (Rikitake et al., 2005). As an inhibitor of Ca^{2+}-dependent protein kinases (PKC and PKA) and an intracellular Ca^{2+} antagonist, it is possible that fasudil may attenuate Ca^{2+}/calmodulin-dependent MLCK activity to reduce MLC phosphorylation and infarct volume. However, given the selection of relatively specific concentrations of fasudil for Rho-kinase, the protective effects observed are less likely to be due to inhibition of these secondary mechanisms (Rikitake et al., 2005). Other mechanisms

including vasodilation through activation of eNOS is more likely to contribute to beneficial effects of Rho-kinase inhibitors. Indeed, in $eNOS^{-/-}$ mice, Rho kinase inhibitors exerted no benefits on cerebral infarct size (Asano et al., 1989).

Several mechanisms including overt openings in paracellular pathways may compromise endothelial barrier function in the presence of OGD. TEER and NaF flux across HBMEC/HA cocultures were measured to assess the barrier function which showed OGD-evoked significant time-dependent decreases in TEER and increases in NaF flux thereby implying a physical breakdown and barrier impairments under OGD. To determine the actual relevance of RhoA to endothelial barrier integrity, HBMEC were transfected with anti-RhoA-IgG or constitutively active recombinant His-RhoA-L63 in that the former increased TEER and decreased paracellular permeability specifically in pathological conditions while the latter exerted the opposite effects. Taken together these findings verified the importance of RhoA in maintaining barrier integrity and showed a requirement for its adequate levels to preserve normal cellular activity (van Nieuw Amerongen et al., 2007). Attenuation of OGD-induced hyperpermeability by Y-27632 lent further support to the involvement of RhoA/Rho-kinase pathway in barrier disruption. Indeed, reduced tracer permeation in ischaemic brains and through endothelial monolayers have also been attributed to Rho-kinase inhibition (Takaishi et al., 1997).

The changes in cell morphology may also contribute to OGD-induced barrier failure. Experiments examining putative structural differences in microfilaments, a key component of cytoskeleton, (Davies et al., 2000) showed that HBMEC grown under normoxia possessed a marginal actin filament distribution while those exposed to OGD took up elongated and cuboidal appearance and developed stress fibres

traversing the cells. Transfection of HBMEC with His-RhoA-L63 or anti-RhoA-IgG induced thick stress fibre formation and preserved normal phenotype, respectively. Moreover, the inhibition of Rho-kinase activity also restored the cell morphology alongside reducing the stress fibres which was similar to the effects exhibited by RhoA inhibition. The cortical actin bands play a pivotal role in the prevention of paracellular flux by participating in formation and stabilisation of intercellular junctions. Once formed, stress fibres can generate a tensile centripetal force to pull junctional molecules inward to break up junctions and create intercellular gaps. Several mechanisms including activation of VEGF and transcriptional factors HIF-1 and NF-κB have been implicated in OGD-mediated junctional disruptions (van Bruggen et al., 1999, Frixione, 2000).

Enhanced phosphorylation of MLC triggered by RhoA/Rho kinase activity may also cause destabilisation of interendothelial cell junctions (Van Aelst and D'Souza-Schorey, 1997, Sahai and Marshall, 2002). Indeed, previous studies including our own have shown that while activation of RhoA in HBMEC via His-RhoA-L63 transfection increased MLC2 phosphorylations possibly through inhibition of myosin phosphatase or activation of MLCK, its inhibition via anti-RhoA-IgG dramatically decreased both phosphorylations (Tinsley et al., 2000, Mark and Davis, 2002, Allen et al., 2010). Given that activation of Rho kinase leads to phosphorylation of the ezrin-radixin-moesin proteins and these in turn provide a regulated linkage between membrane proteins and the cortical cytoskeleton, this mechanism warrants further investigation (Amano et al., 1996, van Bruggen et al., 1999).

To summarise, this study has shown that OGD compromises the structural and functional capacities of an *in vitro* model of human cerebral barrier through the

activation of RhoA/Rho-kinase pathway and consequent induction of the cytoskeletal remodelling.

Chapter 2

Mechanisms involved in Rho-kinase inhibition-dependent normalisation of cerebral barrier under OGD±R

2.1. Aims

1. To investigate whether Y-27632 treatment modulates the effects of OGD±R on pro-oxidant enzyme NADPH oxidase activity, total $O_2^{\bullet-}$ levels, and the protein levels of gp91-phox, antioxidant enzymes CuZn-SOD and catalase,

2. To investigate whether Y-27632 treatment nullifies the effects of OGD±R on the protein levels of RhoA, Rho-kinase-2 and activity of RhoA,

3. To investigate whether Y-27632 treatment restores the OGD±R-mediated modulation of junctional complex and protects the cerebral-barrier disruption.

2.2. Results

2.2.1. Effects of OGD±R in the absence or presence of Y-27632 on total $O_2^{\bullet-}$ levels and protein expressions and/or activity of pro-oxidant and antioxidant enzymes

Oxidative stress is an imbalance in the ROS metabolism caused by an aberration in the expression or activity of pro-oxidant and antioxidant enzymes resulting in an enhanced ROS production and accumulation. Hence, it was important to study the pro-oxidant and antioxidant parameters under same pathological condition to address the probable occurrence of an oxidative stress. Total proteins harvested from HBMEC exposed to OGD±R in the absence or presence of Y-27632 (10 μM) were used to detect the fold differences observed in the protein levels of gp91-phox, a membrane bound subunit of pro-oxidant NADPH oxidase, activity of NADPH oxidase enzyme, total $O_2^{\bullet-}$ levels and protein levels of antioxidant enzymes CuZn-SOD and catalase. Our results appeared to show a significant increase in the protein expression of gp91-phox under OGD±R compared to the HBMEC cultured under normoxia which served as controls, after normalisation against β-actin ($P<0.05$). However, the Y-27632 treatment neutralised the effects of OGD±R as the gp91-phox protein levels were normalised under OGD and significantly alleviated under OGD+R compared to the

controls ($P<0.05$). These results indicate that Y-27632 treatment neutralises the OGD±R-mediated elevation in gp91-phox protein levels (Figure 2.1A).

Since gp91-phox is pivotal for the NADPH oxidase enzyme activity, an increase in its protein expression may represent an increase in the activity of NADPH oxidase enzyme complex. Indeed, the exposure to OGD±R significantly increased the activities of NADPH oxidase enzyme compared to the enzyme activity measured in control HBMEC proteins ($P<0.05$). However, the Y-27632 treatment appeared to restore the OGD±R-mediated elevation in the NADPH oxidase enzyme activities (Figure 2.1B). Since NADPH oxidase enzyme complex is one of the main producers of $O_2^{\bullet-}$, an increase in its activity may increase an overall $O_2^{\bullet-}$ production. Indeed, the OGD±R significantly increased the total $O_2^{\bullet-}$ levels ($P<0.05$). However, Y-27632 treatment abolished the OGD±R-mediated elevation in the total $O_2^{\bullet-}$ levels and restored their levels similar to controls (Figure 2.1C). These data indicate that Rho-kinase activity may be involved in OGD±R-mediated upregulation in NADPH oxidase activity and $O_2^{\bullet-}$ production.

The protein levels of CuZn-SOD remained largely unchanged in HBMEC after OGD. However, a slight but insignificant reduction in its levels was observed after longer OGD+R compared to the controls. The Y-27632 treatment failed to alter the unchanged CuZn-SOD protein levels under OGD. However, its levels were significantly low under longer OGD+R ($P<0.05$) (Figure 2.2A). The protein levels of another antioxidant enzyme catalase were significantly higher in HBMEC subjected to OGD±R compared to the controls ($P<0.05$). However, the Y-27632 treatment abolished the OGD±R-mediated elevation in catalase protein levels and restored its levels similar to the controls. This result indicates that Rho-kinase activity may be

involved in upregulating the catalase protein expression as Y-27632 treated controls showed a significantly low catalase protein levels ($P<0.05$) (Figure 2.2B).

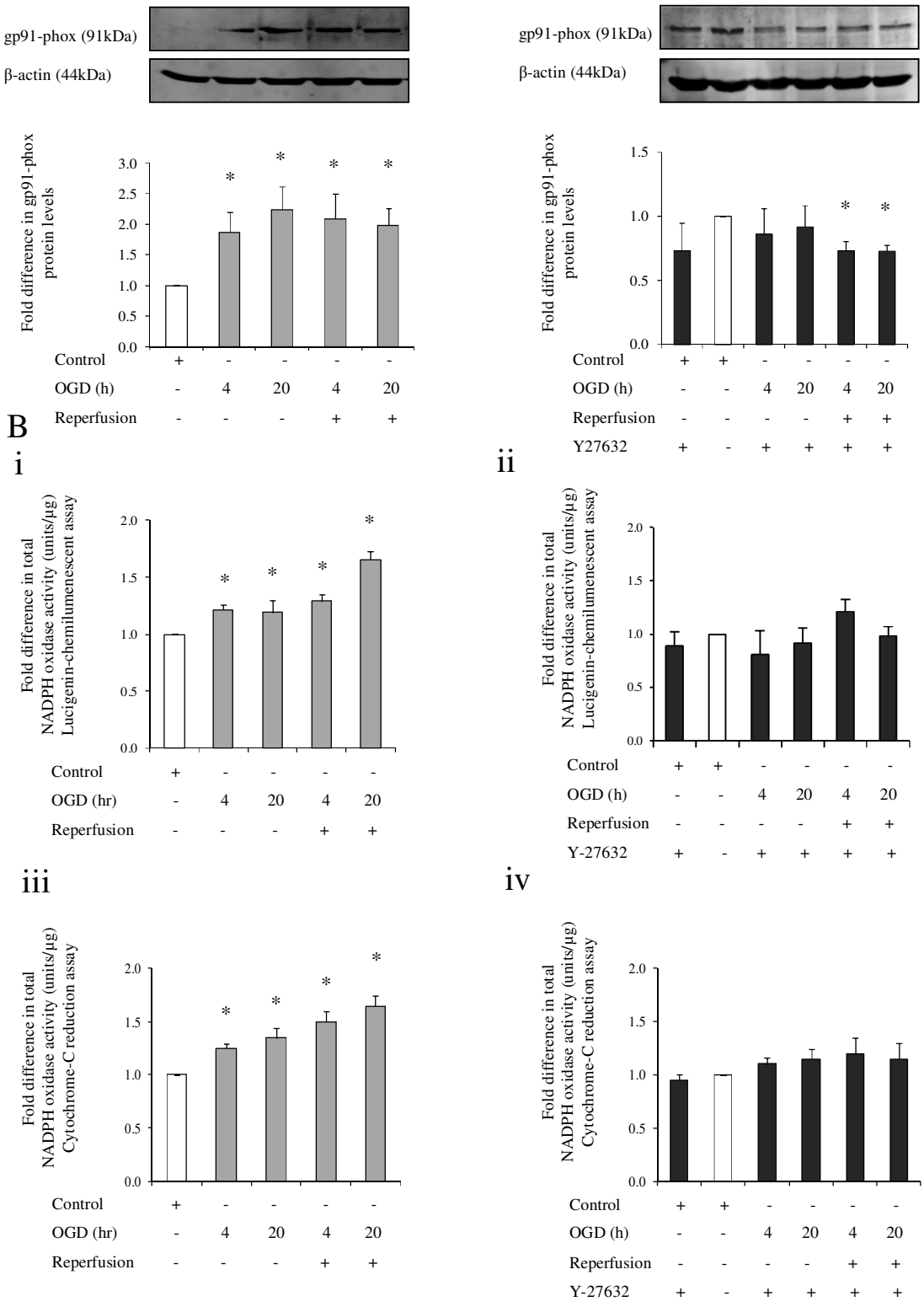
A
i
gp91-phox (91kDa)
β-actin (44kDa)
Fold difference in gp91-phox protein levels
Control + - - - -
OGD (h) - 4 20 4 20
Reperfusion - - - + +
ii
gp91-phox (91kDa)
β-actin (44kDa)
Fold difference in gp91-phox protein levels
Control + + - - - -
OGD (h) - - 4 20 4 20
Reperfusion - - - - + +
Y27632 + - + + + +
B
i
Fold difference in total NADPH oxidase activity (units/µg) Lucigenin-chemilumenescent assay
Control + - - - -
OGD (hr) - 4 20 4 20
Reperfusion - - - + +
ii
Fold difference in total NADPH oxidase activity (units/µg) Lucigenin-chemilumenescent assay
Control + + - - - -
OGD (h) - - 4 20 4 20
Reperfusion - - - - + +
Y-27632 + - + + + +
iii
Fold difference in total NADPH oxidase activity (units/µg) Cytochrome-C reduction assay
Control + - - - -
OGD (hr) - 4 20 4 20
Reperfusion - - - + +
iv
Fold difference in total NADPH oxidase activity (units/µg) Cytochrome-C reduction assay
Control + + - - - -
OGD (h) - - 4 20 4 20
Reperfusion - - - - + +
Y-27632 + - + + + +

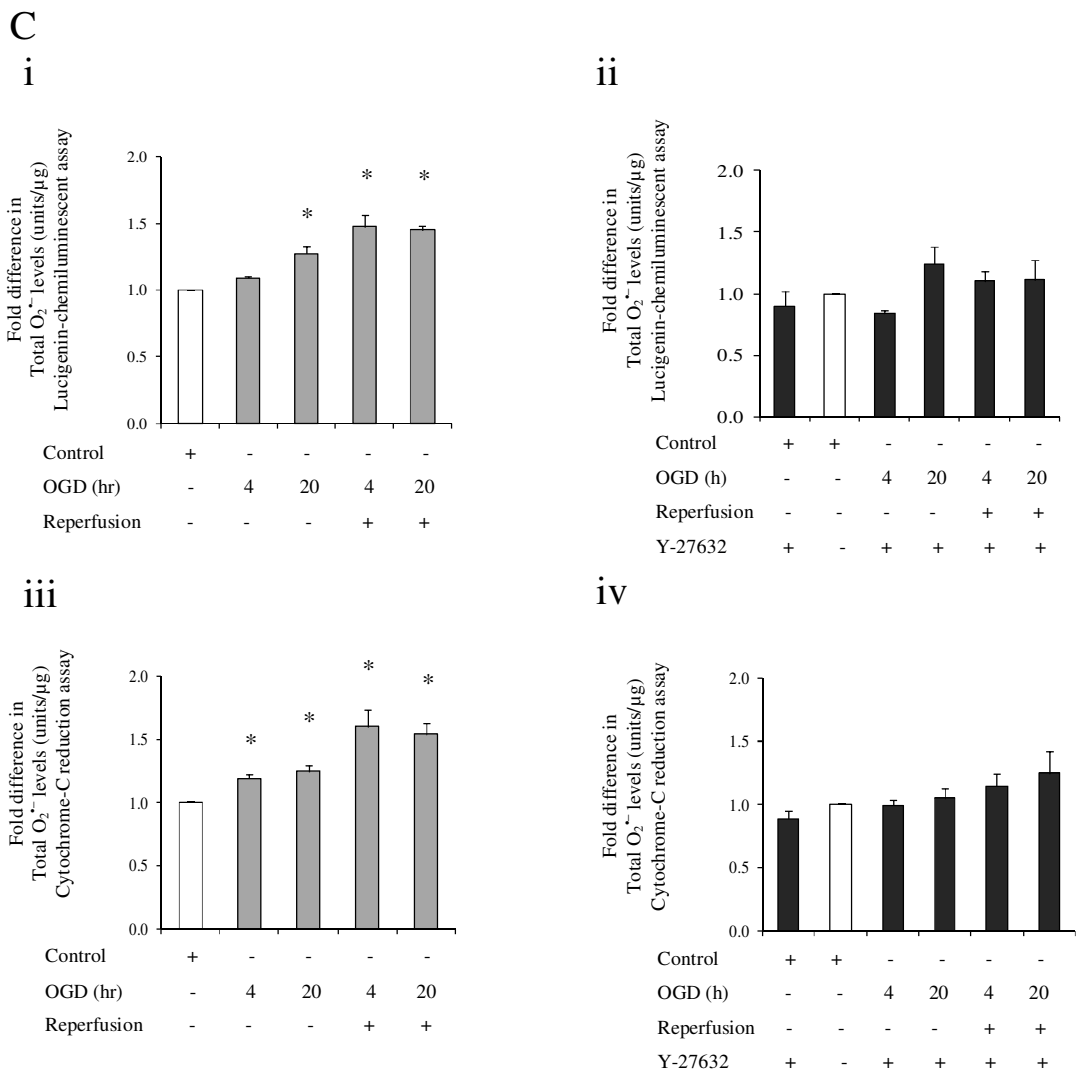

Figure 2.1. (A) Protein levels of gp91-phox, **(B)** NADPH oxidase enzyme activity (units/µg) and **(C)** total superoxide anion levels (units/µg) in HBMEC after OGD±R in the absence or presence of Y-27632 (10 µM). Data are expressed as mean±SEM from 6 different experiments. Statistical analysis was done using ANOVA with Dunnet's *post hoc* test for multiple comparisons (Ai: P=0.022, F=3.937, df1=4, df2=15; Aii: P=0.046, F=3.193, df1=5, df2=12), (Bi: P=0.0015, F=10.21, df1=4, df2=10; Bii: P=0.378, F=1.169, df1=5, df2=12; Biii: P=0.0029, F=8.504, df1=4, df2=10; Biv: P=0.4634, F=0.9898, df1=5, df2=12), (Ci: P=0.0072, F=6.609, df1=4,

df2=10; Cii: P=0.1437, F=2.046, df1=5, df2=12; Ciii: P=0.0038, F=7.946, df1=4, df2=10; Civ: P=0.0700, F=2.753, df1=5, df2=12). *P<0.05 compared to the controls.

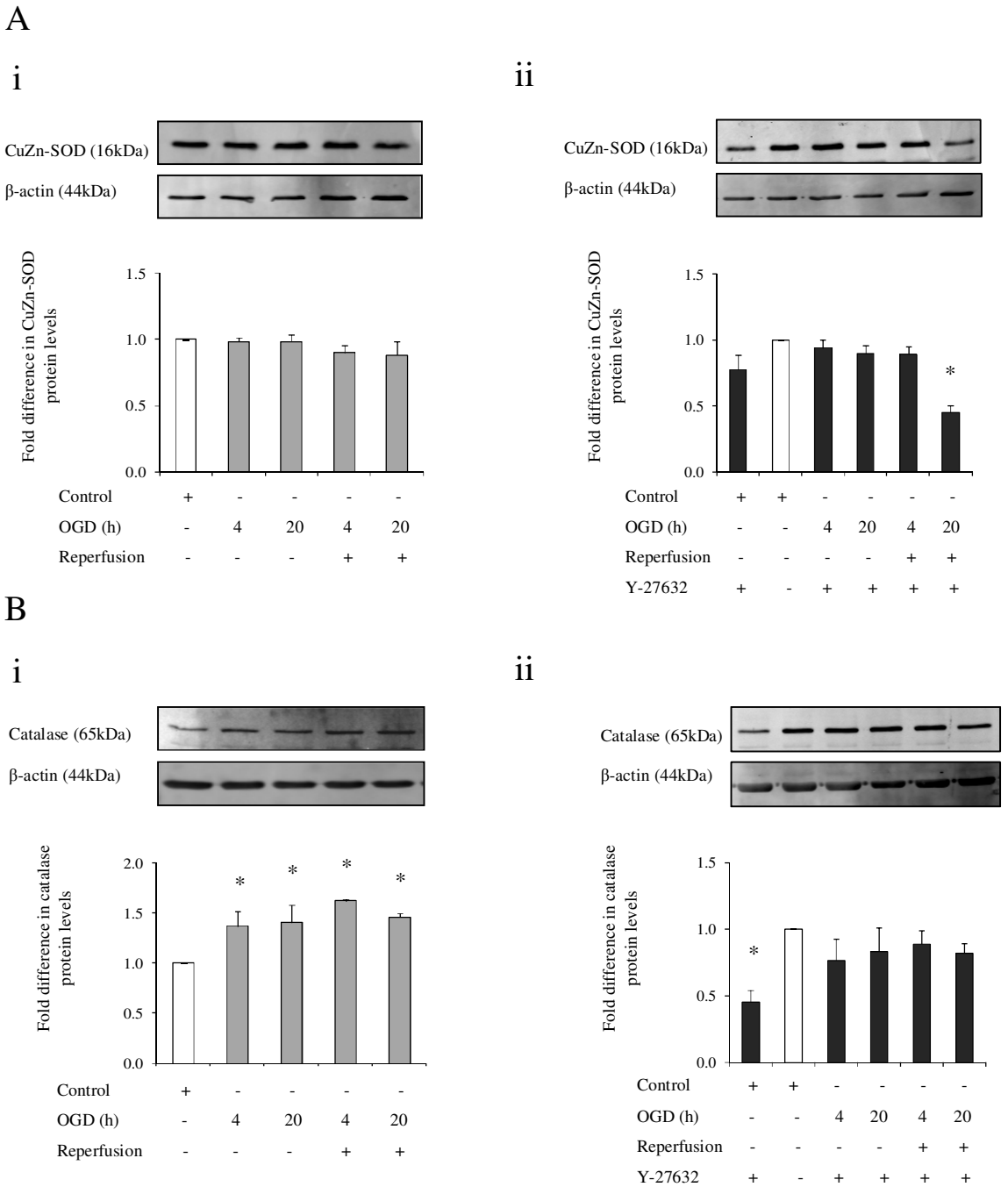

Figure 2.2. Protein levels of **(A)** CuZn-SOD and **(B)** catalase in HBMEC after OGD±R in the absence or presence of Y-27632 (10 μM). Data are expressed as mean±SEM from 3 different experiments. Statistical analysis was done using ANOVA with Dunnet's *post hoc* test for multiple comparisons (Ai: P=0.80, F=0.4022, df1=4, df2=10; Aii: P=0.0011, F=8.711, df1=5, df2=12), (Bi: P=0.006, F=6.842, df1=4, df2=10; Bii: P=0.063, F=2.849, df1=5, df2=12). *P<0.05 compared to the controls.

2.2.2. Effects of OGD±R in the absence or presence of Y-27632 on RhoA, Rho-kinase-2 protein expressions and RhoA activity

HBMEC subjected to OGD±R showed no significant alteration in the total RhoA protein levels. However, their protein levels dramatically decreased after Y-27632 treatment during OGD±R and in Y-27632 treated controls compared to the untreated controls (P<0.05) (Figure 2.3A). Since RhoA-GTP levels represent active RhoA isoform, the RhoA activity was measured after normalising RhoA-GTP protein levels against unchanged total RhoA protein levels in HBMEC. A marked increase in the RhoA activity was recorded in HBMEC subjected to OGD±R (P<0.05). Since Y-27632 treatment attenuated the total RhoA protein levels, the RhoA activity was measured by normalising RhoA-GTP levels with loading control β-actin in Y-27632 treated HBMEC. The Y-27632 treatment abrogated the OGD±R-mediated increase in the RhoA activity and normalised the RhoA-GTP levels similar to the controls. In addition, the Rho-kinase inhibitor treatment significantly attenuated the RhoA activity in HBMEC exposed to short OGD+R (P<0.05) (Figure 2.3A). These data indicate that inhibition of Rho-kinase activity may modulate RhoA protein expression as well as activity.

Since Rho-kinase is the main effector protein of RhoA, the OGD±R-mediated alterations in RhoA expression or activity may induce alterations in Rho-kinase protein levels. Our results show no significant difference in the Rho-kinase-2 protein levels under OGD. However, OGD+R induced an increase in the Rho-kinase-2 levels which were significantly higher only after longer OGD+R compared to the controls ($P<0.05$). In addition, the Y-27632 treatment had no effect on the Rho-kinase-2 protein levels under OGD, but it abolished the OGD+R-mediated elevation and normalised Rho-kinase-2 levels similar to the controls (Figure 2.3B). These results indicate that Y-27632 can regulate the expression of Rho-kinase.

A

i

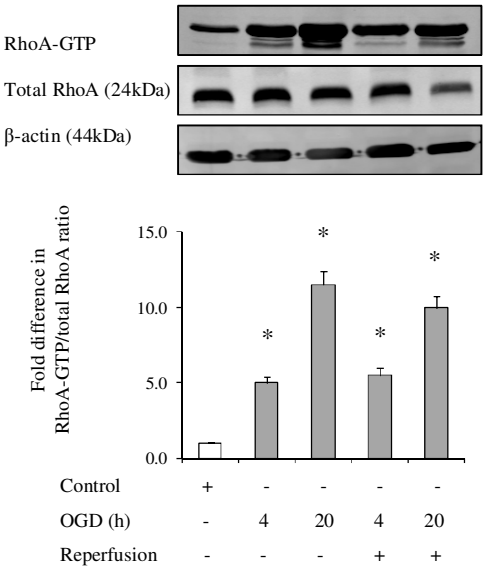

ii

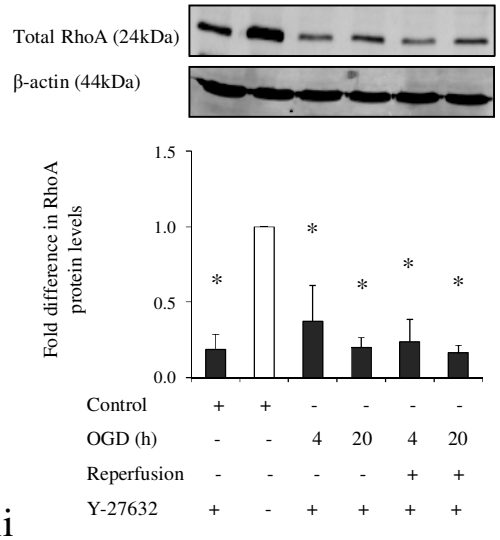

iii

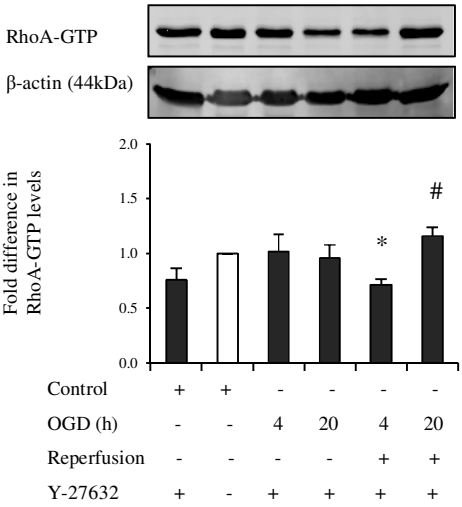

B

i

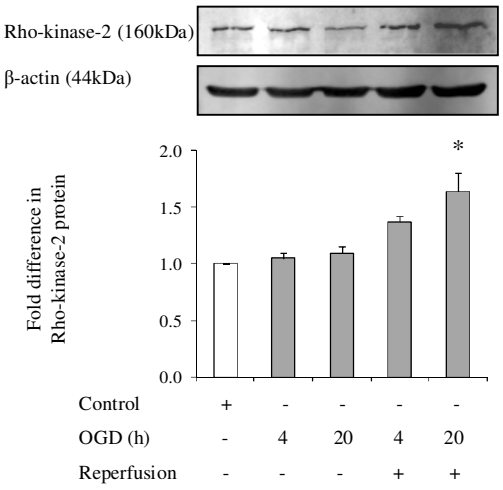

ii

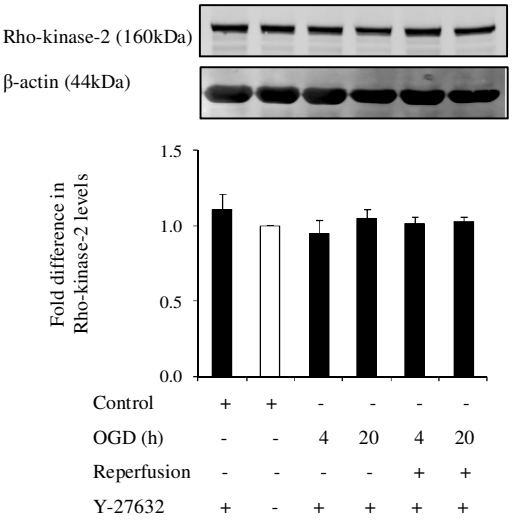

Figure 2.3. (A) Protein expression and activity of RhoA and **(B)** protein levels of Rho-kinase-2 in HBMEC after OGD±R in the absence or presence of Y-27632 (10 μM). Data are expressed as mean±SEM from 4 different experiments. Statistical analysis was done using ANOVA with Dunnet's *post hoc* test for multiple comparisons (Ai: P=0.0001, F=34.4, df1=4, df2=10; Aii: P=0.0045, F=6.234, df1=5, df2=12; Aiii: P=0.0173, F=4.341, df1=5, df2=12), (Bi: P=0.0018, F=9.765, df1=4, df2=10; Bii: P=0.707, F=0.5916, df1=5, df2=12). *P<0.05 compared to the controls, $^{\#}$P<0.05 compared to the OGD (4hr)+R.

2.2.3. Effects of OGD±R in the absence or presence of Y-27632 on junctional complex and cerebral-barrier integrity

Since tight junction and adherens junction proteins seal the adjacent endothelial cells making the cerebral barrier impermeable to the blood driven solutes, the effects of OGD±R in the presence or absence of Y-27632 were studied on the expressions of tight junction proteins occludin and claudin-5, adherens junction protein β-catenin and focal adhesion protein vinculin. OGD±R did not significantly affect the occludin protein expression in HBMEC compared to the control cells cultured under normoxic conditions. However, the Y-27632 treatment during OGD±R and normoxia significantly increased the occludin protein levels compared to the levels in untreated control cells (P<0.05) (Figure 2.4A). In addition, OGD increased the claudin-5 protein levels in a time-dependent manner which appeared to be significantly elevated after longer periods of OGD and OGD+R (P<0.05). In contrast, the Y-27632 treatment neutralised the OGD±R-mediated elevation in the claudin-5 protein levels and restored its levels similar to the control cells (Figure 2.4B). These results indicate that OGD±R can modulate the tight junction protein expression via Rho-kinase activity.

The protein levels of β-catenin did not appear to significantly alter in HBMEC subjected to OGD. However, a marked rise in the β-catenin protein levels was observed after OGD+R compared to the control cells ($P<0.05$). Moreover, the Y-27632 treatment did not alter the β-catenin levels under OGD, but it attenuated its levels after OGD+R and normalised it to the levels observed in control cells (Figure 2.5A). The vinculin protein levels appeared to remain unchanged after OGD±R in the absence or presence of Y-27632 and indicate that OGD±R may not affect the levels of focal adhesion protein (Figure 2.5B).

To study the significance of OGD±R mediated modulation of aforementioned proteins on the BBB, the integrity and function of the *in vitro* model of human BBB were measured by TEER and flux of EBA, respectively. OGD decreased the TEER readings in a time-dependent manner compared to the cocultures exposed to normoxia which served as controls, indicating the physical breakdown of the endothelial barrier ($P<0.05$). Reperfusion after OGD further diminished the coculture integrity ($P<0.05$). These findings were further confirmed by dramatic increases in the flux of EBA across the cocultures compared to the controls ($P<0.05$). These data demonstrate that OGD±R can compromise the cerebral-barrier integrity (Figure 2.6A).

Treatment with Y-27632 improved the TEER readings after short OGD±R. These results were substantiated by concurrent decreases in the flux of EBA across the cocultures which appeared to be similar to flux measured across the cocultures exposed to normoxia in the absence or presence of Y-27632. However, Y-27632 had no affect on the barrier integrity after longer OGD±R as dramatic decrease in TEER readings and concomitant increases in the flux of EBA were recorded across the cocultures compared to the respective measurements across the cocultures exposed to

normoxia and short OGD±R (P<0.05) (Figure 2.6B). These results indicate that Y-27632 is cerebral-barrier protective under short OGD±R.

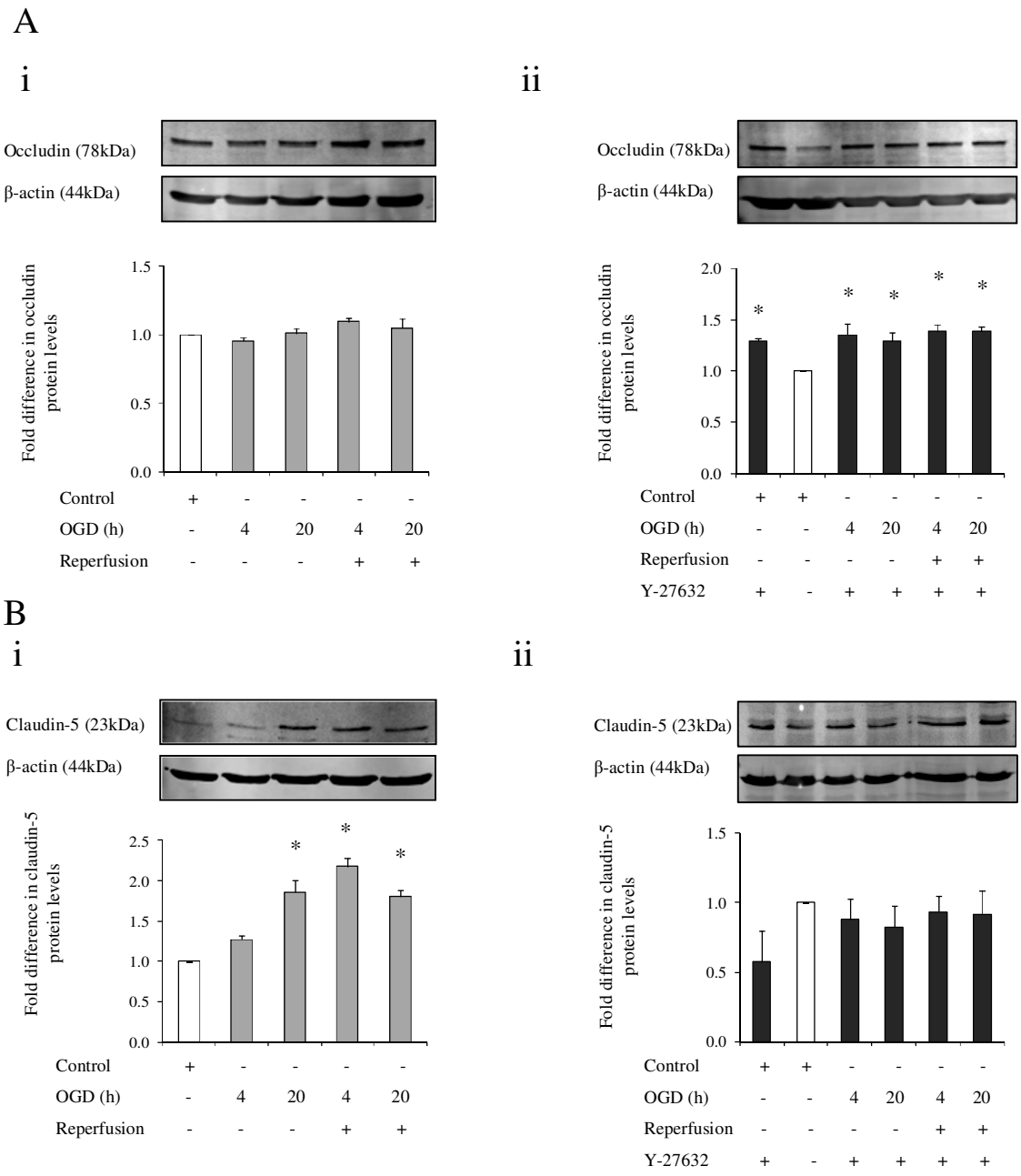

Figure 2.4. Protein expressions of **(A)** occludin and **(B)** claudin-5 in HBMEC after OGD±R in the absence or presence of Y-27632 (10 μM). Data are expressed as mean±SEM from 3 different experiments. Statistical analysis was done using

ANOVA with Dunnet's *post hoc* test for multiple comparisons (Ai: P=0.1448, F=2.18, df1=4, df2=10; Aii: P=0.0105, F=4.992, df1=5, df2=12), (Bi: P<0.0001, F=23.07, df1=4, df2=10; Bii: P=0.7944, F=0.4661, df1=5, df2=12). *P<0.05 compared to the controls, $^{\#}$P<0.05 compared to the OGD (4hr)+R.

A

i

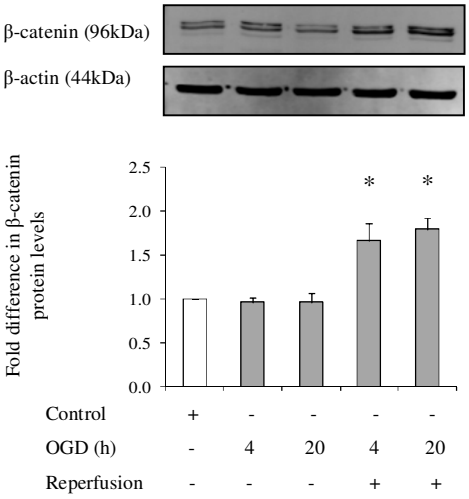

ii

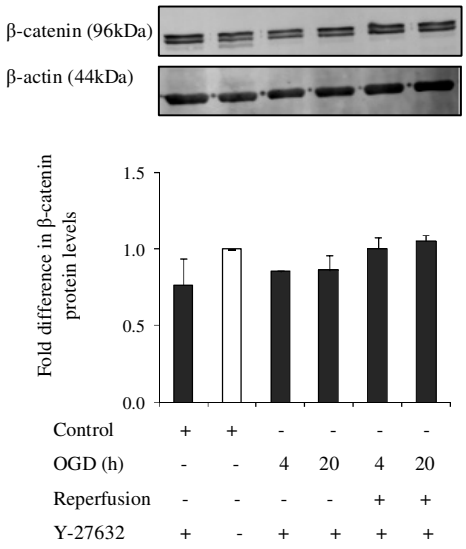

B

i

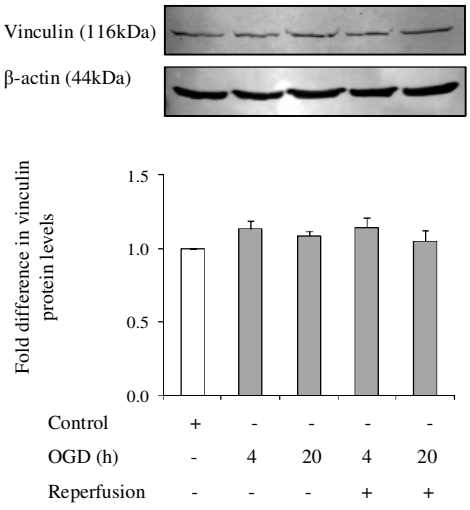

ii

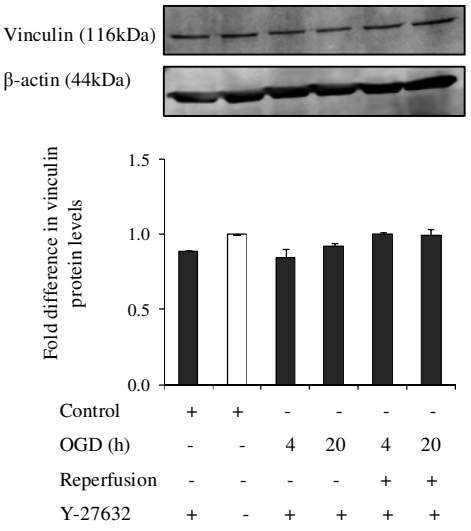

Figure 2.5. Protein expressions of **(A)** β-catenin and **(B)** vinculin in HBMEC after OGD±R in the absence or presence of Y-27632 (10 μM). Data are expressed as mean±SEM from 3 different experiments. Statistical analysis was done using ANOVA with Dunnet's *post hoc* test for multiple comparisons (Ai: P=0.0007, F=12.42, df1=4, df2=10; Aii: P=0.1936, F=1.770, df1=5, df2=12), (Bi: P=0.3645, F=1.213, df1=4, df2=10; Bii: P=0.0404, F=3.338, df1=5, df2=12). *P<0.05 compared to the controls.

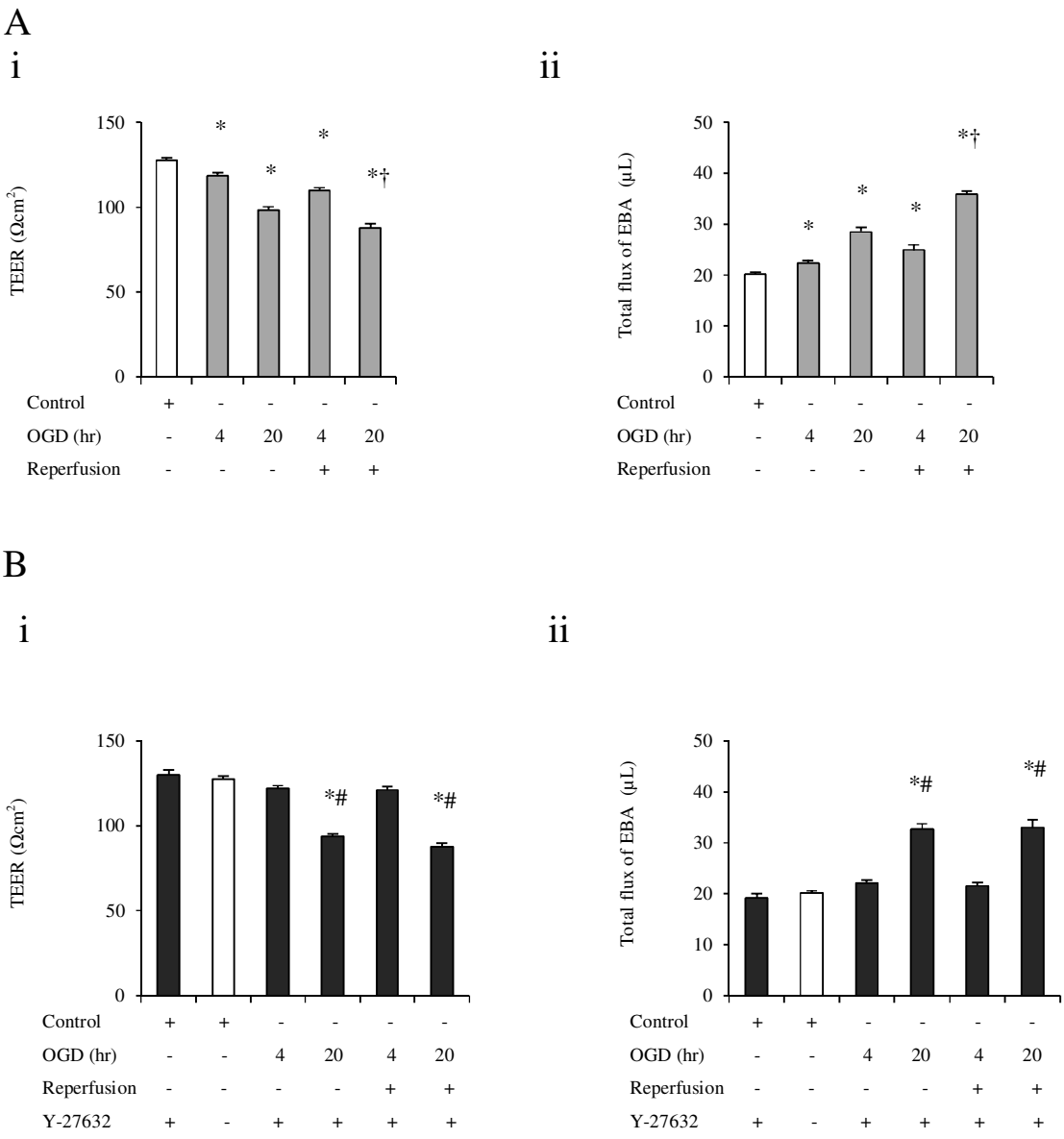

Figure 2.6. Measurement of cerebral-barrier integrity by TEER readings (Ωcm^2), and flux of EBA (μL) across an *in vitro* model of human BBB after OGD±R in the **(A)** absence or **(B)** presence of Y-27632. Data are expressed as mean±SEM from 4 different experiments. Statistical analysis was done using ANOVA with Dunnet's *post hoc* test for multiple comparisons (Ai: $P<0.0001$, $F=65.645$, $df1=4$, $df2=10$; Aii: $P<0.0001$, $F=173.5$, $df1=4$, $df2=10$), (Bi: $P<0.0001$, $F=88.892$, $df1=5$, $df2=12$; Bii: $P<0.0001$, $F=53.853$, $df1=5$, $df2=12$). $^{*}P<0.05$ compared to the controls, $^{\dagger}P<0.05$ compared to longer OGD, $^{\#}P<0.05$ compared to short OGD±R.

2.3. Discussion

The main findings of this study were that in HBMEC, OGD±R accounted for the enhanced activity of pro-oxidant enzyme NADPH oxidase and consequent generation of $O_2^{\bullet-}$, a marker of oxidative stress. OGD±R also upregulated the RhoA activity, and protein expressions of Rho-kinase-2 and antioxidant enzyme catalase. In addition, OGD also altered the endothelial-barrier integrity preserved by tightly sealed HBMEC by modulating the expressions of tight junction protein claudin-5 and adherens junction protein β-catenin. Taken together, these events may in part be responsible for the OGD±R-mediated disruption of the endothelial barrier associated with BBB hyperpermeability. Cotreatment with Y-27632 reversed the OGD±R-mediated affects marked by the normalisation of gp91-phox, catalase, caludin-5, β-catenin and Rho-kinase-2 protein levels, NADPH oxidase and RhoA activities, and total $O_2^{\bullet-}$ levels. Moreover, the Y-27632 treatment in part proved to be cerebral barrier protective by attenuating BBB hyperpermeability under short OGD±R.

During physiological conditions, low levels of ROS are known to act as secondary messengers in maintaining the cellular homeostasis. However, under pathological condition, many ROS generating enzyme complexes including xanthine oxidase, COX, mitochondrial electron transport chain, NOS and NADPH oxidase are activated and generate ROS in abundance leading to oxidative stress. Among these enzyme complexes, NADPH oxidase has attracted much of the attention mainly due to its role in generating $O_2^{\bullet-}$, the foundation molecule of all ROS. Previous studies in our group have shown that HBMEC express p22-phox protein which is a pivotal subunit of NADPH oxidase enzyme complex and enhances the enzyme activity and the $O_2^{\bullet-}$ production under hyperglycaemia (Allen and Bayraktutan, 2009a). In this study we have shown that HBMEC express gp91-phox protein which is also important for the NADPH oxidase enzyme activity and OGD±R enhances its expression which correlates with increases in the NADPH oxidase activity. Since NADPH oxidase activity was measured in the presence of inhibitors for other ROS generating enzymes, it is safe to suggest that NADPH oxidase plays a big role during OGD±R injury. Previous studies also support this rationale and associate the vascular $O_2^{\bullet-}$ produced by NADPH oxidase with the endothelial dysfunction. Moreover, it has been shown that inhibition of NADPH oxidase by apocynin reduces the infarction in animal model of ischaemic stroke (Guzik et al., 2000, Kahles et al., 2007).

Previous research in our group had shown that RhoA and subsequent Rho-kinase activations modulate cytoskeletal-remodelling and impair the coculture integrity under OGD conditions. We had shown that low concentration of Y-27632 (2.5 μM) was ineffective in improving the coculture integrity under OGD±R (Allen et al., 2010). Therefore in this study, the HBMEC were exposed to higher dose of Y-27632 (10 μM) where the cell death was found to be negligible, thus eliminating the cellular

toxicity that may be induced by high dose of Y-27632. Our Y-27632 dosage selection is consistent with the results from a recent study, which demonstrates 10 µM to be the optimal concentration for Y-27632 to exhibit the barrier protective effects on rat BMEC (Ma et al., 2012). To monitor the prophylactic and therapeutic effects of Rho-kinase inhibition, HBMEC were treated with Y-27632 during exposures to different periods of OGD alone and during reperfusion following OGD, respectively. The Y-27632 treatment normalised the gp91-phox protein levels in HBMEC exposed to OGD. However, pronounced decreases in its levels were recorded under short and long OGD±R. The gp91-phox data was substantiated by NADPH oxidase activity, which showed basal NADPH oxidase activities under the influence of Y-27632 during OGD±R and were similar to control HBMEC cultured under normoxia. These data demonstrate the antioxidant properties of Y-27632 and emphasise the Rho-kinase-mediated increase in the expression and activity of the NADPH oxidase enzyme complex. Indeed, a previous study on rat neonatal cardiac myocytes have shown that activated Rho-kinase mediates angiotensin II-induced Rac1 activation and concomitant Rac1-dependent ROS production by NADPH oxidase enzyme activation (Nishida et al., 2005). Our data go hand in hand with the results from study with Dahl salt-sensitive hypertensive rats, which showed that Y-27632 treatment inhibited the increased expression of NADPH oxidase subunits (p22-phox, p47-phox and gp91-phox) in heart tissues from the left ventricle hypertrophy stage and exhibited the cardioprotective mechanisms of Rho-kinase inhibition by suppression of oxidative-stress mediated vascular lesion formations which included medial thickness and perivascular fibrosis (Mita et al., 2005). Recent studies with rat model of angiotensin II-induced cardiovascular hypertrophy, Dahl salt-sensitive hypertensive rats and rat model of liver transplantation with IR injury have demonstrated the dramatic

increases in the vascular NADPH oxidase expressions and endothelial $O_2^{\bullet-}$ production, which were significantly supressed by another Rho-kinase inhibitor, fasudil, and further exhibit the cardioprotective and hepatoprotective effects of Rho-kinase inhibition (Higashi et al., 2003, Shiotani et al., 2004, Takeshima et al., 2012). In support of these studies, the total $O_2^{\bullet-}$ levels measured in HBMEC exposed to OGD±R with Y-27632 treatment also showed basal levels of $O_2^{\bullet-}$ which were similar to the controls and suggest that the Rho-kinase inhibition attenuates NADPH oxidase-derived $O_2^{\bullet-}$ as well as it may also supress other $O_2^{\bullet-}$ generating enzymatic complexes like lipooxygenase-1 and COX-2 (Schmeck et al., 2003, Mita et al., 2005).

Since impaired cellular antioxidant mechanisms may also account for the oxidative stress, it was important to delineate the OGD±R-mediated modulation of antioxidant enzymes CuZn-SOD and catalase in HBMEC. Previous studies have shown that the levels of CuZn-SOD can dictate the extent of an NADPH oxidase-induced oxidative stress in murine coronary arteries subjected to hypoxia-reoxygenation. Indeed, transgenic mice overexpressing human CuZn-SOD reduced NADPH oxidase-derived $O_2^{\bullet-}$ levels along with completely blocking the coronary vasoconstriction (Liu et al., 2004). Hence, the protein level of CuZn-SOD was explored in HBMEC that revealed no change or insignificant reduction under OGD±R. These results were consistent with studies on bovine pulmonary microvascular endothelial cells, which showed a two-fold increase in the $O_2^{\bullet-}$ production along with unchanged CuZn-SOD levels after hypoxia-reoxygenation. However, only after treatment with CuZn-SOD (100 units/mL) during hypoxia prevented the $O_2^{\bullet-}$ generation and attenuated the hyperpermeability (Lum et al., 1992). Since in our experiment the OGD±R resulted in hyperpermeability, the existing CuZn-SOD protein levels may not be sufficient to dismutate the excessive $O_2^{\bullet-}$ generated. Studies on rats with transient focal cerebral

ischaemia followed by reperfusion have also shown a reduced CuZn-SOD immunoreactivity in the ipsilateral striatum along with a reduced antioxidant activity of total SOD and CuZn-SOD in plasma and blood cells reiterating a weak dismutase activity (Matsuda et al., 2009, Kravcukova et al., 2010). The Y-27632 treatment during OGD and short OGD+R had no significant effect on the CuZn-SOD protein levels. However, a significant reduction in its protein level was recorded under long OGD+R. These data indicate the inability of Rho-kinase inhibition to alter CuZn-SOD protein levels, but it may modulate the antioxidant enzyme activity. Indeed, studies with rat model of intestinal IR support this hypothesis, as fasudil hydrochloride, a derivative of fasudil, significantly increased the IR-attenuated SOD antioxidant activity. Similarly in rat MCAO model of focal cerebral IR, the presence of fasudil mesylate, a derivative of fasudil, has been recently shown to increase the SOD activity by 50% in ischaemic cortex and by 58% in ischaemic hippocampus regions of the brain alongside improving the neurological deficits and reduction in cerebral infarct volume (Huang et al., 2008, Li et al., 2009, Li et al., 2011b). Further studies are required to measure the CuZn-SOD activity in HBMEC.

The dismutation of $O_2^{\bullet-}$ by CuZn-SOD and Mn-SOD results in the production of H_2O_2 in cytoplasm and mitochondria, respectively (Gao et al., 2009). However, under physiological state the H_2O_2 accumulation is averted by another antioxidant enzyme catalase, which breaks down H_2O_2 into H_2O. Previous studies in our group have shown that HBMEC express functionally active catalase (Allen and Bayraktutan, 2009a). In this study we have found that the protein levels of catalase increase in HBMEC after OGD±R. The increase in catalase protein levels may be in response to an increased intracellular H_2O_2 levels. Indeed, study with bovine aortic endothelial cells has shown that an increase in the intracellular $O_2^{\bullet-}$ levels leads to elevations in

intracellular H_2O_2 levels (Quijano et al., 2007). In addition, studies with rat skeletal muscle IR injury model support this hypothesis as an elevated tissue catalase activity was observed in this group compared with the sham group (Ozkan et al., 2012). However, recent studies with rat MCAO model of focal cerebral ischaemia have shown a significant reduction in the catalase activity in the brain cortex compared with that of the sham group (Liu et al., 2012). Since in our experiments, the OGD±R increased the BBB permeability, the increased catalase levels may not be sufficient to attenuate the H_2O_2 accumulation. Indeed, recent study on the mitochondrial oxidative stress demonstrated the inability of overexpressed catalase in alleviating the oxidative stress-induced cell death triggered after IR injury (Loor et al., 2011). Moreover, external supplementation with only high dose of catalase (1000 units/mL), which may be beyond physiological levels, have been previously shown to inhibit the reoxygenation-induced hyperpermeability in bovine pulmonary microvascular endothelial cells after hypoxic exposures, further suggesting the importance of H_2O_2 in mediating the response (Lum et al., 1992). As stated earlier, the intracellular levels of H_2O_2 are dependent on the intracellular levels of $O_2^{\bullet-}$. Hence, the Y-27632-mediated normalisation of $O_2^{\bullet-}$ levels may also reduce the H_2O_2 levels and subsequent catalase protein expression or activity. Our data is supportive of this notion as the Y-27632 treatment normalised the catalase protein levels in HBMEC exposed to OGD±R. Thus, treatment with Y-27632 has been shown to regulate the ROS metabolism in HBMEC by limiting elementary ROS i.e. $O_2^{\bullet-}$ production and modulate HBMEC to adjust the cellular antioxidant machinery to maintain cellular homeostasis. Indeed, studies on porcine brain capillary endothelial cells supports our rationale, as Y-27632 treatment completely prevented H_2O_2 (100 μM)-induced actin polymerisation and monolayer permeability (Kahles et al., 2007).

In our previous study, we found that RhoA and its downstream effector Rho-kinase are expressed in HBMEC (Allen et al., 2010). In this study we have observed that the total RhoA levels measured in HBMEC homogenates remained mostly unchanged after OGD±R. However, the relative RhoA activities, measured by RhoA-GTP/total RhoA ratio, were significantly elevated during OGD±R. Our results are consistent with previous studies with human pulmonary artery endothelial cells, human pulmonary artery smooth muscle cells and porcine pulmonary artery smooth muscle cells where RhoA activity appeared to be upregulated in a time-dependent manner under hypoxia (Bailly et al., 2004, Wojciak-Stothard et al., 2012). SinceY-27632 inhibits Rho-kinase activity; we examined its possible role in modulating the RhoA expression and activity to demonstrate the Y-27632 inhibitory effects are not limited to Rho-kinase per se, but might also affect RhoA. Our data show a dramatic reduction in the total RhoA protein levels in HBMEC under Y-27632 treatment during OGD±R. Studies with rat model of diabetes mellitus and Dahl salt-sensitive hypertensive rats are in agreement with our findings and also demonstrate the Y-27632-mediated reduction in RhoA protein expression in heart tissues (Mita et al., 2005, Soliman et al., 2012). In addition, our study has also shown that Y-27632 alleviates the RhoA activity marked by normalised RhoA-GTP levels in HBMEC exposed to OGD±R, which is also consistent with a previous *in vitro* study on mouse BMEC (Stamatovic et al., 2003). Taken together, Y-27632 also appears to regulate the Rho-kinase activity by modulating the expression and activity of RhoA.

Earlier we had shown that RhoA overactivity and subsequent Rho-kinase activation are associated with the stress-fibre formations in HBMEC resulting in increased actin filament contractility and impaired endothelial-barrier function (Allen et al., 2010). Since Rho-kinase-2 is highly expressed in heart and brain tissues, we

investigative the levels of this particular isoform in HBMEC exposed to OGD±R and showed selective increases only in OGD+R groups. However, the unchanged protein levels in OGD may not be representative of level of change in the activity. Indeed, recent studies confirm increased Rho-kinase activities measured by elevated adducin and MYPT phosphorylations, substrates of Rho-kinase, in endothelial cells from ischaemic lesions after focal cerebral ischaemia in rat and mice, respectively. Moreover, the increased Rho-kinase activity was associated with infarct expansion and neurological deficits in these rodents (Rikitake et al., 2005, Yagita et al., 2007). The Y-27632 treatment normalised the OGD+R-mediated increase in Rho-kinase-2 protein levels without altering those in the OGD groups. These data are in partial agreement with previous *in vivo* studies where Rho-kinase inhibition by Y-27632 and fasudil have been shown to supress the Rho-kinase gene expression and activation, which resulted in the inhibition of infarct expansion and subsequently improved the neurological deficits (Mita et al., 2005, Yagita et al., 2007). These results suggest that Y-27632 is a potent inhibitor of RhoA/Rho-kinase signalling pathway.

The vasogenic oedema emerging from the disruption of the BBB represents one of the most severe outcomes of ischaemic stroke. Since the tight junction proteins and adherens junction proteins tightly seal the adjacent endothelial cells to restrict the paracellular permeability, it is possible that the disruption of the BBB may reflect the ischaemia-mediated modulation of these proteins. In this context, our data confirm the ischaemia-mediated modulation of tight junction proteins given the time-dependent increase in claudin-5 protein levels under OGD±R. It is of vital importance that the increases in the claudin-5 protein levels may not be reflective of its peripheral localisation which is critical element for the assembly of tight junctions and the barrier integrity. Recent studies with female Sprague-Dawley rats exposed to either

chronic inflammatory pain, hypoxia or hypoxia-reoxygenation have shown that increased claudin-5 levels in cerebral microvessels are associated with increased paracellular permeability and a loss of BBB function (Brooks et al., 2005, Willis et al., 2010). In addition, the Y-27632 treatment normalised the OGD±R-mediated increases in the claudin-5 protein levels in HBMEC. Since increased claudin-5 protein expressions are associated with barrier dysfunction, the normalisation of claudin-5 levels under OGD±R may suggest an improved endothelial-barrier function. These results indicate that Rho-kinase is involved in modulation of claudin-5 protein expression. Indeed, a previous study has demonstrated the direct correlation of Rho-kinase overactivity with enhanced claudin-5 phosphorylation and subsequent BBB dysfunction (Yamamoto et al., 2008).

Unlike claudin-5 protein levels, our results show no significant differences in the occludin protein expression in HBMEC exposed to normoxic versus OGD±R conditions. Similar to our data, a recent study with rat treated with λ-carrageenan, an inflammatory pain inducer, led to increased substrate permeability across the BBB without altering the β-occludin protein levels in cerebral microvessels. However, the α-occludin levels were decreased by 1.3-fold in the same study (Ronaldson et al., 2009). Studies with rat model of subarachnoid haemorrhage have also shown a reduction in the occludin protein levels in the ipsilateral brain hemisphere emphasising possibility of protein degradation with cerebrovascular pathology. Recent *in vitro* and *in vivo* studies on mice brain endothelial cells and mice model of acute liver failure, respectively, have confirmed that the degradation of occludin proteins is due to an endogenous overexpression of MMP-9 (Chen et al., 2009, Fujii et al., 2012). However, the similar levels of occludin before and after exposure to OGD±R highlight the possible phosphorylation and subsequent disassembly of this

particular transmembrane protein. Indeed, a recent study with rat-MCAO model of global cerebral ischaemia supports this hypothesis, as ischaemic injury increased the BBB breakdown mediated through acute disassembly of occludin protein triggered by its increased phosphorylation (Kaur et al., 2011).

Treatment with Y-27632 during OGD±R increased occludin protein levels in HBMEC. Since occludin is one of the major transmembrane tight junction protein responsible for sealing the gaps between the adjacent endothelial cells, an increase in its levels under the influence of Y-27632 may reflect an improved endothelial barrier integrity. Indeed, recent *in vitro* and *in vivo* studies have shown that the inhibition of Rho-kinase improves the total occludin protein levels and the endothelial-barrier tightness (Fujii et al., 2012, Xie et al., 2012). Moreover, studies with mouse BMEC and bovine retinal endothelial cells have revealed that RhoA, Rho-kinase and PKC-β activations phosphorylate occludin at more than one sites and potentiate the tight junction trafficking, which is accompanied by the functional impairment of the endothelial barrier and prevented by specific inhibitor of aforementioned molecules (Hirase et al., 2001, Yamamoto et al., 2008, Murakami et al., 2012). Hence, further studies are required to examine the phosphorylation status of claudin-5 and occludin and their cellular localisation in HBMEC to investigate the tight junction trafficking under pathological conditions.

Apart from the transmembrane tight junction proteins, the endogenous adherens junction proteins like β-catenin, the primary canonical Wnt pathway activator, also regulates the endothelial permeability and intercellular signalling (Bazzoni and Dejana, 2004, Aisagbonhi et al., 2011). In this study we found that β-catenin levels remain unchanged in HBMEC after short and longer periods of exposures to OGD.

However, their levels elevated after OGD+R. These results illustrate the reperfusion-mediated modulation of the adherens junction proteins. Recent findings from hypoxia-reoxygenation studies on proximal tubular epithelial rat cell line concur with our data, as β-catenin protein levels remain unchanged during hypoxia and hypoxia followed by short phases of reoxygenation (1-6 hours) (Saenz-Morales et al., 2006). Moreover, study on mouse model of myocardial infarction have shown a dramatic activation of canonical Wnt signalling in endothelial cells surrounding infarct area after 4 days of myocardial infarction emphasising the enhanced β-catenin induction during the later stages of pathology. In addition, this study also showed that canonical Wnt/β-catenin signalling triggers the transition of bovine aortic endothelial cells into mesenchymal cells indicated by phenotype modifications and loss of endothelial-cell-specific signature gene CD31 (Aisagbonhi et al., 2011). Since β-catenin supports the transmembrane adherens junction protein VE-cadherin and anchors the focal adhesion complex to actin (Bazzoni and Dejana, 2004), its dissociation from VE-cadherin may introduce gaps and increase paracellular permeability. Indeed, recent studies on human pulmonary microvascular endothelial cells have suggested the ROS-mediated dissociation of β-catenin from VE-cadherin as one of the reasons behind the enhanced endothelial permeability (Makarova et al., 2011). In addition, using transgenic mice and primary brain endothelial cells it has been shown that stabilisation of VE-cadherin-β-catenin complex is pivotal in maintaining the BBB integrity (Liebner et al., 2008).

In the current study, we observed that Y-27632 treatment restored the increased total β-catenin levels during OGD+R conditions which may be related to the stability of the VE-cadherin-β-catenin complex. Furthermore, it has been shown that synthesis and release of growth factors and cytokines destabilise the VE-cadherin adhesion

complex by increasing β-catenin phosphorylation. Hence by regulating the synthesis of cytokines and growth factor, Rho-kinase inhibition may attenuate β-catenin phosphorylation and subsequent dissociation from the VE-cadherin adhesion complex, thereby improving the barrier integrity (Vogelmann et al., 2005). Further studies are required to evaluate the β-catenin phosphorylations levels in HBMEC after OGD±R.

The vinculin, a subunit of focal adhesion complex, protein levels were also investigated in the current study which remained similar in HBMEC exposed to normoxia versus OGD±R conditions. These data are in coherence with results from studies with coronary endothelial cells which illustrated an unchanged vinculin protein levels, and proposed the association of increased vinculin phosphorylation levels with the progression of hyperpermeability during energy depletion in these cells (Muhs et al., 1997). Recent hypoxia-reoxygenation study has also shown unchanged paxillin, another subunit of focal adhesion complex, protein levels in proximal tubular epithelial rat cell line exposed to different hypoxia-reoxygenation combinations (Saenz-Morales et al., 2006). These results suggest that the focal adhesion protein levels are not altered under pathological conditions. Similarly, the Y-27632 treatment did not change the vinculin protein levels in HBMEC under OGD±R. These results suggest that vinculin protein levels are not modulated by either Rho-kinase activation or inhibition. However, phosphorylations of vinculin protein are known to be associated with the hyperpermeability (Muhs et al., 1997). Therefore, further studies are required to delineate the vinculin phosphorylations and their association with OGD±R-mediated hyperpermeability in HBMEC.

Overwhelming evidence exists regarding the critical role of endothelial-barrier in restricting the paracellular permeability and therefore maintaining proper barrier function. In final part of this section, the possible alterations in BBB integrity were assessed by TEER and flux of EBA after exposure to OGD±R using an *in vitro* model of human BBB consisting of HBMEC and HA. We have previously shown that astrocytes are not as dormant as they were initially thought, in that they also possess increased RhoA activity and Rho-kinase expression after OGD±R (Allen et al., 2010). Therefore increased ROS production from astrocytes might also augment the oxidative stress-mediated BBB disruption. A time-dependent decrease in TEER and concurrent increase in the flux of EBA were recorded across the cocultures under OGD. The reperfusion after OGD exacerbated the BBB damage and further reduced the TEER and increased the flux of EBA across the cocultures. This may in part be due to the enhanced oxidative stress-mediated endothelial cell apoptosis (Kahles et al., 2007, Connell et al., 2011, Genovese et al., 2011). The Y-27632 treatment with OGD±R showed cerebral-barrier protective effects as the Rho-kinase inhibitor preserved the coculture integrity during short OGD±R which was confirmed by TEER readings and flux of EBA similar in the cocultures exposed to normoxia versus short OGD±R conditions. However, the Y-27632 treatment was ineffective in protecting the cerebral barrier integrity under longer OGD±R which showed decreased TEER readings and concomitant increase in the flux of EBA. Thus, cocultures exposed to short OGD±R with Y-27632 treatment appeared to have improved integrity and function compared to the cocultures exposed to OGD±R without Y-27632. This may be due to the inhibition of Rho-kinase-mediated induction of apoptosis in HBMEC under OGD±R. It has been shown that RhoA/Rho-kinase pathway is associated with the upregulation of proapoptotic protein Bax which activates the mitochondrial death

pathway and induce apoptosis in cardiomyocytes. Moreover fasudil mesylate has been shown to protect the oxidative stress-mediated apoptosis in rat PC12 cell line derived from rat pheochromocytoma (Del Re et al., 2007, Li et al., 2011a).

In conclusion, the current study has shown that Rho-kinase inhibitor Y-27632 may demonstrate antioxidant properties by attenuating the OGD±R-mediated increase in expression and activity of NADPH oxidase enzyme complex and preventing the excessive ROS formation and accumulation. Y-27632 may also be considered a cerebral barrier protective agent as it has improved the endothelial-barrier integrity and function. Lastly, the RhoA/Rho-kinase signalling pathway appears to orchestrate the endothelial-barrier dysfunction in part by modulating the pro-oxidant, antioxidant enzymes and junctional protein complexes.

Chapter 3

Studies focusing on the molecular mechanisms behind cerebro protective effects of fasudil after ischaemic injury in mice

Previous *in vivo* studies have shown that fasudil, a specific Rho-kinase inhibitor, treatment attenuates the IR-mediated injury by reducing the cerebral infarct volume and exhibit the neuroprotective properties following cerebral ischaemia (Rikitake et al., 2005, Yagita et al., 2007). Hence, the current study was designed to investigate the molecular mechanisms behind cerebro protective effects of fasudil after ischaemic injury in mice. Ischaemic stroke was induced in male mice by MCAO for 60 minutes and the animals received either fasudil or vehicle after ischaemia at: onset of reperfusion, 6 hours post reperfusion and 24 hours post reperfusion. The mice were sacrificed 48 hours after ischaemia and their brain tissues were collected, sliced and homogenised for *in vitro* experiments.

3.1. Aims

To investigate,

1. whether fasudil modulates the IR-mediated effects on cerebral RhoA and Rho-kinase-2 protein levels and RhoA activity,
2. whether fasudil alters the IR-mediated effects on cerebral pro-oxidant enzyme NADPH oxidase expression and activity, total $O_2^{\bullet-}$ levels, antioxidant enzymes CuZn-SOD and catalase protein levels,
3. whether cerebral junctional complex proteins are regulated by fasudil after IR injury.

3.2. Results

3.2.1. Effects of fasudil on cerebral RhoA and Rho-kinase-2 protein expressions and RhoA activity

The homogenised brain sections from a mice model of ischaemic stroke were used to study the effects of fasudil on the RhoA protein expression, activity and Rho-

kinase-2 protein levels after normalisation against β-actin levels. The results have been generated from (a) comparison between protein levels in the contralateral and ipsilateral brain sections from either vehicle-treated group or fasudil-treated group of mice, and (b) comparison of fold differences (ipsilateral/contralateral) in protein expression between vehicle-treated and fasudil-treated mice. Our results appear to show no significant difference in total RhoA protein levels between contralateral and ipsilateral brain sections in either vehicle-treated or fasudil-treated mice. In addition, there was no significant fold difference in the total RhoA levels observed between these mice groups (Figure 3.1). These data appear to indicate that the cerebral total RhoA levels remain unchanged in vehicle-treated and fasudil- treated animals after IR injury.

The total RhoA activity was analysed by measuring the RhoA-GTP/total RhoA ratio in brain sections from vehicle-treated and fasudil-treated groups of mice. There were no significant differences in the total RhoA activities between contralateral and ipsilateral brain sections from either vehicle-treated or fasudil-treated mice. In addition, the fold differences in the total RhoA activities also remain unchanged between these groups (Figure 3.2). These results may indicate that the total RhoA activity does not change in brain sections after IR injury, and fasudil treatment may be ineffective in modulating the RhoA activity.

Similarly, the Rho-kinase-2 levels were also detected in mice brain tissue from the contralateral and ipsilateral sections of vehicle-treated group and fasudil-treated group of mice. No significant differences were observed in the Rho-kinase-2 protein levels between contralateral and ipsilateral brain sections of either vehicle- or fasudil-treated mice. Moreover, the fold difference in the Rho-kinase-2 protein levels also remained

unchanged between these mice groups (Figure 3.3). These results seem to indicate that Rho-kinase-2 protein levels do not change in brain sections after IR injury, and fasudil treatment has no effect on Rho-kinase-2 protein levels in brain sections of mice.

A

Animal	Group	Contralateral (c)	Ipsilateral (i)	Fold difference (i/c)
1	Vehicle	0.68	0.72	1.06
2	Vehicle	1.64	1.77	1.08
3	Vehicle	1.54	1.68	1.09
4	Fasudil	1.15	1.17	1.02
5	Fasudil	0.78	0.78	1.00
6	Fasudil	1.11	1.18	1.06

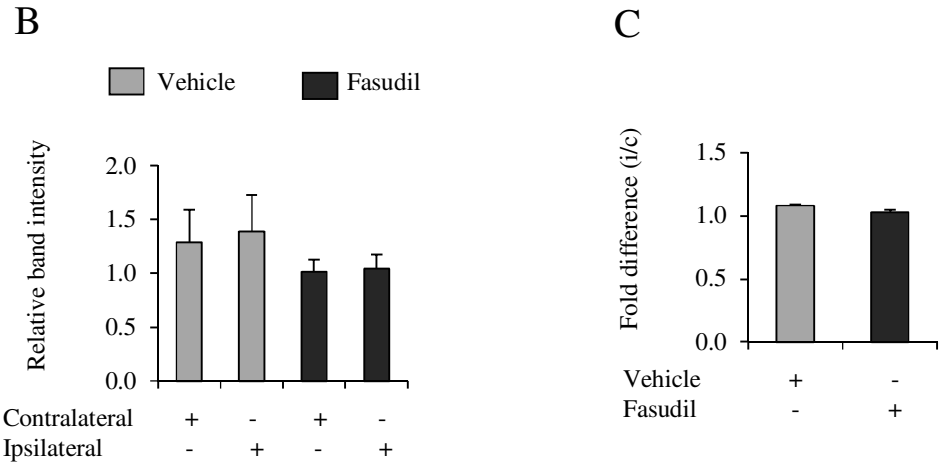

D

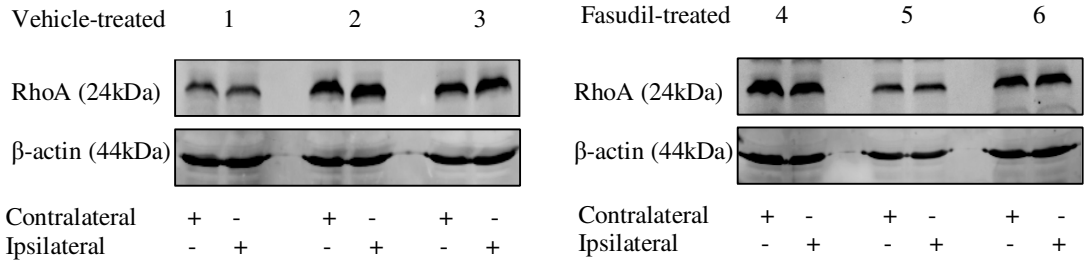

Figure 3.1. Total RhoA protein levels mice brain sections. **(A-D)** Representative Western blots and densitometric analyses of RhoA protein expression in contralateral and ipsilateral brain sections of mice model of ischaemic stroke treated with either

fasudil or vehicle. Univariate comparisons were made using Student's t-test. Data are expressed as mean±SEM, n=3 in each group.

A

Animal	Group	Contralateral (c)	Ipsilateral (i)	Fold difference (i/c)
1	Vehicle	17.89	6.56	0.37
2	Vehicle	0.31	12.1	39.03
3	Vehicle	16.53	16.4	0.99
4	Fasudil	0.4	1.53	3.83
5	Fasudil	1.54	5.65	3.67
6	Fasudil	1.99	13.12	6.59

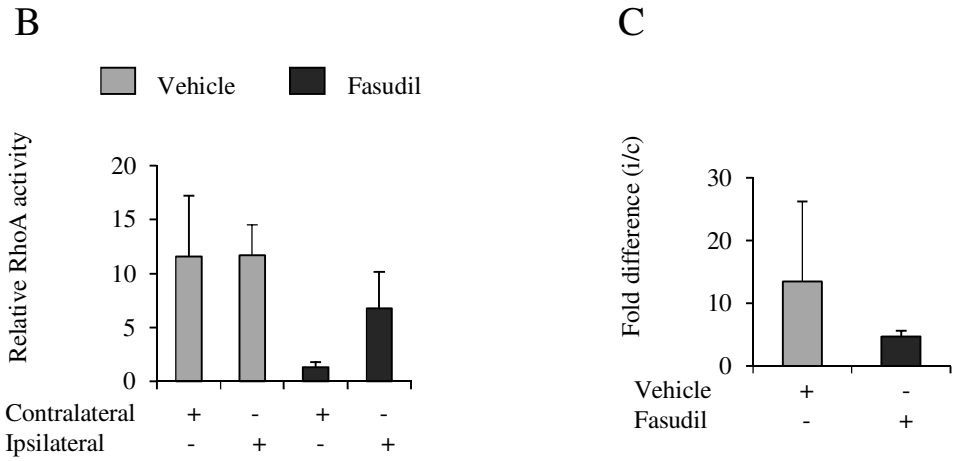

D

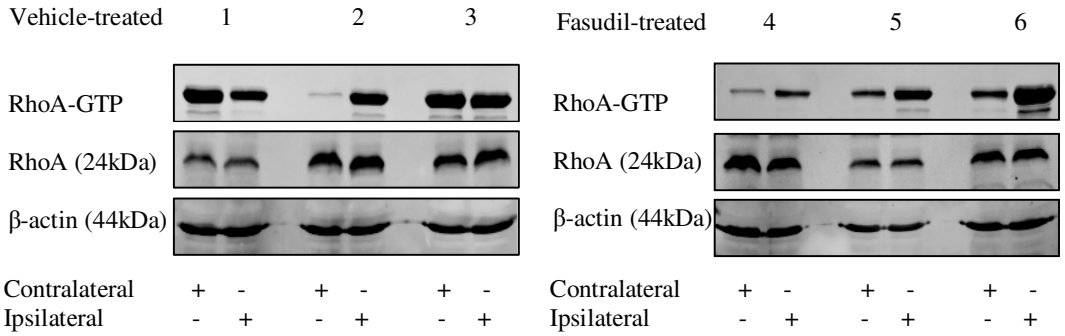

Figure 3.2. Total RhoA activity in mice brain sections. **(A-D)** Representative Western blots and densitometric analyses of RhoA-GTP/total RhoA ratio in contralateral and

ipsilateral brain sections of mice model of ischaemic stroke treated with either fasudil or vehicle. Univariate comparisons were made using Student's t-test. Data are expressed as mean±SEM, n=3 in each group.

A

Animal	Group	Contralateral (c)	Iipsilateral (i)	Fold difference (i/c)
1	Vehicle	6.7	6.7	1.00
2	Vehicle	7.3	7.3	1.00
3	Vehicle	6.9	6.8	0.99
4	Fasudil	6.7	6.7	1.00
5	Fasudil	6.1	6.1	1.00
6	Fasudil	6.3	5.8	0.92

B

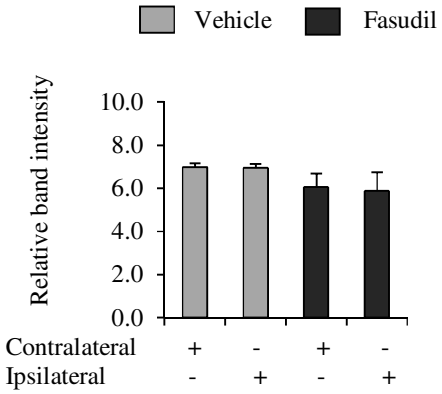

C

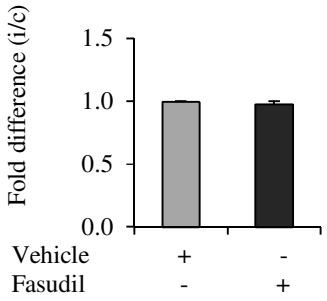

D

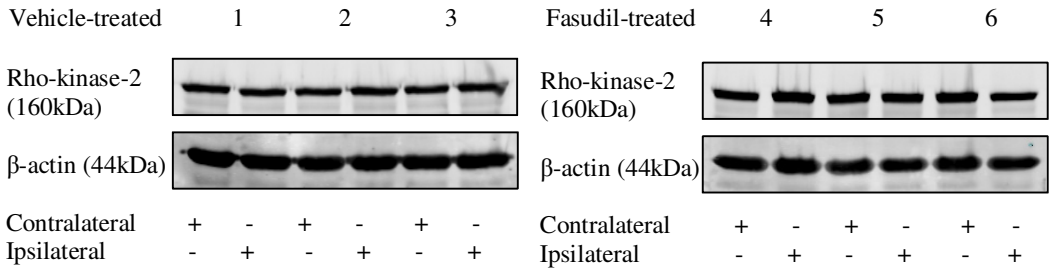

Figure 3.3. Rho-kinase-2 protein levels in mice brain sections. **(A-D)** Representative Western blots and densitometric analyses of Rho-kinase-2 protein expression in

contralateral and ipsilateral brain sections of mice model of ischaemic stroke treated with either fasudil or vehicle. Univariate comparisons were made using Student's t-test. Data are expressed as mean±SEM, n=3 in each group.

3.2.2. Effects of fasudil on cerebral gp91-phox protein levels, NADPH oxidase activity, total $O_2^{\bullet-}$ levels and antioxidant enzyme expressions

Our data show a slight but insignificant reduction in the gp91-phox protein levels in ipsilateral sections compared to contralateral sections in vehicle-treated mice group, which remained unchanged between respective sections in fasudil-treated mice group. Moreover in the ipsilateral brain sections, the fasudil treatment dramatically increased the gp91-phox protein levels compared to the ipsilateral brain sections of vehicle-treated mice ($P<0.05$). There was no significant variation in the fold difference in gp91-phox protein levels in brain sections between these mice groups (Figure 3.4). These results seem to indicate that gp91-phox protein levels do not change between the contralateral and ipsilateral sections of mice brain after IR injury in the presence or absence of fasudil.

In parallel with the gp91-phox data, the total NADPH oxidase enzyme activities measured by lucigenin-enhanced chemiluminescent detection of $O_2^{\bullet-}$ assay indicate a slight but insignificant reduction in the enzyme activity in ipsilateral section compared to contralateral section in vehicle-treated animals. However, the enzyme activities seemed to be similar in respective brain sections of fasudil-treated mice. There was no significant fold difference in the enzyme activities from ipsilateral and contralateral sections of fasudil-treated mice compared to the vehicle-treated mice (Figure 3.5). These results seem to indicate that the NADPH oxidase enzyme activity does not vary in different sides of mice brain after IR insult, and the fasudil treatment

may be ineffective in modulating the enzyme activities in brain sections of ischaemic mice.

To substantiate the differences or similarities observed in NADPH oxidase activity, total $O_2^{\bullet-}$ levels were also measured in the same homogenates of contralateral and ipsilateral brain sections from vehicle-treated and fasudil-treated mice groups via lucigenin-enhanced chemiluminescent detection of $O_2^{\bullet-}$. No significant difference was recorded in the total $O_2^{\bullet-}$ levels between contralateral and ipsilateral brain sections from aforementioned mice groups. In addition, similar fold differences in the total $O_2^{\bullet-}$ levels were recorded between these groups of mice (Figure 3.6). These results indicate that the total $O_2^{\bullet-}$ levels appeared to remain unchanged in different sides of mice brain after IR insult and may also reflect the inefficiency of fasudil in modulating the total $O_2^{\bullet-}$ levels in brain sections of ischaemic mice.

A

Animal	Group	Contralateral (c)	Ipsilateral (i)	Fold difference (i/c)
1	Vehicle	0.053	0.054	1.02
2	Vehicle	0.05	0.052	1.04
3	Vehicle	0.048	0.045	0.94
4	Vehicle	0.04	0.02	0.50
5	Vehicle	0.08	0.06	0.75
6	Vehicle	0.24	0.04	0.17
7	Fasudil	0.047	0.09	1.91
8	Fasudil	0.145	0.15	1.01
9	Fasudil	0.061	0.117	1.92
10	Fasudil	0.021	0.102	4.86
11	Fasudil	0.091	0.11	1.21
12	Fasudil	0.15	0.079	0.53

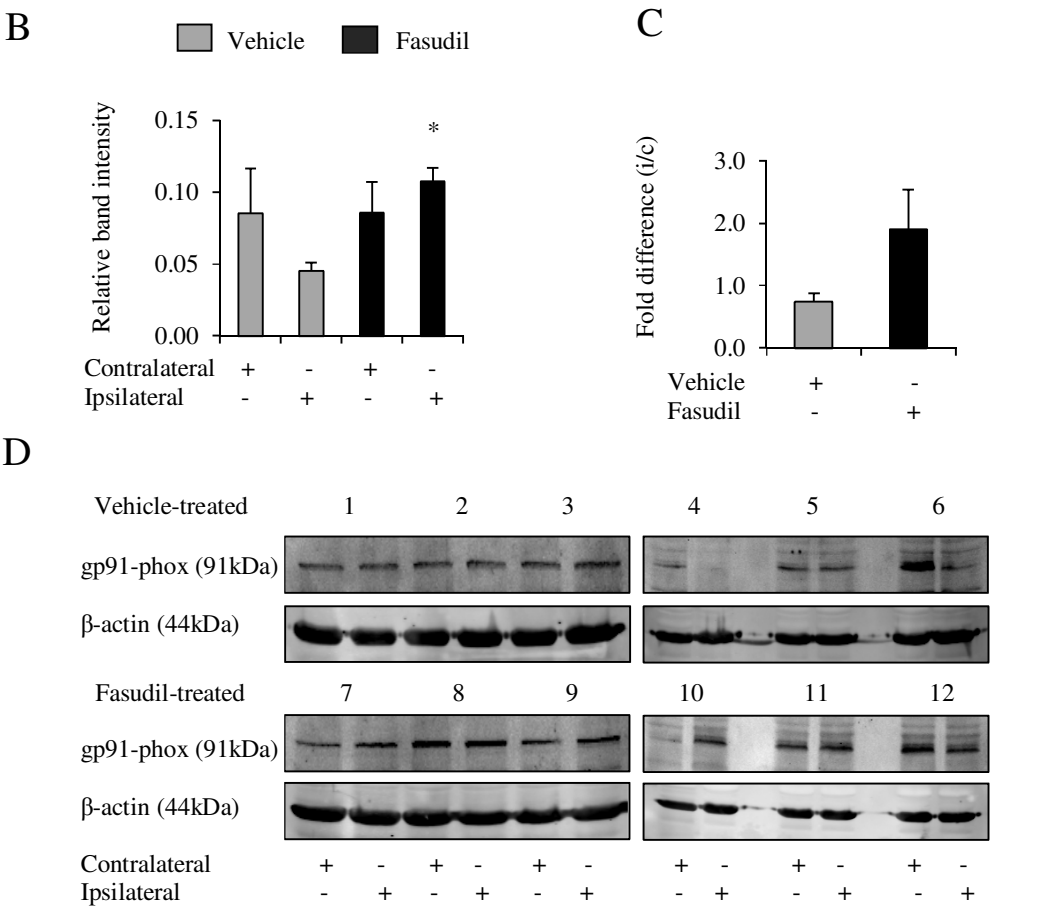

Figure 3.4. The gp91-phox protein levels in mice brain sections. **(A-D)** Representative Western blots and densitometric analyses of gp91-phox protein expression in contralateral and ipsilateral brain sections of mice model of ischaemic

stroke treated with either fasudil or vehicle. Univariate comparisons were made using Student's t-test. Data are expressed as mean±SEM, n=6, $^{*}P<0.05$ compared to the ipsilateral section in vehicle group.

A

Animal	Group	Contralateral (c)	Ipsilateral (i)	Fold difference (i/c)
1	Vehicle	1.28	1.28	1.00
2	Vehicle	1.42	1.07	0.75
3	Vehicle	1.37	1.14	0.83
4	Fasudil	1.05	1.27	1.21
5	Fasudil	1.14	1.1	0.96
6	Fasudil	1.18	0.93	0.79

B

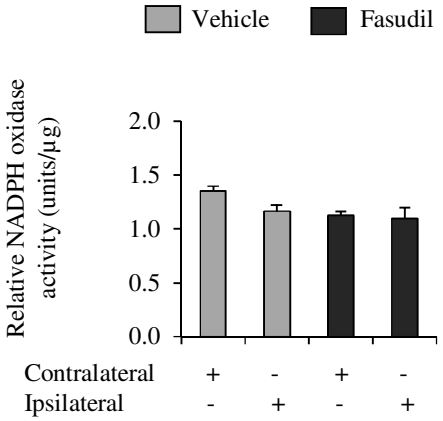

C

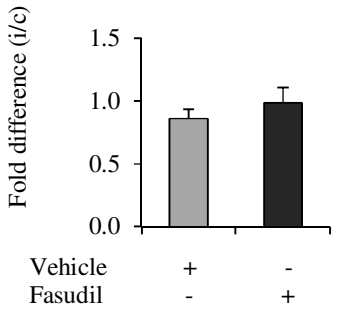

Figure 3.5. The cerebral NADPH oxidase enzyme activity (units/µg). **(A-C)** Relative NADPH oxidase activity and fold difference in contralateral and ipsilateral brain sections of mice model of ischaemic stroke treated with either fasudil or vehicle. Univariate comparisons were made using Student's t-test. Data are expressed as mean±SEM, n=3 in each group.

A

Animal	Group	Contralateral (c)	Ipsilateral (i)	Fold difference (i/c)
1	Vehicle	0.77	0.84	1.09
2	Vehicle	0.7	0.81	1.16
3	Vehicle	0.79	0.72	0.91
4	Fasudil	0.63	0.91	1.44
5	Fasudil	0.8	0.7	0.90
6	Fasudil	0.63	0.75	1.19

B

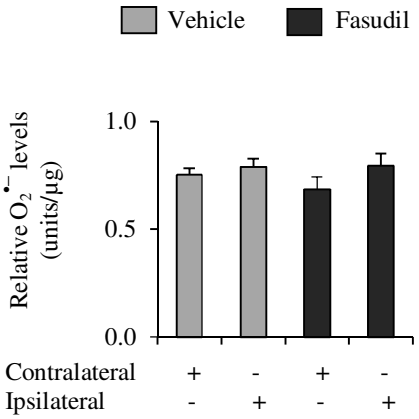

C

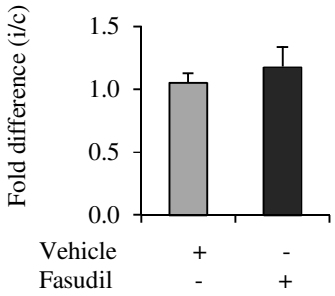

Figure 3.6. The cerebral $O_2^{\bullet-}$ levels (units/µg). **(A-C)** Relative $O_2^{\bullet-}$ levels and fold difference in contralateral and ipsilateral brain sections of mice models of ischaemic stroke treated with either fasudil or vehicle. Univariate comparisons were made using Student's t-test. Data are expressed as mean±SEM, n=3 in each group.

Moreover, our data show no significant variations in the antioxidant enzyme CuZn-SOD protein levels between contralateral and ipsilateral brain sections of either vehicle-treated group or fasudil-treated group of mice. In addition, the fold difference in CuZn-SOD levels was similar in these mice groups (Figure 3.7). These data may indicate that the protein levels of CuZn-SOD do not change after IR insult in mice, and fasudil treatment does not modulate the CuZn-SOD levels.

Similarly, the protein levels of another antioxidant enzyme catalase were also analysed in the brain sections of these mice groups. There was no significant difference observed in the catalase levels between contralateral and ipsilateral brain sections of either vehicle-treated or fasudil-treated mice. A similar fold difference in the catalase levels was also recorded between these mice groups (Figure 3.8). Taken together, these results indicate that IR injury seems to have no effect on the catalase protein levels, and fasudil treatment appears to be largely ineffective in modulating the catalase levels.

A

Animal	Group	Contralateral (c)	Ipsilateral (i)	Fold difference (i/c)
1	Vehicle	9.06	8.57	0.95
2	Vehicle	8.27	7.9	0.96
3	Vehicle	9.02	9.79	1.09
4	Fasudil	8.5	9.3	1.09
5	Fasudil	8.1	7.90	0.98
6	Fasudil	10.63	7.84	0.74

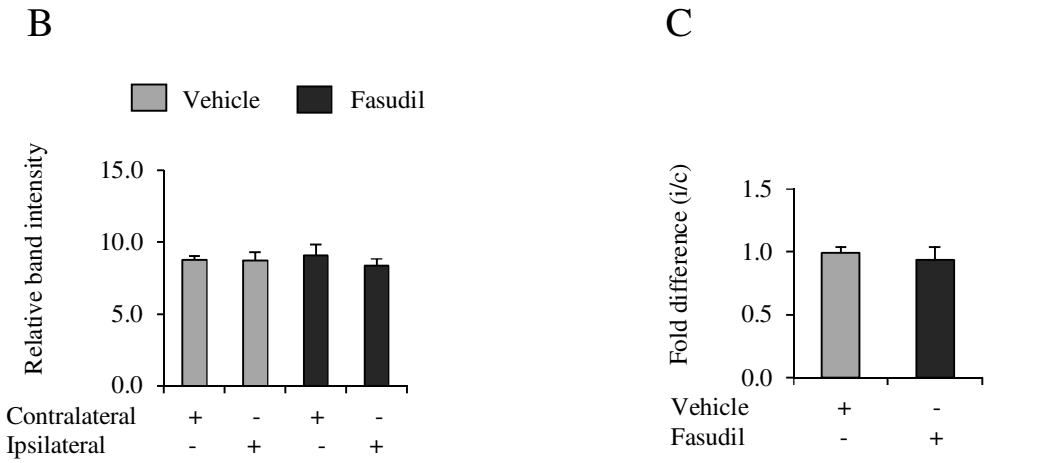

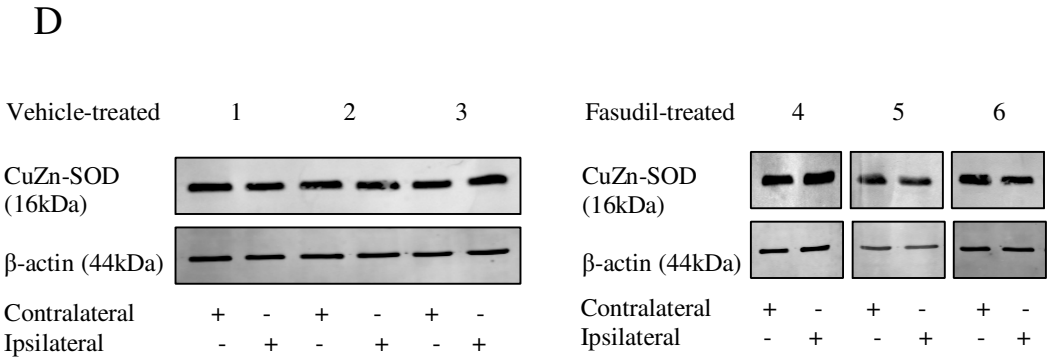

Figure 3.7. CuZn-SOD protein levels in mice brain sections. **(A-D)** Representative Western blots and densitometric analyses of CuZn-SOD protein expression in contralateral and ipsilateral brain sections of mice model of ischaemic stroke treated

with either fasudil or vehicle. Univariate comparisons were made using Student's t-test. Data are expressed as mean±SEM, n=3 in each group.

A

Animal	Group	Contralateral (c)	Ipsilateral (i)	Fold difference (i/c)
1	Vehicle	2.94	2.87	0.98
2	Vehicle	3.09	3.09	1.00
3	Vehicle	2.97	3.19	1.07
4	Fasudil	2.46	2.72	1.11
5	Fasudil	2.4	2.44	1.02
6	Fasudil	2.8	3.32	1.19

B

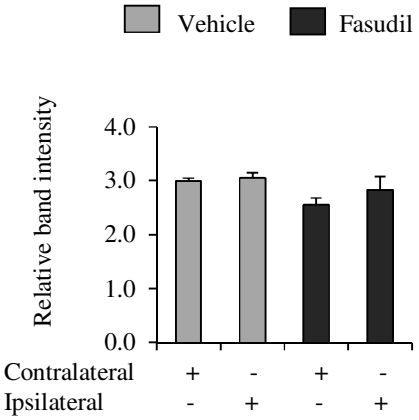

C

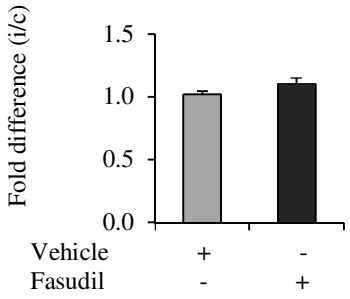

D

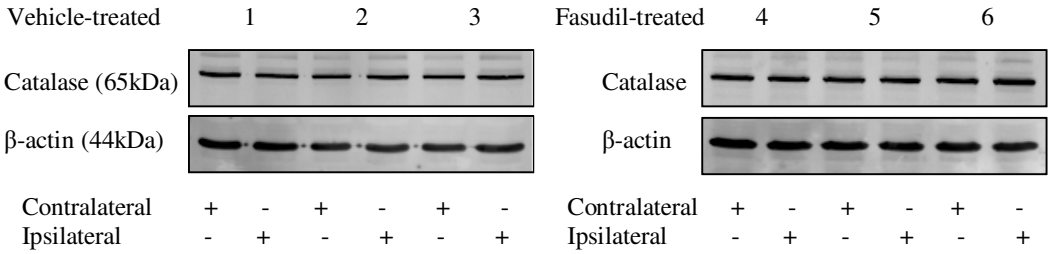

Figure 3.8. Catalase protein levels in mice brain sections. **(A-D)** Representative Western blots and densitometric analyses of catalase protein expression in

contralateral and ipsilateral brain sections of mice model of ischaemic stroke treated with either fasudil or vehicle. Univariate comparisons were made using Student's t-test. Data are expressed as mean±SEM, n=3 in each group.

3.2.3. Effects of fasudil on cerebral occludin and claudin-5 protein levels

Tight junction proteins like occludin and caludin-5 restrict the paracellular permeability and prevent the cerebral oedema formation. Hence, the cerebral levels of these proteins were detected in vehicle-treated and fasudil-treated groups of mice model of ischaemic stroke. There were no significant differences observed in the occludin protein levels between contralateral and ipsilateral brain sections in either of the mice groups. In addition, similar fold difference in the occludin levels was observed between these mice groups (Figure 3.9).

Similarly, the cerebral claudin-5 levels were also detected in the same mice groups. Our data show no significant difference in the claudin-5 levels between contralateral and ipsilateral sections of either vehicle-treated or fasudil-treated mice groups. However, a significant reduction in the claudin-5 levels was observed in contralateral and ipsilateral sections after fasudil treatment compared to the vehicle treatment ($P<0.05$). Moreover, the fold difference in the claudin-5 levels also remained unchanged between the mice groups (Figure 3.10). These results indicate that IR injury appears to have no significant effect on the cerebral occludin and claudin-5 protein levels, and fasudil may supresses the claudin-5 levels in mice brain.

A

Animal	Group	Contralateral (c)	Ipsilateral (i)	Fold difference (i/c)
1	Vehicle	0.1	0.11	1.10
2	Vehicle	0.1	0.1	1.00
3	Vehicle	0.08	0.09	1.13
4	Fasudil	0.07	0.07	1.00
5	Fasudil	0.08	0.07	0.88
6	Fasudil	0.1	0.1	1.00

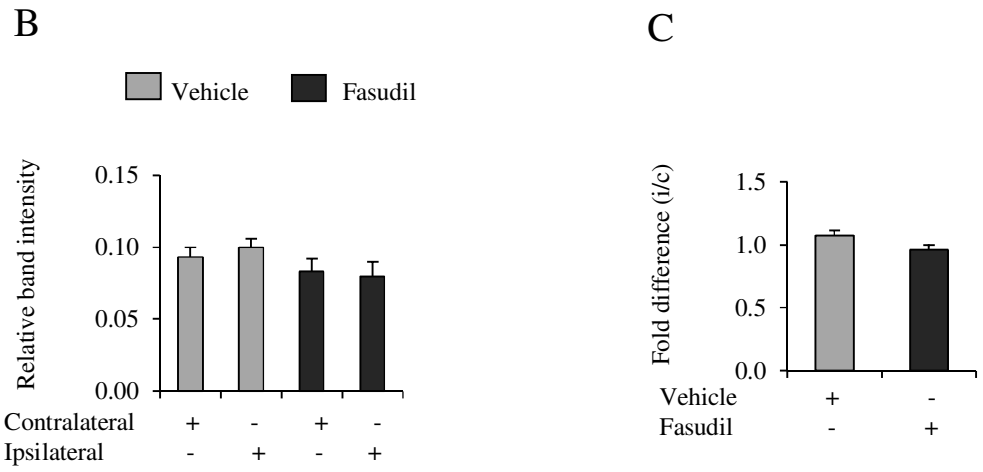

D

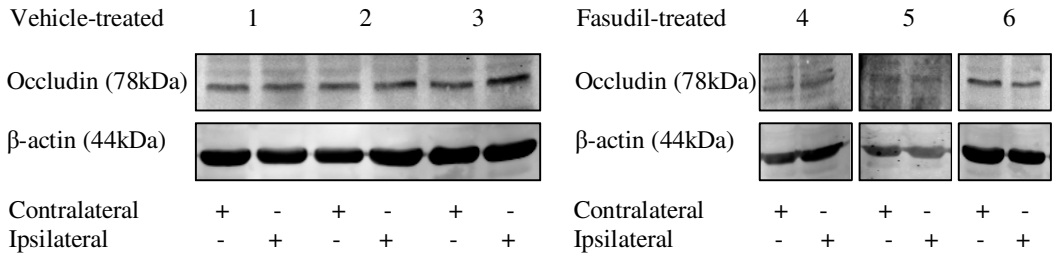

Figure 3.9. Cerebral occludin protein levels in mice. **(A-D)** Representative Western blots and densitometric analyses of occludin protein expression in contralateral and ipsilateral brain sections of mice model of ischaemic stroke treated with either fasudil or vehicle. Univariate comparisons were made using Student's t-test. Data are expressed as mean±SEM, n=3 in each group.

A

Animal	Group	Contralateral (c)	Ipsilateral (i)	Fold difference (i/c)
1	Vehicle	0.42	0.4	0.95
2	Vehicle	0.43	0.29	0.67
3	Vehicle	0.32	0.29	0.91
4	Fasudil	0.11	0.15	1.36
5	Fasudil	0.19	0.16	0.84
6	Fasudil	0.18	0.15	0.83

B

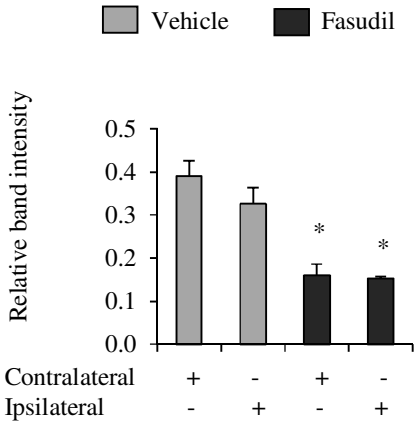

C

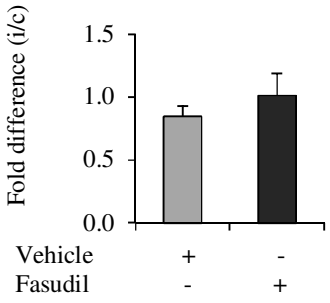

D

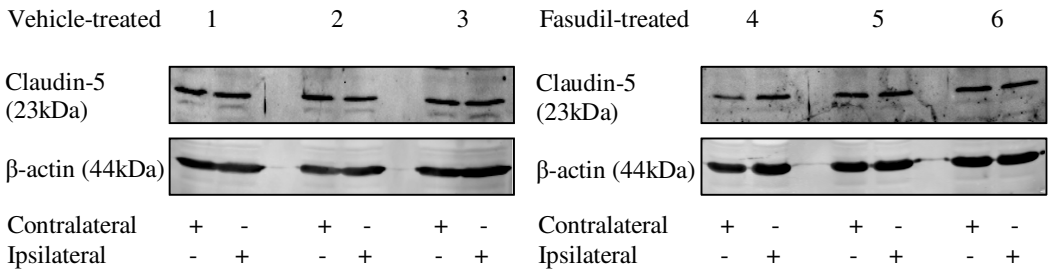

Figure 3.10. Cerebral claudin-5 protein levels in mice. **(A-D)** Representative Western blots and densitometric analyses of claudin-5 protein expression in contralateral and ipsilateral brain sections of mice model of ischaemic stroke treated with either fasudil or vehicle. Univariate comparisons were made using Student's t-test. Data are

expressed as mean±SEM, n=3 in each group, $^{*}P<0.05$ compared to same sections in vehicle group.

3.3. Discussion

In this study, the brain tissue homogenates obtained from mice subjected to MCAO and treated with either vehicle or fasudil, a specific Rho-kinase inhibitor, were used to assess the effects of IR injury and Rho-kinase inhibition on RhoA/Rho-kinase, pro-oxidant enzyme, antioxidant enzyme and junctional complex proteins. Our results show that IR injury had no significant effects on the protein expressions of RhoA, Rho-kinase-2, gp91-phox, CuZn-SOD, catalase, occudin and claudin-5; RhoA and NADPH oxidase enzyme activities and total $O_2^{\bullet-}$ levels. Although fasudil treatment supressed the claudin-5 protein levels, it was ineffective in modulating either expression or activities of other aforementioned proteins. Thus, it appears that different types of cells constituting the complex cerebral tissues maybe stimulated in a different manner under IR stress.

Our previous studies have shown that the activation of RhoA/Rho-kinase modulates the cytoskeletal components like MLC2 and actin, and enhances the cytoskeletal remodelling under IR pathology in HBMEC and HA (Allen et al., 2010). Here, we investigated the expression of RhoA and RhoA-GTP in brain tissues from mice model of ischaemic stroke which were found to remain unchanged after IR injury. Results from previous studies do not support this data as a marked increase in RhoA protein levels have been reported in stroke brain sections and in cellular components of rodent cerebrovasculature after global ischaemia (Brabeck et al., 2003, Zhou et al., 2003). Although the unaltered total RhoA protein data in brain samples were similar to our *in vitro* data observed in HBMEC exposed to OGD±R, the RhoA

activity data were different as two-fold increases were recorded in HBMEC subjected OGD±R. In addition, the fasudil treatment neither affected the RhoA levels nor its activity. These results indicate that the IR injury may not modulate the RhoA activity in the similar manner in all the brain cells. Since cerebral tissues constitute neurons, astrocytes, pericytes, microglia, macrovascular endothelial cells, microvascular endothelial cells and blood cells, an IR-mediated alteration in microvascular endothelial cells may not be reflected in data obtained from complete cerebral tissues. The brain sections from mice treated with either fasudil or vehicle had no difference in the Rho-kinase-2 protein levels, which were consistent with our previously discussed *in vitro* data in HBMEC. However, the unchanged Rho-kinase-2 protein levels may not be representative of change in its activity. Indeed, recent studies confirm increased Rho-kinase activities in the cerebral tissues from ischaemic lesions after focal cerebral ischaemia in rodents (Rikitake et al., 2005, Yagita et al., 2007). Moreover, suppression of Rho-kinase activity by fasudil or Y-27632 in mice models of global ischaemia decreased the kinase activity and the infarct volume and substantiated the role of Rho-kinase to ischaemic cerebral damage (Rikitake et al., 2005).

Oxidative stress, an imbalance in ROS metabolism, exacerbates the cerebral damage under IR injury. Since pro-oxidant NADPH oxidase enzyme complex is one of the major sources of $O_2^{\bullet-}$ production, the expression of gp91-phox, a pivotal subunit of NADPH oxidase, and enzyme activity were studied in brain sections of experimental mice treated with either fasudil or vehicle. Our data show no significant changes in the gp91-phox protein levels, NADPH oxidase activities and total $O_2^{\bullet-}$ levels in mice brain sections after IR injury regardless of the treatment regimen. Recent *in vivo* studies on rat models of liver transplantation with IR injury,

angiotensin II-induced cardiovascular hypertrophy and Dahl salt-sensitive hypertensive rats with cardiovascular abnormalities does not support the current *in vivo* data as marked increase in the gp91-phox protein levels, NADPH oxidase activities and total $O_2^{\bullet-}$ levels were observed in respective tissues under the pathological conditions. In addition, Rho-kinase inhibition either by fasudil or Y-27632 completely suppressed the elevation in gp91-phox protein levels, NADPH oxidase activities and total $O_2^{\bullet-}$ levels (Higashi et al., 2003, Shiotani et al., 2004, Takeshima et al., 2012). Taken together these data indicate that under pathological conditions, Rho-kinase activity may induce oxidative stress by substantially upregulating NADPH oxidase expression, activity and ROS production in different tissues. Since brain is a complex tissue constituting different cell types it is possible that IR injury may not have induced dramatic NADPH oxidase activation in all the cells simultaneously. Indeed, microglia and astrocytes are known to produce enhanced levels of reactive nitrogen species which include nitric oxide and peroxynitrite under IR stress conditions (Askalan et al., 2006, Haynes et al., 2009).

The alteration in physiological levels of antioxidant enzymes like CuZn-SOD and catalase are key determinants of ROS and overall oxidative status. Hence, the protein expressions of CuZn-SOD and catalase were detected in brain sections of ischaemic mice treated with either vehicle or fasudil. Our results show no significant differences in the CuZn-SOD protein levels in the ipsilateral and contralateral brain sections of vehicle-treated and fasudil-treated ischaemic mice. These results are in agreement with our *in vitro* data where protein expression of CuZn-SOD remained unchanged in HBMEC under OGD±R. These results also go hand in hand with a previous *in vitro* study on bovine pulmonary microvascular endothelial cells which showed unchanged CuZn-SOD levels after hypoxia-reoxygenation (Lum et al., 1992). On the contrary,

recent studies on rat models of focal cerebral IR have shown a reduced CuZn-SOD immunoreactivity in the ipsilateral striatum (Matsuda et al., 2009, Kravcukova et al., 2010). In addition, recent studies on rat models of intestinal IR and focal cerebral IR have shown that fasudil treatment ameliorated the SOD activity alongside improving neurological deficits and reducing the cerebral infarction (Huang et al., 2008, Li et al., 2009, Li et al., 2011b). Further experiments are required to measure the CuZn-SOD activity in brains sections of ischaemic mice, and to evaluate the influence of fasudil treatment on enzyme activity.

The antioxidant enzyme catalase is also important in the ROS metabolism as it reduces the excessive H_2O_2 into water and oxygen. Hence, the catalase protein levels were studied in brain sections from ischaemic mice. Our results show no significant difference in the catalase protein expression in the brain sections of vehicle-treated mice and also remain unchanged in brain sections of fasudil-treated mice. These results are different from our *in vitro* data which showed a dramatic increase in the catalase protein expression in HBMEC after OGD±R, and were normalised with Y-27632 treatment. The difference in the catalase protein expression in our *in vitro* and *in vivo* experiments may be due to the variation in the catalase expression in different cellular components of the brain. Since brain is a complex tissue made up of different kinds of cells, the OGD±R-mediated modulation of catalase in microvascular endothelial cells may not be similar in other cells of brain. Hence, further experiments are required to measure catalase protein levels and activity in different cellular components of brain from ischaemic mice.

As discussed in earlier chapters, the integrity of the BBB is heavily dependent on the expression, localisation and stability of tight junction proteins. Variation in these

parameters due to the pathological conditions, destabilise the tight junction protein complexes and compromise the tightness and integrity of the BBB. Therefore, this study investigated the protein levels of tight junction components occludin and claudin-5 in brain sections of mice model of IR treated with either vehicle or fasudil. In addition, the effects of fasudil treatment on the tight junction protein levels were also observed in these *in vivo* samples. There were no significant differences observed in the protein levels of occludin in the brain sections from contralateral and ipsilateral sides of the experimental mice and remained unchanged after fasudil treatment. These results indicate that the total occludin protein levels do not change after IR injury which is consistent with our *in vitro* data from HBMEC exposed to OGD±R. Recent *in vivo* studies with rat models of subarachnoid haemorrhage and acute liver failure have shown a decrease in the occludin levels in the brain samples and do not support the current *in vivo* data (Chen et al., 2009, Fujii et al., 2012). The unchanged occludin level observed in the current study does not dismiss the possibility of occludin phosphorylation and subsequent destabilisation. Indeed, recent *in vivo* studies with rodents have shown that ischaemia-mediated BBB breakdown is due to the acute disassembly of occludin triggered by Rho-kinase-mediated occludin phosphorylation (Yamamoto et al., 2008, Kaur et al., 2011). Although the fasudil treatment did not alter the total ocludin protein levels, it may have decreased the IR-mediated occludin phosphorylation and contributed to stabilise the BBB.

Similarly, the claudin-5 protein expressions were investigated in the *in vivo* brain sections form the experimental mice and the effects of IR injury and fasudil treatment were studied. Our data show no significant difference in the claudin-5 protein levels between the contralateral and ipsilateral brain sections from these mice. Recent *in vivo* data from rat models of chronic inflammatory pain and global hypoxia have

shown an increase in claudin-5 levels in the cerebral microvessels under pathological conditions (Brooks et al., 2005, Willis et al., 2010). These results indicate that the protein levels of caludin-5 vary in different cellular components of brain and this variability may not be reflected in brain tissue which constitutes different kinds of cellular components. Although the claudin-5 protein levels remain unchanged between contralateral and ipsilateral brain sections of fasudil-treated mice, a dramatic reduction in its levels was recorded after the fasudil treatment compared to the vehicle treatment. These results indicate that Rho-kinase modulates the claudin-5 protein level which is consistent with our *in vitro* data in HBMEC exposed to the experimental conditions. In addition, recent *in vivo* studies with rodents have shown that activated Rho-kinase phosphorylates claudin-5 proteins and potentiate the tight junction protein trafficking under pathological conditions (Yamamoto et al., 2008, Kaur et al., 2011).

In conclusion, the data collected from this particular study showed no significant difference in RhoA and NADPH oxidase activities, $O_2^{\bullet -}$ production and RhoA, Rho-kinase-2, gp91-phox, CuZn-SOD, catalase, occludin and claudin-5 protein levels between contralateral and ipsilateral brain sections obtained from mice subjected to MCAO and treated with either vehicle or fasudil. These results were somewhat expected considering the complexity of the brain tissue which comprises of different kinds of cells as mentioned before. All of these cells may not respond to the IR stress simultaneously and in a similar manner. In addition, our *in vitro* data were collected from brain microvascular endothelial cells which are the cellular components of the BBB and may be less than 1% of total brain tissue (Bar, 1983, del Zoppo and Mabuchi, 2003, Cipolla, 2009).

Chapter 4

Studies focusing on the effects of hyperglycaemia on BBB integrity

4.1. Aims

To examine the association of hyperglycaemia with cerebral barrier dysfunction, this study was designed to elucidate,

1. whether hyperglycaemia modulates the RhoA/Rho-kinase/MLC2 pathway, cytoskeletal organisation, junctional complex protein expressions or localisation and cerebral barrier integrity,
2. whether PKC and p38MAPK signalling pathways are involved in the hyperglycaemia-mediated effects,
3. whether inhibition of RhoA/Rho-kinase activities and specific PKC isoforms modulate the hyperglycaemia-mediated PKC overactivity,
4. whether specific PKC-α and PKC-β inhibitors restore the hyperglycaemia-mediated alterations to the RhoA/Rho-kinase/MLC2 pathway, cytoskeletal reorganisation, junctional complex protein expressions or localisation and cerebral barrier integrity,
5. whether PKC-α and PKC-β siRNA protein knockdown attenuate the hyperglycaemic effects on the RhoA activity, MLC2 phosphorylation, junctional complex protein expression and cytoskeletal remodelling.

4.2. Results

4.2.1. Effects of hyperglycaemia on RhoA/Rho-kinase/MLC2 signalling pathway, cytoskeletal reorganisation and junctional complex

The cellular protein levels in HBMEC subjected to different treatments were detected by in-cell Western analysis after normalisation against the α-tubulin levels which served as internal controls. In-cell Western analyses is a new technique to detect and quantify the proteins present in the monolayer of cells in an attempt to minimise the variations in protein levels caused by artifacts in ordinary Western

blotting technique. Hyperglycaemic exposure (25 mM D-glucose) to HBMEC increased the protein expressions of RhoA and Rho-kinase-2 compared to the HBMEC under normoglycaemia (5.5 mM D-glucose) which served as controls ($P<0.05$). However after the glucose normalisation, the hyperglycaemia mediated increase in these proteins was restored ($P<0.05$). The equimolar D-mannitol treatment did not introduce any significant difference in the protein levels and thus eliminated the effects of hyperosmolality playing its part in the hyperglycaemia-mediated alterations. Cotreatment with low dosage of Y-27632 (2.5 μM) under hyperglycaemia appeared to have no effect on the increased protein expressions of RhoA and Rho-kinase-2 and supports the fact that Y-27632 is an inhibitor of Rho-kinase activity (Figure 4.1A, B). Since the total RhoA levels measured in HBMEC homogenates remained largely unchanged among various treatment regimens after normalisation against the β-actin, the relative RhoA activities were calculated after normalising total RhoA-GTP isoforms levels against the total RhoA protein levels (RhoA-GTP/total RhoA ratio). Hyperglycaemia introduced a 2-fold increase in the RhoA activity compared to the controls ($P<0.05$), which was independent of a rise in osmolality and were effectively neutralised by glucose normalisation and inhibition of RhoA by electroporation of anti-RhoA-IgG to HBMEC ($P<0.05$). In contrast, the treatment with low dose of Y-27632 with hyperglycaemia failed to restore the elevated RhoA-GTP levels in HBMEC (Figure 4.1C). These results indicate that hyperglycaemia modulates RhoA/Rho-kinase signalling and glucose normalisation abrogated the hyperglycaemia-mediated alterations.

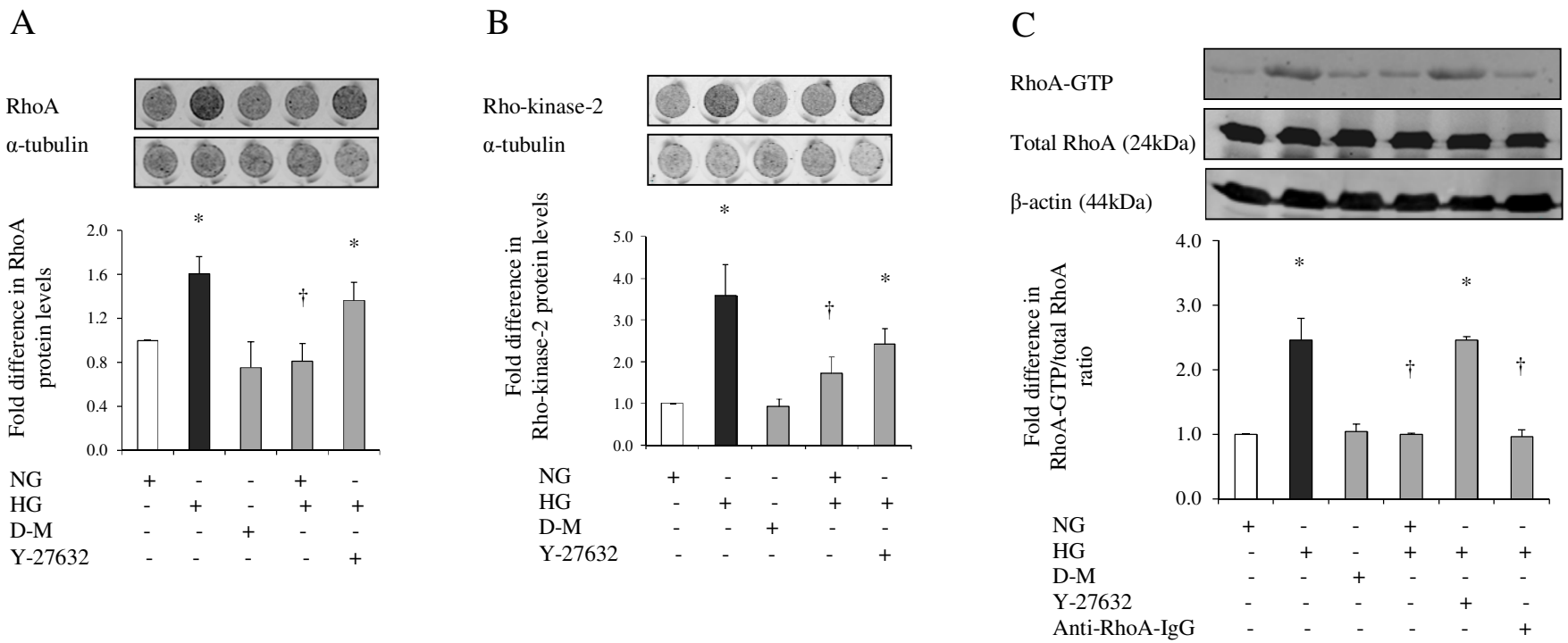

Figure 4.1. Hyperglycaemia modulates RhoA/Rho-kinase signalling. Representative protein levels and corresponding densitometric analyses of **(A)** RhoA, **(B)** Rho-kinase-2 and **(C)** RhoA activities in HBMEC after normalisation against α-tubulin and β-actin. HBMEC were exposed to NG (5.5 mM D-Glucose), HG (25 mM D-glucose), D-M (5.5 mM D-glucose+19.5 mM D-mannitol), Y-27632 (2.5 μM)+HG and electroporated with anti-RhoA-IgG before HG. Data are expressed as mean±SEM from 4 different experiments. Statistical analysis was done using ANOVA

with Dunnet's *post hoc* test for multiple comparisons (A: $P<0.0001$, $F=18.07$, $df1=4$, $df2=15$), (B: $P<0.0001$, $F=12.737$, $df1=4$, $df2=15$), (C: $P<0.0001$, $F=61.285$, $df1=5$, $df2=12$) $^{*}P<0.05$ versus NG, $^{\dagger}P<0.05$ versus HG.

Since MLC2 is one of the known downstream targets of Rho-kinase, a change in their phosphorylation status may be an indication of the Rho-kinase activity under hyperglycaemia. There were no significant changes in the total MLC2 protein levels in HBMEC treated with hyperglycaemia alone or in the presence of Y-27632 and in HBMEC treated with D-mannitol compared with the controls. However, hyperglycaemia increased the levels of MLC2 mono-phosphorylation (p-MLC2-Ser^{19}) and di-phosphorylation (p-MLC2-Thr^{18}/Ser^{19}) in HBMEC measured after normalisation against the total MLC2 protein levels which appeared to be unaffected by hyperglycaemic challenge ($P<0.05$). The hyperglycaemia-induced increases in the levels of MLC2-mono/di-phosphorylations were independent of hyperosmolality and were restored by glucose normalisation and treatment with Y-27632 ($P<0.05$). As MLC2 phosphorylations are dependent on Rho-kinase activity, these results illustrate the role of hyperglycaemia-mediated Rho-kinase overactivity in modulating the MLC2 phosphorylation levels (Figure 4.2).

To examine the effects of hyperglycaemia-mediated MLC2 phosphorylations on HBMEC architecture, the actin filaments were detected by Rhodamine-labelled phalloidin dye. While cells cultured under normoglycaemia and D-mannitol displayed a cortical actin stainings, those exposed to hyperglycaemia developed stress fibres traversing across the cells and acquired morphological changes characterised by cuboidal or elongated appearances. Normalisation of glucose levels reinstated cortical actin staining and cellular morphology which were fully preserved by inhibition of

RhoA and Rho-kinase by anti-RhoA-IgG electroporation and Y-27632 treatment, respectively, during hyperglycaemic insult (Figure 4.3). These results suggest that hyperglycaemia induces the cytoskeletal remodelling by activation of RhoA/Rho-kinase signalling pathway.

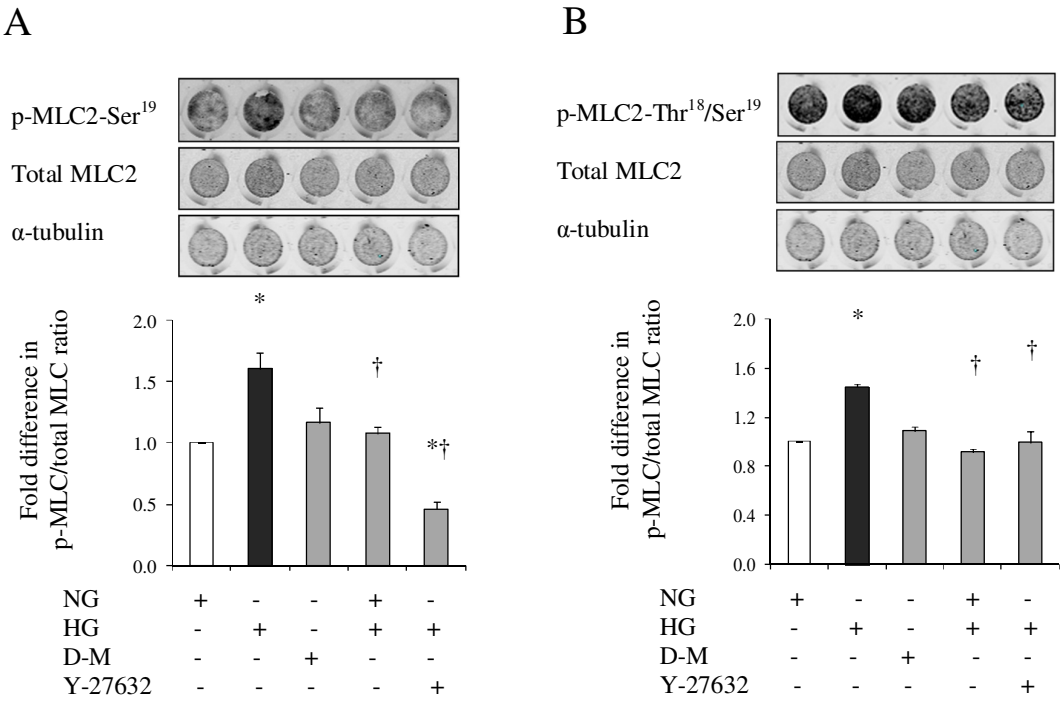

Figure 4.2. Representative in-cell Westerns and densitometric analyses of (**A**) p-MLC2-Ser^{19}, and **(B)** p-MLC2-Thr^{18}/Ser^{19} in HBMEC after normalisation against total MLC2 and α-tubulin. HBMEC were exposed to NG (5.5 mM D-Glucose), HG (25 mM D-glucose), D-M (5.5 mM D-glucose + 19.5 mM D-mannitol) and cotreated with Y-27632 (2.5 μM) plus HG. Data are expressed as mean±SEM from 4 different experiments. Statistical analysis was done using ANOVA with Dunnet's *post hoc* test for multiple comparisons (A: P<0.0001, F=21.312, df1=4, df2=15), (B: P<0.0001, F=37.151, df1=4, df2=10). *P<0.05 compared to NG, †p<0.05 compared to HG.

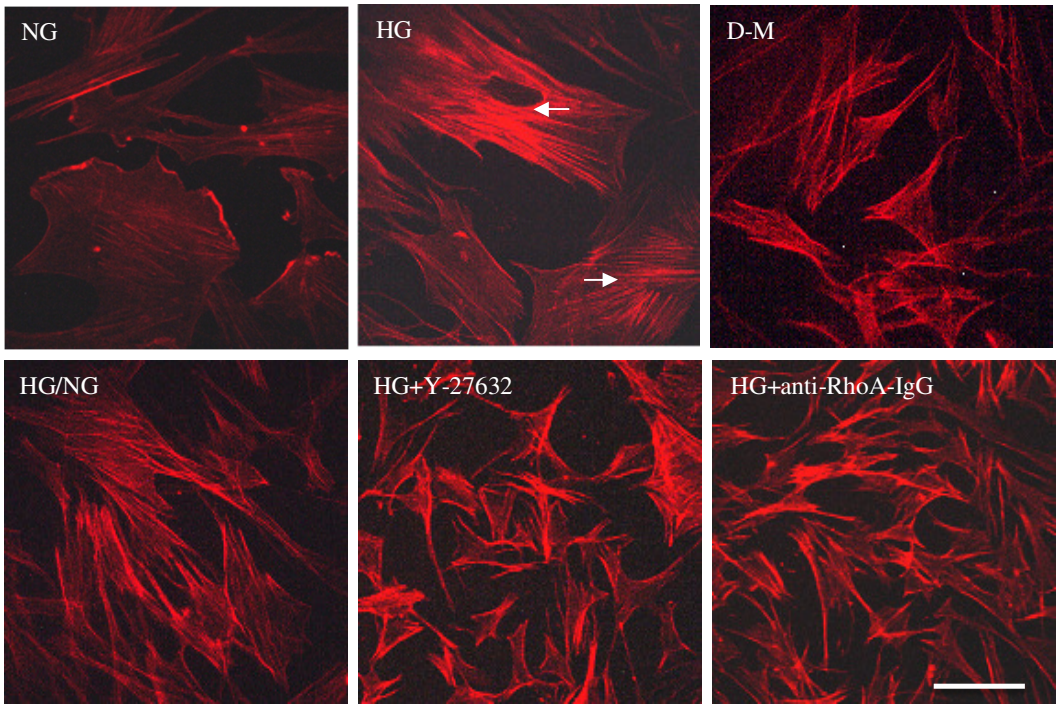

Figure 4.3. Actin microfilament stainings in HBMEC exposed to normoglycaemia (NG; 5.5 mM D-glucose), hyperglycaemia (HG; 25 mM D-glucose), D-mannitol (D-M; 5.5 mM D-glucose + 19.5 mM D-mannitol), HG followed by NG, HG+Y-27632 (2.5 µM) and electroporated with anti-RhoA-IgG (3 µg) before HG. The cells were fixed, permeabilised, blocked, and incubated with Rhodamine-labelled phalloidin dye. Arrows represent the stress fibre formations during hyperglycaemic exposure. Data are collected from 3 different experiments. Bar scale: 50 µm.

Given the effects of hyperglycaemia on cytoskeleton, it was highly likely that hyperglycaemia could compromise the expression and respective localisation of tight junction proteins occludin and ZO-1. In support this notion the in-cell Western analyses showed that hyperglycaemia reduced the occludin protein levels in HBMEC compared to the normoglycaemic controls ($P<0.05$). Where the increases in osmolality failed to affect the occludin levels. However, the decreases in occludin levels were restored by normalisation of glucose levels and supression of Rho-kinase activity via Y-27632 ($P<0.05$) (Figure 4.4A). In addition, the cellular levels of ZO-1 protein remained unchanged in HBMEC treated with hyperglycaemia alone or in the presence of Y-27632. Similarly, the ZO-1 protein levels also remained unaffected by hyperosmolality and the glucose normalisation (Figure 4.4B)

These data were corroborated with studies focusing on the cellular localisations of occludin and ZO-1 in that while complete peripheral stainings were observed under normoglycaemic conditions, hyperglycaemia disrupted the uniform peripheral occludin and ZO-1 stainings observed by partial disappearance of occludin and regular introduction of gaps in ZO-1 stainings by either relocalisation or degradation of these proteins at cell borders (Figure 4.5 A, B). These changes in the occludin and ZO-1 localisations were independent of hyperosmolality. Moreover, the complete peripheral stainings of these proteins were restored after glucose normalisation and inhibition of RhoA and Rho-kinase by anti-RhoA-IgG electroporation and Y-27632 treatment, respectively, during hyperglycaemia. These results indicate that hyperglycaemia modulates tight junction complex in part via RhoA/Rho-kinase signalling pathway.

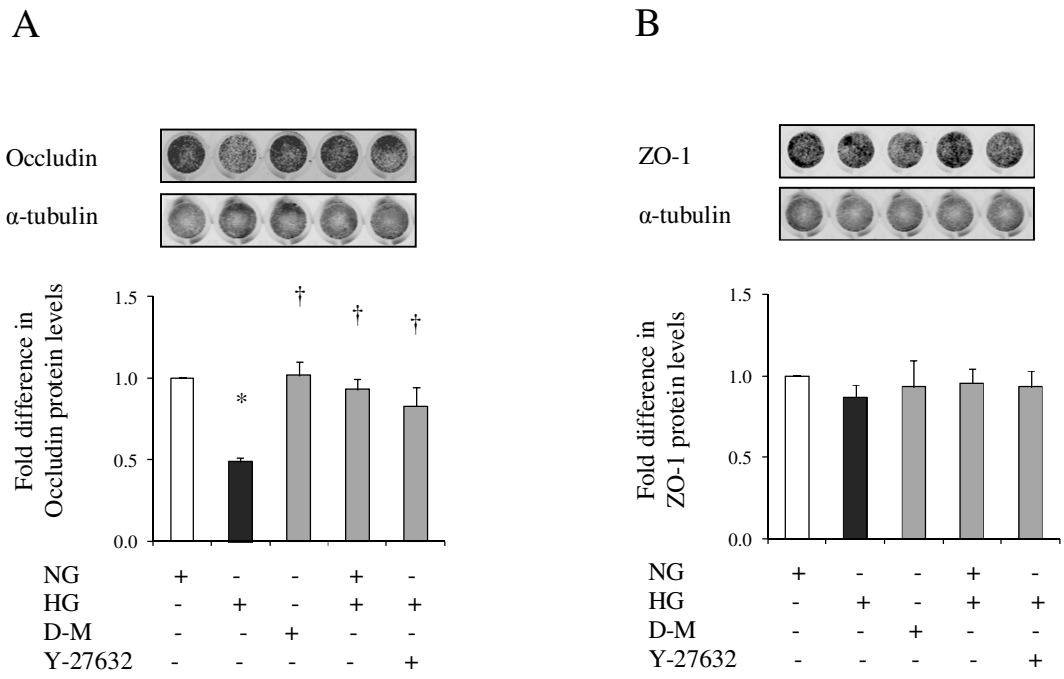

Figure 4.4. Representative in-cell Westerns and densitometric analyses of (**A**) occludin, and (**B**) ZO-1 in HBMEC after normalisation against α-tubulin. HBMEC were exposed to NG (5.5 mM D-Glucose), HG (25 mM D-glucose), D-M (5.5 mM D-glucose + 19.5 mM D-mannitol) and cotreated with Y-27632 (2.5 µM) plus HG. Data are expressed as mean±SEM from 4 different experiments. Statistical analysis was done using ANOVA with Dunnet's *post hoc* test for multiple comparisons (A: $P<0.0001$, $F=10.548$, $df1=4$, $df2=15$), (B: $P=0.848$, $F=0.339$, $df1=4$, $df2=15$). $^{*}P<0.05$ compared to NG, $^{\dagger}P<0.05$ compared to HG.

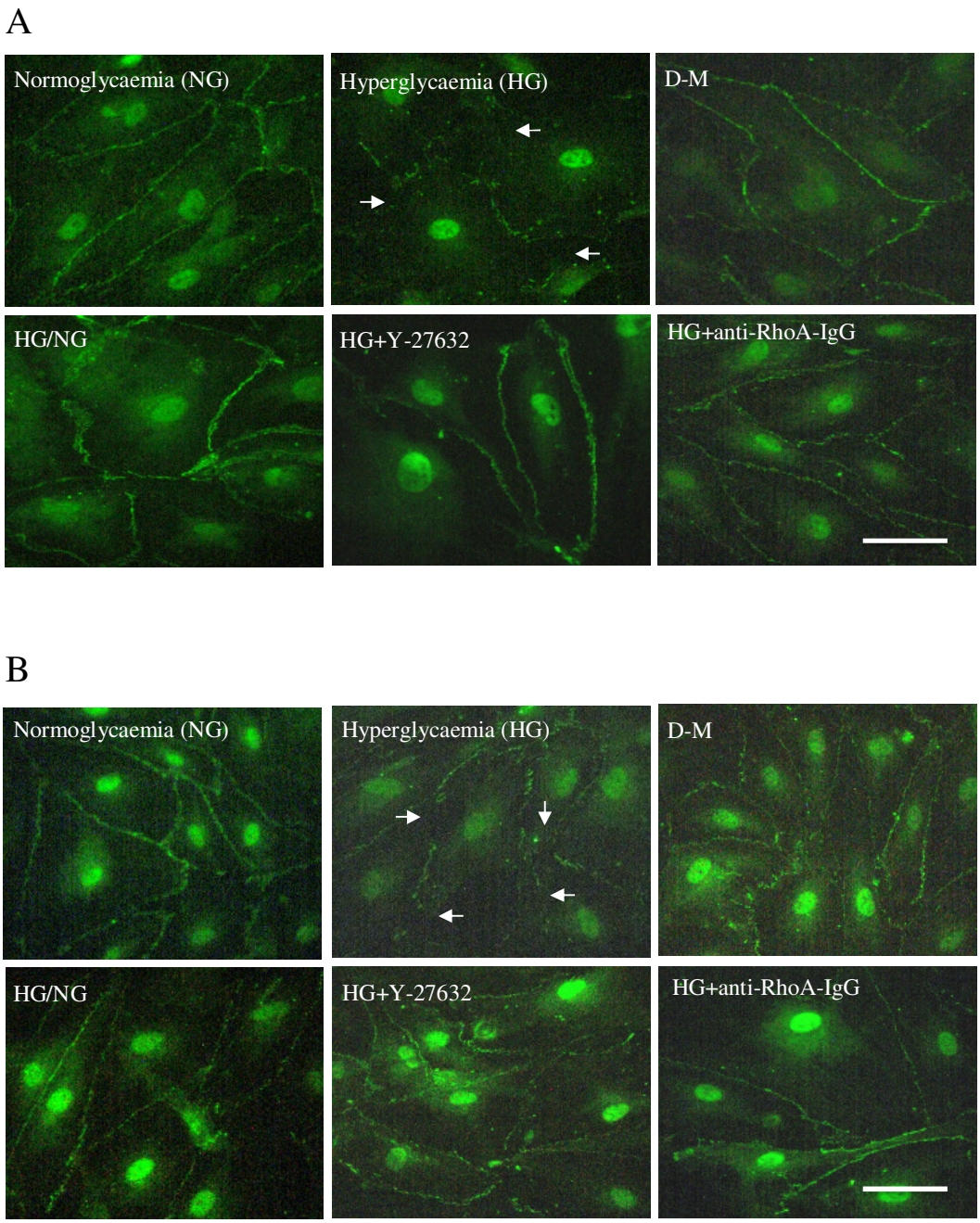

Figure 4.5. Hyperglycaemia disrupts tight junction complex. **(A)** occludin and **(B)** ZO-1 localisation in HBMEC detected by FITC-stainings. Arrows represent the gap formations after hyperglycaemic exposures. HBMEC were subjected to normoglycaemia (NG; 5.5 mM D-glucose), hyperglycaemia (HG; 25 mM D-glucose), D-mannitol (D-M; 5.5 mM D-glucose + 19.5 mM D-mannitol), HG followed by NG,

HG+Y-27632 (2.5 μM) and electroporated with anti-RhoA-IgG (3 μg) before exposing to HG. Data are collected from 3 different experiments. Bar scale: 50 μm.

The functional outcome of the hyperglycaemia-mediated changes observed in the aforementioned proteins were studied by measuring TEER values and the flux of permeability marker EBA across an *in vitro* model of human BBB. Hyperglycaemia compromised the *in vitro* cerebral-barrier integrity as evidenced by decrease in TEER values, and concomitant increase in the flux of EBA compared to those observed across cocultures subjected to normoglycaemia which served as controls ($P<0.05$) (Figure 4.6 A, B). However, suppression of RhoA and Rho-kinase activities by anti-RhoA-IgG electroporation and Y-27632, respectively, abrogated these defects and improved the cerebral-barrier function as observed by improvement in the TEER readings and concurrent reduction in the flux of EBA across the cocultures ($P<0.05$). Furthermore during hyperglycaemia, inhibitions of PKC and p38MAPK signalling pathways in HBMEC by cotreatments with a general PKC inhibitor Bis-I (5 μM) and a p38MAPK inhibitor SB203580 (10 μM), respectively, have also been shown to be cerebral-barrier protective as they maintained the normal barrier function similar to those observed in normoglycaemic cocultures (Figure 4.6 A, B). Taken together, these data indicate the involvements of RhoA, Rho-kinase, PKC and p38MAPK in the pathogenesis of hyperglycaemia-mediated cerebral-barrier breakdown.

A

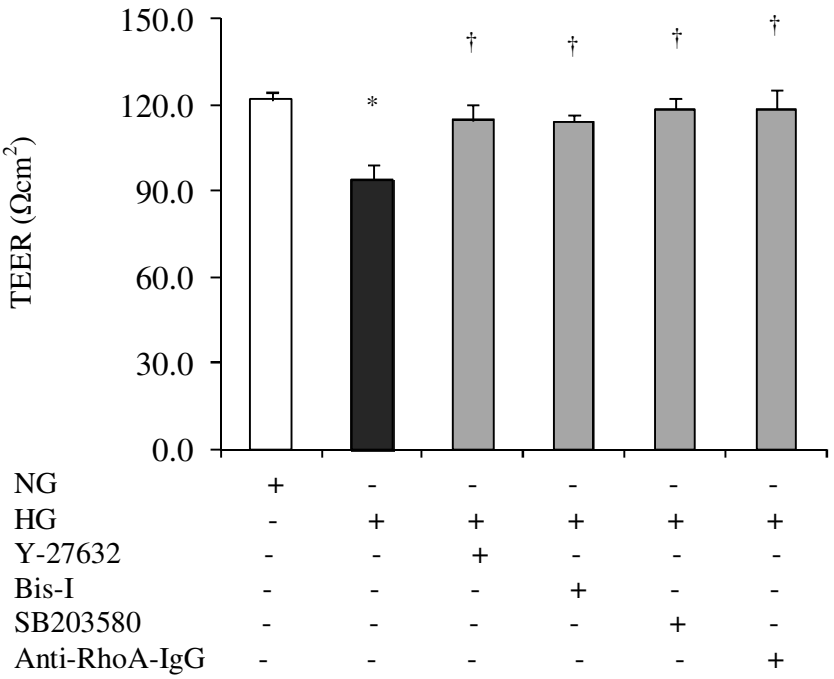
150.0
120.0
90.0
60.0
30.0
0.0
TEER (Ωcm2)
*
†
†
†
†
NG + - - - - -
HG - + + + + +
Y-27632 - - + - - -
Bis-I - - - + - -
SB203580 - - - - + -
Anti-RhoA-IgG - - - - - +

B

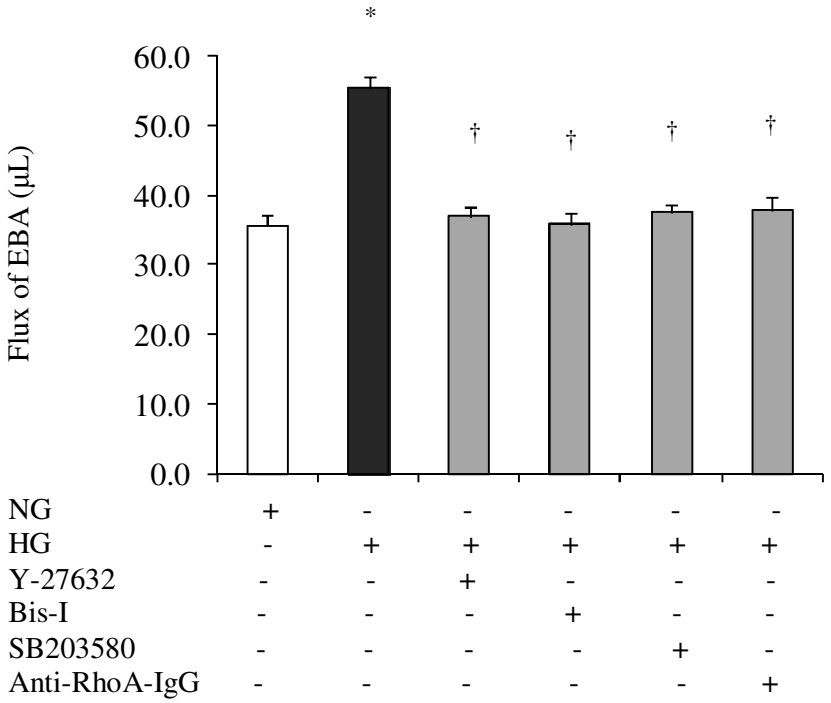
60.0
50.0
40.0
30.0
20.0
10.0
0.0
Flux of EBA (μL)
*
†
†
†
†
NG + - - - - -
HG - + + + + +
Y-27632 - - + - - -
Bis-I - - - + - -
SB203580 - - - - + -
Anti-RhoA-IgG - - - - - +

Figure 4.6. Measurement of integrity and function of an *in vitro* model of human BBB. **(A)** Transendothelial electrical resistance (TEER) (Ωcm^2) and **(B)** flux of EBA (µL) across the cocultures after exposures to normoglycaemia (NG; 5.5 mM D-Glucose), hyperglycaemia (HG; 25 mM D-glucose) alone or in the presence of inhibitors against Rho-kinase (Y-27632; 2.5 µM), PKC (Bis-I; 5 µM), p38MAPK (SB203580; 10 µM), and establishing cocultures with anti-RhoA-IgG (3µg) electroporated HBMEC before exposing to HG. Data are expressed as mean±SEM from 6 different experiments. Statistical analysis was done using ANOVA with Dunnet's *post hoc* test for multiple comparisons (A: $P<0.0001$, $F=32.597$, $df1=5$, $df2=30$), (B: $P<0.0001$, $F=23.589$, $df1=5$, $df2=30$). $^{*}P<0.05$ compared to NG, $^{\dagger}P<0.05$ compared to HG.

4.2.2. PKC-mediated modulation of RhoA/Rho-kinase/MLC2 pathway under hyperglycaemia

Since the inhibitions of RhoA/Rho-kinase, PKC and p38MAPK pathways exerted cerebral-barrier protective effects, in subsquent studies we aimed to determine the possible existence of a cross-talk between them. In relation to this, the cotreatment of HBMEC with either Bisindolylmaleimide-I (Bis-I) or SB203580 under hyperglycaemia did not alter the hyperglycaemia-mediated elevations observed in cellular RhoA protein levels. However, only the treatment with Bis-I normalised the Rho-kinase-2 protein levels ($P<0.05$). These data indicate that PKC signalling might be upstream to the Rho-kinase-2. In addition, cotreatment with SB203580 under hyperglycaemia did not affect the hyperglycaemia evoked Rho-kinase-2 levels (Figure 4.7 A, B). To further explore the link between these particular signalling pathways and RhoA/Rho-kinase/MLC2 system, the levels of MLC2 phosphorylation were observed in cells treated with PKC and p38MAPK inhibitors. It is of note here that the total MLC2 protein levels were unaffected in cells exposed to hyperglycaemic conditions in the absence or presence of Bis-I and SB203580. The treatment with Bis-I but not SB203580 attenuated the hyperglycaemia-evoked MLC2 mono- and di-phosphorylations when normalised against total MLC2 levels ($P<0.05$), thereby confirming the PKC-mediated modulation of Rho-kinase expression and activity (Figure 4.8 A, B).

To elucidate the effects of PKC-mediated modulation of RhoA/Rho-kinase/MLC2 signalling on HBMEC architecture, the cytoskeletal component, F-actin, was visualised. As stated before, the cells cultured under normoglycaemia displayed cortical actin stainings while those exposed to hyperglycaemia developed stress fibres traversing across the cells and acquired morphological changes characterised by

cuboidal or elongated appearances. Cotreatment with Bis-I reinstated cortical actin staining and dramatically reduced stress fibres alongside restoring the cellular morphology similar to that of HBMEC subjected to normoglycaemic conditions (Figure 4.8C). As the treatments with SB203580 slightly reduced the MLC2 diphosphorylation levels, it is safe to suggest that a separate pathway may be involved in p38MAPK inhibitor-dependent cerebral-barrier protection ($P<0.05$).

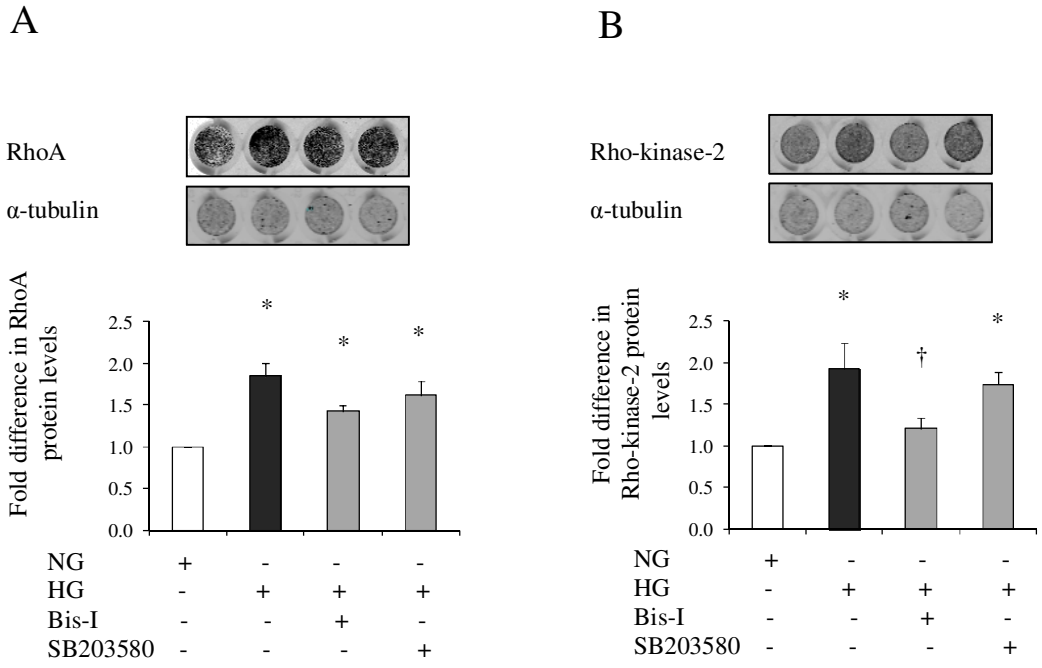

Figure 4.7. PKC modulates RhoA/Rho-kinase pathway. Representative in-cell Westerns and densitometric analyses of **(A)** RhoA, and **(B)** Rho-kinase-2 proteins in HBMEC after normalisation against α-tubulin. HBMEC were exposed to normoglycaemia (NG; 5.5 mM D-Glucose), hyperglycaemia (HG; 25 mM D-glucose) alone and in the presence of either Bis-I (5 μM) or SB203580 (10 μM). Data are expressed as mean±SEM from 4 different experiments. Statistical analysis was done using ANOVA with Dunnet's *post hoc* test for multiple comparisons (A: P=0.001,

F=12.401, df1=3, df2=12), (B: P=0.023, F=5.570, df1=3, df2=8). *P<0.05 compared to NG, †P<0.05 compared to HG.

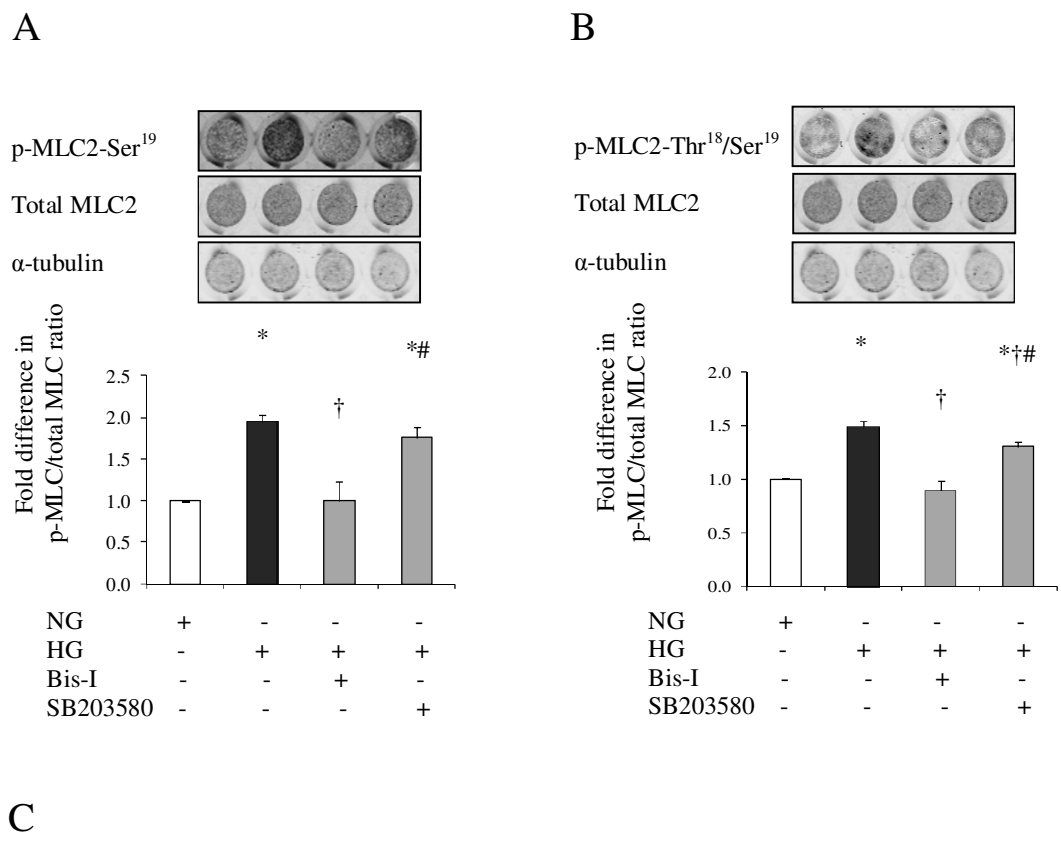

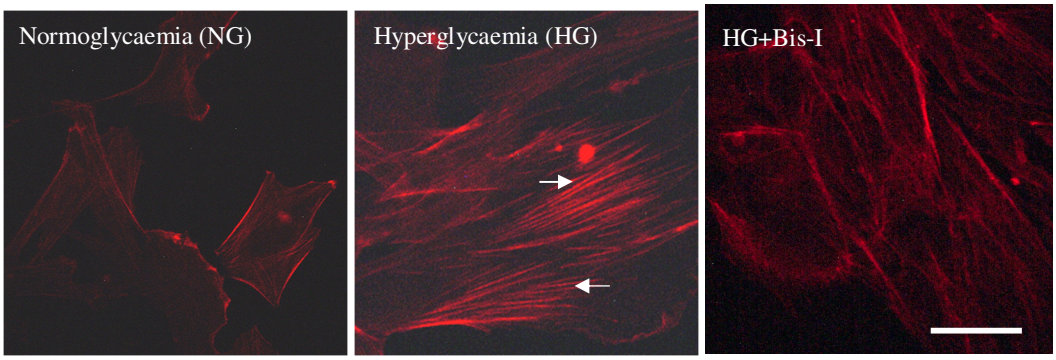

Figure 4.8. PKC modulates MLC2 mono/di- phosphorylations. Representative in-cell Westerns and densitometric analyses of **(A)** p-MLC2-Ser[19], and **(B)** p-MLC2-Thr[18]/Ser[19] in HBMEC after normalisation against total MLC2 and α-tubulin. **(C)** F-

actin stainings with Rhodamine-labelled phalloidin dye. HBMEC were exposed to normoglycaemia (NG; 5.5 mM D-Glucose), hyperglycaemia (HG; 25 mM D-glucose) alone and cotreated with either Bis-I (5 μM) or SB203580 (10 μM). Arrows represent stress fibre formations. Data are expressed as mean±SEM from 3 different experiments. Statistical analysis was done using ANOVA with Dunnet's *post hoc* test for multiple comparisons (A: P=0.002, F=12.857, df1=3, df2=8), (B: P=0.003, F=11.102, df1=3, df2=8). *P<0.05 compared to NG, †P<0.05 compared to HG, $^{\#}$P<0.05 compared to HG+Bis-I. Bar scale: 50 μm.

4.2.3. Effects of RhoA/Rho-kinase and isoform-specific PKC inhibitors on total PKC activity

In order to assess the effects of RhoA and Rho-kinase on total PKC activity, to further address the crosstalk between these signalling molecules, and to determine the relative contributions of specific PKC isoforms to the hyperglycaemia-mediated changes observed in PKC activity, the total PKC activities (units/mL) were measured in HBMEC exposed to normoglycaemia versus hyperglycaemia alone and in the presence of specific inhibitors for PKC-α, PKC-β, PKC-β_{II}, and PKC-δ isoforms. It was observed that hyperglycaemia significantly increased the total PKC activity (P<0.05), which was normalised by inhibition of RhoA and Rho-kinase by anti-RhoA-IgG electroporation and Y-27632 treatment, repectively, thus confirming the existence of the cross-talk and interdependence between these signalling pathways (P<0.05) (Figure 4.9A). The specific inhibitors of PKC-α (Ro-32-0432, 1 μM), PKC-β (LY333531, 0.5 μM), PKC-β_{II} (CGP53353, 1 μM) and PKC-δ (rottlerin, 5 μM) also attenuated the hyperglycaemia-mediated increases in the total PKC activity (P<0.05). Moreover, a dramatic attenuation was observed with PKC-α, PKC-β and PKC-δ inhibitors that reduced the PKC activity below the levels observed in normal cells

which might indicate the inhibition of constitutive activity as well ($P<0.01$) (Figure 4.9B). These data indicate that the bulk of PKC activity is governed by PKC-α, PKC-β and PKC-δ isoforms.

A

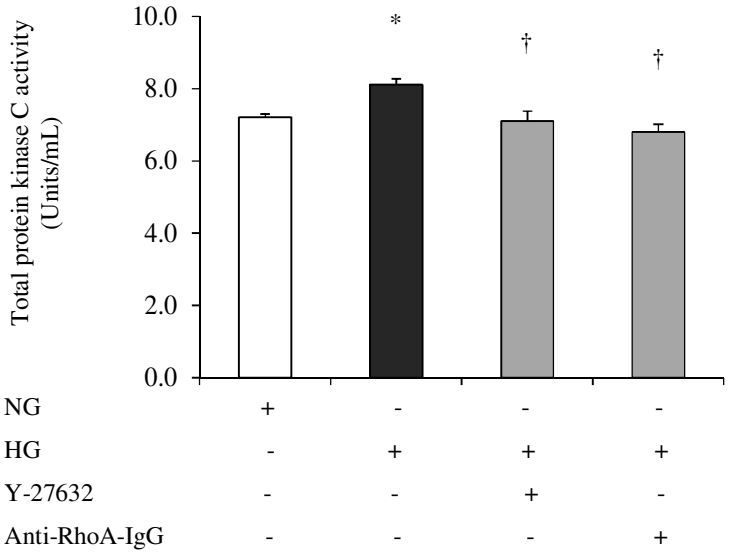

B

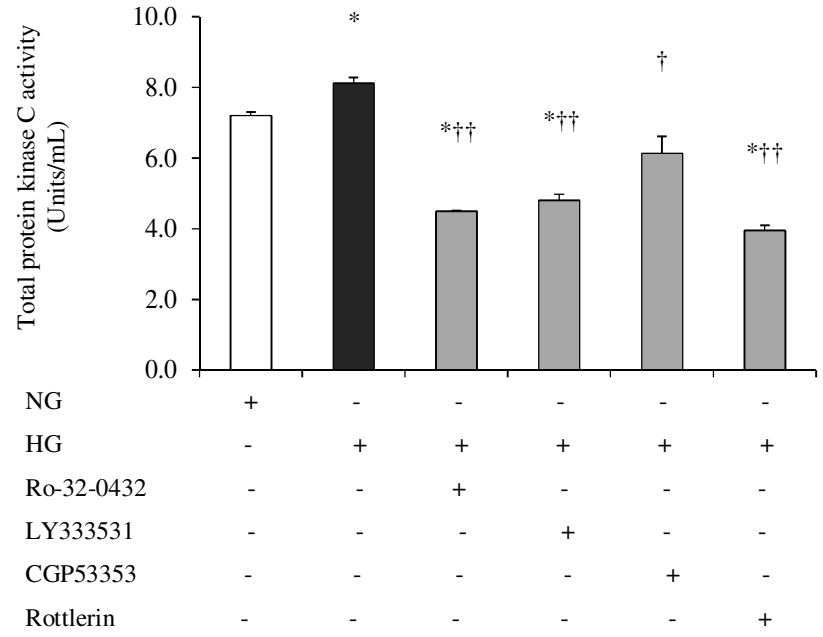

Figure 4.9. Inhibition of RhoA/Rho-kinase signalling and PKC isoforms attenuate the PKC overactivity under hyperglycaemia. **(A)** Total PKC activity (units/mL) measured in HBMEC subjected to normoglycaemia (NG; 5.5 mM D-glucose), hyperglycaemia (HG; 25 mM D-glucose) alone and in the presence of Y-27632 (2.5 μM), and anti-RhoA-IgG electroporation (3 μg) before HG. **(B)** Total PKC activity was measured in HBMEC exposed to NG, HG alone and with inhibitors of PKC-α (Ro-32-0432; 1 μM), PKC-β (LY333531; 0.5 μM), PKC-β_{II} (CGP53353; 1 μM), and PKC-δ (rottlerin; 5 μM). Data are expressed as mean±SEM from 5 different experiments. Statistical analysis was done using ANOVA with Dunnet's *post hoc* test for multiple comparisons (A: P=0.006, F=8.894, df1=3, df2=8), (B: P<0.0001, F=51.767, df1=5, df2=12). *P<0.05 compared to NG, †P<0.05 compared to HG, ††P<0.01 compared to HG.

4.2.4. Effects of PKC-α and PKC-β inhibitors on the BBB integrity, RhoA/Rho-kinase/MLC2 pathway, cytoskeletal reorganisation and junctional complex

Since we examined the effects of specific PKC isoform inhibitors in attenuating the hyperglycaemia-mediated PKC overactivity, these inhibitors were used to study their cerebral-barrier protective effects under hyperglycaemia. Despite reducing total PKC activity, the specific inhibitors of PKC-β_{II} and PKC-δ appeared to be inaffective in improving the hyperglycaemia-induced barrier damage which was confirmed by a marked decrease in the TEER values and concomitant increases in the flux of EBA across the cocultures ($P<0.05$) (Figure 4.10 A, B). However, the inhibition of PKC-α or PKC-β isoforms in cocultures exposed to hyperglycaemia improved the coculture integrity and function by increasing TEER and decreasing flux of EBA across the cocultures compared to the cocultures under hyperglycaemia ($P<0.05$) (Figure 4.10 A, B). This data substantiated our previous results and strengthened the focus on PKC-α and PKC-β isoforms in the forthcoming studies.

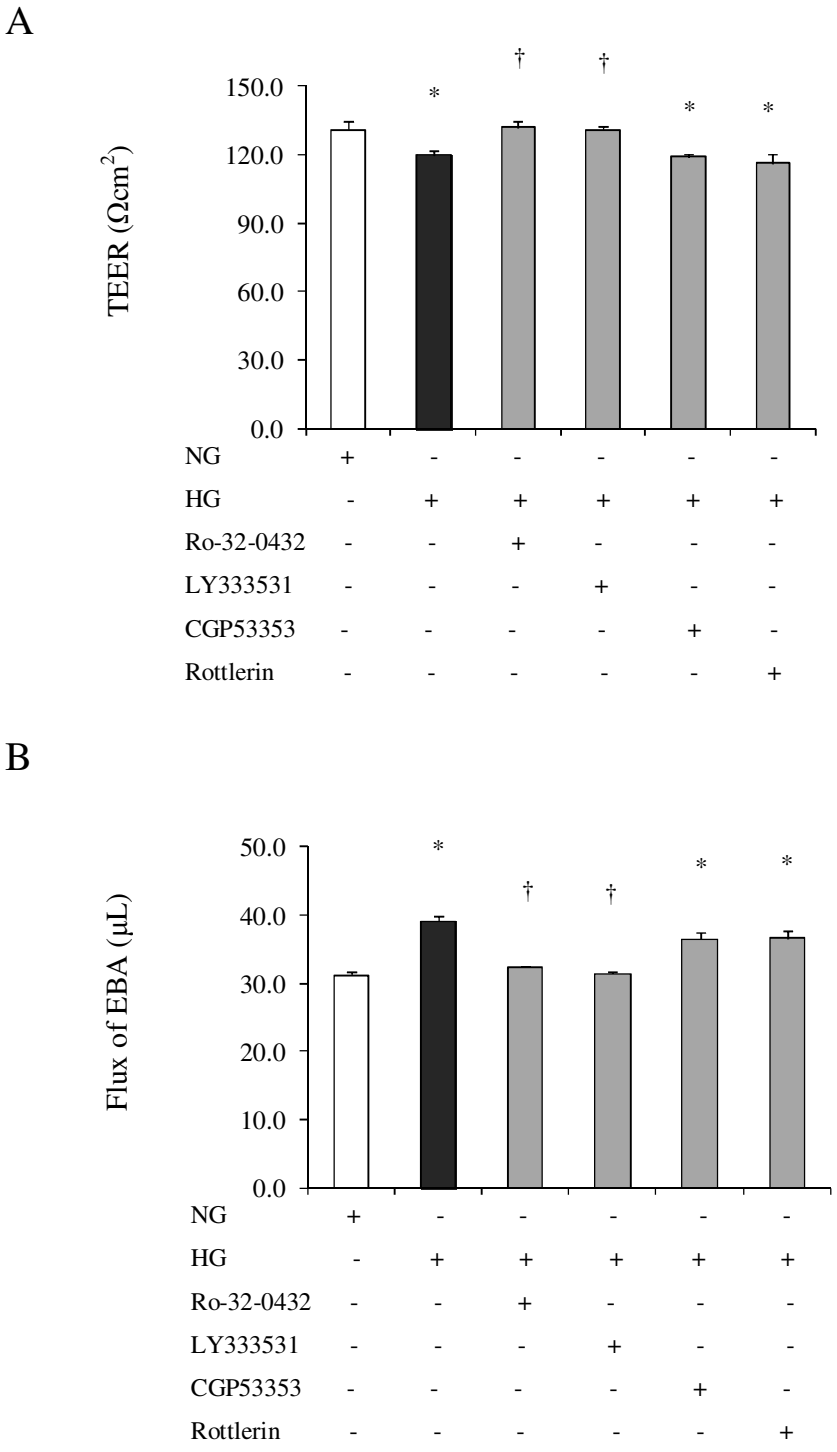

Figure 4.10. Effects of isoform-specific PKC inhibitors on the integrity and function of an *in vitro* model of human BBB. **(A)** Transendothelial electrical resistance (TEER) (Ωcm^2) and **(B)** flux of EBA (µL) across the cocultures after exposures to

normoglycaemia (NG; 5.5 mM D-glucose), hyperglycaemia (HG; 25 mM D-glucose), and HG with inhibitors of PKC-α (Ro-32-0432; 1 μM), PKC-β (LY333531; 0.5 μM), PKC-β_{II} (CGP53353; 1 μM), and PKC-δ (rottlerin; 5 μM). Data are expressed as mean±SEM from 5 different experiments. Statistical analysis was done using ANOVA with Dunnet's *post hoc* test for multiple comparisons (A: $P<0.0001$, $F=18.874$, $df1=5$, $df2=12$), (B: $P<0.001$, $F=16.245$, $df1=5$, $ddf2=12$). $^{*}P<0.05$ compared to NG, $^{\dagger}P<0.05$ compared to HG.

Having investigated the effects of inhibitors for PKC-α and PKC-β isoforms in attenuating the PKC overactivity and improving the coculture integrity, we aimed to elucidate whether these inhibitors regulate the RhoA/Rho-kinase signalling pathway. The use of rottlerin was discontinued in further experiements because of its multiple specificities for other kinase enzymes. It was observed that specific inhibition of PKC-α and PKC-β isoforms decreased the cellular RhoA protein levels in a dose-dependent manner, where statistical significance was achieved only with the highest doses of inhibitors used in the study (5 μM) ($P<0.05$) (Figure 4.11A). In addition, cotreatment with these inhibitors attenuated the hyperglycaemia-mediated 2-fold increase in the relative RhoA activities ($P<0.05$). These results indicate that PKC-α and PKC-β isoforms are involved in hyperglycaemia-mediated RhoA activation in HBMEC (Figure 4.11B). However, the effects of these inhibitors on Rho-kinase-2 protein levels were different. While different doses of PKC-β inhibitor and low doses of PKC-α inhibitor appeared to be ineffective against the hyperglycaemia-mediated increases in Rho-kinase-2 protein levels, only the high dose of PKC-α inhibitor (5 μM) normalised the Rho-kinase-2 levels and indicates that PKC activity regulates the Rho-kinase-2 expression (Figure 4.11C).

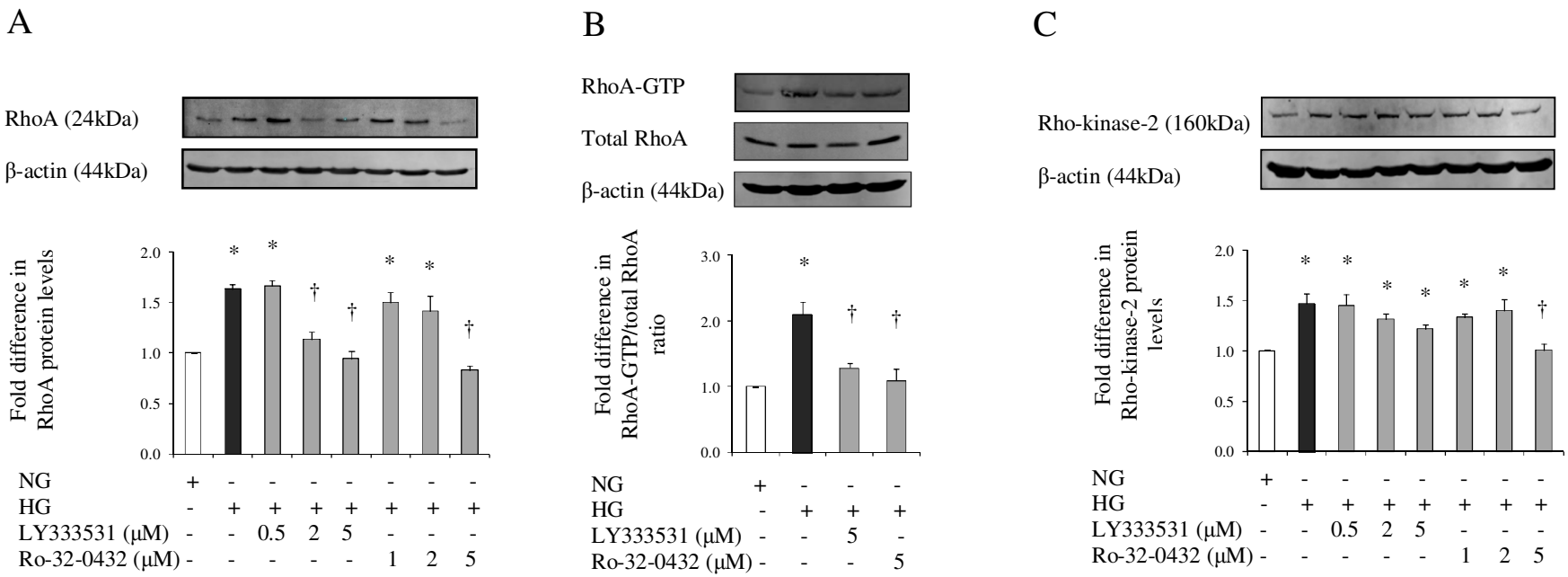

Figure 4.11. PKC-α and PKC-β isoforms-modulate RhoA/Rho-kinase signalling pathway. Representative Western blots and densitometric analyses of **(A)** RhoA protein levels, **(B)** RhoA activities and **(C)** Rho-kinase-2 protein levels in HBMEC exposed to normoglycaemia (NG; 5.5 mM D-glucose), hyperglycaemia (HG; 25 mM D-glucose), and HG with inhibitors of PKC-β (LY333531; 0.5-5 μM) and PKC-α (Ro-32-0432; 1-5 μM) after normalisation against β-actin. Data are expressed as mean±SEM from 5 different experiments. Statistical analysis was done using

ANOVA with Dunnet's *post hoc* test for multiple comparisons (A: $P<0.0001$, $F=8.771$, $df1=7$, $df2=16$), (B: $P<0.0001$, $F=27.706$, $df1=3$, $df2=8$), (C: $P=0.002$, $F=5.979$, $df1=7$, $df2=16$). $^{*}P<0.05$ compared to NG, $^{\dagger}P<0.05$ compared to HG.

To further study the importance of PKC-α and PKC-β isoforms in regulating the RhoA/Rho-kinase pathway, we investigated the levels of MLC2 mono- and di-phosphorylations. There were no significant differences in the total MLC2 protein levels in HBMEC exposed to varying doses of PKC-α and PKC-β isoform specific inhibitors. However, a dose-dependent decrease in the hyperglycaemia-evoked p-MLC2-Ser^{19} levels were recorded after normalisation against total MLC2 levels in HBMEC cotreated with these inhibitors under hyperglycaemia ($P<0.01$). In addition, the effects of these inhibitors on MLC2 di-phosphorylation levels (p-MLC2-Thr^{18}/Ser^{19}) were different. While inhibitors for PKC-β attenuated the hyperglycaemia-evoked p-MLC2-Thr^{18}/Ser^{19} levels in a dose-dependent manner ($P<0.05$), varying doses of PKC-α inhibitor appeared to be inaffective in modulating the p-MLC2-Thr^{18}/Ser^{19} levels (Figure 4.12 A, B).

To elucidate the effects of PKC-α and PKC-β-mediated modulation of RhoA/Rho-kinase/MLC2 signalling on cellular architecture, actin filaments was visualised in HBMEC exposed to hyperglycaemia in the absence or presence of PKC-α and PKC-β inhibitors. While the cells cultured under normoglycaemia displayed cortical actin stainings, those exposed to hyperglycaemia developed thick bundles of stress fibres and acquired elongated morphological appearances. Cotreatment with either PKC-α or PKC-β inhibitors reinstated cortical actin staining and dramatically reduced stress fibres alongside restoring the cellular morphology similar to that of HBMEC subjected to normoglycaemic conditions. (Figure 4.12C). Thus, these results indicate

that both PKC-α and PKC-β isoforms regulate the cytoskeletal remodelling. However, the therapeutic effects of the PKC-β inhibition appear to be more sustainable during the hyperglycaemic insult.

A

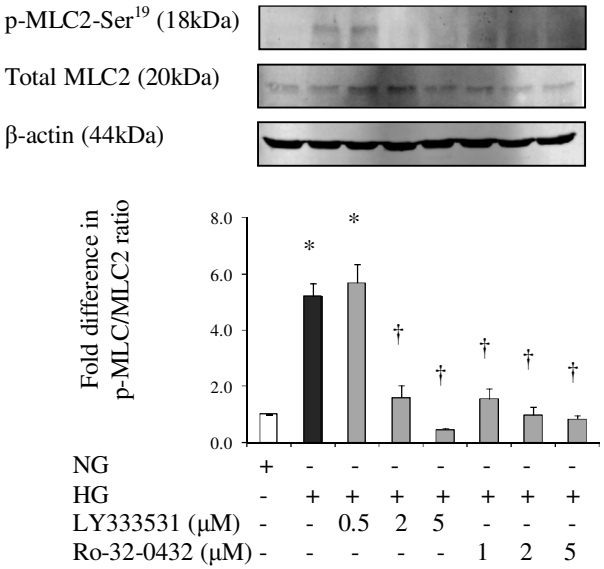
p-MLC2-Ser19 (18kDa)
Total MLC2 (20kDa)
β-actin (44kDa)
Fold difference in p-MLC/MLC2 ratio
8.0
6.0
4.0
2.0
0.0
NG + - - - - - - -
HG - + + + + + + +
LY333531 (μM) - - 0.5 2 5 - - -
Ro-32-0432 (μM) - - - - - 1 2 5

B

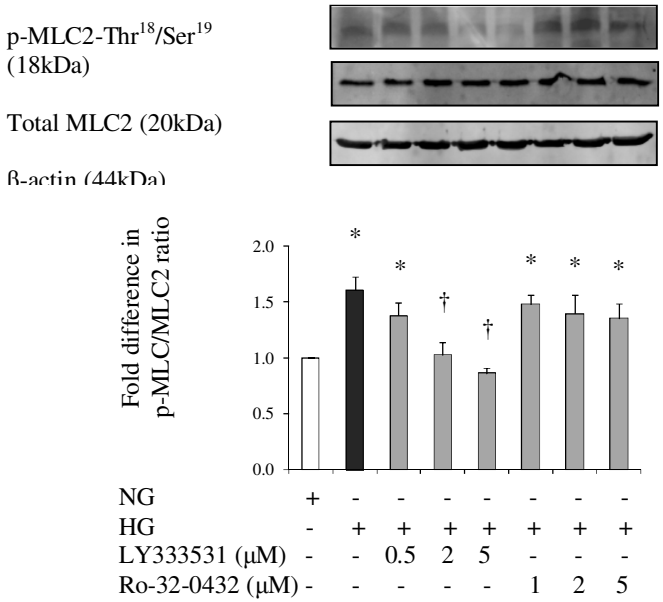
p-MLC2-Thr18/Ser19 (18kDa)
Total MLC2 (20kDa)
β-actin (44kDa)
Fold difference in p-MLC/MLC2 ratio
2.0
1.5
1.0
0.5
0.0
NG + - - - - - - -
HG - + + + + + + +
LY333531 (μM) - - 0.5 2 5 - - -
Ro-32-0432 (μM) - - - - - 1 2 5

C

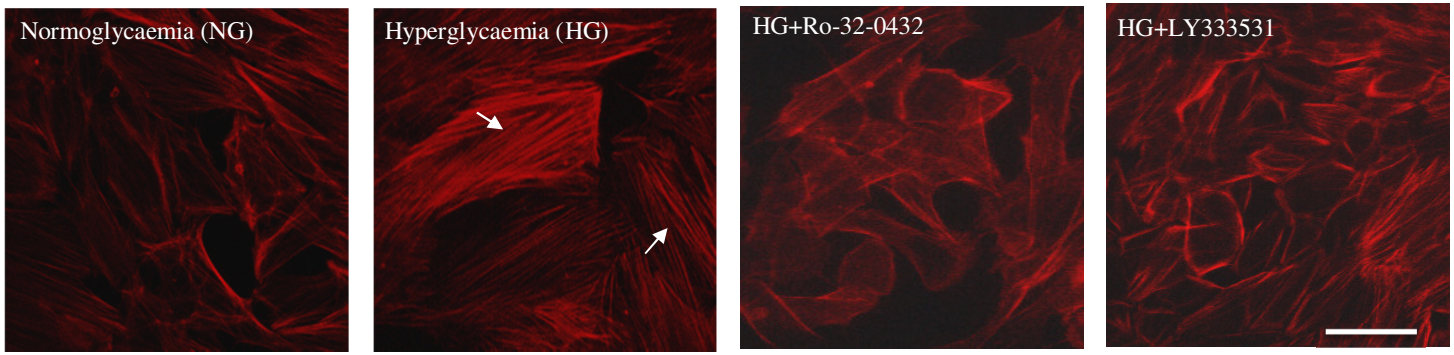
Normoglycaemia (NG)
Hyperglycaemia (HG)
HG+Ro-32-0432
HG+LY333531

Figure 4.12. Effect of PKC-α and PKC-β inhibitors on MLC2 phosphorylation and cytoskeletal reorganisation. Representative Western blots and densitometric analyses of **(A)** p-MLC2-Ser^{19}, **(B)** p-MLC2-Thr^{18}/Ser^{19} in HBMEC subjected to normoglycaemia (NG; 5.5 mM D-glucose), hyperglycaemia (HG; 25 mM D-glucose), and HG with inhibitors of PKC-β (LY333531; 0.5-5 μM), PKC-α (Ro-32-0432; 1-5 μM) after normalisation against total MLC2 levels and β-actin. **(C)** F-actin stainings in HBMEC exposed to aforementioned conditions. Following the treatments, the cells were fixed, permeabilised, blocked, incubated with Rhodamine-labelled phalloidin dye and identified by 40X magnification on fluorescent microscope. Arrows represent the stress fibre formations. Data are expressed as mean±SEM from 5 different experiments. Statistical analysis was done using ANOVA with Dunnet's *post hoc* test for multiple comparisons (A: $P<0.0001$, $F=37.543$, $df1=7$, $df2=16$), (B: $P<0.0001$, $F=8.564$, $df1=7$, $df2=16$). $^{*}P<0.05$ compared to NG, $^{\dagger}P<0.05$ compared to HG. Bar scale: 50 μm.

Given the effects of PKC-α and PKC-β inhibitors in improving the integrity and function of cerebral barrier under hyperglycaemia, it was highly likely that these effects emerge from the induction of tighter assembly of junctions via regulation of tight junction proteins. In support of this notion, treatment with different doses of PKC-α and PKC-β inhibitors appeared to abolish the hyperglycaemia-mediated supression of occludin protein expression in HBMEC and improved its levels to that observed in HBMEC under normoglycaemic condition ($P<0.05$) (Figure 4.13A). However, the effects of these inhibitors on ZO-1 protein levels was slightly different. While the PKC-β inhibitor increased the ZO-1 protein levels in a dose-dependent manner ($P<0.05$), the varying doses of PKC-α inhibitor appeared to be ineffective in modulating the ZO-1 protein levels compared to the ZO-1 levels observed in HBMEC

under normoglycaemia (Figure 4.13B). These data indicate the clinical importance of the PKC-β inhibition in improving the tight junction protein levels and indeed the cerebral-barrier integrity.

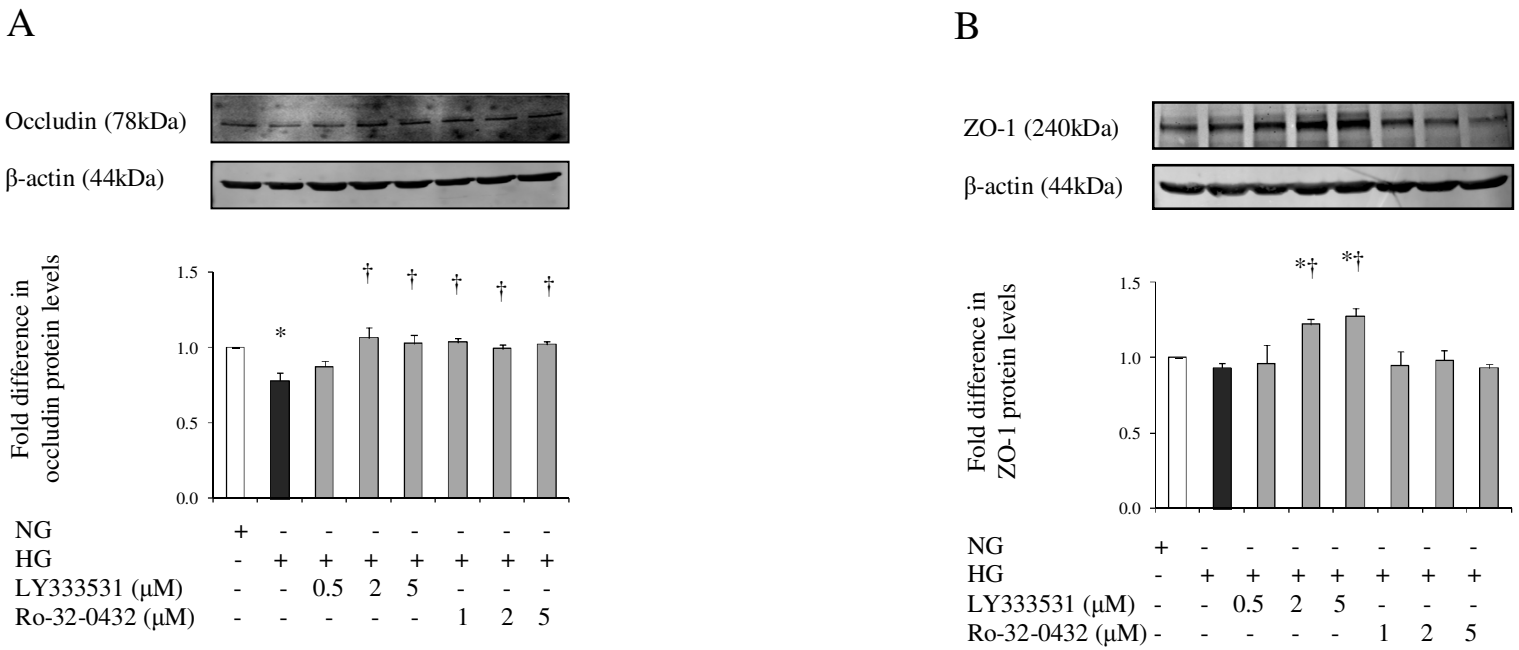

Figure 4.13. PKC-α and PKC-β inhibitors improve tight junction protein levels. Representative Western blots and densitometric analyses of **(A)** occludin, **(B)** ZO-1 in HBMEC subjected to normoglycaemia (NG; 5.5 mM D-glucose), hyperglycaemia (HG; 25 mM D-glucose), and HG with inhibitors of PKC-β (LY333531; 0.5-5 μM) and PKC-α (Ro-32-0432; 1-5 μM) after normalisation against β-actin. Data are expressed as

mean±SEM from 5 different experiments. Statistical analysis was done using ANOVA with Dunnet's *post hoc* test for multiple comparisons (A; P=0.002, F=5.572, df1=7, df2=16), (B: P=0.005, F=4.651, df1=7, df2=16). *P<0.05 compared to NG, †P<0.05 compared to HG.

4.2.5. Effects of PKC-α and PKC-β protein knockdown by siRNA transfection on the RhoA activity, MLC2 phosphorylation, cytoskeletal reorganisation and junctional complex

Although the PKC isoform inhibitors used in this study have high specificity for PKC-α and PKC-β isoforms, they are also specific for other PKC isoforms with low IC_{50} values. Hence to eliminate the non-target specific effects of these inhibitors, the siRNA gene knockdown studies were carried out to confirm the effects of these pharmacological inhibitors. Under normal and hyperglycaemic conditions, HBMEC were transfected with equal amounts (50-100 nM) of either non-target, PKC-α or PKC-β siRNA oligonucleotides via lipid based transfection reagents. The successful siRNA transfection and protein knockdown were confirmed by a dramatic reduction in the protein levels of PKC-α and PKC-β isoforms by 80% and 50%, respectively, compared to the non-target siRNA transfected HBMEC which served as negative controls ($P<0.05$) (Figure 4.14A). The decrease in protein levels of either isoforms alleviated the relative RhoA activities as a marked reduction in the RhoA-GTP levels were recorded after normalisation against total RhoA levels ($P<0.05$) (Figure 4.14B). These results confirm the role of PKC-α and PKC-β isoforms in the activation of RhoA-driven signalling pathways.

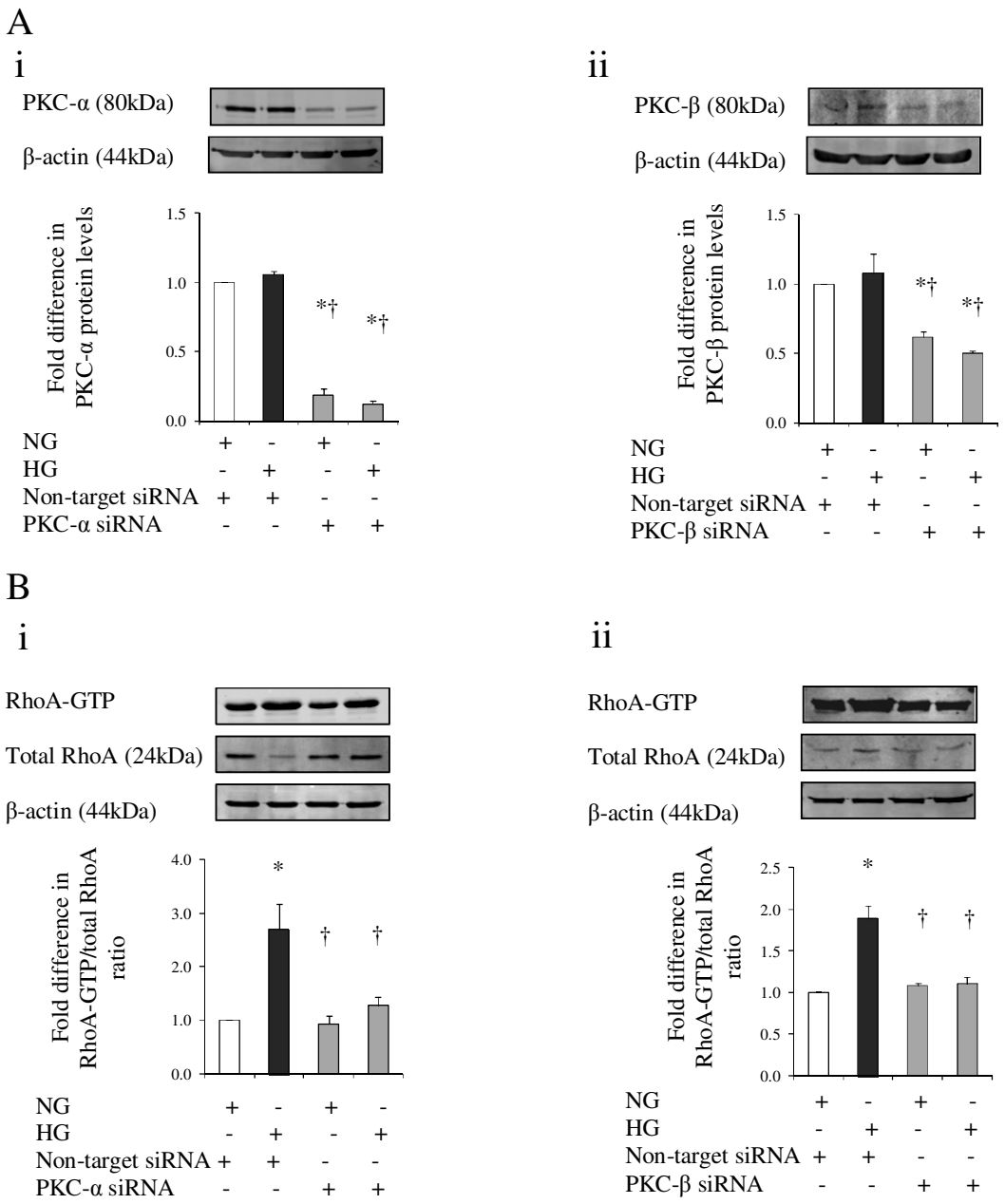

Figure 4.14. PKC-α and PKC-β gene knockdown and their effect on the relative RhoA activity. Representative Western blots and densitometric analyses of **(A)** PKC-α and PKC-β, and **(B)** relative RhoA activities in HBMEC transfected with PKC-α, PKC-β and non-target siRNA before exposure to normoglycaemia (NG; 5.5 mM D-glucose) and hyperglycaemia (HG; 25 mM D-glucose) for 72 hours. Data are expressed as mean±SEM from 4 different experiments. Statistical analysis was done using ANOVA with Dunnet's *post hoc* test for multiple comparisons (Ai: P<0.0001,

F=793.944, df1=3, df2=8; Aii: P<0.0001, F=44.8, df1=3, df2=8), (Bi: P=0.006, F=9.214, df1=3, df2=8, Bii: P<0.0001, F=20.75, df1=3, df2=8). *P<0.05 compared to NG, †P<0.05 compared to HG.

The role of PKC isoforms in hyperglycaemia-evoked MLC2 phosphorylation was further studied in PKC-α or PKC-β knockdown HBMEC. A dramatic reduction in the p-MLC2-Ser^{19} and p-MLC2-Thr^{18}/Ser^{19} protein levels were recorded in PKC-β knockdown HBMEC compared to the negative controls under hyperglycaemic conditions (P<0.05) (Figure 4.15A). These results confirm that PKC-β plays a pivotal role in enhanced MLC2 mono- and di-phosphorylations under hyperglycaemia. The PKC-α knockdown significantly decreased the hyperglycaemia-evoked p-MLC2-Ser^{19} levels in HBMEC compared to the negative controls (P<0.05). However, the PKC-α knockdown was ineffective in modulating the hyperglycaemia-evoked MLC2 di-phosphorylation (Figure 4.15B). These results go hand in hand with the previous pharmacological data and highlight the significance of PKC-β inhibition.

Since MLC2 phosphorylations enhance the cytoskeletal reorganisation, the effects of PKC-α and PKC-β isoforms were studied by exploring the F-actin localisation in siRNA transfected HBMEC to investigate their role in the hyperglycaemia-evoked cytoskeletal remodelling. The HBMEC serving as negative controls showed faint marginal F-actin stainings with spindle shape cellular morphology under normoglycaemia. However, hyperglycaemic exposure induced thick bundles of stress fibre formations traversing across the cells along with cells attaining an elongated morphology. The PKC-α knockdown in HBMEC induced thick cortical F-actin stainings under normoglycaemia and appeared to reduce the stress fibre formations and restore the cellular morphology under hyperglycaemia. However, a dramatic

reduction in the stress fibre formation along with thick cortical stainings and cobble-stone or spindle cellular morphologies were recorded in the PKC-β knockdown HBMEC under hyperglycaemia which seemed identical to the siRNA transfected HBMEC under normoglycaemia (Figure 4.16). Thus, these results confirm the therapeutic potential of PKC-β knockdown in attenuating the hyperglycaemia-evoked cytoskeletal remodelling.

To demonstrate whether formation of compact junctional complexes is involved in PKC-α and PKC-β inhibition-mediated protection of cerebral barrier integrity, the levels of occludin and ZO-1 proteins were investigated in non-target versus PKC-α and PKC-β siRNA-transfected HBMEC. Exposure of HBMEC to hyperglycaemia markedly decreased occludin protein expression without significantly altering the ZO-1 protein levels. However, inhibition of PKC-β dramatically enhanced the expressions of both occludin and ZO-1 under hyperglycaemic conditions while selectively improving occludin levels under normoglycaemia ($P<0.05$) (Figure 4.17A). Inhibition of PKC-α on the other hand, prevented hyperglycaemia-mediated decreases in occludin expression without affecting that of ZO-1 (Figure 4.17B). These data reiterate the clinical importance of PKC-β inhibition in improving the tight junction protein levels and indeed the cerebral barrier integrity.

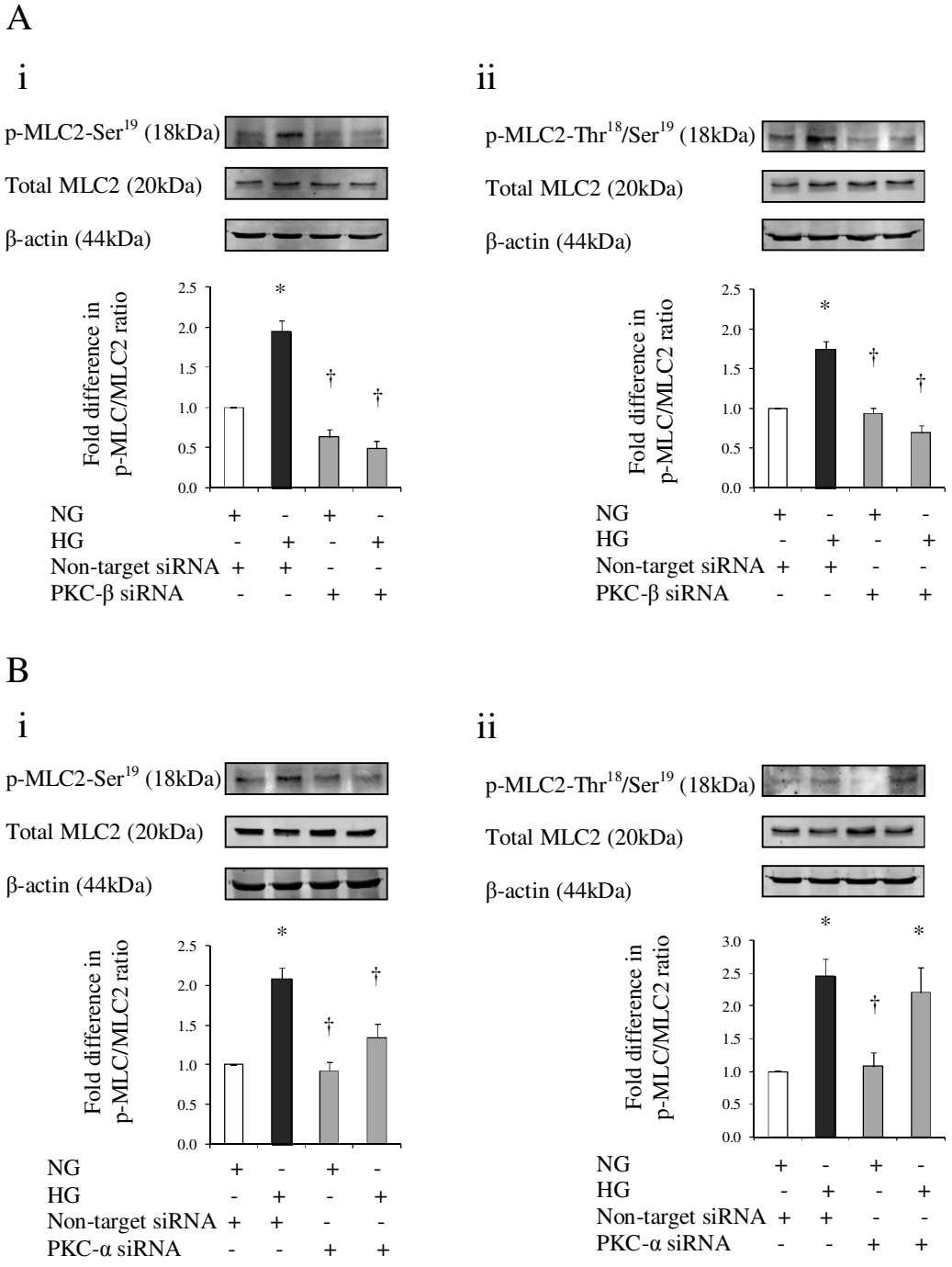

Figure 4.15. PKC-α and PKC-β gene knockdown attenuates the MLC2 phosphorylations. Representative Western blots and densitometric analyses of p-MLC2-Ser^{19} and p-MLC2-Thr^{18}/Ser^{19} levels in **(A)** PKC-β, and **(B)** PKC-α knockdown HBMEC. The cells were transfected with PKC-α, PKC-β and non-target siRNA before exposure to normoglycaemia (NG; 5.5 mM D-glucose) and

hyperglycaemia (HG; 25 mM D-glucose) for 72 hours. Data are expressed as mean±SEM from 5 different experiments. Statistical analysis was done using ANOVA with Dunnet's *post hoc* test for multiple comparisons (Ai: P<0.0001, F=47.581, df1=3, df2=8; Aii: P<0.0001, F=32.65, df1=3, df2=8), (Bi: P=0.001, F=17.021, df1=3, df2=8; Bii: P=0.010, F=7.539, df1=3, df2=8). *P<0.05 compared to NG, †P<0.05 compared to HG.

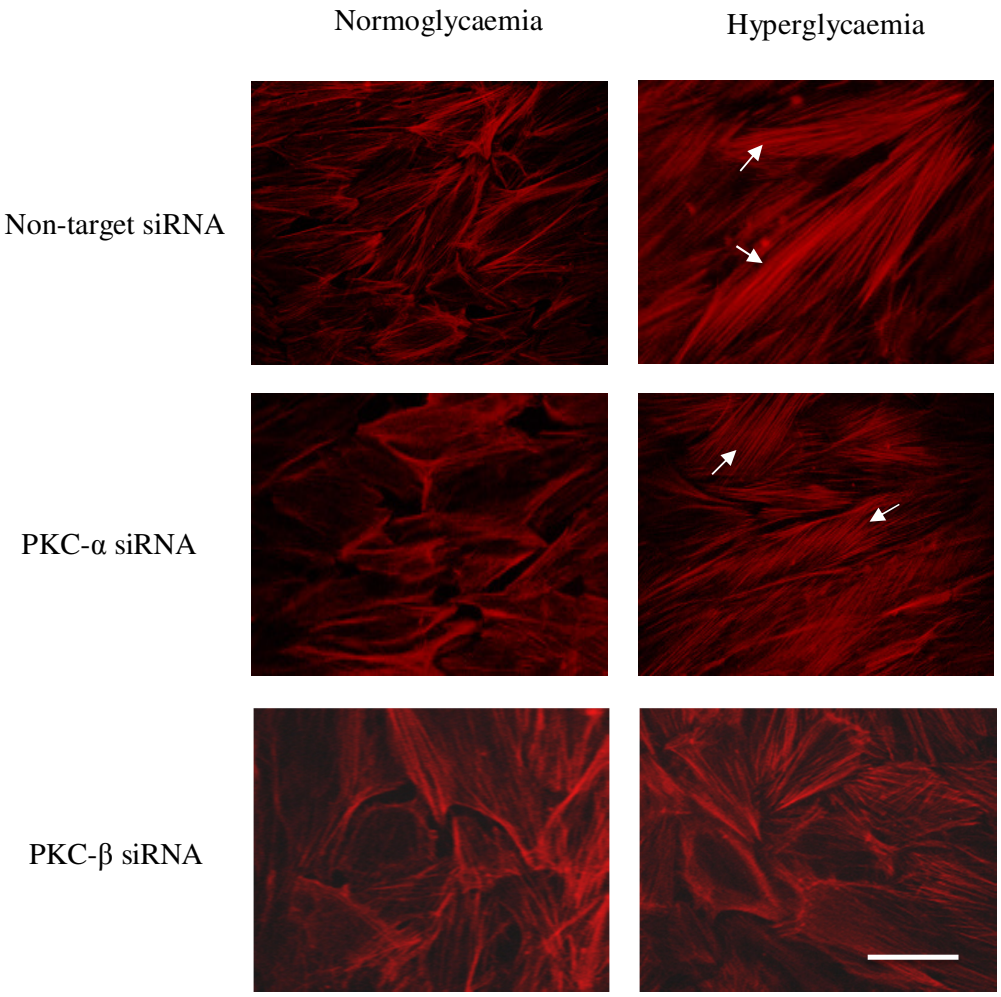

Figure 4.16. PKC-α and PKC-β gene knockdown studies to investigate the hyperglycaemia-induced cytoskeletal remodelling. HBMEC were transfected with PKC-α siRNA (50 nM), PKC-β siRNA (100 nM) and non-target siRNA (50-100 nM)

before exposure to normoglycaemia (5.5 mM D-glucose) and hyperglycaemia (25 mM D-glucose) for 72 hours. Following the treatments, the cells were fixed, permeabilised, blocked, and incubated with Rhodamine-labelled phalloidin dye. The cells were incubated with DAPI and were identified by 40X magnification on fluorescent microscope. Arrows represent the stress fibre formations after the hyperglycaemia exposure. Data are collected from 5 different experiments. Bar scale: 50 μm.

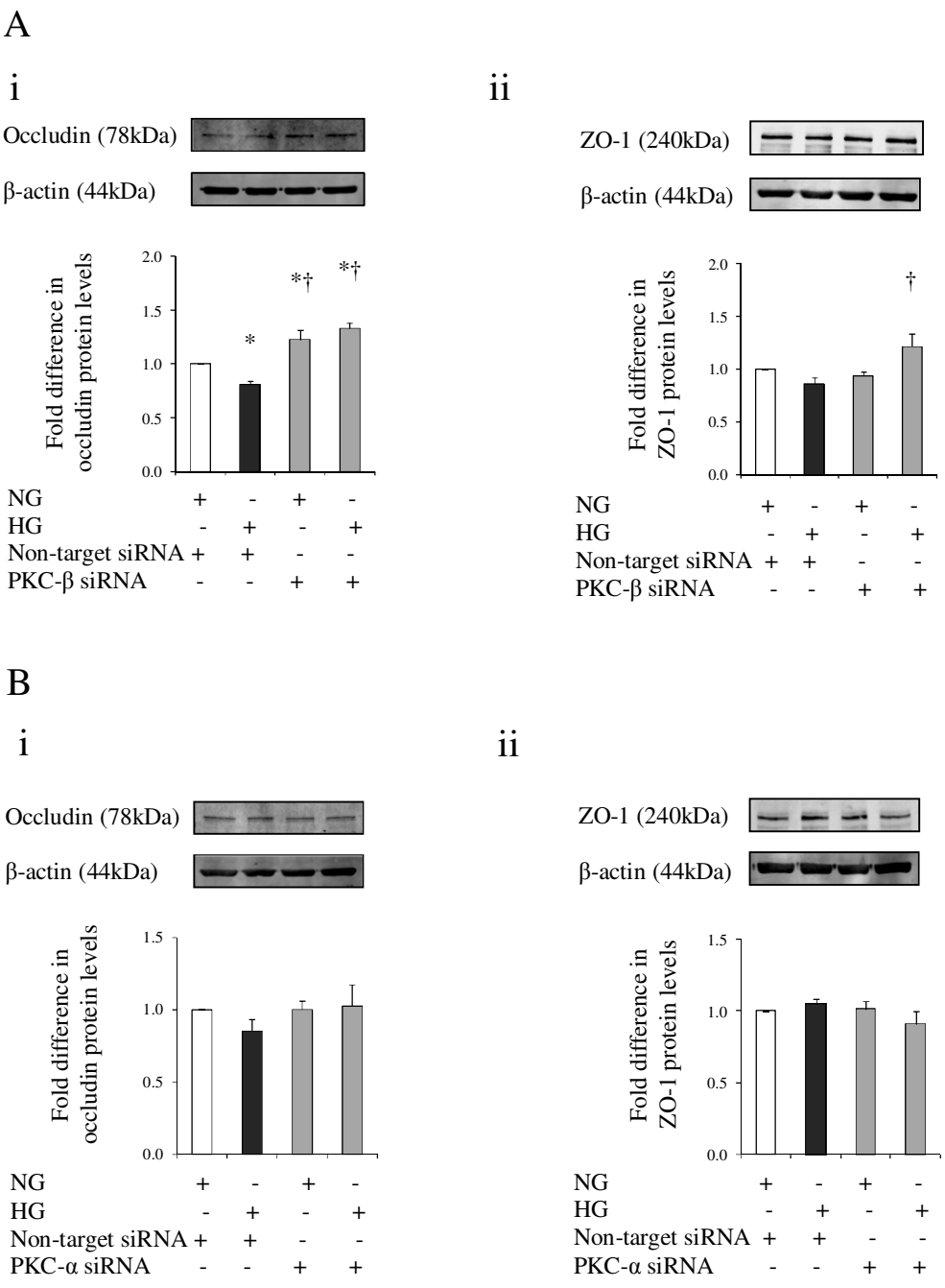

Figure 4.17. PKC-α and PKC-β gene knockdown modulate tight junction complex. Representative Western blots and densitometric analyses of occludin and ZO-1 protein levels in **(A)** PKC-β, and **(B)** PKC-α knockdown HBMEC. The cells were transfected with PKC-α, PKC-β and non-target siRNA before exposure to normoglycaemia (NG; 5.5 mM D-glucose) and hyperglycaemia (HG; 25 mM D-

glucose) for 72 hours. Data are expressed as mean±SEM from 3 different experiments. Statistical analysis was done using ANOVA with Dunnet's *post hoc* test for multiple comparisons (Ai: P=0.003, F=11.484, df1=3, df2=8; Aii: P=0.004, F=10.193, df1=3, df2=8), (Bi: P=0.522, F=0.813, df1=3, df2=8; Bii: P=0.077, F=3.328, df1=3, df2=8). *P<0.05 compared to NG, †P<0.05 compared to HG.

4.3. Discussion

Brain oedema emerging from disruption of the BBB constitutes one of the leading causes of mortality after a stroke and appears to be more prevalent in stroke patients with diabetes than those without thereby implying a prominent role for hyperglycaemia in the BBB breakdown (Ergul et al., 2009). The current study investigated whether the overactivation of RhoA/Rho-kinase/MLC2 pathway is implicated in hyperglycaemia-mediated barrier damage. Using a microplate-based immunocytochemical assay i.e. in-cell Western analysis, designed to detect proteins in their cellular context to produce more relevant results via elimination of cell lysis-derived artefacts, this study has shown that hyperglycaemia elicits significant increases in HBMEC RhoA and Rho-kinase-2 protein expressions and RhoA activity. Since equimolar concentrations of D-mannitol did not affect cell viability, protein expression or enzyme activity, it is safe to suggest that all the aforementioned alterations are a consequence of hyperglycaemia itself rather than a rise in osmolality or cell death. It is of note that the presence of such close link between hyperglycaemia and RhoA/Rho-kinase pathway overactivity is also documented in basilar artery sections of type-1 diabetic rats and in endothelial cells originated from different species and parts of vascular tree such as human saphenous vein and bovine aorta (Miao et al., 2002, Rikitake and Liao, 2005b, Iwasaki et al., 2008).

Hyperglycaemia represents a common phenomenon in stroke patients, with up to ~65-70% of patients known to manifest hyperglycaemia at some stage within 48 hours of stroke onset as a result of diabetes or acute stress response. Clinical evidence regarding the extent of glycaemic control in acute ischaemic stroke patients is limited. However, given the close correlation between hyperglycaemia and poor outcomes, typically defined by enhanced mortality or dependence 90 days after the event, it remains important to monitor and reduce blood glucose levels in an effective manner (Capes et al., 2001, Baird et al., 2002). Indeed, normalisation of glucose levels in the current study returned the increases observed in RhoA, Rho-kinase-2 protein expression and RhoA activity to the levels obtained in control groups and provided some mechanistic evidence for the benefits that may be produced by efficacious glycaemic control. Unlike glycaemic control, the specific inhibition of Rho-kinase-2 by Y-27632, a competitive-ATP inhibitor, failed to normalise the expression and activity of RhoA and Rho-kinase-2. Thus, ruling out the existence of a negative feedback mechanism by which the bioavailability of Rho-kinase may influence RhoA expression and activity. Since equimolar concentrations of D-mannitol did not alter protein expressions and activity, it is safe to suggest that the outlined alterations are due to glucose *per se* rather than a glucose-mediated rise in osmolality. Similarly, these alterations cannot be attributed to differences in cell numbers and viability because the protein levels observed in each experiment were normalised against α-tubulin that was detected concurrently as an internal standard. Moreover, as the electroporation process diminished cell viability by ~23%, the number of cells seeded were increased by 30% following this procedure to enable all experimental groups to reach confluence simultaneously.

Studies investigating the effects of hyperglycaemia on *in vitro* barrier integrity and function demonstrated substantial decreases in the TEER values which were indicative of the physical disruptions to the endothelial barrier and lead to concomitant rise in the EBA flux across the cocultures. In addition, the inhibitions of signalling molecules like Rho-kinase (Y-27632), PKC (Bis-I), and p38MAPK (SB203580) improved the coculture integrity by attenuating the hyperglycaemia-induced endothelial-barrier disruptions characterised by an improved TEER and reduced EBA flux; and demonstrated the detrimental effects of these signalling pathways under hyperglycaemia. Since changes in cytoskeleton may contribute to the hyperglycaemia-induced barrier failure, the status of actin filament formation and distribution was comparatively studied. Cells cultured under normoglycaemic conditions displayed a cortical actin staining while those subjected to hyperglycaemia possessed actin stress fibres traversing the cells and appeared predominantly elongated and somewhat cuboidal. The appearance of stress fibres coincided with enhanced MLC2 mono- and di-phosphorylation at Ser^{19} and/or Thr^{18} possibly through the activations of MLCK and Rho-kinase, and/or inhibition of MLCP (Fukata et al., 2001, van Nieuw Amerongen and van Hinsbergh, 2001). Once the actin stress bundles are formed, they lead to the intercellular gap formations by compromising tight junctions via generation of a tensile centripetal force to pull the tight junction proteins inward (Sumi et al., 2001, Allen et al., 2010). Normalisation of glucose levels along with inhibition of RhoA or Rho-kinase before and during hyperglycaemic challenge by anti-RhoA-IgG electroporation and Y-27632, respectively, prevented stress fibre formation, restored actin staining in cell periphery and abolished the barrier disruptive effects of hyperglycaemia. Despite significantly reducing p-MLC2-Ser^{19} levels compared with normoglycaemia and hyperglycaemia HBMEC, Y-27632 cotreatments

normalised the p-MLC2-Thr^{18}/Ser^{19} levels and failed to affect total MLC2 expression, suggesting the notion that diphosphosphorylated isoform may make up the main constituent of total MLC2 under hyperglycaemic conditions. Apart from MLC2, RhoA/Rho-kinase pathway can also phosphorylate adducin, LIMK and ERM proteins which link a number of proteins such as spectrin and cofilin to cortical actin and modulate actin filament (de)stabilisation (Matsui et al., 1998, Ohashi et al., 2000, Sumi et al., 2001). Moreover, RhoA/Rho-kinase pathway-mediated changes in actin cytoskeleton are also implicated in diminished expression, phosphorylation (at Ser^{1177}) and activity of eNOS and thus reduced availability of NO, a barrier protective agent, while inhibition of Rho activity by statins are known to produce the opposite effects (Rikitake and Liao, 2005a).

Impaired organisation of the tight junction proteins which seal the edges between adjacent endothelial cells to control paracellular permeability may also be a key determinant of hyperglycaemia-evoked barrier failure. Indeed, a discontinuous pattern of the transmembrane occludin and the cytoplasmic ZO-1 staining at cell borders coupled with the reduced expressions of the occludin in hyperglycaemic cells confirmed this hypothesis. Normalisation of glucose levels and inhibition of RhoA or Rho-kinase-2 significantly improved the occludin protein levels and restored the occludin and ZO-1 staining to the cell periphery. These concurred with the findings of previous *in vivo* studies which correlated the levels of tight junction proteins with enhanced retinal hyperpermeability, and insulin-mediated glycaemic control of diabetic animals significantly ameliorated the reduced cerebral contents of occludin and ZO-1 (Antonetti et al., 1998, Chehade et al., 2002, Barber and Antonetti, 2003, Hawkins et al., 2007). More importantly the inhibition of RhoA/Rho-kinase pathway is clinically relevant in restoring the occludin and ZO-1 levels and cytoplasmic

trafficking under hyperglycaemia. This might also be due to an increased RhoA/Rho-kinase-mediated phosphorylation of tight junction proteins triggering their cytoplasmic trafficking. Recent *in vitro* and *in vivo* studies on brain endothelial cells supports this hypothesis and demonstrates three specific sites of phosphorylation on occludin and claudin-5 after RhoA/Rho-kinase activation which were accompanied by functional impairment of barrier and prevented by specific Rho-kinase inhibitor (Yamamoto et al., 2008). However, the contribution of increased matrix metalloproteinase activities to diabetes-induced loss of cerebral tight junction proteins and subsequent BBB hyperpermeability cannot be dismissed (Hawkins et al., 2007).

After having established a critical role for RhoA/Rho-kinase pathway in hyperglycaemia-mediated cerebral-barrier damage, the aforementioned cerebral-barrier protection by inhibition of the PKC and p38MAPK signalling were further studied since recent research on these signalling pahways have documented the hyperglycaemia-mediated increases in both kinase activities. (Geraldes and King, 2010, Rane et al., 2010). To address whether regulation of RhoA/Rho-kinase pathway may in part be involved in the aforementioned barrier protective effects, the level of RhoA and Rho-kinase-2 protein expressions, p-MLC2-Ser^{19} and p-MLC2-Thr^{18}/Ser^{19} were investigated in HBMEC subjected to hyperglycaemia in the absence and presence of Bis-I or SB203580. Although RhoA protein levels were not modified by either compound, Rho-kinase-2 expression, p-MLC2-Ser^{19} and p-MLC2-Thr^{18}/Ser^{19} were significantly diminished by Bis-I alone, thereby indicating that PKC is modulating the RhoA/Rho-kinase pathway to deteriorate barrier function. Enhanced expression, translocation and activity of several PKC isoforms, namely PKC-α, PKC-β_I, PKC-β_{II} and PKC-δ have previously been observed in hyperglycaemic retinal endothelial cells amongst which PKC-β_{II} is closely linked to the occludin

phosphorylation and blood-retinal barrier hyperpermeability in diabetic rats (Park et al., 2000, Harhaj et al., 2006). In addition, the inhibition of PKC also reduced the hyperglycaemic stress fibre formations and restored the endothelial morphology, thereby confirming the PKC-driven cytoskeletal reoganisation to be in part responsible for the endothelial hyperpermeability.

Despite the inability of SB203580 to suppress RhoA/Rho-kinase protein expressions and MLC2 mono- and di-phosphorylations in hyperglycaemic cells, the inhibition of p38MAPK has been extremely efficacious in preventing hyperglycaemia-induced barrier dysfunction. These data imply that p38MAPK exerts its deleterious effects on the *in vitro* barrier utilising mechanisms other than RhoA/Rho-kinase pathway but do not dismiss the possibility that p38MAPK may act downstream of Rho-kinase. In fact, RhoA/Rho-kinase complex-mediated stimulation of linear kinase cascades leading to p38MAPK activation has recently been shown in endothelial cells, supporting the hypothesis that this pathway may act upstream of p38MAPK (Marinissen et al., 2001, Edlund et al., 2002, Shimada and Rajagopalan, 2010). Besides, mitogen activated protein-extracellular signal-regulated kinase (ERK) kinase kinase-1 molecules including ERK and p38MAPK may directly regulate MLC2 phosphorylation and impair endothelial function and cytoskeleton (Usatyuk and Natarajan, 2004, Deng et al., 2011). In the latter study, inhibitions of ERK and p38MAPK have been shown to partially attenuate 4-hydroxy-2-nonenal-mediated barrier disruption and actin remodelling in bovine lung microvascular endothelial cells (Usatyuk and Natarajan, 2004).

Hence, to further explore the abovementioned PKC modulation of RhoA/Rho-kinase pathway, the present study investigated the molecular mechanisms by which

hyperglycaemia-evoked PKC activity was linked with the cytoskeletal remodelling and the HBMEC barrier dysfunction. The results show that hyperglycaemia dramatically increases the total PKC activity and different PKC isoforms have variable sensitivity and activity under hyperglycaemic pathology where PKC-α, PKC-β and PKC-δ are highly sensitive as reported previously in retinal endothelial cells (Park et al., 2000). Moreover, the PKC-α and PKC-β isoforms are key signalling molecules modulating the hyperglycaemia-mediated endothelial-barrier dysfunction as inhibition of their activity by specific inhibitors Ro-32-0432 (PKC-α) and LY333531 (PKC-β) attenuated the hyperglycaemia-evoked total PKC activity possibly by competitive inhibition with respect to ATP, and the hyperglycaemia-induced hyperpermeability by restoring the endothelial-barrier integrity as observed by the coculture data across the *in vitro* model of human BBB.

These results are consistent with the recent findings which also demonstrated that by knocking down PKC-α expression and by blocking the PKC-β activity (LY333531), both mouse BMEC and HUVEC showed an improvement in their barrier functionality in part by improving the cell antioxidant and antiapoptotic ability (Stamatovic et al., 2003, Stamatovic et al., 2006, Wei et al., 2010a, Xu et al., 2010). Our results have shown that although the treatment with specific inhibitor CGP53353 (PKC-β_{II}) under hyperglycaemia normalised the total PKC activity, it was ineffective in improving the endothelial-barrier integrity compared with LY333531 which was used half of CGP53353 dosage. The answer may be in the IC_{50} values of these molecules, i.e. CGP53353 has the IC_{50} values of 3,800 nM and 410 nM for PKC-β_I and PKC-β_{II}, respectively, and LY333531 has the IC_{50} values of 4.7 nM and 5.9 nM for PKC-β_I and PKC-β_{II}, respectively. Although rottlerin, an alleged PKC-δ-specific inhibitor, has been shown to alleviate the total PKC activity under hyperglycaemia,

there are questions about its specificity because it inhibits many other protein kinases as explained in detail in a recent review (Davies et al., 2000). These results have shown that Y-27632 treatment normalised the hyperglycaemia-evoked total PKC activity indicating a Rho-kinase-dependent PKC activation under hyperglycaemia. However like other PKC isoform specific inhibitors, Y-27632 attenuates the activity of its target molecules by competing with ATP and also has a lower affinity for PKC isoforms. This might be the reason for the abovementioned phenomenon but our recent RhoA knockdown studies examining the crosstalk between RhoA/Rho-kinase and PKC pathways have found that an inverse crosslink does exists between RhoA protein levels and PKC-α activity only under pathological condition like hyperglycaemia. This data substantiates the therapeutic importance of the multiple target drugs which can reduce the side effects of their other constituents. In addition for the first time a direct crosslink was also observed between RhoA protein level and PKC-β activity indicating inter-dependent mechanistic cascades under hyperglycaemic stress (Srivastava and Bayraktutan, 2010, Srivastava et al., 2012).

Previous studies in our group have shown the hyperglycaemia-mediated disruption of the *in vitro* BBB integrity which was restored by the non-specific PKC inhibitor (Bis-I) (Allen and Bayraktutan, 2009a). Hence, the current studies have identified the hyperglycaemia-evoked conventional PKC isoforms i.e. PKC-α and PKC-β to be in part responsible for the endothelial-barrier dysfunction as the effects of hyperglycaemia i.e. decreased TEER values and hyperpermeability across the coculture models were reverted under the influence of Ro-32-0432 and LY333531 respectively, and highlights the therapeutic potential of these inhibitors. Our results are in coherence with previous findings and point to the PKC-α and PKC-β-mediated endothelial barrier dysfunction (Mehta et al., 2001, Wei et al., 2010b).

The exposure of bovine aortic endothelial cells to hyperglycaemia has been linked with barrier hyperpermeability and dysfunction due to an increased activity of the components of plasminogen-plasmin system which are regulated in part by the activated RhoA/Rho-kinase pathway (Iwasaki et al., 2008). This study has shown that hyperglycaemia-evoked PKC overactivity is in part associated with the activation of RhoA/Rho-kinase pathway. The dose-dependent decrease in total RhoA, Rho-kinase levels and a significant decrease in the total RhoA activity in HBMEC under treatment with PKC-α and PKC-β inhibitors further substantiates this hypothesis and demonstrates the importance of the pharmacological intervention of PKC-α and PKC-β isoforms as a tool in modulating the components of RhoA/Rho-kinase pathway. Our gene knockdown studies involving PKC-α and PKC-β siRNA transfection in HBMEC confirms the above findings and demonstrate the PKC-mediated RhoA activation. These results are consistent with recent findings where PKC-α was shown to phosphorylate the Rho-GDI resulting in its dissociation from RhoA-GDP which facilitated in the RhoA activation by p115Rho-GEF (Mehta et al., 2001, Peng et al., 2011). Recent *in vitro* studies on mesangial cells are consistant with the current study and manifest the PKC-β_I-mediated RhoA activation in part by the ROS formation and accumulation under hyperglycaemia (Zhang et al., 2011).

Consistent with the previous findings, the decrease in the intracellular RhoA and RhoA-GTP levels had a direct impact in reducing the hyperglycaemia-evoked MLC2 mono- and di-phosphorylation (p-MLC2-Ser^{19}, p-MLC2-Thr^{18}/Ser^{19}) levels under the influence of isoform-specific PKC inhibitors. Since the isoform-specific PKC inhibitors have multiple targets of varying specificity, as indicated by Ro-32-0432 having 4-fold specificity for PKC-β isoform, it was imperative to find the most important PKC isoform between α and β for therapeutic importance. Hence the gene

knockdown studies have shown that although both PKC-α and PKC-β gene knockdown resulted in protein reductions by approximately 80% and 50%, respectively, and attenuated the RhoA activity, it was the PKC-β knockdown which normalised the hyperglycaemia-evoked MLC2 mono- and di-phosphorylation levels, albeit PKC-α knockdown reduced only the hyperglycaemia-evoked MLC2 mono-phosphorylation levels. Thus, these data emphasise on the therapeutic importance of PKC-β inhibition under hyperglycaemia.

The F-actin staining results substantiated the reduction in MLC2 phosphorylation as hyperglycaemia-mediated stress fibre formations were mitigated under the influence of general PKC and isoform-specific PKC inhibitors for PKC-α and PKC-β, and replaced with a thick and prominent cortical stainings. The modulation of these cytoskeletal components i.e. MLC2 and actin reverted the hyperglycaemia-mediated morphological changes in HBMEC and the cells resumed their typical cobblestone morphology similar to control cells under normoglycaemia. This might be due to the decrease in the inward force exerted by stress fibres under hyperglycaemia since most of the filamentous-actin reverted back to their granular-actin form. These results were further substantiated by gene knockdown studies as PKC-β gene knockdown-HBMEC displayed a thick cortical staining with reduction in stress fibres whereas, the effects of hyperglycaemia prevailed in the PKC-α knockdown HBMEC. Interestingly, these data highlight the importance of PKC-β and MLC2 di-phosphorylation levels in modulating the hyperglycaemia-mediated stress fibre formation and disappearance.

To further support the coculture results, the hyperglycaemia-mediated downregulation of the transmembrane tight junction protein occludin was attenuated by cotreatment with either PKC-α or PKC-β inhibitors under hyperglycaemia. The

total occludin protein levels were either normalised or upregulated under the dose-dependent treatment of these inhibitors. The significance of these results was exemplified by increased coculture barrier integrity. However, the cytoplasmic component of the tight junction complex i.e. ZO-1 showed significant increase only under the influence of PKC-β inhibitor. These data confirms the role of PKC-α and PKC-β isoforms in modulating the tight junction protein expression and their overactivity is in part involved in the degradation and/or disruption of tight junction protein complexes. Since the PKC-α and PKC-β isoform-specific inhibitors also target other PKC isoforms with low specificity and selectivity, these data were further substantiated with gene knockdown studies which highlighted the therapeutic importance of PKC-β knockdown as the protein levels of occludin and ZO-1 significantly improved under hyperglycaemia compared with the PKC-α knockdown. This improvement in the occludin protein levels by PKC-β protein knockdown under hyperglycaemia may be due to a decrease in occludin ubiquitination as explained in detail in recent *in vitro* and *in vitro* studies which concluded that inhibition of PKC-β activation blocks occludin phosphorylation, ubiquitination and tight junction protein trafficking in bovine retinal vascular endothelial cells resulting in a decreased vascular permeability (Murakami et al., 2012). These results are also in coherence with previous studies showing the degradation of tight junction proteins under the influence of *Acanthamoeba* metabolite and the attenuation in *Clostridium difficile* toxin A-mediated tight junction translocation when subjected to PKC-α and PKC-β antagonists. Consistent to the earlier results the inhibition of RhoA and Rho-kinase activity has also been shown to be pivotal in preventing the monocyte chemoattractant protein-1-induced reorganization of tight junction proteins and alterations in

endothelial permeability (Chen et al., 2002, Stamatovic et al., 2003, Khan and Siddiqui, 2009).

In conclusion, the current study has shown that hyperglycaemia disrupts the endothelial-barrier function by potentiating the MLC2 phosphorylation-mediated cytoskeletal remodelling and disrupting the tight junction protein assembly. Inhibition of RhoA, Rho-kinase and PKC signalling molecules restored the aforementioned hyperglycaemic effects and demonstrated the cerebrovascular protection by ameliorating the endothelial-barrier integrity. A schematic representation of the proposed PKC/RhoA/Rho-kinase signalling pathway is shown in figure 4.18.

After successfully evaluating the significance of PKC-β overactivity in hyperglycaemia-evoked PKC/RhoA/Rho-kinase pathway, it will be interesting to further study the role of specific PKC-β isoforms (β_I, β_{II}) in modulating the NF-κB, a transcription factor, activation which may induce the RhoA overactivity as recently reported in the BMEC (He et al., 2011).

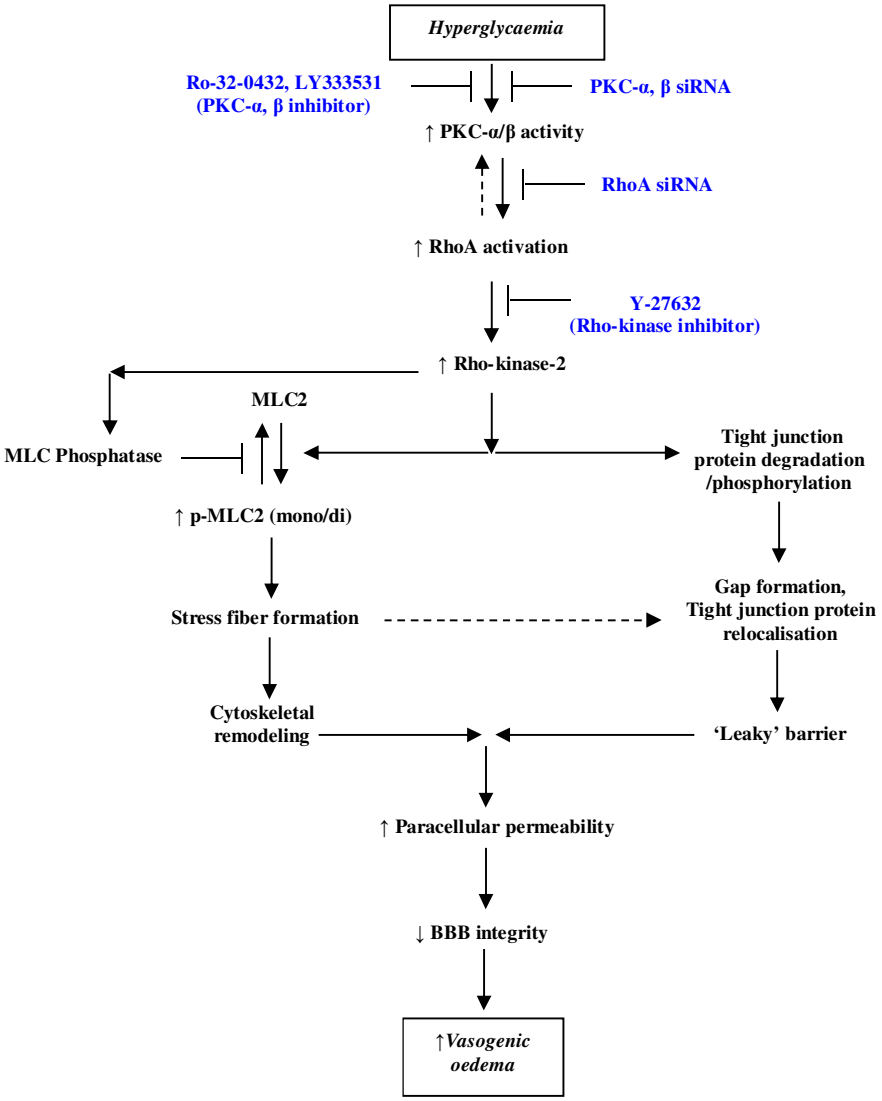

Figure 4.18. The hyperglycaemia-evoked PKC/RhoA/Rho-kinase signalling pathway modulating the BBB integrity via modulation of cytoskeletal remodelling and tight junction localisation. MLC2: Myosin light chain-2; p-MLC2: phosphorylated-MLC2.

General discussion

The endothelial cells form the innermost layer of all the blood vessels and synthesise a number of physiological elements such as nitric oxide to maintain vascular homeostasis. In brain, the microvascular endothelial cells form tightly sealed barrier termed as the BBB, which limit the paracellular permeability to a number of selective blood-driven solutes. However, the pathological conditions like IR and hyperglycaemia alter the physiological functions of the endothelial cells by activating many intercellular stress-sensitive and inflammation-sensitive signalling pathways which collectively threaten the integrity of the BBB.

The outlined studies in the thesis set out to highlight the molecular mechanisms of hyperglycaemia and ischaemia-mediated BBB disruption, a characteristic feature of ischaemic stroke, by investigating the OGD±R-activated RhoA/Rho-kinase signalling cascade, which is related to both the oxidant-dependent and oxidant-independent mechanisms of injury. Tissue oedema has been reported as a result of IR injury in many organs including brain which is a leading cause of death after ischaemic stroke (Bounds et al., 1981, McCord, 1985, Werns and Lucchesi, 1990). Hence, the current OGD studies focused on some of the key molecular mechanisms responsible for the brain oedema which include cytoskeletal remodelling, activation of prooxidant NADPH oxidase enzyme complex, induction of the oxidative stress, and modulation of the tight junction and adherens junction proteins. Moreover the significance of these molecular mechanisms were also studied by evaluating their effects on the BBB integrity and the functionality.

The overall results generated throughout these studies confirm these hypotheses and have shown that OGD compromises the BBB integrity by activation of RhoA-GTPase. The activation of these molecular switches disseminate the stress-induced

signals by activation of their main effector protein Rho-kinase. The activated Rho-kinase initiates the alterations in the phosphorylation status and reorganisation of key cytoskeletal components i.e. myosin and actin, thereby enhancing stress fibre formation and cytoskeletal remodelling.

Since the RhoA/Rho-kinase pathway has been associated with many vascular abnormalities including oxidative stress (Shiotani et al., 2004), our next study under OGD±R pathology investigated the role of Rho-kinase in activation of oxidant-dependent mechanisms responsible for the BBB disruption. Previous *in vitro* studies with bovine pulmonary microvessel endothelial cells have shown that reoxygenation of endothelial cells disrupts the endothelial-barrier integrity and increases the paracellular permeability (Lum et al., 1992). Moreover, recent *in vivo* studies on rats have shown increased paracellular permeability in brain microvessels followed by brain oedema formation under conditions of hypoxia and subsequent reoxygenation (Mark and Davis, 2002, Witt et al., 2008). Hence, the results obtained from our OGD±R studies have shown that the enhanced expression and activity of pro-oxidant NADPH oxidase enzyme complex potentiated the ROS production and accumulation, which may have resulted in the oxidative stress-mediated cerebral-barrier disruption. Moreover, it appeared that the OGD±R-induced oxidative stress was being regulated by RhoA/Rho-kinase as interference with this pathway by specific inhibitors attenuated the NADPH activation and checked the enhanced ROS production and accumulation, which proved to be cerebrovascular protective by improving the endothelial-barrier integrity.

In addition, the OGD±R-mediated modulation of tight junction and adherens junction protein levels were also studied in HBMEC and data presented in the thesis

have highlighted the role of RhoA/Rho-kinase pathway in modulating tight junction and adherens junction proteins. Recent *in vitro* and *in vivo* studies are in coherence with our data and have shown that activations of RhoA and/or Rho-kinase phosphorylates the occludin and claudin-5 tight junction proteins thereby triggering their relocalisation, inducing gap formations, and potentiating the loss in the endothelial-barrier integrity (Yamamoto et al., 2008). In contrast, the specific inhibition of Rho-kinase reverted these effects and improved the barrier integrity, which is in conjunction with our data and also corelates the improved occludin levels after Rho-kinase inhibition to the enhanced endothelial-barrier integrity. The studies with mice brian sections to investigate the effects of fasudil on aforementioned proteins after ischaemic injury appeared to have no significant results. This may be due to the complexity of the brain tissue which is composed of different kinds of cells which may not respond to the IR stress in the similar manner.

Brain oedema emerging from disruption of the BBB constitutes one of the leading causes of mortality after a stroke and appears to be more prevalent in stroke patients with diabetes than those without thereby implying a prominent role for hyperglycaemia in the BBB breakdown. Although hyperglycaemia represents a common pathology in ischaemic stroke patients, about two-thirds of whom are diagnosed as hyperglycaemic at some stage within the first 48 hours of the event due to acute stress response or previously diagnosed diabetes, the mechanisms by which it may compromise the cerebral barrier integrity and/or exacerbate vascular damage remain largely unknown. Identification of these mechanisms is of particular importance given the limitations of tPA (tissue plasminogen activator), the currently approved sole therapeutic agent, which has a short treatment window for recanalisation (within 4.5 h of stroke onset) and is inherently associated with elevated

risk of haemorrhagic transformation, especially in hyperglycaemic patients. Bearing these in mind, the current studies focused on the relevance of two apparently distinct pathways, namely PKC and RhoA/Rho-kinase/MLC2 to hyperglycaemia-mediated barrier damage using an *in vitro* model of human BBB composed of HBMEC and HA. It is thought that elucidating the nature of correlation between these pathways that collectively regulate vasomotor function, cell proliferation, survival, migration, oxidative stress, immune responses and modulate the productions of extracellular matrix and cytokines may prove extremely beneficial in identifying novel targets for future therapeutic approaches (Ishii et al., 1998, Nonaka et al., 2000, Kowluru, 2001, Kelly et al., 2003). The results outlined in this thesis have confirmed that exposures to longer periods of hyperglycaemic insult disrupts the BBB integrity by activating RhoA/Rho-kinase, promoting the cytoskeletal remodelling and perturbing the tight junction protein expression and localisations.

The hyperglycaemic pathology was further scrutinised to delineate the signalling molecules dictating the RhoA and Rho-kinase activities. The PKC isoform-specific activation of RhoA and Rho-kinase has been shown to be the driving force behind the RhoA/Rho-kinase-mediated aforementioned alterations disrupting the BBB and introducing hyperpermeability. The specific PKC-α and PKC-β pharmacological inhibitions and their gene knockdown studies illustrated the hyperglycaemia-mediated PKC-α and PKC-β overactivities governs the RhoA/Rho-kinase pathway and modulate the tight junction protein expression and localisation. Recent *in vitro* and *in vivo* studies support our data and show the PKC-β-mediated phosphorylation and ubiquitination of occludin along with trafficking of tight junction proteins in bovine retinal vascular endothelial cells to be responsible for the enhanced vascular permeability (Murakami et al., 2012).

Although OGD±R and hyperglycaemia are two distinct pathological conditions, the deleterious effects of these pathologies seem to originate from the induction of oxidative stress, activation of inflammatory responses and activation of proteases through common signalling pathway like RhoA/Rho-kinase (Shiotani et al., 2004, Ando et al., 2011, Zhang et al., 2011). The activations of RhoA and Rho-kinase have been shown to enhance the cytoskeletal remodelling and modulate the tight junction protein expression and/or localisation. Interestingly, the pharmacological inhibition of RhoA/Rho-kinase normalised the endothelial morphology, increased the endothelial-barrier tightness and improved the cerebral-barrier properties under the aforementioned pathological conditions. Figure 8 illustrates the similarities between the effects of OGD±R and hyperglycaemia on HBMEC studied in this thesis. Moreover, recent *in vitro* and *in vivo* studies have addressed the interdependent link between the pro-oxidant enzyme-mediated oxidative stress and the PKC-β-mediated RhoA activation under hyperglycaemia by demonstrating a positive feedback loop which also involves Rho-kinase, caveolae (Zhang et al., 2011, Soliman et al., 2012). Hence, the aforementioned studies in this thesis have demonstrated that specific pharmacological inhibition of PKC-β overactivity has been cerebrovascular protective and may be used as an effective novel agent to; (a) improve post-stroke survival rate, (b) reduce the occurrence of the secondary strokes, and (c) abate the occurrence of other similar vascular abnormalities including myocardial infarction.

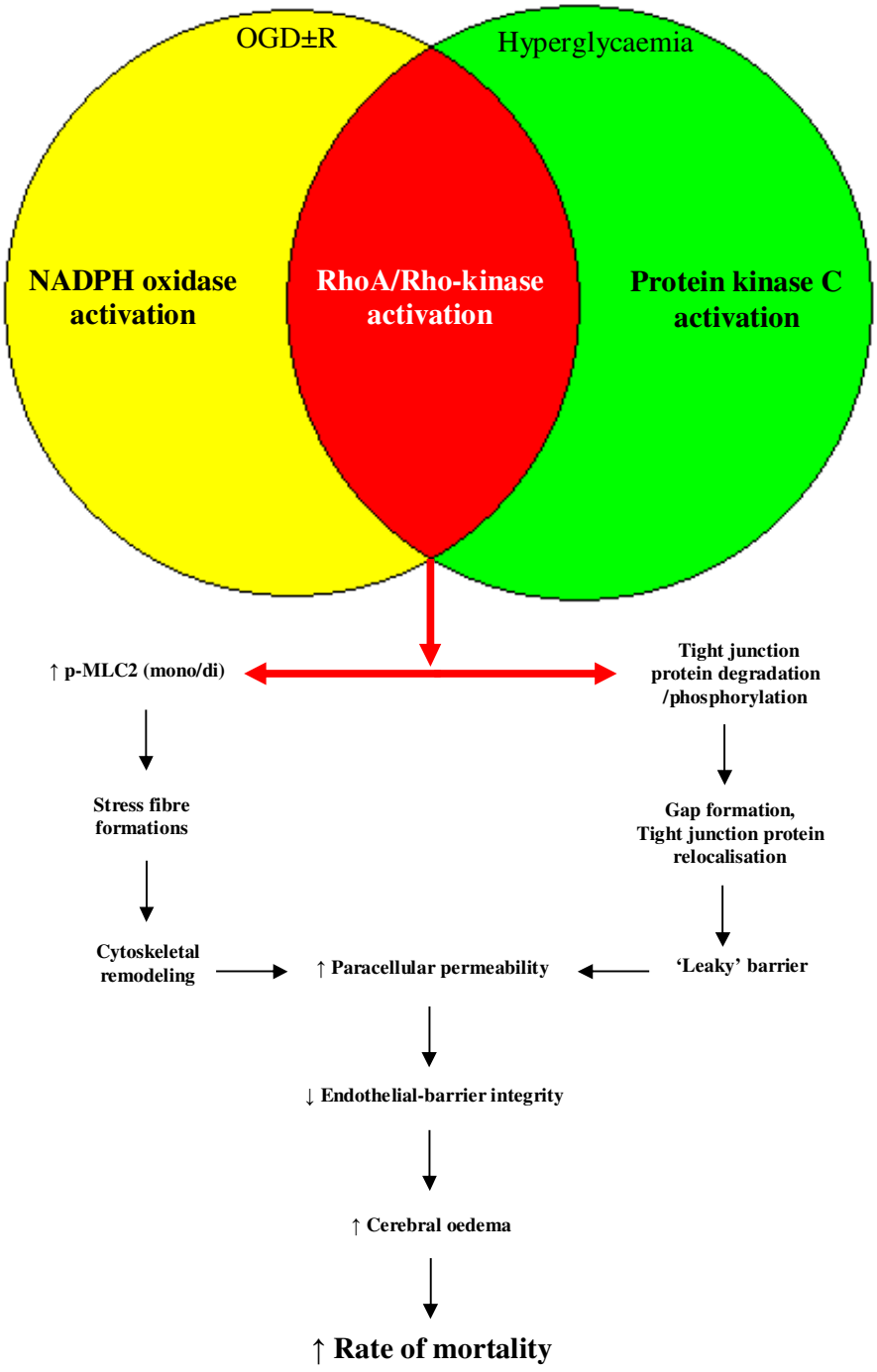

Figure 8. Diagrammatic representation of the similarities between the effects OGD±R and hyperglycaemia using HBMEC and the *in vitro* model of BBB.

Limitations

And

Future directions

1. Limitations to the current studies

The data presented in this thesis are derived from *in vitro* experiments using mainly HBMEC and an *in vitro* model of human BBB comprising of HBMEC and HA. The outlined findings exhibit the molecular mechanisms behind the hyperglycaemia and OGD±R-mediated modulation of the endothelial-barrier integrity. It remains critical to confirm the role of PKC/RhoA/Rho-kinase signalling pathway potentiated under aforementioned pathologies, and to dissect the cooperative or additive roles of diabetes to ischaemic stroke-mediated cerebral-barrier complications in *in vivo* settings by using rodent models of diabetes, ischaemic stroke, and a combination of two.

The *in vitro* model of human BBB was established by coculturing the HBMEC and HA. However, it is essential to further improve the human BBB model by including pericytes and microglia in the BBB architecture because of their significant role during ischaemic stress by enhancing the ROS, cytokine, and chemokine productions which exacerbate the ischaemic injury. Moreover, it is also essential to study the significance of diabetes and ischaemia-mediated BBB dysfunction on the neuronal viability by measuring the rate of neuronal apoptosis during and after the pathological conditions because area of cerebral infarction largely constitutes the dead neurons in ischaemic stroke.

Some of the immunocytochemistry experiments which include the tight junction protein stainings were carried out in HBMEC under hyperglycaemic pathology as illustrated in the thesis. However, these experiments failed during the longer OGD exposures to the HBMEC because majority of HBMEC cultured on coverslips came

off the surface during OGD exposures. Hence, short OGD exposures and time-dependent observations are suggested to address this issue.

2. Future directions

Since stability of tight junction proteins and adherens junction proteins is critical in maintaining the BBB integrity, the OGD or hyperglycaemia-mediated alterations in the expression and relocalisation of these proteins warrants further investigation. By using cell fractionation techniques, different components of HBMEC or HA i.e. membrane fraction, cytoplasmic fraction, nuclear fraction, and actomyosin fraction; can be used to detect the rate of destabilisation and cytoplasmic trafficking for these proteins. Since adherens junction proteins like β-catenin act as transcription factors and modulate the protein expression of claudin-5, the cell fractionation data will confirm the hypothesis and will be useful in addressing the phosphorylation and subsequent relocalisation of tight junction proteins from cell periphery. Moreover it will be interesting to study the role of transcription factors like NF-κB and AP-1 in the destabilisation of these proteins under aforementioned pathologies by investigating the activation and translocation of these transcription factors from cytoplasm to nucleus and their transcription regulation at binding sites at promoter region on the genes by using techniques like chromatin immunoprecipitaions (ChIP).

As mentioned earlier, PKC overactivity regulates the RhoA/Rho-kinase signalling. However, little is known about the molecular mechanisms behind this regulation. Hence, it will be interesting to delineate the role of PKC isoforms in regulating the expression/activity of the activator of RhoA-GTPase i.e. GEFs, GAPs and GDI in HBMEC.

Our recent publication showed the OGD-mediated RhoA/Rho-kinase overactivity in astrocytes (Allen et al., 2010). Since RhoA/Rho-kinase overactivities are linked with ROS generation, it will be interesting to study the pro-oxidant and antioxidant parameters and ROS metabolism in HBMEC and HA cocultures to compare any differences from single cell set ups.

Recent studies on cardiomyocytes have shown that RhoA/Rho-kinase pathway plays an important role in the cell survival as increased RhoA/Rho-kinase activity can upregulate the proapoptotic marker gene Bax and induce apoptosis (Del Re et al., 2007). Indeed, *in vitro* studies with rat PC12 cell line have shown that H_2O_2 exposure increases the Bax mRNA and protein levels and induce apoptosis. Inhibition of Rho-kinase by fasudil mesylate reversed the H_2O_2-mediated effects and improved cell survival rates (Li et al., 2011a). Since the oxidative stress in endothelial cells during IR injury might induce apoptosis, it will be interesting to study the effects of Rho-kinase inhibitors on the apoptotic genes like Bax and Bcl-2 in HBMEC and HA to further substantiate the cerebrovascular protective effects of these inhibitors.

References

Aghajanian A, Wittchen E, Campbell S, Burridge K (2009) Direct activation of RhoA by reactive oxygen species requires a redox-sensitive motif. PLoS One 4:e8045.

Aisagbonhi O, Rai M, Ryzhov S, Atria N, Feoktistov I, Hatzopoulos AK (2011) Experimental myocardial infarction triggers canonical Wnt signaling and endothelial-to-mesenchymal transition. Dis Model Mech 4:469-483.

Akopov S, Zhang L, Pearce W (1998) Regulation of Ca2+ sensitization by PKC and rho proteins in ovine cerebral arteries: effects of artery size and age. Am J Physiol 275:H930-939.

Allen C, Bayraktutan U (2008) Risk factors for ischaemic stroke. Int J Stroke 3:105-116.

Allen C, Bayraktutan U (2009a) Antioxidants attenuate hyperglycaemia-mediated brain endothelial cell dysfunction and blood-brain barrier hyperpermeability. Diabetes Obes Metab 11:480-490.

Allen C, Bayraktutan U (2009b) Oxidative stress and its role in the pathogenesis of ischaemic stroke. Int J Stroke 4:461-470.

Allen C, Srivastava K, Bayraktutan U (2010) Small GTPase RhoA and its effector rho kinase mediate oxygen glucose deprivation-evoked in vitro cerebral barrier dysfunction. Stroke 41:2056-2063.

Amano M, Chihara K, Kimura K, Fukata Y, Nakamura N, Matsuura Y, Kaibuchi K (1997) Formation of actin stress fibers and focal adhesions enhanced by Rho-kinase. Science 275:1308-1311.

Amano M, Chihara K, Nakamura N, Fukata Y, Yano T, Shibata M, Ikebe M, Kaibuchi K (1998) Myosin II activation promotes neurite retraction during the action of Rho and Rho-kinase. Genes Cells 3:177-188.

Amano M, Chihara K, Nakamura N, Kaneko T, Matsuura Y, Kaibuchi K (1999) The COOH terminus of Rho-kinase negatively regulates rho-kinase activity. J Biol Chem 274:32418-32424.

Amano M, Ito M, Kimura K, Fukata Y, Chihara K, Nakano T, Matsuura Y, Kaibuchi K (1996) Phosphorylation and activation of myosin by Rho-associated kinase (Rho-kinase). J Biol Chem 271:20246-20249.

Ando K, Ishibashi T, Ohkawara H, Inoue N, Sugimoto K, Uekita H, Hu CJ, Okamoto Y, Takuwa Y, Takeishi Y (2011) Crucial role of Membrane Type 1 Matrix

Metalloproteinase (MT1-MMP) in RhoA/Rac1-dependent signaling pathways in thrombin-stimulated endothelial cells. J Atheroscler Thromb 18:762-773.

Ando-Akatsuka Y, Saitou M, Hirase T, Kishi M, Sakakibara A, Itoh M, Yonemura S, Furuse M, Tsukita S (1996) Interspecies diversity of the occludin sequence: cDNA cloning of human, mouse, dog, and rat-kangaroo homologues. J Cell Biol 133:43-47.

Antonetti D, Barber A, Khin S, Lieth E, Tarbell J, Gardner T (1998) Vascular permeability in experimental diabetes is associated with reduced endothelial occludin content: vascular endothelial growth factor decreases occludin in retinal endothelial cells. Penn State Retina Research Group. Diabetes 47:1953-1959.

Arber S, Barbayannis F, Hanser H, Schneider C, Stanyon C, Bernard O, Caroni P (1998) Regulation of actin dynamics through phosphorylation of cofilin by LIM-kinase. Nature 393:805-809.

Arita R, Hata Y, Nakao S, Kita T, Miura M, Kawahara S, Zandi S, Almulki L, Tayyari F, Shimokawa H, Hafezi-Moghadam A, Ishibashi T (2009) Rho kinase inhibition by fasudil ameliorates diabetes-induced microvascular damage. Diabetes 58:215-226.

Asano T, Suzuki T, Tsuchiya M, Satoh S, Ikegaki I, Shibuya M, Suzuki Y, Hidaka H (1989) Vasodilator actions of HA1077 in vitro and in vivo putatively mediated by the inhibition of potein-kinase. Br J Pharmacol 98:1091-10100.

Askalan R, Deveber G, Ho M, Ma J, Hawkins C (2006) Astrocytic-inducible nitric oxide synthase in the ischemic developing human brain. Pediatr Res 60:687-692.

Aspenström P (1999) Effectors for the Rho GTPases. Curr Opin Cell Biol 11:95-102.

Assenza G, Zappasodi F, Squitti R, Altamura C, Ventriglia M, Ercolani M, Quattrocchi C, Lupoi D, Passarelli F, Vernieri F, Rossini P, Tecchio F (2009) Neuronal functionality assessed by magnetoencephalography is related to oxidative stress system in acute ischemic stroke. Neuroimage 44:1267-1273.

Bailly K, Ridley AJ, Hall SM, Haworth SG (2004) RhoA activation by hypoxia in pulmonary arterial smooth muscle cells is age and site specific. Circ Res 94:1383-1391.

Baird T, Parsons M, Barber P, Butcher K, Desmond P, Tress B, Colman P, Jerums G, Chambers B, Davis S (2002) The influence of diabetes mellitus and hyperglycaemia on stroke incidence and outcome. J Clin Neurosci 9:618-626.

Ballabh P, Braun A, Nedergaard M (2004) The blood-brain barrier: an overview: structure, regulation, and clinical implications. Neurobiol Dis 16:1-13.

Bamburg J, McGough A, Ono S (1999) Putting a new twist on actin: ADF/cofilins modulate actin dynamics. Trends Cell Biol 9:364-370.

Bar T (1983) Patterns of vascularization in the developing cerebral-cortex. Ciba Foundation Symposia 100:20-36.

Barber A, Antonetti D (2003) Mapping the blood vessels with paracellular permeability in the retinas of diabetic rats. Invest Ophthalmol Vis Sci 44:5410-5416.

Bayraktutan U (2002) Free radicals, diabetes and endothelial dysfunction. Diabetes Obes Metab 4:224-238.

Bazzoni G, Dejana E (2004) Endothelial cell-to-cell junctions: Molecular organization and role in vascular homeostasis. Physiol Rev 84:869-901.

Beckers C, van Hinsbergh V, van Nieuw Amerongen G (2010) Driving Rho GTPase activity in endothelial cells regulates barrier integrity. Thromb Haemost 103:40-55.

Bonnardel-Phu E, Wautier J, Schmidt A, Avila C, Vicaut E (1999) Acute modulation of albumin microvascular leakage by advanced glycation end products in microcirculation of diabetic rats in vivo. Diabetes 48:2052-2058.

Bounds JV, Wiebers DO, Whisnant JP, Okazaki H (1981) Mechanisms and timing of deaths from cerebral infarction. Stroke 12:474-477.

Boureux A, Vignal E, Faure S, Fort P (2007) Evolution of the Rho family of ras-like GTPases in eukaryotes. Mol Biol Evol 24:203-216.

Brabeck C, Mittelbronn M, Bekure K, Meyermann R, Schluesener HJ, Schwab JM (2003) Effect of focal cerebral infarctions on lesional RhoA and RhoB expression. Arch Neurol 60:1245-1249.

Bretscher A (1983) Purification of an 80,000-dalton protein that is a component of the isolated microvillus cytoskeleton, and its localization in nonmuscle cells. J Cell Biol 97:425-432.

Brooks TA, Hawkins BT, Huber JD, Egleton RD, Davis TP (2005) Chronic inflammatory pain leads to increased blood-brain barrier permeability and

tight junction protein alterations. Am J Physiol-Heart Circ Physiol 289:H738-743.

Brouns R, De Deyn P (2009) The complexity of neurobiological processes in acute ischemic stroke. Clin Neurol Neurosurg 111:483-495.

Brownlee M (2001) Biochemistry and molecular cell biology of diabetic complications. Nature 414:813-820.

Burridge K, Wennerberg K (2004) Rho and Rac take center stage. Cell 116:167-179.

Caldwell R, Bartoli M, Behzadian M, El-Remessy A, Al-Shabrawey M, Platt D, Liou G, Caldwell R (2005) Vascular endothelial growth factor and diabetic retinopathy: role of oxidative stress. Curr Drug Targets 6:511-524.

Capes S, Hunt D, Malmberg K, Pathak P, Gerstein H (2001) Stress hyperglycemia and prognosis of stroke in nondiabetic and diabetic patients: a systematic overview. Stroke 32:2426-2432.

Carlier M, Laurent V, Santolini J, Melki R, Didry D, Xia G, Hong Y, Chua N, Pantaloni D (1997) Actin depolymerizing factor (ADF/cofilin) enhances the rate of filament turnover: implication in actin-based motility. J Cell Biol 136:1307-1322.

Chehade J, Haas M, Mooradian A (2002) Diabetes-related changes in rat cerebral occludin and zonula occludens-1 (ZO-1) expression. Neurochem Res 27:249-252.

Chen F, Ohashi N, Li W, Eckman C, Nguyen JH (2009) Disruptions of Occludin and Claudin-5 in Brain Endothelial Cells In Vitro and in Brains of Mice with Acute Liver Failure. Hepatology 50:1914-1923.

Chen ML, Pothoulakis C, LaMont JT (2002) Protein kinase C signaling regulates ZO-1 translocation and increased paracellular flux of T84 colonocytes exposed to Clostridium difficile toxin A. J Biol Chem 277:4247-4254.

Chevrier V, Piel M, Collomb N, Saoudi Y, Frank R, Paintrand M, Narumiya S, Bornens M, Job D (2002) The Rho-associated protein kinase p160ROCK is required for centrosome positioning. J Cell Biol 157:807-817.

Chikumi H, Fukuhara S, Gutkind J (2002) Regulation of G protein-linked guanine nucleotide exchange factors for Rho, PDZ-RhoGEF, and LARG by tyrosine phosphorylation: evidence of a role for focal adhesion kinase. J Biol Chem 277:12463-12473.

Chrissobolis S, Budzyn K, Marley P, Sobey C (2004) Evidence that estrogen suppresses rho-kinase function in the cerebral circulation in vivo. Stroke 35:2200-2205.

Chrissobolis S, Faraci FM (2008) The role of oxidative stress and NADPH oxidase in cerebrovascular disease. Trends Mol Med 14:495-502.

Chrissobolis S, Sobey C (2006) Recent evidence for an involvement of rho-kinase in cerebral vascular disease. Stroke 37:2174-2180.

Cipolla MJ (2009) The Cerebral Circulation. San Rafael (CA): Morgan & Claypool Life Sciences.

Citi S, Cordenonsi M (1998) Tight junction proteins. Biochim Biophys Acta 1448:1-11.

Connell BJ, Saleh MC, Khan BV, Saleh TM (2011) Apocynin may limit total cell death following cerebral ischemia and reperfusion by enhancing apoptosis. Food Chem Toxicol 49:3063-3069.

Davies SP, Reddy H, Caivano M, Cohen P (2000) Specificity and mechanism of action of some commonly used protein kinase inhibitors. Biochem J 351:95-105.

De Smet F, Segura I, De Bock K, Hohensinner P, Carmeliet P (2009) Mechanisms of vessel branching: filopodia on endothelial tip cells lead the way. Arterioscler Thromb Vasc Biol 29:639-649.

Dejana E, Orsenigo F, Lampugnani MG (2008) The role of adherens junctions and VE-cadherin in the control of vascular permeability. J Cell Sci 121:2115-2122.

Del Re DP, Miyamoto S, Brown JH (2007) RhoA/Rho kinase up-regulate bax to activate a mitochondrial death pathway and induce cardiomyocyte apoptosis. J Bio Chem 282:8069-8078.

del Zoppo G, Ginis I, Hallenbeck JM, Iadecola C, Wang X, Feuerstein GZ (2000) Inflammation and stroke: putative role for cytokines, adhesion molecules and iNOS in brain response to ischemia. Brain Pathol 10:95-112.

del Zoppo GJ, Mabuchi T (2003) Cerebral microvessel responses to focal ischemia. J Cereb Blood Flow Metab 23:879-894.

Deng M, Chacko S, Ding W, Xia Y, John M (2011) MLCK-independent phosphorylation of MLC20 and its regulation by MAP kinase pathway in human bladder smooth muscle cells. Cytoskeleton 68:139-149.

Denker BM, Nigam SK (1998) Molecular structure and assembly of the tight junction. Am J Physiol 274:F1-9.

Di Cunto F, Imarisio S, Hirsch E, Broccoli V, Bulfone A, Migheli A, Atzori C, Turco E, Triolo R, Dotto G, Silengo L, Altruda F (2000) Defective neurogenesis in citron kinase knockout mice by altered cytokinesis and massive apoptosis. Neuron 28:115-127.

Didion S, Lynch C, Baumbach G, Faraci F (2005) Impaired endothelium-dependent responses and enhanced influence of Rho-kinase in cerebral arterioles in type II diabetes. Stroke 36:342-347.

Edlund S, Landström M, Heldin C, Aspenström P (2002) Transforming growth factor-beta-induced mobilization of actin cytoskeleton requires signaling by small GTPases Cdc42 and RhoA. Mol Biol Cell 13:902-914.

Endoh M, Maiese K, Wagner J (1994) Expression of the inducible form of nitric oxide synthase by reactive astrocytes after transient global ischemia. Brain Res 651:92-100.

Ergul A, Li W, Elgebaly M, Bruno A, Fagan S (2009) Hyperglycaemia, diabetes and stroke: Focus on the cerebrovasculature. Vasc Pharmacol 51:44-49.

Essler M, Hermann K, Amano M, Kaibuchi K, Heesemann J, Weber P, Aepfelbacher M (1998) Pasteurella multocida toxin increases endothelial permeability via Rho kinase and myosin light chain phosphatase. J Immunol 161:5640-5646.

Etienne-Manneville S, Hall A (2002) Rho GTPases in cell biology. Nature 420:629-635.

Feng J, Ito M, Ichikawa K, Isaka N, Nishikawa M, Hartshorne D, Nakano T (1999a) Inhibitory phosphorylation site for Rho-associated kinase on smooth muscle myosin phosphatase. J Biol Chem 274:37385-37390.

Feng J, Ito M, Kureishi Y, Ichikawa K, Amano M, Isaka N, Okawa K, Iwamatsu A, Kaibuchi K, Hartshorne D, Nakano T (1999b) Rho-associated kinase of chicken gizzard smooth muscle. J Biol Chem 274:3744-3752.

Ferrari R, Ceconi C, Curello S, Alfieri O, Visioli O (1993) Myocardial damage during ischaemia and reperfusion. Eur Heart J 14 Suppl G:25-30.

Flavin MP, Coughlin K, Ho LT (1997) Soluble macrophage factors trigger apoptosis in cultured hippocampal neurons. Neuroscience 80:437-448.

Frixione E (2000) Recurring views on the structure and function of the cytoskeleton: A 300-year epic. Cell Motil Cytoskeleton 46:73-94.

Fujii M, Duris K, Altay O, Soejima Y, Sherchan P, Zhang JH (2012) Inhibition of Rho kinase by hydroxyfasudil attenuates brain edema after subarachnoid hemorrhage in rats. Neurochem Int 60:327-333.

Fukai T, Ushio-Fukai M (2011) Superoxide Dismutases: Role in Redox Signaling, Vascular Function, and Diseases. Antioxid Redox Signal 15:1583-1606.

Fukata Y, Amano M, Kaibuchi K (2001) Rho-Rho-kinase pathway in smooth muscle contraction and cytoskeletal reorganization of non-muscle cells. Trends Pharmacol Sci 22:32-39.

Fukata Y, Oshiro N, Kinoshita N, Kawano Y, Matsuoka Y, Bennett V, Matsuura Y, Kaibuchi K (1999) Phosphorylation of adducin by Rho-kinase plays a crucial role in cell motility. J Cell Biol 145:347-361.

Furuse M, Hirase T, Itoh M, Nagafuchi A, Yonemura S, Tsukita S (1993) Occludin: a novel integral membrane protein localizing at tight junctions. J Cell Biol 123:1777-1788.

Furuse M, Sasaki H, Fujimoto K, Tsukita S (1998) A single gene product, claudin-1 or -2, reconstitutes tight junction strands and recruits occludin in fibroblasts. J Cell Biol 143:391-401.

Gallagher P, Garcia J, Herring B (1995) Expression of a novel myosin light chain kinase in embryonic tissues and cultured cells. J Biol Chem 270:29090-29095.

Gallagher P, Herring B, Stull J (1997) Myosin light chain kinases. J Muscle Res Cell Motil 18:1-16.

Gao Q, Zhao X, Ahmad M, Wolin MS (2009) Mitochondrial-derived hydrogen peroxide inhibits relaxation of bovine coronary arterial smooth muscle to hypoxia through stimulation of ERK MAP kinase. Am J Physiol-Heart Circ Physiol 297:H2262-2269.

Garcia J, Lazar V, Gilbert-McClain L, Gallagher P, Verin A (1997) Myosin light chain kinase in endothelium: molecular cloning and regulation. Am J Respir Cell Mol Biol 16:489-494.

Gehrmann J, Matsumoto Y, Kreutzberg GW (1995) Microglia: intrinsic immuneffector cell of the brain. Brain Res Brain Res Rev 20:269-287.

Genovese T, Mazzon E, Paterniti I, Esposito E, Bramanti P, Cuzzocrea S (2011) Modulation of NADPH oxidase activation in cerebral ischemia/reperfusion injury in rats. Brain Res 1372:92-102.

Geraldes P, King G (2010) Activation of protein kinase C isoforms and its impact on diabetic complications. Circ Res 106:1319-1331.

Gloor SM, Wachtel M, Bolliger MF, Ishihara H, Landmann R, Frei K (2001) Molecular and cellular permeability control at the blood-brain barrier. Brain Res Brain Res Rev 36:258-264.

Goldstein L, Adams R, Becker K, Furberg C, Gorelick P, Hademenos G, Hill M, Howard G, Howard V, Jacobs B, Levine S, Mosca L, Sacco R, Sherman D, Wolf P, del Zoppo G (2001) Primary prevention of ischemic stroke: A statement for healthcare professionals from the Stroke Council of the American Heart Association. Stroke 32:280-299.

Gong M, Iizuka K, Nixon G, Browne J, Hall A, Eccleston J, Sugai M, Kobayashi S, Somlyo A, Somlyo A (1996) Role of guanine nucleotide-binding proteins--ras-family or trimeric proteins or both--in Ca2+ sensitization of smooth muscle. Proc Natl Acad Sci U S A 93:1340-1345.

González-Mariscal L, Betanzos A, Nava P, Jaramillo BE (2003) Tight junction proteins. Prog Biophys Mol Biol 81:1-44.

Guntaka SR, Samak G, Seth A, LaRusso NF, Rao R (2011) Epidermal growth factor protects the apical junctional complexes from hydrogen peroxide in bile duct epithelium. Lab Invest 91:1396-1409.

Guzik TJ, West NEJ, Black E, McDonald D, Ratnatunga C, Pillai R, Channon KM (2000) Vascular superoxide production by NAD(P)H oxidase - Association with endothelial dysfunction and clinical risk factors. Circ Res 86:E85-90.

Harhaj N, Felinski E, Wolpert E, Sundstrom J, Gardner T, Antonetti D (2006) VEGF activation of protein kinase C stimulates occludin phosphorylation and contributes to endothelial permeability. Invest Ophthalmol Vis Sci 47:5106-5115.

Hart M, Jiang X, Kozasa T, Roscoe W, Singer W, Gilman A, Sternweis P, Bollag G (1998) Direct stimulation of the guanine nucleotide exchange activity of p115 RhoGEF by Galpha13. Science 280:2112-2114.

Hartshorne D (1998) Myosin phosphatase: subunits and interactions. Acta Physiol Scand 164:483-493.

Hawkins B, Lundeen T, Norwood K, Brooks H, Egleton R (2007) Increased blood-brain barrier permeability and altered tight junctions in experimental diabetes

in the rat: contribution of hyperglycaemia and matrix metalloproteinases. Diabetologia 50:202-211.

Hawkins BT, Davis TP (2005) The blood-brain barrier/neurovascular unit in health and disease. Pharmacol Rev 57:173-185.

Hayashi K, Nakao S, Nakaoke R, Nakagawa S, Kitagawa N, Niwa M (2004) Effects of hypoxia on endothelial/pericytic co-culture model of the blood-brain barrier. Regul Pept 123:77-83.

Haynes RL, Folkerth RD, Trachtenberg FL, Volpe JJ, Kinney HC (2009) Nitrosative stress and inducible nitric oxide synthase expression in periventricular leukomalacia. Acta Neuropathol 118:391-399.

He F, Peng J, Deng XL, Yang LF, Wu LW, Zhang CL, Yin F (2011) RhoA and NF-κB are involved in lipopolysaccharide-induced brain microvascular cell line hyperpermeability. Neuroscience 188:35-47.

Heo W, Meyer T (2003) Switch-of-function mutants based on morphology classification of Ras superfamily small GTPases. Cell 113:315-328.

Higashi M, Shimokawa H, Hattori T, Hiroki J, Mukai Y, Morikawa K, Ichiki T, Takahashi S, Takeshita A (2003) Long-term inhibition of Rho-kinase suppresses angiotensin II-induced cardiovascular hypertrophy in rats in vivo: effect on endothelial NAD(P)H oxidase system. Circ Res 93:767-775.

Hink U, Li H, Mollnau H, Oelze M, Matheis E, Hartmann M, Skatchkov M, Thaiss F, Stahl RA, Warnholtz A, Meinertz T, Griendling K, Harrison DG, Forstermann U, Munzel T (2001) Mechanisms underlying endothelial dysfunction in diabetes mellitus. Circ Res 88:E14-22.

Hirase T, Kawashima S, Wong EYM, Ueyama T, Rikitake Y, Tsukita S, Yokoyama M, Staddon JM (2001) Regulation of tight junction permeability and occludin phosphorylation by RhoA-p160ROCK-dependent and -independent mechanisms. J Biol Chem 276:10423-10431.

Hou ST, MacManus JP (2002) Molecular mechanisms of cerebral ischemia-induced neuronal death. Int Rev Cytol 221:93-148.

Huang L, He Z, Guo L, Wang H (2008) Improvement of cognitive deficit and neuronal damage in rats with chronic cerebral ischemia via relative long-term inhibition of Rho-kinase. Cell Mol Neurobiol 28:757-768.

Huber JD, Egleton RD, Davis TP (2001) Molecular physiology and pathophysiology of tight junctions in the blood-brain barrier. Trends Neurosci 24:719-725.

Ishii H, Koya D, King GL (1998) Protein kinase C activation and its role in the development of vascular complications in diabetes mellitus. J Mol Med (Berl) 76:21-31.

Ishizaki T, Maekawa M, Fujisawa K, Okawa K, Iwamatsu A, Fujita A, Watanabe N, Saito Y, Kakizuka A, Morii N, Narumiya S (1996) The small GTP-binding protein Rho binds to and activates a 160 kDa Ser/Thr protein kinase homologous to myotonic dystrophy kinase. EMBO J 15:1885-1893.

Ito U, Nagasao J, Kawakami E, Oyanagi K (2007) Fate of disseminated dead neurons in the cortical ischemic penumbra: ultrastructure indicating a novel scavenger mechanism of microglia and astrocytes. Stroke 38:2577-2583.

Iwasaki H, Okamoto R, Kato S, Konishi K, Mizutani H, Yamada N, Isaka N, Nakano T, Ito M (2008) High glucose induces plasminogen activator inhibitor-1 expression through Rho/Rho-kinase-mediated NF-kappaB activation in bovine aortic endothelial cells. Atherosclerosis 196:22-28.

Jin H, Yamashita H, Nagano Y, Fukuba H, Hiji M, Ohtsuki T, Takahashi T, Kohriyama T, Kaibuchi K, Matsumoto M (2006) Hypoxia-induced upregulation of endothelial small G protein RhoA and Rho-kinase/ROCK2 inhibits eNOS expression. Neurosci Lett 408:62-67.

Jin L, Ying Z, Webb R (2004) Activation of Rho/Rho kinase signaling pathway by reactive oxygen species in rat aorta. Am J Physiol Heart Circ Physiol 287:H1495-1500.

Kacimi R, Giffard RG, Yenari MA (2011) Endotoxin-activated microglia injure brain derived endothelial cells via NF-κB, JAK-STAT and JNK stress kinase pathways. J Inflamm (Lond) 8:7.

Kahles T, Luedike P, Endres M, Galla HJ, Steinmetz H, Busse R, Neumann-Haefelin T, Brandes RP (2007) NADPH oxidase plays a central role in blood-brain barrier damage in experimental stroke. Stroke 38:3000-3006.

Kaneko T, Amano M, Maeda A, Goto H, Takahashi K, Ito M, Kaibuchi K (2000) Identification of calponin as a novel substrate of Rho-kinase. Biochem Biophys Res Commun 273:110-116.

Kaur J, Tuor UI, Zhao Z, Barber PA (2011) Quantitative MRI reveals the elderly ischemic brain is susceptible to increased early blood-brain barrier permeability following tissue plasminogen activator related to claudin 5 and occludin disassembly. J Cereb Blood Flow Metab 31:1874-1885.

Kawano Y, Fukata Y, Oshiro N, Amano M, Nakamura T, Ito M, Matsumura F, Inagaki M, Kaibuchi K (1999) Phosphorylation of myosin-binding subunit (MBS) of myosin phosphatase by Rho-kinase in vivo. J Cell Biol 147:1023-1038.

Kelly DJ, Zhang YA, Hepper C, Gow RM, Jaworski K, Kemp BE, Wilkinson-Berka JL, Gilbert RE (2003) Protein kinase C beta inhibition attenuates the progression of experimental diabetic nephropathy in the presence of continued hypertension. Diabetes 52:512-518.

Khan NA, Siddiqui R (2009) Acanthamoeba affects the integrity of human brain microvascular endothelial cells and degrades the tight junction proteins. Int J Parasitol 39:1611-1616.

Kimura K, Ito M, Amano M, Chihara K, Fukata Y, Nakafuku M, Yamamori B, Feng J, Nakano T, Okawa K, Iwamatsu A, Kaibuchi K (1996) Regulation of myosin phosphatase by Rho and Rho-associated kinase (Rho-kinase). Science 273:245-248.

Kowluru RA (2001) Diabetes-induced elevations in retinal oxidative stress, protein kinase C and nitric oxide are interrelated. Acta Diabetologica 38:179-185.

Koyama M, Ito M, Feng J, Seko T, Shiraki K, Takase K, Hartshorne D, Nakano T (2000) Phosphorylation of CPI-17, an inhibitory phosphoprotein of smooth muscle myosin phosphatase, by Rho-kinase. FEBS Lett 475:197-200.

Kravcukova P, Danielisova V, Nemethova M, Burda J, Gottlieb M (2010) Effects of one-day reperfusion after transient forebrain ischemia on circulatory system in the rat. Gen Physiol Biophys 29:113-121.

Kumar P, Shen Q, Pivetti C, Lee E, Wu M, Yuan S (2009) Molecular mechanisms of endothelial hyperpermeability: implications in inflammation. Expert Rev Mol Med 11:e19.

Lassegue B, Griendling KK (2010) NADPH Oxidases: Functions and pathologies in the vasculature. Arterioscler Thromb Vasc Biol 30:653-661.

Laufs U, Endres M, Stagliano N, Amin-Hanjani S, Chui D, Yang S, Simoncini T, Yamada M, Rabkin E, Allen P, Huang P, Böhm M, Schoen F, Moskowitz M, Liao J (2000) Neuroprotection mediated by changes in the endothelial actin cytoskeleton. J Clin Invest 106:15-24.

Leung T, Chen X, Manser E, Lim L (1996) The p160 RhoA-binding kinase ROK alpha is a member of a kinase family and is involved in the reorganization of the cytoskeleton. Mol Cell Biol 16:5313-5327.

Leung T, Manser E, Tan L, Lim L (1995) A novel serine/threonine kinase binding the Ras-related RhoA GTPase which translocates the kinase to peripheral membranes. J Biol Chem 270:29051-29054.

Li Q, Huang X-J, He W, Ding J, Jia J-T, Fu G, Wang H-X, Guo L-J (2009) Neuroprotective potential of fasudil mesylate in brain ischemia-reperfusion injury of rats. Cell Mol Neurobiol 29:169-180.

Li Q, Liu D, Huang XJ, Guo LJ (2011a) Fasudil Mesylate protects PC12 Cells from oxidative stress injury via the Bax-mediated pathway. Cell Mol Neurobiol 31:243-250.

Li Y, Yao J-H, Hu X-W, Fan Z, Huang L, Jing H-R, Liu K-X, Tian X-F (2011b) Inhibition of Rho kinase by fasudil hydrochloride attenuates lung injury induced by intestinal ischemia and reperfusion. Life Sci 88:104-109.

Liao J, Laufs U (2005) Pleiotropic effects of statins. Annu Rev Pharmacol Toxicol 45:89-118.

Liao J, Seto M, Noma K (2007) Rho kinase (ROCK) inhibitors. J Cardiovasc Pharmacol 50:17-24.

Liebner S, Corada M, Bangsow T, Babbage J, Taddei A, Czupalla CJ, Reis M, Felici A, Wolburg H, Fruttiger M, Taketo MM, von Melchner H, Plate KH, Gerhardt H, Dejana E (2008) Wnt/beta-catenin signaling controls development of the blood-brain barrier. J Cell Biol 183:409-417.

Liu H, Zhang X, Du Y, Ji H, Li S, Li L, Xing Y, Zhang X, Dong L, Wang C, Zhao K, Ji Y, Cao X (2012) Leonurine protects brain injury by increased activities of UCP4, SOD, CAT and Bcl-2, decreased levels of MDA and Bax, and ameliorated ultrastructure of mitochondria in experimental stroke. Brain Res 1474:73-81.

Liu JQ, Zelko IN, Folz RJ (2004) Reoxygenation-induced constriction in murine coronary arteries - The role of endothelial NADPH oxidase (gp91(phox)) and intracellular superoxide. J Biol Chem 279:24493-24497.

Loor G, Kondapalli J, Iwase H, Chandel NS, Waypa GB, Guzy RD, Hoek TLV, Schumacker PT (2011) Mitochondrial oxidant stress triggers cell death in simulated ischemia-reperfusion. Biochim Biophys Acta 1813:1382-1394.

Lu DY, Liou HC, Tang CH, Fu WM (2006) Hypoxia-induced iNOS expression in microglia is regulated by the PI3-kinase/Akt/mTOR signaling pathway and activation of hypoxia inducible factor-1alpha. Biochem Pharmacol 72:992-1000.

Lu YZ, Lin CH, Cheng FC, Hsueh CM (2005) Molecular mechanisms responsible for microglia-derived protection of Sprague-Dawley rat brain cells during in vitro ischemia. Neurosci Lett 373:159-164.

Lum H, Barr DA, Shaffer JR, Gordon RJ, Ezrin AM, Malik AB (1992) Reoxygenation of endothelial-cells increases permeability of oxidant-dependent mechanisms. Circ Res 70:991-998.

Ma T, Liu L, Wang P, Xue Y (2012) Evidence for involvement of ROCK signaling in bradykinin-induced increase in murine blood-tumor barrier permeability. J Neurooncol 106:291-301.

Makarova AM, Lebedeva TV, Nassar T, Higazi AA, Xue J, Carinato ME, Bdeir K, Cines DB, Stepanova V (2011) Urokinase-type plasminogen activator (uPA) induces pulmonary microvascular endothelial permeability through Low density lipoprotein Receptor-related Protein (LRP)-dependent activation of endothelial nitric-oxide synthase. J Biol Chem 286:23044-23053.

Margaill I, Plotkine M, Lerouet D (2005) Antioxidant strategies in the treatment of stroke. Free Radic Biol Med 39:429-443.

Marinissen M, Chiariello M, Gutkind J (2001) Regulation of gene expression by the small GTPase Rho through the ERK6 (p38 gamma) MAP kinase pathway. Genes Dev 15:535-553.

Mark K, Davis T (2002) Cerebral microvascular changes in permeability and tight junctions induced by hypoxia-reoxygenation. Am J Physiol Heart Circ Physiol 282:H1485-1494.

Martìn-Padura I, Lostaglio S, Schneemann M, Williams L, Romano M, Fruscella P, Panzeri C, Stoppacciaro A, Ruco L, Villa A, Simmons D, Dejana E (1998) Junctional adhesion molecule, a novel member of the immunoglobulin superfamily that distributes at intercellular junctions and modulates monocyte transmigration. J Cell Biol 142:117-127.

Masuda M, Betancourt L, Matsuzawa T, Kashimoto T, Takao T, Shimonishi Y, Horiguchi Y (2000) Activation of rho through a cross-link with polyamines catalyzed by Bordetella dermonecrotizing toxin. EMBO J 19:521-530.

Masumoto A, Mohri M, Shimokawa H, Urakami L, Usui M, Takeshita A (2002) Suppression of coronary artery spasm by the Rho-kinase inhibitor fasudil in patients with vasospastic angina. Circulation 105:1545-1547.

Matsuda S, Umeda M, Uchida H, Kato H, Araki T (2009) Alterations of oxidative stress markers and apoptosis markers in the striatum after transient focal cerebral ischemia in rats. J Neural Transm 116:395-404.

Matsui T, Amano M, Yamamoto T, Chihara K, Nakafuku M, Ito M, Nakano T, Okawa K, Iwamatsu A, Kaibuchi K (1996) Rho-associated kinase, a novel serine/threonine kinase, as a putative target for small GTP binding protein Rho. EMBO J 15:2208-2216.

Matsui T, Maeda M, Doi Y, Yonemura S, Amano M, Kaibuchi K, Tsukita S (1998) Rho-kinase phosphorylates COOH-terminal threonines of ezrin/radixin/moesin (ERM) proteins and regulates their head-to-tail association. J Cell Biol 140:647-657.

McCord JM (1985) Oxygen-derived free-radicals in postischemic tissue-injury. N Engl J Med 312:159-163.

Mehta D, Rahman A, Malik A (2001) Protein kinase C-alpha signals rho-guanine nucleotide dissociation inhibitor phosphorylation and rho activation and regulates the endothelial cell barrier function. J Biol Chem 276:22614-22620.

Miao L, Calvert J, Tang J, Parent A, Zhang J (2001) Age-related RhoA expression in blood vessels of rats. Mech Ageing Dev 122:1757-1770.

Miao L, Calvert J, Tang J, Zhang J (2002) Upregulation of small GTPase RhoA in the basilar artery from diabetic (mellitus) rats. Life Sci 71:1175-1185.

Miller AA, Drummond GR, Sobey CG (2006) Novel isoforms of NADPH-oxidase in cerebral vascular control. Pharmacol Ther 111:928-948.

Mita S, Kobayashi N, Yoshida K, Nakano S, Matsuoka H (2005) Cardioprotective mechanisms of Rho-kinase inhibition associated with eNOS and oxidative stress-LOX-1 pathway in Dahl salt-sensitive hypertensive rats. J Hypertension 23:87-96.

Miyagi Y, Carpenter R, Meguro T, Parent A, Zhang J (2000) Upregulation of rho A and rho kinase messenger RNAs in the basilar artery of a rat model of subarachnoid hemorrhage. J Neurosurg 93:471-476.

Muhs A, Noll T, Piper HM (1997) Vinculin phosphorylation and barrier failure of coronary endothelial monolayers under energy depletion. Am J Physiol-Heart Circ Physiol 273:H608-H617.

Murakami T, Frey T, Lin C, Antonetti DA (2012) Protein kinase cβ phosphorylates occludin regulating tight junction trafficking in vascular endothelial growth factor-induced permeability in vivo. Diabetes 61:1573-1583.

Nakagawa O, Fujisawa K, Ishizaki T, Saito Y, Nakao K, Narumiya S (1996) ROCK-I and ROCK-II, two isoforms of Rho-associated coiled-coil forming protein serine/threonine kinase in mice. FEBS Lett 392:189-193.

Nakajima K, Honda S, Tohyama Y, Imai Y, Kohsaka S, Kurihara T (2001) Neurotrophin secretion from cultured microglia. J Neurosci Res 65:322-331.

Narumiya S, Ishizaki T, Watanabe N (1997) Rho effectors and reorganization of actin cytoskeleton. FEBS Lett 410:68-72.

Narumiya S, Tanji M, Ishizaki T (2009) Rho signaling, ROCK and mDia1, in transformation, metastasis and invasion. Cancer Metastasis Rev 28:65-76.

Neumann J, Gunzer M, Gutzeit HO, Ullrich O, Reymann KG, Dinkel K (2006) Microglia provide neuroprotection after ischemia. FASEB J 20:714-716.

Nishida M, Tanabe S, Maruyama Y, Mangmool S, Urayama K, Nagamatsu Y, Takagahara S, Turner JH, Kozasa T, Kobayashi H, Sato Y, Kawanishi T, Inoue R, Nagao T, Kurose H (2005) G alpha(12/13)- and reactive oxygen species-dependent activation of c-Jun NH2-terminal kinase and p38 mitogen-activated protein kinase by angiotensin receptor stimulation in rat neonatal cardiomyocytes. J Biol Chem 280:18434-18441.

Nonaka A, Kiryu J, Tsujikawa A, Yamashiro K, Miyamoto K, Nishiwaki H, Honda Y, Ogura Y (2000) PKC-beta inhibitor (LY333531) attenuates leukocyte entrapment in retinal microcirculation of diabetic rats. Invest Ophthalmol Vis Sci 41:2702-2706.

Oh YT, Lee JY, Lee J, Lee JH, Kim JE, Ha J, Kang I (2010) Oleamide suppresses lipopolysaccharide-induced expression of iNOS and COX-2 through inhibition of NF-kappaB activation in BV2 murine microglial cells. Neurosci Lett 474:148-153.

Ohashi K, Nagata K, Maekawa M, Ishizaki T, Narumiya S, Mizuno K (2000) Rho-associated kinase ROCK activates LIM-kinase 1 by phosphorylation at threonine 508 within the activation loop. J Biol Chem 275:3577-3582.

Ohtaki M, Tranmer B (1994) Pretreatment of transient focal cerebral ischemia in rats with the calcium antagonist AT877. Stroke 25:1234-1239; discussion 1240.

Otero K, Martínez F, Beltrán A, González D, Herrera B, Quintero G, Delgado R, Rojas A (2001) Albumin-derived advanced glycation end-products trigger the disruption of the vascular endothelial cadherin complex in cultured human and murine endothelial cells. Biochem J 359:567-574.

Ozkan F, Senayli Y, Ozyurt H, Erkorkmaz U, Bostan B (2012) Antioxidant effects of propofol on tourniquet-induced ischemia-reperfusion injury: An experimental study. J Surg Res 176:601-607.

Palmeri D, van Zante A, Huang CC, Hemmerich S, Rosen SD (2000) Vascular endothelial junction-associated molecule, a novel member of the immunoglobulin superfamily, is localized to intercellular boundaries of endothelial cells. J Biol Chem 275:19139-19145.

Park J, Takahara N, Gabriele A, Chou E, Naruse K, Suzuma K, Yamauchi T, Ha S, Meier M, Rhodes C, King G (2000) Induction of endothelin-1 expression by glucose: an effect of protein kinase C activation. Diabetes 49:1239-1248.

Peng J, He F, Zhang C, Deng X, Yin F (2011) Protein kinase C-α signals P115RhoGEF phosphorylation and RhoA activation in TNF-α-induced mouse brain microvascular endothelial cell barrier dysfunction. J Neuroinflammation 8:28.

Petty M, Wettstein J (2001) Elements of cerebral microvascular ischaemia. Brain Res Brain Res Rev 36:23-34.

Petty MA, Lo EH (2002) Junctional complexes of the blood-brain barrier: permeability changes in neuroinflammation. Prog Neurobiol 68:311-323.

Quijano C, Castro L, Peluffo G, Valez V, Radi R (2007) Enhanced mitochondrial superoxide in hyperglycemic endothelial cells: direct measurements and formation of hydrogen peroxide and peroxynitrite. Am J Physiol Heart Circ Physiol 293:H3404-H3414.

Raat N, Shiva S, Gladwin M (2009) Effects of nitrite on modulating ROS generation following ischemia and reperfusion. Adv Drug Deliv Rev 61:339-350.

Rane M, Song Y, Jin S, Barati M, Wu R, Kausar H, Tan Y, Wang Y, Zhou G, Klein J, Li X, Cai L (2010) Interplay between Akt and p38 MAPK pathways in the regulation of renal tubular cell apoptosis associated with diabetic nephropathy. Am J Physiol Renal Physiol 298:F49-61.

Ridley A (2001a) Rho family proteins: coordinating cell responses. Trends Cell Biol 11:471-477.

Ridley A (2001b) Rho GTPases and cell migration. J Cell Sci 114:2713-2722.

Ridley A, Hall A (1992) The small GTP-binding protein rho regulates the assembly of focal adhesions and actin stress fibers in response to growth factors. Cell 70:389-399.

Ridley A, Paterson H, Johnston C, Diekmann D, Hall A (1992) The small GTP-binding protein rac regulates growth factor-induced membrane ruffling. Cell 70:401-410.

Riento K, Ridley A (2003) Rocks: multifunctional kinases in cell behaviour. Nat Rev Mol Cell Biol 4:446-456.

Rikitake Y, Kim H, Huang Z, Seto M, Yano K, Asano T, Moskowitz M, Liao J (2005) Inhibition of Rho kinase (ROCK) leads to increased cerebral blood flow and stroke protection. Stroke 36:2251-2257.

Rikitake Y, Liao J (2005a) Rho GTPases, statins, and nitric oxide. Circ Res 97:1232-1235.

Rikitake Y, Liao J (2005b) Rho-kinase mediates hyperglycemia-induced plasminogen activator inhibitor-1 expression in vascular endothelial cells. Circulation 111:3261-3268.

Ronaldson PT, DeMarco KM, Sanchez-Covarrubias L, Solinsky CM, Davis TP (2009) Transforming growth factor-beta signaling alters substrate permeability and tight junction protein expression at the blood-brain barrier during inflammatory pain. J Cereb Blood Flow Metab 29:1084-1098.

Saenz-Morales D, Escribese MM, Stamatakis K, Garcia-Martos M, Alegre L, Conde E, Perez-Sala D, Mampaso F, Garcia-Bermejoa ML (2006) Requirements for proximal tubule epithelial cell detachment in response to ischemia: Role of oxidative stress. Exp Cell Res 312:3711-3727.

Sahai E, Marshall CJ (2002) RHO-GTPases and cancer. Nat Rev Cancer 2:133-142.

Sandoval KE, Witt KA (2008) Blood-brain barrier tight junction permeability and ischemic stroke. Neurobiol Dis 32:200-219.

Sato M, Tani E, Fujikawa H, Kaibuchi K (2000) Involvement of Rho-kinase-mediated phosphorylation of myosin light chain in enhancement of cerebral vasospasm. Circ Res 87:195-200.

Satoh S, Kobayashi T, Hitomi A, Ikegaki I, Suzuki Y, Shibuya M, Yoshida J, Asano T (1999) Inhibition of neutrophil migration by a protein kinase inhibitor for the treatment of ischemic brain infarction. Jpn J Pharmacol 80:41-48.

Satoh S, Utsunomiya T, Tsurui K, Kobayashi T, Ikegaki I, Sasaki Y, Asano T (2001) Pharmacological profile of hydroxy fasudil as a selective rho kinase inhibitor on ischemic brain damage. Life Sci 69:1441-1453.

Schlessinger J (1993) How receptor tyrosine kinases activate Ras. Trends Biochem Sci 18:273-275.

Schmeck B, Brunsch M, Seybold J, Krull M, von Eichel-Streiber C, Suttorp N, Hippenstiel S (2003) Rho protein inhibition blocks cyclooxygenase-2 expression by proinflammatory mediators in endothelial cells. Inflammation 27:89-95.

Schwartz M (2004) Rho signalling at a glance. J Cell Sci 117:5457-5458.

Seasholtz T, Majumdar M, Brown J (1999) Rho as a mediator of G protein-coupled receptor signaling. Mol Pharmacol 55:949-956.

Selemidis S, Sobey CG, Wingler K, Schmidt HHHW, Drummond GR (2008) NADPH oxidases in the vasculature: Molecular features, roles in disease and pharmacological inhibition. Pharmacol Ther 120:254-291.

Shimada H, Rajagopalan L (2010) Rho-kinase mediates lysophosphatidic acid-induced IL-8 and MCP-1 production via p38 and JNK pathways in human endothelial cells. FEBS Lett 584:2827-2832.

Shin D, Kang J, Ha J, Kang H, Park S, Kim I, Kim S (2008) Cystamine prevents ischemia-reperfusion injury by inhibiting polyamination of RhoA. Biochem Biophys Res Commun 365:509-514.

Shiotani S, Shimada M, Suehiro T, Soejima Y, Yosizumi T, Shimokawa H, Maehara Y (2004) Involvement of Rho-kinase in cold ischemia-reperfusion injury after liver transplantation in rats. Transplantation 78:375-382.

Siehler S (2009) Regulation of RhoGEF proteins by G12/13-coupled receptors. Br J Pharmacol 158:41-49.

Singh U, Kunar M, Kao Y, Baker K (2001) Role of transglutaminase II in retinoic acid-induced activation of RhoA-associated kinase-2. EMBO J 20:2413-2423.

Solaini G, Harris D (2005) Biochemical dysfunction in heart mitochondria exposed to ischaemia and reperfusion. Biochem J 390:377-394.

Soliman H, Gador A, Lu YH, Lin G, Bankar G, Macleod KM (2012) Diabetes-induced increased oxidative stress in cardiomyocytes is sustained by a positive feedback loop involving Rho-kinase and PKCβ2. Am J Physiol Heart Circ Physiol 303:H989-1000.

Son HY, Han HS, Jung HW, Park YK (2009) Panax notoginseng Attenuates the Infarct Volume in Rat Ischemic Brain and the Inflammatory Response of Microglia. J Pharmacol Sci 109:368-379.

Sonoda N, Furuse M, Sasaki H, Yonemura S, Katahira J, Horiguchi Y, Tsukita S (1999) Clostridium perfringens enterotoxin fragment removes specific claudins from tight junction strands: Evidence for direct involvement of claudins in tight junction barrier. J Cell Biol 147:195-204.

Srivastava K, Bayraktutan U (2010) Hyperglycaemia perturbs blood-brain barrier by inducing redistribution of tight junction proteins. Cerebrovasc Dis 29:suppl 2.

Srivastava K, Shao B, Bayraktutan U (2012) Hyperglycaemia-evoked protein kinase C augments the endothelial-barrier dysfunction through RhoA/ROCK pathway. Int J Stroke 7:58.

Stamatovic SM, Dimitrijevic OB, Keep RF, Andjelkovic AV (2006) Protein kinase Calpha-RhoA cross-talk in CCL2-induced alterations in brain endothelial permeability. J Biol Chem 281:8379-8388.

Stamatovic SM, Keep RF, Kunkel SL, Andjelkovic AV (2003) Potential role of MCP-1 in endothelial cell tight junction 'opening': signaling via Rho and Rho kinase. J Cell Sci 116:4615-4628.

Stenmark KR, Fagan KA, Frid MG (2006) Hypoxia-induced pulmonary vascular remodeling - Cellular and molecular mechanisms. Circ Res 99:675-691.

Sumi T, Matsumoto K, Nakamura T (2001) Specific activation of LIM kinase 2 via phosphorylation of threonine 505 by ROCK, a Rho-dependent protein kinase. J Biol Chem 276:670-676.

Sydow K (2003) Diabetes mellitus, oxidative stress and endothelial dysfunction. International Congress Series 1253:125-138.

Takai Y, Sasaki T, Tanaka K, Nakanishi H (1995) Rho as a regulator of the cytoskeleton. Trends Biochem Sci 20:227-231.

Takaishi K, Sasaki T, Kotani H, Nishioka H, Takai Y (1997) Regulation of cell-cell adhesion by Rac and Rho small G proteins in MDCK cells. J Cell Biol 139:1047-1059.

Takemoto M, Liao J (2001) Pleiotropic effects of 3-hydroxy-3-methylglutaryl coenzyme a reductase inhibitors. Arterioscler Thromb Vasc Biol 21:1712-1719.

Takemoto M, Sun J, Hiroki J, Shimokawa H, Liao J (2002) Rho-kinase mediates hypoxia-induced downregulation of endothelial nitric oxide synthase. Circulation 106:57-62.

Takeshima H, Kobayashi N, Koguchi W, Ishikawa M, Sugiyama F, Ishimitsu T (2012) Cardioprotective Effect of a Combination of Rho-Kinase Inhibitor and P38 MAPK Inhibitor on Cardiovascular Remodeling and Oxidative Stress in Dahl Rats. J Atheroscler Thromb 19:326-336.

Tinsley JH, de Lanerolle P, Wilson E, Ma WY, Yuan SY (2000) Myosin light chain kinase transference induces myosin light chain activation and endothelial hyperpermeability. Am J Physiol Cell Physiol 279:C1285-1289.

Turrin NP, Rivest S (2006) Tumor necrosis factor alpha but not interleukin 1 beta mediates neuroprotection in response to acute nitric oxide excitotoxicity. J Neurosci 26:143-151.

Uehata M, Ishizaki T, Satoh H, Ono T, Kawahara T, Morishita T, Tamakawa H, Yamagami K, Inui J, Maekawa M, Narumiya S (1997) Calcium sensitization of smooth muscle mediated by a Rho-associated protein kinase in hypertension. Nature 389:990-994.

Usatyuk P, Natarajan V (2004) Role of mitogen-activated protein kinases in 4-hydroxy-2-nonenal-induced actin remodeling and barrier function in endothelial cells. J Biol Chem 279:11789-11797.

Van Aelst L, D'Souza-Schorey C (1997) Rho GTPases and signaling networks. Genes Dev 11:2295-2322.

van Bruggen N, Thibodeaux H, Palmer JT, Lee WP, Fu L, Cairns B, Tumas D, Gerlai R, Williams SP, Campagne MV, Ferrara N (1999) VEGF antagonism reduces edema formation and tissue damage after ischemia/reperfusion injury in the mouse brain. J Clin Invest 104:1613-1620.

van Nieuw Amerongen G, van Hinsbergh V (2001) Cytoskeletal effects of rho-like small guanine nucleotide-binding proteins in the vascular system. Arterioscler Thromb Vasc Biol 21:300-311.

van Nieuw Amerongen GP, Beckers CML, Achekar ID, Zeeman S, Musters RJP, van Hinsbergh VWM (2007) Involvement of Rho kinase in endothelial barrier maintenance. Arterioscler Thromb Vasc Biol 27:2332-2339.

Vandenbroucke E, Mehta D, Minshall R, Malik A (2008) Regulation of endothelial junctional permeability. Ann N Y Acad Sci 1123:134-145.

Vlassara H, Palace M (2002) Diabetes and advanced glycation endproducts. J Intern Med 251:87-101.

Vogelmann R, Nguyen-Tat MD, Giehl K, Adler G, Wedlich D, Menke A (2005) TGF beta-induced downregulation of E-cadherin-based cell-cell adhesion depends on PI3-kinase and PTEN. J Cell Sci 118:4901-4912.

Vorbrodt AW, Dobrogowska DH (2003) Molecular anatomy of intercellular junctions in brain endothelial and epithelial barriers: electron microscopist's view. Brain Res Brain Res Rev 42:221-242.

Wang Q, Tang XN, Yenari MA (2007) The inflammatory response in stroke. J Neuroimmunol 184:53-68.

Wei L, Sun D, Yin Z, Yuan Y, Hwang A, Zhang Y, Si R, Zhang R, Guo W, Cao F, Wang H (2010a) A PKC-beta inhibitor protects against cardiac microvascular ischemia reperfusion injury in diabetic rats. Apoptosis 15:488-498.

Wei L, Yin Z, Yuan Y, Hwang A, Lee A, Sun D, Li F, Di C, Zhang R, Cao F, Wang H (2010b) A PKC-beta inhibitor treatment reverses cardiac microvascular barrier dysfunction in diabetic rats. Microvasc Res 80:158-165.

Werns SW, Lucchesi BR (1990) Free-radicals and ischemic tissue-injury. Trends Pharmacol Sci 11:161-166.

Willis CL, Meske DS, Davis TP (2010) Protein kinase C activation modulates reversible increase in cortical blood-brain barrier permeability and tight junction protein expression during hypoxia and posthypoxic reoxygenation. J Cereb Blood Flow Metab 30:1847-1859.

Witt KA, Mark KS, Sandoval KE, Davis TP (2008) Reoxygenation stress on blood-brain barrier paracellular permeability and edema in the rat. Microvasc Res 75:91-96.

Wojciak-Stothard B, Ridley A (2002) Rho GTPases and the regulation of endothelial permeability. Vascul Pharmacol 39:187-199.

Wojciak-Stothard B, Zhao L, Oliver E, Dubois O, Wu Y, Kardassis D, Vasilaki E, Huang M, Mitchell JA, Louise H, Prendergast GC, Wilkins MR (2012) Role

of RhoB in the Regulation of Pulmonary Endothelial and Smooth Muscle Cell Responses to Hypoxia. Circ Res 110:1423-1434.

Wolburg H, Lippoldt A (2002) Tight junctions of the blood-brain barrier: development, composition and regulation. Vascul Pharmacol 38:323-337.

Wood PL (1995) Microglia as a unique cellular target in the treatment of stroke: potential neurotoxic mediators produced by activated microglia. Neurol Res 17:242-248.

Xie H, Xue YX, Liu LB, Liu YH, Wang P (2012) Role of RhoA/ROCK signaling in endothelial-monocyte-activating polypeptide II opening of the blood-tumor barrier. J Mol Neurosci 46:666-676.

Xu Y, Wang S, Feng L, Zhu Q, Xiang P, He B (2010) Blockade of PKC-beta protects HUVEC from advanced glycation end products induced inflammation. Int Immunopharmacol 10:1552-1559.

Yagita Y, Kitagawa K, Sasaki T, Terasaki Y, Todo K, Omura-Matsuoka E, Kaibuchi K, Hori M (2007) Rho-kinase activation in endothelial cells contributes to expansion of infarction after focal cerebral ischemia. J Neurosci Res 85:2460-2469.

Yamamoto M, Ramirez SH, Sato S, Kiyota T, Cerny RL, Kaibuchi K, Persidsky Y, Ikezu T (2008) Phosphorylation of claudin-5 and occludin by rho kinase in brain endothelial cells. Am J Pathol 172:521-533.

Yang H, Roberts LJ, Shi MJ, Zhou LC, Ballard BR, Richardson A, Guo ZM (2004) Retardation of atherosclerosis by overexpression of catalase or both Cu/Zn-superoxide dismutase and catalase in mice lacking apolipoprotein E. Circ Res 95:1075-1081.

Yang N, Higuchi O, Ohashi K, Nagata K, Wada A, Kangawa K, Nishida E, Mizuno K (1998) Cofilin phosphorylation by LIM-kinase 1 and its role in Rac-mediated actin reorganization. Nature 393:809-812.

Yasuda Y, Tateishi N, Shimoda T, Satoh S, Ogitani E, Fujita S (2004) Relationship between S100beta and GFAP expression in astrocytes during infarction and glial scar formation after mild transient ischemia. Brain Res 1021:20-31.

Yenari MA, Xu L, Tang XN, Qiao Y, Giffard RG (2006) Microglia potentiate damage to blood-brain barrier constituents: improvement by minocycline in vivo and in vitro. Stroke 37:1087-1093.

Zhang Y, Pardridge WM (2001) Rapid transferrin efflux from brain to blood across the blood-brain barrier. J Neurochem 76:1597-1600.

Zhang Y, Peng F, Gao B, Ingram AJ, Krepinsky JC (2011) High glucose-induced RhoA activation requires caveolae and PKC-beta1-mediated ROS generation. Am J Physiol Renal Physiol 302:F159-172.

Zhou CM, Li Y, Nanda A, Zhang JH (2003) HBO suppresses Nogo-A, Ng-R, or RhoA expression in the cerebral cortex after global ischemia. Biochem Biophys Res Commun 309:368-376.

Appendices

1. Appendix I

Recipe for Western blotting buffers and gels

The following buffers were used detected the protein bands by Western blotting technique in HBMEC lysates.

1. 10X Running buffer (1 Litre)

24.2 g	Tris-base
144.0 g	Glycine
10.0 g	SDS
1000 mL	distilled water

2. 1X Running buffer (1 Litre)

100 mL	10X Running buffer
900 mL	distilled water

3. 10X Transfer buffer (1 Litre)

24.2 g	Tris-base
144.0 g	Glycine
1000 mL	distilled water

4. 1X Transfer buffer (2 Litres)

200 mL	10X Transfer buffer
400 mL	methanol (100%)
1400 mL	distilled water

5. 10X TBST (1 Litre)

24.2 g	Tris-base
87.6 g	Sodium Chloride
1000 mL	distilled water
	pH 7.4-7.6

10 mL Tween-20

6. 1X TBST (1 Litre)

100 mL 10X TBST

900 mL distilled water

7. Blotto blocking buffer (5%)

2.5 g Blotto milk

50 mL 1X TBST

8. Ammonium persulphate (APS; 10%)

0.5 g Ammonium persulphate

5 mL distilled water

9. L-Tris buffer (1.87 M, 0.5 Litres)

113.6 g Tris-base

500 mL distilled water

pH 8.8 adjusted with Conc. Hydrochloric acid

10. U-Tris buffer (1.25 M, 0.5 Litres)

75.7 g Tris-base

500 mL distilled water

pH 6.8 adjusted with Conc. Hydrochloric acid

Polyacrylamide gel electrophoresis (PAGE) recipe

Gel components	**Resolving (7.5%)**	**(10%)**	**(15%)**	**Stacking (4%)**
	(mL)	(mL)	(mL)	(mL)
Ultra-pure water	7.600	6.201	3.405	3.680
40% w/v Acrylamide	2.740	3.653	5.475	0.490
2% Bis-acrylamide	1.460	1.946	2.920	0.260
L-Tris (1.87 M)	3.000	3.000	3.000	-
U-Tris (1.25 M)	-	-	-	0.500
10% SDS	0.150	0.150	0.150	0.050
10% APS	0.100	0.100	0.100	0.040
TEMED	0.015	0.015	0.015	0.010

2. Appendix II

Antibodies detecting proteins of human and mouse origin by Western blotting

The following human proteins were detected in HBMEC lysates.

	Proteins	Size (kDa)	Gel (%)	Antibody Conc.	Quantity (µg)
1.	CuZn-SOD	16	15	(1:5000)	2.5
2.	Catalase	65	10	(1:2000)	15
3.	gp91-phox	91	10	(1:300)	50
4.	RhoA	24	15	(1:300)	25
5.	Rho-kinase-2	160	7.5	(1:1000)	25
6.	MLC2	20	15	(1:300)	25
7.	p-MLC2-Ser^{19}	18	15	(1:300)	25
8.	p-MLC2Thr^{18}/Ser^{19}	18	15	(1:300)	25
9.	Occludin	78	10	(1:700)	25
10.	ZO-1	240	7.5	(1 µg/mL)	25
11.	Claudin-5	23	15	(1:500)	50
12.	β-catenin	96	10	(1:5000)	10
13.	Vinculin	116	10	(1:1000)	25
14.	PKC-α	80	10	(1:300)	25
15.	PKC-β	80	10	(1:75)	25
16.	β-actin	44	10	(1:30,000)	2.5

3. Appendix III

siRNA oligonucleotide sequences targeting human PKC isoforms

The following siRNA oligonucleotides were used for gene silencing in HBMEC.

1. ON-TARGET plus SMART pool, human PKC-β_I, 5 nmol

1. GGUCAUGCUUUCAGAACGA
2. CCUGUCAGAUCCCUACGUA
3. GAUUUGGGAUUGGGAUUUG
4. UCAUUGUCCUCGUAAGAGA

2. ON-TARGET plus SMART pool, human PKC-α, 5 nmol

1. UCACUGCUCUAUGGACUUA
2. GAAGGGUUCUCGUAUGUCA
3. UUAUAGGGAUCUGAAGUUA
4. UAAGGAACCACAAGCAGUA

4. Appendix IV

Recipe for the buffers used in total PKC activity

The following buffers were used for measuring the total PKC activity in the HBMEC lysates.

1. PKC extraction buffer

25 mM	Tris-HCl (pH 7.4)
0.5 mM	EDTA
0.5 mM	EGTA
0.05%	Triton X-100
10 mM	β-mercaptoethanol
1 µg/mL	Leupeptin
1 µg/mL	Aprotinin

2. PepTag C1 peptide

L-R-R-A-S-L-G

0.4 µg/µL in water

3. PepTag PKC reaction 5X buffer

100 mM	HEPES (pH 7.4)
6.5 mM	$CaCl_2$
5 mM	DTT
50 mM	$MgCl_2$
5 mM	ATP